The Pennsylvania State University

The Graduate School

College of Engineering

THE DEVELOPMENT OF ULTRAHIGH STRENGTH LOW ALLOY CAST STEELS WITH INCREASED TOUGHNESS

A Dissertation in

Industrial Engineering

by

Paul C. Lynch

Submitted in Partial Fulfillment

of the Requirements

for the Degree of

Doctor of Philosophy

May 2011

The dissertation of Paul C. Lynch was reviewed and approved* by the following:

Robert C. Voigt
Professor of Industrial Engineering
Dissertation Adviser
Chair of Committee

Richard A. Wysk
Professor Emeritus of Industrial Engineering

Edward C. DeMeter
Professor of Industrial Engineering

Chantal Binet
Material Process Researcher, Center for Innovative Sintered Products

Paul M. Griffin
Peter and Angela Dal Pezzo Chair Professor
Head of the Department of Industrial Engineering

*Signatures are on file in the Graduate School

Abstract

This work describes the initial work on the development of the next generation of ultrahigh strength low alloy (UHSLA) cast steels. These UHSLA cast steels have both ultrahigh strength levels and good impact toughness. The influence of heat treatment, secondary processing using hot isostatic processing (HIP), and chemical composition on the microstructure and properties of UHSLA cast steels have been evaluated. The extent of microsegregation reduction expected during the heat treatment of UHSLA cast steels has also been estimated by diffusion modeling. This new family of UHSLA cast steels is similar in composition and properties to UHSLA wrought steels. However, the heat treatment and secondary processing of the UHSLA cast steels is used to develop microstructures and properties typically developed through thermomechanical processing and heat treatment for wrought UHSLA steels.

Two martensitic UHSLA steels, 4340+ (silicon modified 4340) and ES-1 were investigated for this study. For the 4340+ alloy, heat treatment variables evaluated include homogenization temperature and time, tempering temperature, and austempering temperature and time. For the ES-1 alloy, heat treatment variables evaluated include homogenization temperature and time, austenization temperature, cryogenic treatment, and tempering temperature. The effect of high temperature hot isostatic processing (HIP) on the 4340+ and ES-1 alloys was also investigated. Tensile properties, charpy v-notch impact toughness (CVN), microstructures, and fractographs have all been characterized after heat treatment. The effects of HIP on microporosity reduction in the ES-1 alloy were also investigated.

The experiments carried out on the investment cast 4340+ alloy have shown that increasing the homogenization temperature can increase CVN without changing the ultimate tensile strength (UTS) or yield strength (YS) of the cast material. By replacing the homogenization step in the conventional heat treatment process with a high temperature HIP treatment, both the CVN and ductility of the alloy was found to increase while maintaining comparable ultimate tensile strength (UTS) and yield strength (YS) levels as compared to the original homogenization treatment. Austempering the (IC) 4340+ material led to a significant increase in CVN and ductility at the expense of UTS and yield strength as the primarily martensitic microstructure was converted to a mixed martensitic-bainitic structure.

Excellent impact and tensile properties were possible with vacuum degassed ES-1 cast ingot material when the material was subject to a high temperature HIP homogenization cycle prior to heat treatment. A high temperature HIP homogenization cycle following by a second high temperature homogenization cycle, high temperature austenization cycle, and a low temperature tempering step had the potential to produce cast ES-1 ingot material with 40 ft-lbs. of CVN impact toughness at -40°F while possessing 15% elongation, yield strength > 190 ksi., and an ultimate tensile strength of > 250 ksi. The impact transition behavior of this material showed evidence of the excellent impact toughness exhibited by the material across a wide range of temperatures (-100°F to +212°F). The lower shelf energy for the cast + HIP ES-1 alloy could not be estimated from the impact toughness vs. temperature curves shown, because the lower shelf energy for this alloy occurs at a temperature below -100°F, the lowest impact testing temperature in the study.

A high temperature HIP homogenization treatment of cast ES-1 ingot material significantly reduces both the average number of pores and the average area fraction or average % porosity. A high temperature homogenization treatment (without pressure) significantly increased the average number and average area fraction (% porosity) of the cast ES-1 material.

No retained austenite was found in the as cast, as quenched, or fully heat treated ES-1 ingot samples that were analyzed using XRD analysis. Cryo-treatment led to a small improvement in hardness at the expense of -40°F impact toughness.

An initial heat of induction melted, aluminum deoxidized investment cast ES-1 with 0.06 wt % of aluminum showed that the average -40°F and +72°F impact toughness, % elongation, and UTS and YS of the fully heat treated investment cast + HIP ES-1 material lagged significantly behind that of the vacuum degassed cast + HIP ES-1 ingot material. Even though the % elongation and impact toughness of the investment cast ES-1 material changed between heat treatment conditions, the average UTS and YS values remained relatively unchanged throughout the heat treatments for the investment cast study. Etched micrographs of the investment cast ES-1 material showed evidence of significant differences in microsegregation reduction between the samples homogenized at 2125°F for 4 hours and those not homogenized at 2125°F for 4 hours. SEM fracture surface work performed on the investment cast material clearly showed that the induction melted investment and aluminum killed cast material contained

significant amounts of MnS and Al_2O_3 inclusions that were not discovered in the vacuum degassed cast ingot material.

Lastly, the results of a third heat of induction melted, aluminum deoxidized investment cast ES-1 material possessing just 0.01wt% of aluminum showed that the decrease in aluminum content from the first experimental heat did not improve the mechanical properties of the investment cast material.

Casting section size (cooling rate) is shown to directly influence the amount of segregation reduction possible during HIP or homogenization treatments of UHSLA steel castings. The segregation reduction possible depends not only on the alloys present and the homogenization time and temperature, but also on the DAS of cast steels. Model estimates show that little, if any diffusion of substitutional alloying elements will occur during the homogenization of steels castings with DAS $\geq$ 200 μm regardless of the homogenization temperature. Throughout this study, high temperature (1950°F - 2125°F) HIP cycles as well as high temperature homogenization cycle improved the impact toughness of UHSLA cast steels. Diffusion modeling suggests that high temperature HIP cycle can also significantly reduce the microsegregation of substitutional alloying elements and can therefore replace the homogenization step in the heat treatment of UHSLA cast steels. The research suggests that HIP processing improves the toughness by significantly reducing microporosity formed during solidification.

TABLE OF CONTENTS

LIST OF FIGURES

LIST OF TABLES

AKNOWLEDGEMENTS

The completion of the PhD. degree is the end of a great education at Penn State, but it is also an exciting beginning. The completion of this degree will allow me to fulfill a dream working as a University instructor where I will able to focus on teaching, advising, and mentoring the next generation of our nation's youth. I must dedicate the completion of this degree to my late father, Charles R. Lynch. Being a first generation college graduate, my dad always encouraged me to seek more education and ***always*** work extremely hard. The values and work ethic that my parents instilled in me at a very young age have carried me to where I am today.

I would like to thank my wife, Alex for her continued support of me. It has been a stressful ride, but we only hope that it will pay off in a rewarding profession and prosperous life for our family. I would also like to thank my mom, Barbara Lynch for her unconditional support throughout my education. Next, I must thank my committee members. I must thank my advisor, Dr. Bob Voigt, for his support throughout the past 5+ years. Dr. Voigt was both an advisor and a mentor to me throughout my time at Penn State. Dr. Voigt never lost his faith in me; he mentored me through good times and bad. I must thank Dr. Richard Wysk for his support of me throughout the past 5+ years. Dr. Wysk and I worked great together as an IE 450 team and we became great friends in the process. Our hard work in IE 450 is still not forgotten as we routinely receive emails and phone calls to this day from our IE 450 students. Dr. Edward DeMeter is another faculty member that I need to thank as Dr. DeMeter and I became friends when he was my undergraduate professor back in 2002. Dr. DeMeter has always led by example; he works extremely hard and as a student of his it motivated me to work equally as hard. I learned a great deal from Dr. DeMeter and enjoyed working alongside him in SME. I must thank Dr. Chantal Binet. I am very thankful to have Dr. Binet on this committee as she has brought a wealth of steel knowledge to the committee.

Next, I need to thank Ms. Rachel Abrahams. I cannot thank Rachel enough for all that she has done for me. Rachel is like a sister to me. She is one of the smartest and nicest people I have ever met. It was a great experience working with Rachel the past 5+ years.

I must also thank the undergraduate students that worked on this project with me. Alicia Keppler came on board and worked very hard when I began working on the project. After Alicia graduated, Ms. Michelle Leunis dedicated a large amount of her time working with me in the lab for almost 2 years on this project. Kyle Paret and I spent many hours during the Spring and Summer of 2010 discussing diffusion modeling and the data for the model. We also spent a lot of time heat treating and preparing samples for EPMA in an attempt to "find dendrites" and validate assumptions for the working Excel model. My thanks go out to Ms. Alyssa DeYoung for both helping to refine this document and putting in many hours in the lab working on this project.

I must thank Kristina Cowan for her unending support in the CISP metallography lab. In the industrial engineering FAME lab, Dan Supko, Bill Genet, and Randy Wells also provided unending support with cutting and heat treating material to make this research possible.

I cannot forget all the people in industry and on the AMC/SAIC/CIDR team that helped me throughout the past 5 years. Some of which include: Kenneth Murphy (ACIPCO), Rick Boyd (Nova Precision Casting), Morris Dilmore (EAFB), James Ruhlman (Cherokee Technical Specialists), Steven Adams (SAIC), Thornton White (AMC), Malcolm Blair (SFSA), Raymond Monroe (SFSA), Dr. John DuPont (Lehigh University), and all the folks at McConway & Torley in Kutztown, PA.

Thank you to Mr. Clayton Mulcahey at Bodycote for all the HIPing services Bodycote provided for Penn State. Thank you to Mr. Roy Starr at Westmoreland Mechanical Testing & Research. Roy provided unending technical support throughout all the mechanical testing that was carried out.

I must give a send a special thank you to Mark Bidoli, Matt Sullivan, Maureen "Mo" Lynn, and all members of the Penn State Metalcasting Advisory Board. I truly appreciate what you have done for me and continue to do for the Penn State Metalcasting program. In addition, I must thank Bill Sorensen and Pam Lechner of FEF for their support of me and the Penn State Metalcasting program.

Finally, I cannot forget about the great support network of friends I had around me throughout all my years of graduate school. I must thank the entire staff (Linda Hosterman, Erin Ammerman, Shelly Regel, Sharon Frazier, Lisa Fuoss, Olga Covasa, Susan Williams) in 310 Leonhard Building that keep the IE Department running. I must thank Mrs. Elena Joshi and the entire DUS staff for mentoring and helping me become a successful academic advisor. Last but not least- I must also thank all of my graduate school friends for their sincere friendship and support. It was a great experience!!!

Chapter 1

Introduction

The current study is being carried out as a result of the defense industry demand for affordable ultrahigh strength low alloy (UHSLA) cast steels with improved impact toughness for high strain rate applications and for lightweight military components. The term "ultrahigh strength" steel is typically used to describe wrought steels with yield strengths of 200 ksi. and above. Low alloy steels are characterized by a carbon content that is typically below 0.45% with total alloy contents up to 8%. UHSLA steels have traditionally been developed mainly to meet requirements of higher strength. Special alloying and processing techniques are required to develop adequate toughness. By lowering carbon contents and adding appropriate microalloying elements such as tungsten and coupling these changes with proper heat treatments, UHS alloys with improved impact properties can be designed.

Most of the research and development that has been carried out has been completed on wrought products that typically rely on thermomechanical processing to develop desired microstructures and mechanical properties. Ultrahigh strength cast steel alloy development has been lagging behind wrought steel alloy development. A huge potential exists both for defense and commercial applications if affordable UHSLA cast steels can be developed with ultrahigh strength and improved impact toughness. UHSLA cast steels can offer lightweight performance because their high strength-to-weight ratio approaches that of commonly used titanium alloys. By comparison, UHSLA steels are much cheaper to produce than titanium alloys and alloys containing large amounts of expensive alloying elements such as nickel, titanium, and cobalt. UHSLA cast steels can be procured with more ease from an extensive network of suppliers. In an attempt to capitalize on these potential advantages of UHSLA cast steels, this work has focused on the development of ultrahigh strength cast steels at yield strength levels greater than 180ksi. with improved impact toughness.

A review of the literature shows that the physical metallurgy and processing of wrought UHSLA steels for structural applications has been widely studied. The mechanical properties achievable using conventional heat treatments for wrought UHSLA steels are well known. A few recent studies have focused on studying the impact toughness achievable for UHSLA steels using non conventional heat treatment practices such as higher homogenization and austenization

temperatures, austempering, and hot isostatic processing (HIP). Although the chemistries, and physical metallurgy principles for achieving high strength and toughness in wrought and cast UHSLA steels are expected to be similar, it is in the processing steps, where a distinct difference can be expected. The heat treatment process is the critical component in improving the mechanical properties of cast UHSLA steels. Very little work has been completed on developing processing guidelines and conventional quench and temper heat treatments for cast UHSLA steel. In addition, processing improvements possible by austempering and hot isostatic processing (HIP) prior to heat treatment have not been investigated.

Previous efforts to develop UHSLA steels for structural, aerospace, and ballistic applications have primarily been carried out on wrought 4340, and next-generation derivative alloys based on 4340 (300M and D-6AC) steels. 4340 steel is considered the industry standard for which ultrahigh strength steel comparisons are commonly made. When conventionally heat treated by quench and temper (Q&T) heat treatments, 4340, 300M, and D-6AC alloys exhibit very high strengths with limited toughness. The intermediate alloy, high fracture toughness steels, Aermet 100 and AF 1410, were developed to exhibit both acceptable strength and toughness using standard heat treatment practices. However, alloy costs are very high for these materials because of their high Ni and Co contents.

The initial part of this work is focused on developing a silicon modified 4340 steel (referred to as 4340+ or 300M), based on recent generation wrought UHSLA steels and de**v**eloping cast heat treatment processing guidelines to result in yield strength levels greater than 200ksi with improved impact toughness. The second part of this work is focused on developing a cast Fe-C-W-Si steel, ES-1. This lower carbon content alloy is expected to achieve yield strengths greater than 180 ksi. with excellent low temperature impact toughness. Heat treatment cycles for the materials must be able to reduce the as-cast alloy micro-segregation levels to insure adequate toughness. Lastly, a diffusion model was developed as part of this work to estimate the percent reduction in cast steel alloying element microsegregation expected from heat treatment.

The primary objectives of the experiments carried out as part of this development study were to investigate the physical metallurgy and structure/property/processing relationships for the cast 4340+ and ES-1 alloys. A single heat of investment cast 4340+ test bars was procured from which heat treatment processing trials were conducted. The conventional Q & T heat

treatment variables studied for the 4340+ alloy were homogenization temperature and tempering temperature. Austempering treatments at multiple temperatures and times were carried out on the 4340+ alloy; high temperature HIP was also carried out on the 4340+ material.

A single heat of cast ES-1 ingot material and three heats of investment cast ES-1 material were also procured. The heat treatment variables studied included homogenization temperature and time, austenization temperature, HIP, and tempering temperature. The heat treatment development effort was focused on characterizing the impact transition behavior and developing low temperature impact toughness. In addition to the experimental heat treatment test matrix, additional cryogenic treatments were carried out on the cast ES-1 ingot material in an attempt to isolate the possible effects of retained austenite on the heat treated properties of the ES-1 material. Parallel material characterization studies were carried out to evaluate the influence of micro-segregation and micro-porosity on the resultant properties. Diffusion models were developed and validated with the literature to assist in the identification of appropriate heat treatment processing cycles for cast alloys.

Throughout the studies, tensile and impact specimens were machined and tested to evaluate the effects of specific heat treatment variables on strength and toughness. Unetched and etched samples from each of the heat treatment conditions were examined using optical microscopy to characterize microstructural changes in the material with different heat treatments. Scanning electron microscopy (SEM) work was completed to characterize the fracture surfaces throughout the studies, and x-ray diffraction work was carried out to quantify retained austenite in the cast ES-1 alloy.

Chapter 2

Literature Review

2.1 Background of Ultrahigh Strength Steels

The term ultrahigh-strength steels (UHS) was used to describe wrought steels capable of developing a minimum yield strength of 200 ksi. (1380MPa) [1]. Ultrahigh-strength steels are typically divided into three separate classes. The first class of ultrahigh strength steels is the low-alloy steel class of ultrahigh-strength steels typically based on the widely specified 4340 steel. The second class of ultrahigh-strength steels is the high-alloy secondary hardening steels based on the cobalt containing AF1410 steel. The third class of ultrahigh-strength steels is the high-alloy maraging steels typically based on the 18%Ni steel [1]. Although the focus of this study is on ultrahigh strength low-alloy steels, it is very important to discuss high-alloy maraging steels and high-alloy secondary hardening steels because of their superior impact toughness at high strength levels when compared to the ultrahigh strength low-alloy steels. The ultrahigh strength low-alloy steels are more readily available and have a much lower cost when compared to the high-alloy maraging and secondary hardening steels.

The three classes of ultrahigh strength steels will be discussed in detail. Along with the compositions of ultrahigh strength steels in each class and their typical mechanical properties, the alloying strategies and strengthening mechanisms that separate the three classes of ultrahigh strength steels from each other will be discussed. First, the roles of alloys in strengthening and toughening of steels is discussed. Almost all of this research has been focused on the development of wrought ultrahigh strength steels; however the physical metallography of these steels are similar to the cast UHSLA steels that are the focus of this study.

2.1.1 Roles of Alloys in Strengthening and Toughening of Steels

Steel alloying elements are typically put into two categories according to how they interact with carbon. Steel alloying elements can be categorized as: (1) carbide forming elements, including Mn, Cr, Mo, W, V, Nb, Ti, and Zr or (2) non carbide forming elements, including Ni, Co, Cu, Si, P, and Al.

The following contains a review of the effects of common alloying elements in steels and discusses their role in strengthening and toughening steels:

2.1.1.1 Carbon (C)

The primary hardening element in steels is carbon; carbon strengthens steel through solid solution strengthening and carbide dispersion strengthening. Carbon has a high tendency for macrosegregation during solidification. It also has a strong tendency to segregate at crystal defects in the lattice (i.e. grain boundaries, dislocations). Alloy carbides commonly form in alloyed steels that can have different characteristics than the conventional iron carbides (Fe_3C) [2]. Hardness and strength are largely determined by carbon content and the heat treatment process for plain carbon steels (**Figures 2.1 – Figure 2.3**). This same effect of carbon content on the strength and hardness of wrought steels also plays a role in the strength and ductility of cast steel alloys (**Figure 2.2**). Increasing the carbon content of steels increases the strength and hardness, but ductility and weldability typically decrease [2-4]. The impact toughness of plain carbon steels decreases as the carbon content increases (**Figure 2.4**) [3].

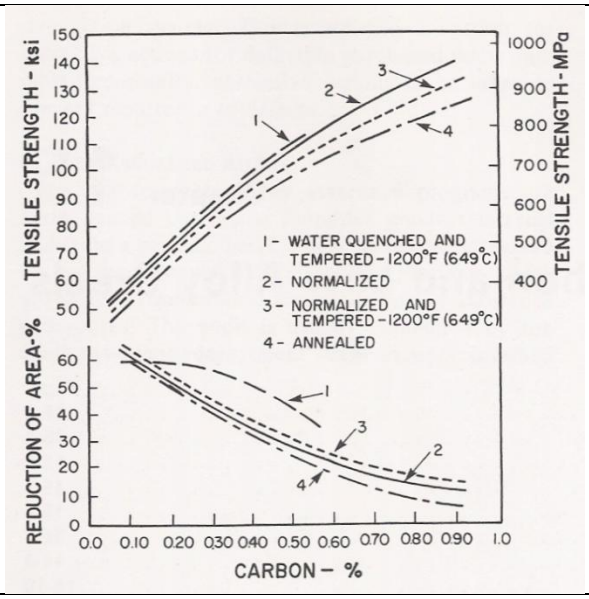

Figure 2.1: Tensile strength vs. carbon content and reduction of area vs. carbon content of cast carbon steels [3].

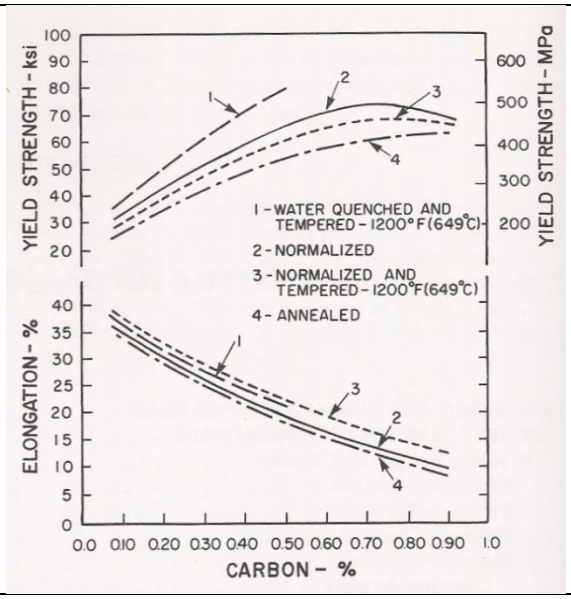

Figure 2.2: Tensile strength vs. carbon content and % elongation vs. carbon content of cast carbon steels [3].

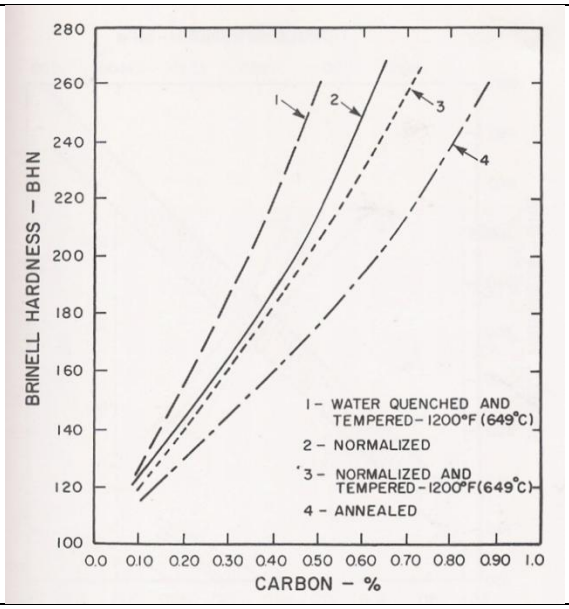

Figure 2.3: Hardness vs. carbon content of cast carbon steels [3].

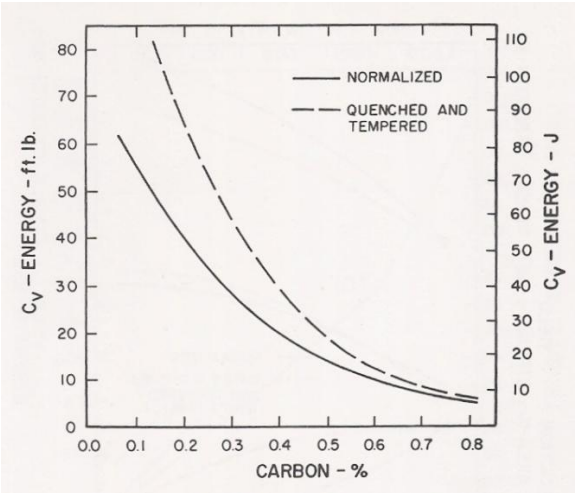

Figure 2.4: Room Temperature Charpy V-notch impact toughness vs. carbon content of cast carbon steels [3].

2.1.1.2 Silicon (Si)

Silicon contents of up to 0.3% are common in all steel alloys because silicon is a principal deoxidizer used in the processing of steel [2,5]. Silicon combines with oxygen in molten steel to form silicates, reducing the gas porosity during solidification. Silicon is a noncarbide forming element that dissolves in austenite, ferrite, or martensite matrixes. Silicon is a ferrite-stabilizing element that dissolves in ferrite (α iron) when the silicon content is below 0.30%. In solid solution, silicon will increase the strength of conventional ferrite matrixes without decreasing ductility. However, for plain carbon steels, as the Si content goes above 0.40%, a marked decrease in ductility in plain carbon steels is realized [2,5]. Silicon also promotes the decarburization of steels during heat treatment and can form silicon oxides, which can lower wear and fatigue resistance of steels [6].

In the development of some ultrahigh strength low alloy steels, greater than 1% silicon is added to help promote deeper hardenability while preventing embrittlement when the steel is tempered at 300-600ºF which is required for very high strength [7]. The reason for this is that the solubility of silicon in cementite is very, very low. As a result, the nucleation and growth of cementite (Fe_3C) in the early stages of tempering is severely slowed because silicon must first diffuse away from the regions of cementite formation [5, 8]. Since the cementite formation and

the formation of coarse crack enhancing carbides during tempering is slowed by silicon, fine transition carbides in the martensitic matrix remain at higher tempering temperatures. Retained austenite also remains stable at higher tempering temperatures in the presence of silicon. Austenite retention in high strength steels has been a subject of study in bainitic microstructures of high strength steels, where high silicon steels have been observed to contain ferrite and austenite structures instead of conventional ferrite and cementite austempered structures [5, 9, 10,11].

2.1.1.3 Manganese (Mn)

Manganese is virtually present in all most all steels in the amount of 0.30% or more. It is a deoxidizer and a sulfur stabilizer. Manganese is an austenite former and can be a weak carbide former as it only dissolves in cementite. Mn levels are typically restricted to <2% to avoid severe segregation problems during solidification. However, Mn can interact with impurities such as P, Sn, Sb, and S resulting in segregation to grain boundaries and temper embrittlement [2,3]. Manganese increases the hardness of tempered martensite by inhibiting the coalescence of carbides and limiting ferrite grain growth [12]. At levels of less than 2%, Mn can improve the tensile strength of cast steels [2,3]. This is evident in **Figure 2.5** for conventional C-Mn cast steels [3].

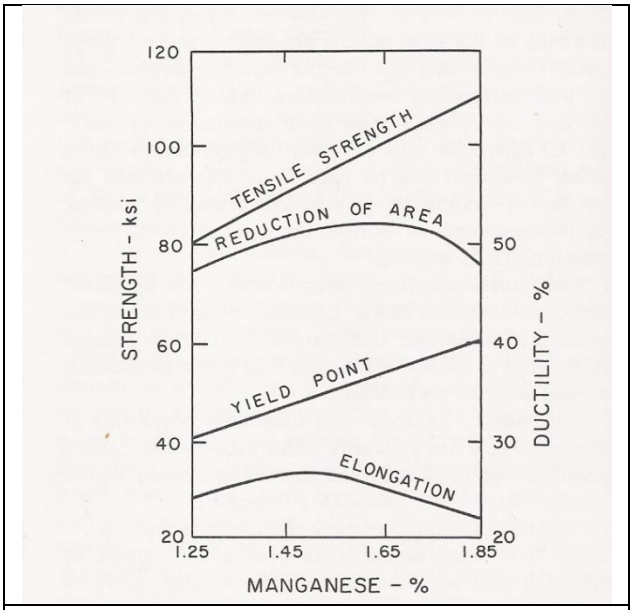

Figure 2.5: Strength and ductility of Mn alloyed C-Mn cast steels with 0.34% C, normalized and tempered at 700ºF (371ºC)[3].

2.1.1.4 Molybdenum (Mo)

Similar to manganese, molybdenum is a very important alloying element in most alloy steels. Mo additions to steel produce fine-grained steels, increase hardenability, and improve alloy fatigue strength; it also promotes solid solution strengthening in austenitic alloys. Molybdenum (like tungsten, vanadium, and chromium) is a strong-carbide forming element that is used to achieve secondary hardening during tempering. It must be fully dissolved in austenite during austenization in order to be incorporated during quenching into martensite with sufficient supersaturation for secondary hardening during tempering [2,13]. **Figure 2.6** below shows the effect of varying levels of Mo on the tempering resistance and secondary hardening during the tempering of a 0.35% steel.

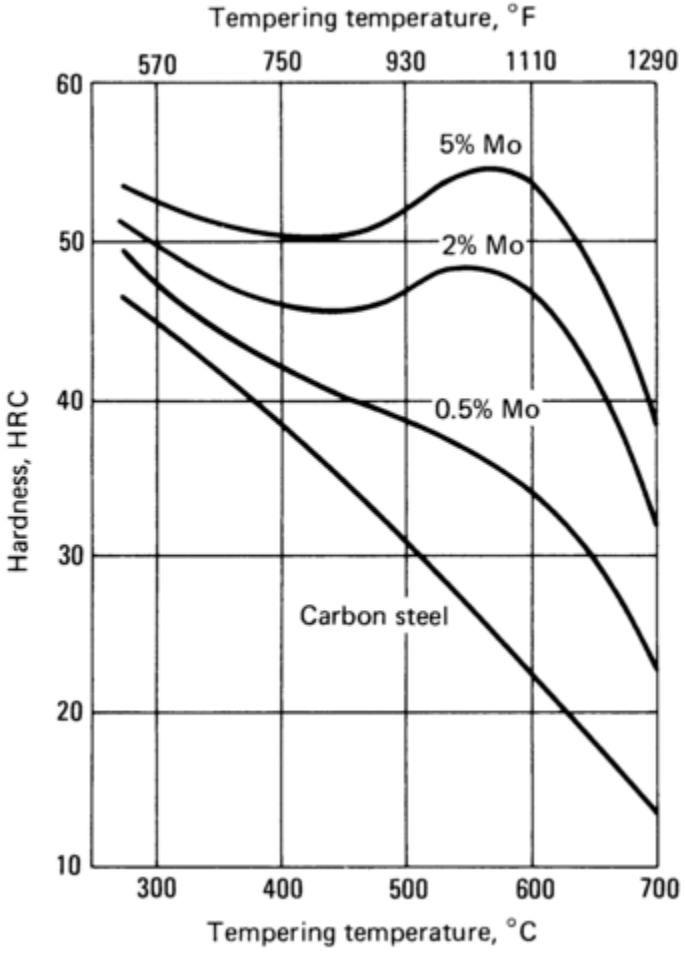

Figure 2.6: Retardation of softening and secondary hardening during the tempering of wrought 0.35% C steel with different levels of molybdenum [14].

2.1.1.5 Aluminum (Al)

Aluminum is typically used in steels as a deoxidizer. Aluminum can also be effective in controlling grain growth during subsequent heat treatment; aluminum forms coarse brittle nitrides in the presence of nitrogen. The aluminum content in steels is kept low; the level should be just enough to act as a grain refiner and deoxidizer of the melt [2, 15].

2.1.1.6 Chromium (Cr)

Chromium is one of the most important alloying elements in steels. Chromium in levels in excess of 12% Cr are required for corrosion resistance in stainless steels. Although chromium is known for its corrosion and oxidation resistance, Cr is often added to low alloy steels to increase hardenability. Chromium is a medium carbide forming element. Chromium behaves a lot like Mo and can be expected to retard the softening of martensite at all temperatures [14]. In low Cr content steels, only alloyed cementite $(Fe,Cr)_3C$ forms. As the Cr/C ratio rises, chromium carbides $(Cr, Fe)_7C_3$ or $(Cr, Fe)_{23}C_6$ or both can be expected to form. Chromium carbides are hard and wear-resistant; complex chromium-iron carbides slowly go into solution in austenite [2,15-16]. Longer time at temperature may be necessary to allow a complete solutionizing before quenching to form martensite [2, 15-16]. Adding Cr to steels has a tendency to interact with impurities such as P, Sn, Sb, and As. These impurities can segregate to grain boundaries and induce temper embrittlement at intermediate tempering temperatures [2,15-16].

2.1.1.7 Nickel (Ni)

Nickel is very unique among steel alloying elements; Ni forms a continuous series of solid solutions with iron and does not exhibit a tendency to form carbides. Nickel is an austenite forming element; Ni is effective at lowering the temperature of the austenite (γ) to ferrite (α) transformation. When Ni is introduced in amounts up to about 5% in Fe-Ni alloys, it increases strength and hardness without inducing a comparable reduction in ductility. Nickel increases the strength of steel by solution hardening ferrite. It also raises steel hardenability, and when used in combination with Cr and Mo, it produces even greater hardenability, impact toughness, and fatigue resistance in steels [2,15-16].

2.1.1.8 Vanadium (V)

Like molybdenum, vanadium is a very strong carbide forming element. In fact, vanadium is a stronger carbide former than Mo and Cr and can therefore be expected to have a much more potent effect at the same alloy levels [12]. Vanadium dissolves in austenite, which strongly increases its hardenability, but undissolved vanadium carbides can decrease hardenability [2]. Vanadium is used as an alloying element in steel for two main reasons. First, the vanadium carbides help to refine the austenite grain structure of the steel casting alloy. Second, vanadium is used to precipitation harden the ferrite (α) phase. The precipitation of fine vanadium carbide and vanadium nitrides in ferrite can develop a significant increase in strength and impact toughness. A manganese content of 1% or more is found to enhance the precipitation hardening effect of vanadium, particularly when the nitrogen content is at least 0.01%. As a result of secondary hardening upon tempering, vanadium helps to increase hot-hardness and improve wear resistance. Vanadium has also been reported to slow the rate of temper embrittlement of Mo-bearing steels [2, 15-16].

2.1.1.9 Tungsten (W)

Like chromium, molybdenum, and vanadium, tungsten is a strong carbide forming alloying element. The behavior of W is very similar to that of Mo in steels. Tungsten was the first alloying element used in the development of tool steels; high temperature heat treatment of tungsten steels developed superior cutting ability [2,15]. The addition of tungsten will produce a larger carbide volume than other alloying elements at the same carbon level because of the M_2C stoichiometry of the tungsten rich carbide phase. Tungsten carbides promote a fine final grain structure by preventing austenite grain growth at high temperatures. **Figure 2.7** shows the effects of tungsten on carbide formation in a low alloy steel. Adding W to steel will help produce a finer carbide structure, more, and finer carbides when compared to other carbide forming alloys. This results in higher hardness, creep strength and better wear resistance at high temperatures [17].

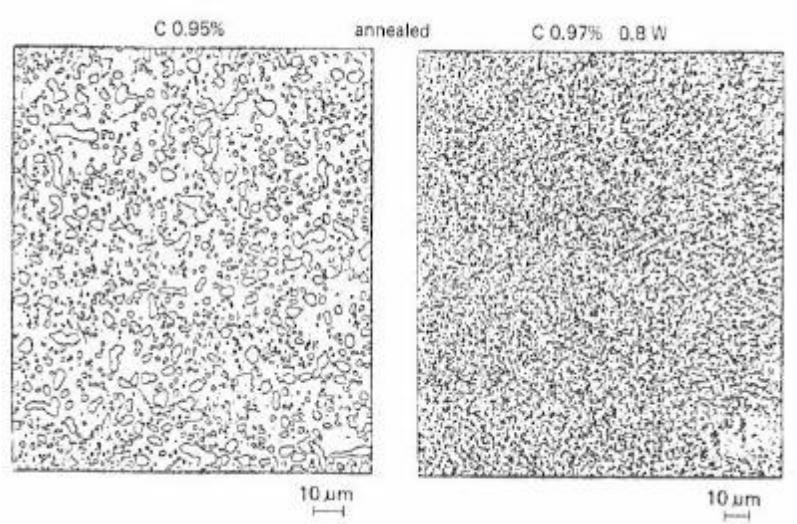

Figure 2.7: Influence of tungsten on the carbide formation in high carbon wrought steel; tungsten produces a larger carbide volume than other alloying elements promoting a fine final grain structure by preventing austenite grain growth at high temperatures [17].

However, W and Mo have been reported to impair scaling resistance during heat treatment [2,15].

2.1.1.9.1 The Effects of Tungsten (W) in UHSLA Steels

Until recently, all UHSLA steels have not relied on tungsten (W) as a primary alloying element. However, the presence of W in newly developed UHSLA cast steels makes their compositions unique. The newly developed UHSLA cast steels containing tungsten have not been thoroughly studied. As mentioned, the addition of tungsten can be expected to produce a larger carbide volume fraction than other alloying elements at the same carbon level. During austenization from sufficiently high temperatures, the W carbides will fully or partially dissolve in the austenite- depending on the austenization temperature. After quenching, the W remains in supersaturated solution in the martensite. **Figure 2.8** illustrates the tempering response in tungsten alloyed steel as compared to carbon steel without tungsten [17]. In plain carbon steels, simple iron carbides form during tempering. These carbides continue to coalesce and grow at higher tempering temperatures, causing hardness and strength to decrease. In tungsten containing steels, delayed tungsten carbide formation leads to a secondary hardening effect upon tempering. Since tungsten has a larger atomic radius than other alloying elements in steels, it takes much more energy for diffusion than many other alloying elements [17, 18]. At lower temperatures W can actually inhibit the diffusion of other elements in steel resulting in a drop in hardness and strength at lower tempering temperatures. Tungsten alloy (W_2C) carbides only

precipitate from the matrix of the martensite above about 400ºC (752ºF). Since these carbides are very fine, they cause a precipitation hardening effect, which leads to increases in hardness and strength when tempering above 500ºC (932ºF). If tempering temperatures are much higher than about 500ºC (932ºF), the fine tungsten carbides begin to coalesce and grow, which leads to an eventual decrease in hardness and strength. It is the combination of tungsten dissolving in the austenite phase, followed by a transformation to martensite upon quenching, and a precipitation of fine carbides during tempering around 500ºC (932ºF) that leads to improved mechanical properties due to precipitation or "secondary" hardening of tungsten containing steels [18].

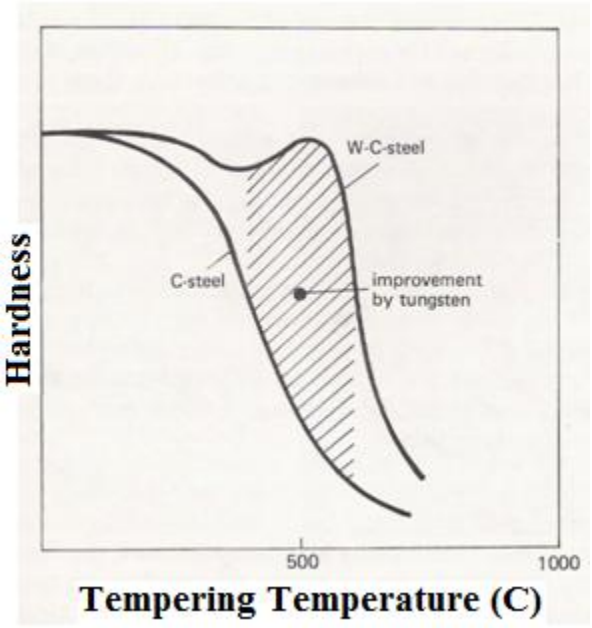

Figure 2.8: Effect of tungsten on the tempering behavior of steel [17].

Most of the previous work on the effects of tungsten in steel has been carried out on tool steels. In a study by Hong et al. (2000) on the effect of the addition of tungsten to 9Cr-Mo steels, it was found that as the amounts of tungsten added to the 9Cr-Mo increased, the toughness decreased. The three steels studied were: M10 steel (9Cr-1Mo), W18 steel (9Cr-0.5Mo-1.8W), and W27 steel (9Cr-0.1Mo-2.7W) with 0.1wt. % carbon. **Figure 2.9 (a)** shows that at certain tempering temperatures, the M10 steel actually had higher impact toughness than the W18 steel that contained about 1.8% W. **Figure 2.9 (b)** shows that the W27 (with 2.7% W) exhibited higher toughness than any other steel for all of the tempering temperatures [19].

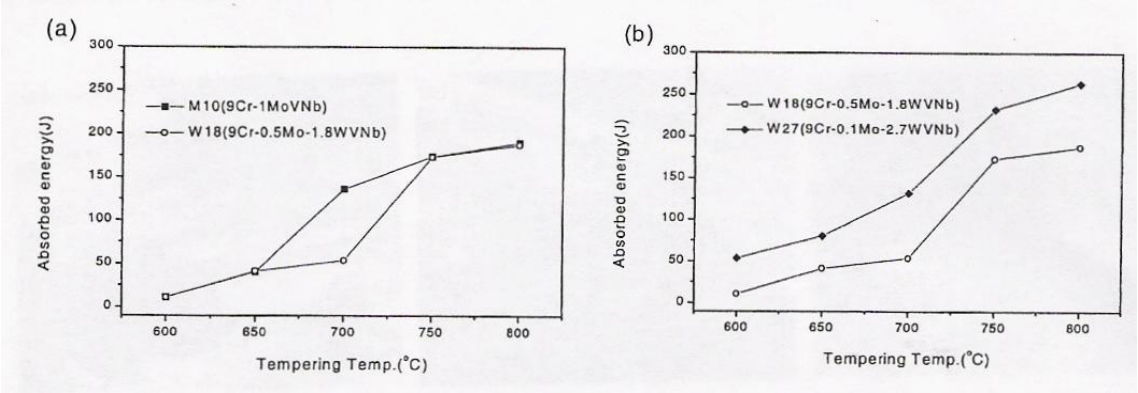

Figure 2.9: Influence of W on the impact toughness of wrought Cr-Mo steels as a function of tempering temperature: **(a)** M10 and W18 (1.8% W) steels; **(b)** W18 and W27 (2.7% W) steels [19].

The deterioration in toughness observed in **Figure 2.9 (a)** was attributed to the 1.8% tungsten addition slowing dislocation recovery to a higher tempering temperature [19]. The W27 steel produced a normalized microstructure that contained both martensite and delta-ferrite. 0.3 vol. % of the soft delta ferrite found in the W27 steel absorbed more impact energy and thus increased the impact toughness of the W27 steel in spite of its higher W content [19].

2.1.1.10 Titanium(Ti)

Titanium (Ti) is a very strong carbide and nitride former [2]. The effects of titanium are similar to those of vanadium and niobium, but titanium carbides and nitrides are more stable than those of Nb and V. Like Nb and V, titanium is an effective grain growth inhibitor because its nitrides and carbides are very stable and difficult to dissolve in austenite [2, 15-16]. If Ti dissolves in austenite, the hardenability of alloy steels could strongly increase due to the presence of Mn and Cr in steels; Mn and Cr decrease the stability of Ti carbides in steels [2]. Titanium is most effective in fully killed (aluminum deoxidized) steels because of its strong deoxidizing effects [16].

2.1.1.11 Cobalt (Co)

Cobalt (Co) is a non carbide forming element in steels. In plain carbon steels, Co decreases hardenability, but when combined with Cr, Co increases the hardenability of Cr-Mo alloy steels [2]. Cobalt also decreases the solubility of Mo in the matrix of maraging steels, which in turn increases the volume fraction of Mo-rich precipitate in these steels [20]. Maraging

steels depend on the precipitation of these fine intermetallics to develop very high strength and impact toughness. Cobalt is also known to increase hardenability in steels by increasing the martensite start temperature and reducing the amount of retained austenite expected upon quenching. Cobalt also has been reported to inhibit austenite grain growth at higher austenization temperatures [2].

2.1.1.12 Phosphorus (P)

Phosphorus in trace amounts can provide benefits to cast steels, but it is mainly looked at as an undesirable tramp element. Phosphorus dissolves in ferrite and increases the strength of steels by solid solution strengthening [2, 15-16]. However, larger amounts of phosphorus (>0.10%) can lead to a decrease in ductility and impact toughness of steels along with increasing the tendency of causing cold-shortness [2,16]. Phosphorus has a tendency to segregate during solidification. When phosphorus segregates at grain boundaries, it can cause temper embrittlement. This is especially true for Mn, Cr, Mn-Si, Cr-Ni, and Cr-Mn steels. It has also been reported to increase the yield strength of austenitic Cr-Ni steels by providing a driving force for precipitation hardening [2].

2.1.1.13 Sulphur (S)

Sulphur is also a tramp element in steels. Sulfur has a very strong tendency to segregate to prior austenite grain boundaries. Increasing amounts of sulphur can cause red or hot shortness because of the low-melting sulfide eutectics that form along the grain boundaries. Sulfur has a negative effect on ductility, impact toughness, weldability, and surface quality of steels [2]. Sulfur must be kept low in all steels, including UHSLA steels to insure maximum toughness.

2.2 Ultrahigh Strength Low Alloy (UHSLA) Steel Development

Low alloy steels have carbon contents that are typically at or below 0.45% with up to 8% total alloy content. In terms of classification, the Steel Founders' Society of America states that if a cast steel alloy contains more than the following amounts of a single alloying element, the alloy is classified as a low alloy cast steel [3]:

Table 2.1: Maximum alloying element concentrations in low alloy cast steels [3].

Manganese	1.00%
Silicon	0.80%
Nickel	0.50%
Copper	0.50%
Chromium	0.25%
Molybdenum	0.10%
Vanadium	0.05%
Tungsten	0.05%

Ultrahigh strength low alloy steels (UHSLA) have been available in wrought form for some time. UHSLA cast steels at yield strength levels above 130 ksi. have not received much attention because the end use applications of UHSLA cast steels rarely called for yield strength levels above 130ksi. UHSLA steels are developed mainly to meet requirements of higher strength than traditional carbon and high strength low alloy (HSLA) steels. UHSLA steels can be expected to exhibit superior hardenability than carbon steels. Even though UHSLA steels are more expensive to produce than plain carbon steels, the cost of UHSLA cast steels is still far lower than that of cast titanium alloys and intermediate or high alloy steels. UHSLA cast steels can be expected to have strength-to-weight ratios that exceed those of titanium alloys, and can be procured at lower cost and with more ease from a number of suppliers.

The bulk of the UHSLA steel literature is for wrought UHSLA steels. The cast UHSLA steels are similar, but have important differences that must be carefully studied. This review will focus on the previous work that has been completed on UHSLA steel and the process control necessary to achieve properties. The following portion of the literature review will provide a background on the development of these wrought UHSLA steels, their strengthening mechanism and its influence on strength and toughness. The groundwork will be laid for the current study on the development of the cast 4340+ and tungsten alloyed UHSLA steels with increased impact toughness.

2.2.1 Wrought UHSLA Steel Compositions

Much of the focus on the development of ultrahigh strength low alloy steels has been completed on wrought ultrahigh strength low alloys 4340, 4330V, 4335V, 300M (i.e. 4340+), D6AC, and HY-TUF steels for structural, aerospace, and ballistic applications. The chemical compositions of these UHSLA alloys can be found in **Table 2.2**.

Table 2.2: Nominal compositions for wrought ultrahigh strength low alloy steels along with their corresponding AMS specifications [21, 22].

Alloy	AMS	% C	%Mn	%Si	% Cr	%Ni	%Mo	% V
Wrought Alloys								
4340	6454, 6414	0.40	0.7	0.3	0.8	1.8	0.3	
D6AC	6431, 6439	0.45	0.7	0.2	1.0	0.6	1.0	0.10% V
300M	6417, 6419, 6257	0.43	0.8	1.6	0.9	1.8	0.4	
4330V	6411	0.30	0.9	0.3	0.9	1.8	0.4	0.07% V
4335V	6435, 6429	0.35	0.8	0.5	0.8	1.8	0.4	0.2% V
HY-TUF	6425	0.25	1.35	1.0	0.3	1.8	0.4	

2.2.1.1 4340 Steel

AISI/SAE 4340 steel is an ultrahigh strength low alloy steel being used in industry for various applications. 4340 steel is considered the industry standard for which other ultrahigh strength steel comparisons are commonly made. The 4340 steel is a variation of the 4130 and 4140 alloys. The 4340 and 4140 alloys both possess about 0.4% carbon, but the 4340 alloy contains additional nickel for enhanced hardenability. The 4340 alloy has deep hardenability with high ductility, toughness, strength, and high fatigue and creep resistance. The 4340 alloy is considered immune to temper embrittlement and does not soften readily at higher tempering temperatures. The 4340 alloy can be nitrided and is mainly used to make parts such as fasteners, gears, pinions, shafts, crankshafts, piston rods, and structural members for aircraft [23]. The 4330V and 4335V alloys contain less carbon than the 4340 alloy with a corresponding V addition to recover some of the strength losses from lower carbon contents. The typical mechanical properties for wrought 4330V, 4335V, and 4340 steel along with other newly developed UHSLA steels are shown in **Table 2.3.** Strength and toughness expectations for these wrought UHSLA steels shown in this table are based on design allowable rather than average or typical properties.

Table 2.3: Mechanical properties of wrought UHSLA steels [21, 22, 24].

Alloy Specification	MMPDS Basis	UTS (ksi)	YS (ksi)	EL (%)	CVN (ft-lbs)* RT/-40°F
4330V	S	220	185	10	25/ 16 (-65F)
D-6AC	S	220	190	12	18/ 16.3 (-65F)
4340	S	260	217	10	18/-
300M (.4C)	S	270	220	8	18/15
4335V	S	240	210	10	NA
HY-TUF	S	220	185	10	NA

*Impact values are properties that are not typically specified.

2.2.1.2 300 M (4340+) Steel

The 300M alloy is silicon modified 4340 alloy (referred to as 4340+ throughout this study). The 300M alloy has about four times the amount of silicon found in the 4340 alloy. 300M also has slightly more carbon and molybdenum than 4340. In addition, 300M contains the strong carbide forming element vanadium (V) [23]. The typical mechanical properties for wrought 300M (4340+) steel are shown in **Table 2.3**.

2.2.1.3 D-6AC Steel

D-6A and D-6AC steel are two ultrahigh strength low alloy steels that were developed for aircraft and missile structural applications. The main difference between D-6A and D-6AC is in the melting practice for each of the steels. The D-6A steel is air melted while the D-6AC material is vacuum arc remelted followed by air melting to reduce the levels of tramp alloying elements. These steels are designed primarily for excellent room temperature properties with tensile strengths of 1800 to 2000MPa (260 to 290 ksi). D-6A steel contains slightly more carbon, chromium, and molybdenum than 4340. It also contains about 0.05 to 0.10% vanadium. D-6A steel has a very high yield to tensile strength ratio, combined with good ductility. This alloy is a deeper hardening alloy when compared to 4340 and does not undergo temper embrittlement [23,25]. The typical mechanical properties for heat treated D-6AC steel are shown in **Table 2.3**.

2.2.1.4 Hy-Tuf Steel

Hy-Tuf is a high-strength low alloy steel that is used for landing gear, flap tracks, and structural applications. Hy-Tuf steel contains 0.25 wt % carbon, whereas the 4340 alloy contains 0.40wt % carbon. The alloy possesses high silicon (1%) and high manganese (1.35%) contents [24]. The typical mechanical properties for heat treated D-6AC steel are shown in **Table 2.3**. This alloy has been designed to have somewhat lower strength than 4340 steel with improved toughness and ductility.

2.2.1.5 Ultrahigh-Strength Low-alloy Steels: Transition Carbide Strengthening

Ultrahigh strength low-alloy steels undergo strengthening due to the development of transition carbides during the early stages of tempering. Krauss [26] provided a review of the microstructure, deformation, and fracture of low-temperature-tempered UHSLA steels. The fine structure of lath martensite that forms in these UHSLA steels consists of high densities of tangled dislocations. During tempering, fine intralath transition carbides form at low temperatures (stage I tempering, up to 250ºC (482ºF)), with the crystallography of the as-quenched martensite crystals remaining unchanged. As a result of these fine transition carbides, the UHSLA steels tempered in the stage I tempering range maintain high strength. At intermediate tempering temperatures (stage II; 250ºC-400ºC (482ºF-752ºF)), any interlath-retained austenite transforms to ferrite and carbide. These aligned carbides form when the interlath-retained austenite transforms to carbides, resulting in tempered martensite embrittlement in addition to a decrease in strength. By increasing the tempering temperature (stage III, 250ºC-700ºC (482ºF-1292ºF), the transition carbide morphologies are replaced by mixtures of ferrite and cementite that lead to increased toughness at the cost of strength. Ultrahigh strength levels in these medium-carbon UHSLA steels can be achieved only through low-temperature tempering (stage I). The strengthening mechanism in UHSLA steels that sets it apart from other steels with is effective transition carbides without tempered martensite embrittlement [1].

Throughout this section, it can be seen that the wrought UHSLA steels have very high strengths, but the tradeoff for strength is impact toughness. Often times, UHSLA quenched and tempered steels are not used at yield strengths above 200ksi because of the subpar toughness of the alloys at these high strength levels [27]. High-alloy maraging steels and high-alloy

secondary hardening steels have superior impact toughness when compared to the ultrahigh strength low-alloy steels at similar strength levels.

2.3 High Strength Steels with High Impact Toughness

Throughout the discussion of UHSLA steels, it was evident that for standard heat treatments, gains in impact toughness are typically possible at the expense of yield strength. Maraging steels and secondary hardening steels are heavily alloyed steels that possess high impact toughness at ultrahigh strength levels. These high alloy steels contain large amounts of cobalt and nickel, making the steels very expensive. Maraging steels are essentially carbon-free martensitic steels which employ substitutional elements allowing for age hardening of the alloys. Secondary hardening steels are a class of quenched and tempered steels which contain sufficient amounts of the carbide-forming elements chromium, molybdenum, and vanadium [1].

2.3.1 High-Alloy Maraging Steels: Intermetallic Precipitate Strengthening

The high impact toughness exhibited by the high-alloy maraging steels is a result of the precipitation of intermetallic compounds that are typically finer than the transition carbides found in quenched and tempered ultrahigh strength low-alloy steels. The very fine intermetallic precipitates provide increased resistance to fracture [20, 1, 28]. In both ultrahigh strength low-alloy steels and in high-alloy maraging steels, fracture typically occurs by void nucleation, growth, and coalescence. Voids typically nucleate by the fracture of Ti(C,N) inclusions in maraging steels and at the interfaces between MnS inclusions and the matrix of 4340 type steels. The main difference between high-alloy maraging steels and ultrahigh strength low-alloy steels is with regard to void growth and coalescence. In ultrahigh strength low-alloy steels, when coarser carbide particles are fractured they cause sheets of voids that help to link together large voids [1]. In maraging steels, carbide particles are not present, because of the very low amounts of carbon in the alloys. In high-alloy maraging steels, primary voids will form aging precipitates until they are impinged, causing the voids to eventually grow together, leading to final fracture. The high-alloy maraging steels contain between 18 and 25 weight % nickel (**Table 2.4**). The typical alloy designations are 18 Ni (250), 18 Ni (300), etc. The number in parentheses indicates the ultimate tensile strength of the alloy.

Table 2.4: Chemical compositions of wrought ultrahigh strength, high fracture toughness steels strengthened by maraging, intermetallic precipitate strengthening (wt%) [1].

Designation	C	Mn	Si	Cr	Ni	Mo	Co	Other
18Ni(250) Maraging	0.03 max	0.12 max	0.12 max	—	17–19	4.6–5.1	7–8.5	0.3–0.5 Ti 0.05–0.15 Al
18Ni(300) Maraging	0.03 max	0.12 max	0.12 max	—	18–19	4.6–5.2	8–9.5	0.5–0.8 Ti 0.05–0.15 Al
18Ni(350) Maraging	0.01 max	0.10 max	0.10 max	—	17–18	3.5–4.0	12–13	1.6–2.0 Ti 0.1–0.2 Al
Garrison NiSiCr steel	0.34	0.49	1.88	1.02	2.89	—	—	—

When a maraging steel is quenched from the solutionizing temperature, a soft but heavily dislocated martensite is formed. The high nickel content actually lowers the M_s temperature to less than about 150ºC (302ºF). However, when the material is reheated to lower temperatures, the martensite remains. Austenite is not reformed until the steel is held between 500ºC and 600ºC (932ºF and 1112ºF). At aging temperatures around 400ºC or 500ºC (752ºF or 932ºF), intermetallic phases precipitate, accelerated by the high dislocation density present in the parent martensite structure. Molybdenum and titanium are responsible for Ni_3Mo, Ni_3Ti and Laves phase Fe_2Mo precipitates. In addition to nickel, the second primary alloying element that is used for high-alloy maraging and secondary hardening steels is cobalt. Cobalt additions actually reduce the solubility of Mo in the matrix; this allows for more Mo to form Mo-rich precipitates. The formation of the precipitates described can lead to a very high volume fraction of precipitate in the alloy. This results in very high strength levels accompanied by very good ductility and high impact toughness [20].

2.3.2 Secondary Hardening Steels: Fine Alloy Carbide Strengthening

High alloy maraging steels have very little, if any, carbon. The secondary hardening steels, often called the Ni-Co-Mo or Ni-Co-Cr intermediate alloy steels (**Table 2.5**) possess a fair amount of carbon.

Table 2.5: Chemical compositions of wrought ultrahigh strength, high fracture toughness steels [1].

Alloy	% C	%Mn	%Si	% Cr	%Ni	%Mo	%Co
AF 1410	0.15	<0.1	<0.1	2	10	1	14
AeroMet 100	0.23	<0.1	<0.1	3.3	12	1.2	14

High strength and high toughness can be achieved by adding alloying elements to the steel to form alloy carbides and precipitates that are thermodynamically more stable than

cementite. This is particularly true for a number of nitrides and borides. Nitrogen and boron are increasingly used in steels in small but significant concentrations for their nitride and boride forming characteristics. As shown in **Figure 2.10**, the enthalpies of formation show that many compounds are more stable than iron carbide. Many nitrides and borides are more stable than iron carbide. The strong carbide forming elements, Cr, Mo, V, W, and Ti all form carbides that have higher enthalpies of formation than iron carbide. The secondary hardening steels also contain amounts of nickel, cobalt, and copper, which do not form carbide phases. Thus, they do not give secondary hardening. For the carbide forming elements Cr, Mo, V, W, and Ti to diffuse fast enough to allow alloy carbides to nucleate and grow, the tempering temperature must be sufficiently high (i.e. 500ºC-600ºC (752ºF-1112ºF)).

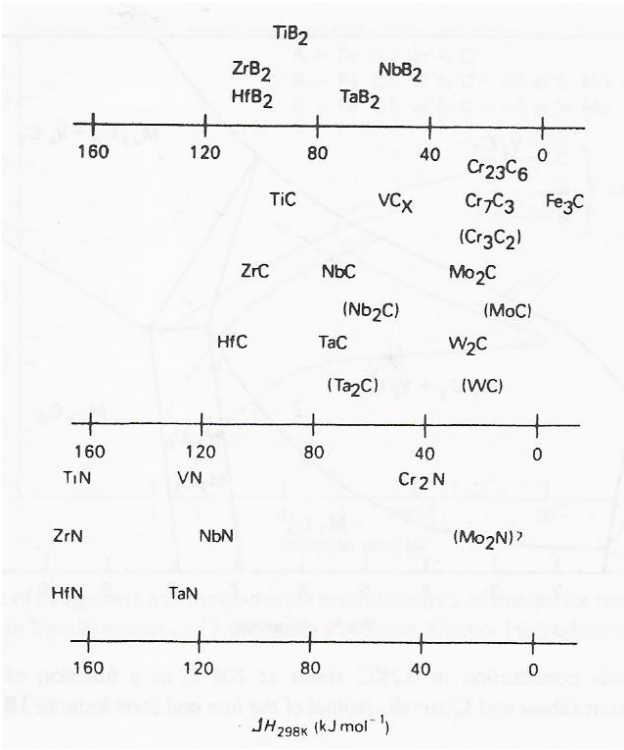

Figure 2.10: The enthalpies of formation of borides, carbides, and nitrides in iron [20].

Very large, coarse precipitates are undesirable for mechanical properties. The coarsening rate of precipitates or carbides depends on the diffusion coefficient of the solute atom. This is what makes the secondary hardening family of alloy steels special. These alloys have the ability to form fine alloy carbide dispersions in the range 500ºC-600ºC (752ºF-1112ºF) that will remain fine even after prolonged tempering. This allows for the development of very high strength levels with good toughness. Secondary hardening is best observed in steels that contain

molybdenum, vanadium, tungsten, titanium, and chromium steels. The age-hardening reactions cause relatively coarse cementite dispersions to be replaced by much finer alloy carbide dispersions. Maintaining very fine carbide dispersion is the key to secondary hardening. The secondary hardening process is dependent on time and temperatures [1,20] which can be expressed as:

$P = T(k + \log t)$ [20], where **Equation 2.1**

T = absolute temperature,

t = tempering time (in hours),

k = constant (typically 20 for alloy steels)

If this expression (the Holloman-Jaffe parameter) is plotted vs. hardness, an understanding of the effect of higher tempering temperatures and longer tempering times on hardness can be evaluated (**Figure 2.11**) [20].

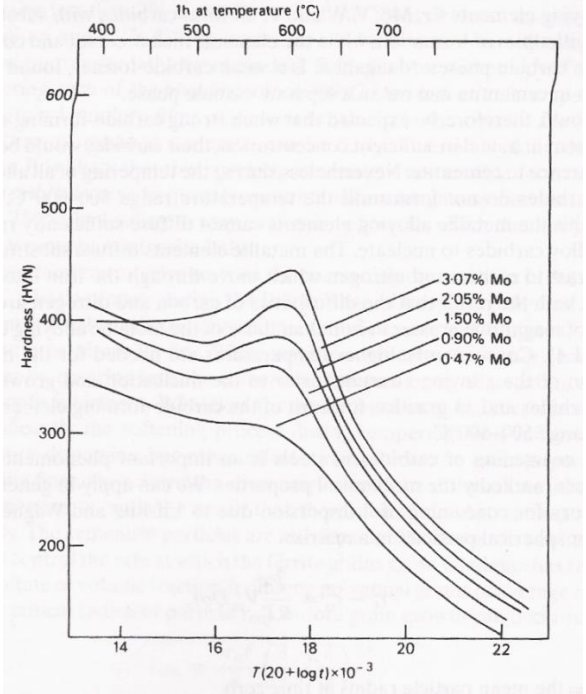

Figure 2.11: The effect of tempering temperature and % Mo on the hardness of quenched 0.1 wt% C wrought steels [20].

2.3.2.1 AF1410 Steel

AF1410 steel is a secondary hardening steel that was designed mainly for structural components in aircraft. As shown in **Table 2.5**, this alloy contains large amounts of nickel and cobalt. The combination of strength and toughness exceeds that of other commercial steels. This alloy has been used in place of titanium for certain aircraft components. The microstructure of the AF1410 alloy consists of a very highly dislocated Fe-Ni lath martensite that is produced after quenching from the austenization temperature. This highly dislocated Fe-Ni lath martensite helps to give the alloy high toughness. The ultimate tensile strength of AF1410 is typically 235ksi. while also possessing a Charpy impact toughness of 60 ft-lbs. at room temperature (**Table 2.6**). Multi step aging of this alloy produces a very complex series of carbide morphology changes. Different complex carbide precipitation occurs at different tempering temperature ranges; much work has been done to find temperature ranges that yield maximum tensile strength or maximum impact toughness. Work has also been done to develop an aging cycle that yields the best combination of strength and toughness [25, 29].

Table 2.6: Typical mechanical properties of wrought intermediate alloy steels [21, 24].

Alloy Specification	MMPDS Basis	UTS (ksi)	YS (ksi)	EL (%)	CVN (ft-lbs)* RT/-40°F
AF1410 (Fe-Ni-Ci Alloy)	S	235	215	12	60/53
Aeromet 100 (Fe-Ni-Co Alloy)	S	290	245	10	42/30

2.3.2.2 Aermet 100

Aermet 100 is another secondary age-hardenable martensitic Ni-Co-Cr steel alloy, which provides a unique combination of tensile strength and toughness (**Table 2.6**). The alloy provides excellent mechanical properties when hardened by vacuum heat treatment with inert gas cooling and has a low ductile-to-brittle transition temperature [30]. Optimal Aermet 100 properties have been reported through a multi-step ageing treatment, which consists of an initial high-temperature short-time austenite precipitation treatment followed by a lower-temperature aging. The multi-step ageing treatment gives rise to what is known as “disperse-phase” transformation toughening that arises from precipitated austenite [1].

For wrought UHSLA steels, it is evident that for standard heat treatments, gains in impact toughness are possible at the expense of yield strength. It was also evident that the high ductile

to brittle transition of UHSLA steels typically yields subpar impact toughness at low temperatures. It will be important to experiment with non standard heat treatment practices to try to improve the low temperature impact toughness of the UHSLA steels without significantly lowering yield strength. The high-alloy maraging steels and the secondary hardening steels have improved properties, but the high amounts of nickel and cobalt make them very expensive to produce.

Only a very limited amount of work has been done to develop next generation ultrahigh strength low alloy cast steels beyond 4340. The casting specifications, heat treatment guidelines, and chemistries for the ultrahigh strength low alloy cast steels have not yet been established.

2.4 High Strength Steel Castings

The development of cast steel material grades historically have been based on pre-existing wrought grades with minor compositional differences to insure adequate castability or more flexibility with respect to tramp and residual alloying element control.

There are numerous specifications for cast low-alloy steels that are designed to meet the specific functional requirements of the intended use of the casting. For example, the specification for end use can be structural strength and resistance to wear, heat, and corrosion. Traditionally, the American Iron and Steel Institute (AISI) and the Society of Automotive Engineers (SAE) have differentiated the various types of wrought steel by principal alloying elements. Cast steel grades do not follow the same compositional ranges specified by AISI and SAE designations for wrought steels.

When steel castings are purchased, they are typically purchased to meet specified end use mechanical property requirements. Some restrictions may be put on chemical composition. **Table 2.7** shows the American Society of Testing and Materials (ASTM 148) cast alloy steel specifications for those cast steels that have properties comparable to the wrought UHSLA steels discussed [31]. ASTM specifications for cast steels, such as ASTM A148 are property-based specifications that do not directly link specified composition limits to supplemental mechanical property limits. Although ASTM A148 includes property specifications for low alloy cast steels with yield strength minimums of 180ksi. and 210 ksi., these grades of material are rarely if ever used in practice. A recent survey of steel foundries indicates that most foundries use cast steel

yield strength values of less than 130 ksi. At the highest specified strength levels, impact toughness requirements are included in ASTM A148 to assure adequate toughness.

Table 2.7: Mechanical property specifications for cast UHSLA steels (ASTM A148) [21, 31].

	UTS (ksi)	YS (ksi)	El (%)	RA (%)	RT CVN (ft-lbs)*	Residual
160-145	160	145	6	12	-	<0.05 % P < 0.06 % S
165-150/L	165	150	5	20	20	< 0.020% P
210-180/L	210	180	4	15	15	< 0.020% S
260-210/L	260	210	3	6	6	

*Impact properties are specified in L specifications only.

Table 2.8 describes nominal compositions for common investment cast UHSLA steels. Supplemental requirements in ASTM A732 for investment castings suggest that UHSLA investment castings should not be specified at yield strengths above 170 ksi. At the present time there are no widely accepted specifications for many of the next generation investment cast UHSLA steels. The current version of the MMPDS Handbook (formerly Mil Handbook) includes specific guidance on the use of the investment cast high alloy steels 17-4PH and 15-5PH, but lacks guidelines for both conventional UHSLA steels and possible next generation UHSLA investment cast steels. The 4XXX low alloy steels and next generation UHSLA steel variants based on 4XXX represent the most popular steels specified at high strength levels. However, the elongation and toughness are limited by the formation of coarse intermetallics associated with tramp and residual elements common in steel melts [32].

Table 2.8: Nominal Compositions for Investment Cast UHSLA Steels (ASTM A732) [24].

Alloy	AMS	% C	%Mn	%Si	% Cr	%Ni	%Mo	Other
Investment Cast Alloys								
IC 4340	5330	0.4	0.85	0.5	0.8	1.8	0.25	Cu < 0.5, W < 0.1
IC 4330	5328	0.3	0.55	0.5	0.8	1.8	0.25	Cu < 0.5, W < 0.1
IC 4140	5338	0.4	0.85	0.5	0.95	-	0.20	Cu < 0.5 Ni < 0.5
IC 4130	5236	0.3	0.55	0.5	0.95	-	0.20	Cu < 0.5

Comparisons of wrought and cast specifications for UHSLA steels suggest that alloy and process development opportunities exist to use and specify low alloy investment cast materials at higher strength levels with increased toughness. Higher yield strengths together with adequate toughness have been achieved in particular in AISI 43XX steels and next generation 43XX derivative alloys using low tempering temperatures. The addition of silicon up to 1-2% is a typical alloy addition in the derivative alloys to retard the formation of cementite and avoid temper embrittlement [32-34]. The silicon has also made these alloys easier to cast due to increased fluidity enabled by the silicon additions. In addition, the silicon modified variants of steels have been found to decrease susceptibility to stress corrosion cracking which has been widely cited as a problem in UHSLA steels [35].

Much work still needs to be done to develop appropriate heat treatment guidelines for UHSLA steel casting alloys at high yield strengths. In addition to developing non standard heat treatment processes for the current generation of ultrahigh strength UHSLA cast steels, focus should also be put on the development of experimental UHSLA steels. At the forefront of the experimental steels in development for structural, aerospace, and ballistic applications is a new tungsten alloyed UHSLA steel, Eglin steel.

2.5 Eglin Steel

Eglin steel, also referred to as ES-1, is a high to ultrahigh strength, low to medium carbon, high ductility, low alloy steel that is currently being developed by the United States Air Force for applications such as, missile components, ordnance components, and airframe components [36, 37]. The alloy may also have a promising future as a commercial alloy that can be used to make pressure vessels, hydraulic and mechanical press components; locomotive, automotive, and truck components, including die block steels for manufacturing of components;

and bridge structural members. A 2009 U.S. Patent for this wrought alloy was granted to inventors Dilmore and Ruhlman. The assignee of the patent was Ellwood National Forge Company. **Table 2.9** shows the mechanical properties achievable for wrought Eglin Steel that has been heat treated using conventional steel heat treatment processes.

Table 2.9: Mechanical properties for wrought Eglin steel test series included in patent 7,537,727 B2 [36].

Mechanical Properties Table for Eglin Steel Test Series

Composition	HR UTS ksi	HR YTS ksi	HR STF %	HRHT UTS ksi	HRHT YTS ksi	HRHT STF %	LR UTS ksi	LR YTS ksi	LR STF %	Hardness Rc	CI RT ft. lbs	CI −40° F. ft. lb.
ES-1	263.7	224.5	16.6	215.7	191.4	15.9	246.7	193.9	18.4	45.6	56.2	42.7
std. dev.	3.1	4.0	0.3	3.6	7.0	0.7	1.4	2.2	0.4	0.1	2.6	0.3
ES-2	261.2	231.9	15.5	216.1	197.4	15.1	244.4	201.9	17.5	46.6	27.3	20.0
std. dev.	2.0	3.3	0.3	7.1	6.0	0.6	1.0	0.2	0.3	0.2	1.9	1.0
ES-3	247.5	218.4	16.6	202.6	187.8	16.0	233.6	186.4	18.0	45.4	44.8	21.3
std. dev.	3.4	3.5	0.5	2.0	2.7	1.0	0.7	1.1	0.2	0.2	2.8	3.9
ES-4	264.3	229.0	16.3	218.4	198.0	16.0	248.3	199.1	17.5	46.5	39.6	24.2
std. dev.	1.6	4.5	0.4	1.2	2.1	0.8	1.4	0.6	0.4	0.2	0.6	3.6
ES-5	291.9	244.8	15.1	233.3	210.6	15.2	270.2	216.0	16.6	48.3	26.2	22.3
std. dev.	0.8	5.5	0.5	2.1	0.5	0.3	1.1	1.6	0.3	0.18	2.2	0.8

HR UTS-High Rate Ultimate Tensile Strength
HR YTS-High Rate Yield Tensile Strength
HR STF-High Rate Strain-To-Failure
HRHT UTS-High Rate High Temperature (900° F.) Ultimate Tensile Strength
HRHT YTS-High Rate High Temperature (900° F.) Yield Tensile Strength
HRHT STF-High Rate High Temperature (900° F.) Strain-To-Failure
LR UTS-Low Rate Ultimate Tensile Strength
LR YTS-Low Rate Ultimate Yield Strength
LR STF-Low Rate Strain-To-Failure
Hardness Rockwell "C"
CI, RT-Charpy "V" Notch Impact @ Room Temperature
CI, −40° F.-Charpy "V" Notch Impact @ −40° F.

The ES-1 wrought alloy has the potential to achieve yield strengths of 190ksi. with Charpy impact toughness above 50ft. lbs at room temperature and above 40 ft. lbs at -40ºF.

In the Eglin steel patent, the following weight percentages (**Table 2.10**) were given for the alloy composition:

Table 2.10: Chemical composition limits and typical compositions of wrought Eglin steel as shown in U.S. patent 7,537,727 B2 [36].

Element	Limit Weight %	Typical
Carbon (C)	0.16-0.35%	.28
Manganese (Mn)	0.85% Maximum	.74
Silicon (Si)	1.25% Maximum	1.00
Chromium (Cr)	1.50-3.25%	2.75
Nickel (Ni)	5.00% Maximum	1.03
Molybdenum (Mo)	0.55% Maximum	.36
Tungsten (W)	0.70-3.25%	1.17
Vanadium (V)	0.05-0.30%	.06
Copper (Cu)	0.50% Maximum	.10
Phosphorous (P)	0.015% Maximum	.012
Sulfur (S)	0.012% Maximum	.003
Calcium (Ca)	0.02% Maximum	.02
Nitrogen (N)	0.14% Maximum	.0073
Aluminum (Al)	0.05% Maximum	.011
Iron (Fe)	Balance	Balance

Interestingly, as shown in **Table 2.10**, the typical chemistry needed to obtain desired strength and impact properties only contains about 1% nickel [36]. What makes Eglin steel unique is that it possesses such a small amount of nickel and no cobalt, but it still possesses both high strength and high ductility using standard heat treatment practices. The alloy is also claimed to possess performance characteristics (i.e. high impact toughness at low temperatures) that are typically only associated with steels that contain high levels of nickel. Since the alloy lacks large amounts of nickel and cobalt, it has the potential to provide a high performance steel composition that avoids the high production costs associated with high alloy steels [36,37].

Similar to the UHSLA steels, certain alloying element additions help provide the desirable properties for Eglin steel. Silicon is included in Eglin steel to enhance toughness and stabilize austenite. Chromium is included in the alloy to enhance strength and hardenability; molybdenum is also added to increase hardenability. Vanadium and nickel are added to increase toughness and tungsten is added to increase strength and wear resistance [36]. Tungsten was not mentioned as an alloying element in the UHSLA steels previously mentioned; Eglin steel contains about 1% tungsten. None of the principle alloying elements in ES-1 wrought steel are expected to cause castability or performance problems in cast variants.

Based on the mechanical property data given in **Table 2.9**, Eglin steel has the potential to be a very special ultrahigh strength low alloy steel in both wrought and cast form with acceptable strength and impact toughness at low cost. Looking at the composition data in **Table 2.10** above, it is the high amount of silicon combined with a lower carbon content, the addition of tungsten, and the low amount of nickel that make the Eglin steel composition different from other ultrahigh strength low alloy steels currently used. To help explain the superior properties of this alloy compared to many of the ultrahigh strength low alloy steels discussed earlier, some focus should be placed on these differences in alloy composition.

Alloying elements greatly influence austenite retention upon quenching [20]. Retained austenite in small percentages has been reported to significantly increase the fracture toughness of 4340 steel without a decrease in strength. However, challenges in measuring small amounts of retained austenite in steel confound studies to clarify the role of retained austenite on the properties of UHS steels. Eglin steel contains multiple austenite stabilizing elements in carbon, nickel, manganese, and nitrogen. Although silicon is characterized as a ferrite stabilizing element, high-silicon bearing, ultrahigh strength low alloy steels have been shown to have improvements in fracture toughness after low temperature tempering as a result of stabilization of retained ductile high-carbon austenite in the alloy [1, 38].

The development of retained austenite during quenching and its subsequent stabilization during low temperature tempering needs to be further studied in the silicon alloyed steels. Within this analysis, the potential for Eglin steel to possess retained austenite after quenching and tempering needs to be explored. Work also needs to be done on the processing of the ES-1 alloy, namely the development of specific heat treatment processes so that the alloy can be consistently manufactured with optimum mechanical properties.

2.6 Processing of Cast Steels

The mechanical properties of cast steels are a direct result of their chemical composition and the processing steps carried out after casting solidification. The steel melting practice, solidification conditions, and the heat treatment processes are all extremely important in controlling the quality of the alloy melt, the microstructure development within the alloy, and ultimately the mechanical properties of the final casting.

2.6.1 Steel Melting Practices

Most of the previous work that has been done on high strength and ultrahigh strength low alloy cast steels was completed some time ago. Since the 1960s and 1970s, cleaner steel melting practices have been designed and others have been honed to produce higher quality, clean steel melts with reduced oxygen, sulfur, and phosphorus contents [1]. By utilizing premium melt processes, steel producers can help to increase toughness and yield strength in the end product by reducing the number of detrimental inclusions and oxides in the steel from the very first step in the melting process [1, 39]. Conventional induction air melting of steel is still a very common melting practice today. Four of the premium melting processes that are used to produce the highest quality ferrous melts containing minimal amounts of oxygen, sulfur, and phosphorus are Argon-Oxygen Decarburization (AOD), Vacuum Induction Melting (VIM), Electroslag Remelting (ESR), and Vacuum Arc Remelting (VAR). It is common for an electric arc melt to be transferred to an AOD vessel for refining.

Within the AOD vessel, oxygen, argon and nitrogen are blown into the molten metal bath to achieve decarburization. After the desired carbon content is reached, alloying elements, lime and ferro-silicon or aluminum are added to reduce chromium and other metallic elements that were oxidized during the decarburization process. Achieving very low levels of sulfur (S) is one of the primary benefits of the AOD process. In addition, various residual elements can be removed due to their high vapor pressures. By injecting inert gas into the bath, unwanted gas impurities can be removed. When compared to straight, air melted, electric furnace steel products, AOD processed steels offer improved cleanliness as a result of possessing lower amounts of non-metallic inclusions [40].

The vacuum induction process uses a completely enclosed and airtight vessel under vacuum. The VIM furnace consists of a refractory vessel or crucible that is surrounded by a water-cooled copper induction coil. VIM furnaces are often used as the initial starting point for premium alloy melting; the alloy melt is then typically moved to one or more additional melting or melt refining processes. A large amount of ferrous alloys used in the defense, aerospace, and power generation applications begin their melting journey in a VIM furnace.

The Electroslag Remelting (ESR) process is a secondary refining process that is used to further refine many alloys; ESR combines fully controlled melting conditions with fully controlled solidification conditions. The ESR process uses consumable electrodes produced by

VIM or conventional air melting to transfer power into the melt. The electrode passes electrical current into the slag of the melt and it heats the slag until it is molten. The molten slag is then responsible for melting the alloy electrode. Since the slag is less dense than the molten metal, the slag remains on the top of the melt. As droplets form on the bottom of the consumable alloy electrode, they form a metal pool below the slag. This metal pool is then solidified quite rapidly in a water cooled mold that extracts the heat that was created during the melting process. An ESR ingot is formed that has minimal chemical segregation that is fully dense and has an improved inclusion distribution. Along with protecting the molten metal from contamination, the ESR slag also helps remove non-metallic oxides and free oxygen and sulfur.

In the VAR process, a DC current is passed through an electrode that melts similar to the ESR process, but now the electrode is inside of a vacuum melting chamber that is a water-cooled copper crucible. The ingot is subsequently resolidified in a water-cooled copper mold. Solidification of the ingot is very highly controlled in the VAR process. The tight solidification control during this VAR process helps to eliminate macrosegregation in the ingot and to reduce microsegregation. The concentration of non-metallic inclusions is significantly reduced in VAR; VAR helps to remove gases and tramp elements. Melting in the water-cooled copper crucible eliminates unwanted reactions between the metal and crucible refractory material. The VAR melting process can help to provide a very clean steel that has a homogeneous microstructure [39]. The problem with the premium melting processes is cost; each step added to the melting process increases the cost of the end product.

It is important to keep in mind the different melting practices used for different heats of material throughout the study of the mechanical properties of ultrahigh strength steels, because reducing the amount of non-metallic inclusions in the steel melt can significantly influencing the toughness of these steels [1, 39, 41]. The presence of undissolved carbides and sulfide inclusions can lower the fracture toughness of quenched and tempered steels such as 4340, 4130, and 300M by 25-50% [41]. After the casting is poured, microstructural refinement and improvements in mechanical properties are the responsibility of the heat treatment procedure.

2.6.2 Solidification and Segregation

Steel castings will solidify with a complex dendritic solidification structure (**Figure 2.12A**). The dendrites contain both primary and secondary dendrite arms, which grow

simultaneously. Thinner casting sections typically cool faster and thus possess smaller secondary dendrite arm spacing (DAS). In large cast ingots or large casting section sizes, the resulting DAS is larger. The distribution of the alloying elements between the dendrites and the interdendritic material in the solidified alloy depend on cooling rate and the partition ratios of the alloying elements. The difference in alloying element concentrations within the core of the dendrite arms and the intercellular regions is described as microsegregation [42]. Microsegregation shown in **Figure 2.12B** can have a negative impact on the mechanical properties of castings. Long time, high temperature heat treatments (namely homogenization) has the potential to lower the concentration gradients resulting from microsegregation through solid state diffusion [43].

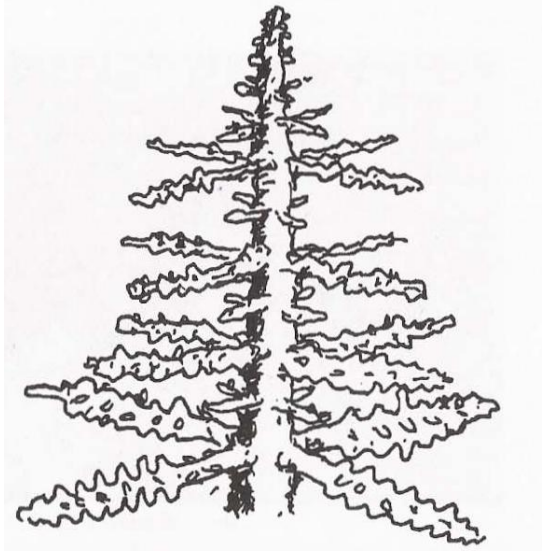

Figure 2.12A

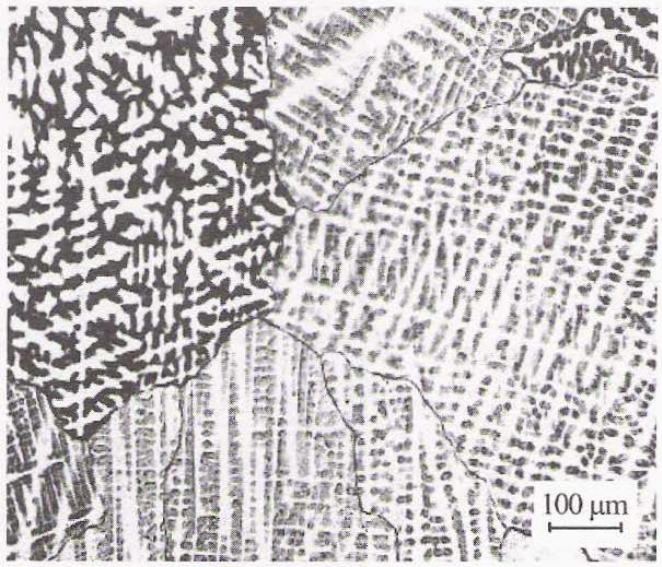

Figure 2.12B

Figure 2.12: (A) A 3-dimensional dendrite schematic; (B) The microscopic inhomogenities (microsegregation) between dendritic (white) and interdendritic areas (dark) within the solid grains of a cast alloy [43].

The heat treatment of wrought ultrahigh strength steels has received a fair amount of attention; however, the heat treatment of the next generation of ultrahigh strength cast steels has not received much attention to date. The next section will discuss the different steps in steel heat treatment and discuss some of the areas that need to be explored in the development of the next generation of ultrahigh strength low alloy cast steels with improved impact toughness.

2.6.3 Steel Heat Treatment

Heat treatment also called the thermal treatment of steels is carried out on steels to cause desired changes in the metallurgical structure and thus in the properties of the steel. The first

step in a typical ultrahigh strength low alloy cast steel heat treatment process is homogenization. In this initial step, the steel is heated to a high-temperature austenitic state and slowly cooled (typically air cooled). The structures that are typically produced after carrying out this homogenizing step are very stable. The structure produced has a low level of residual stresses locked within the part. The second step in a typical cast steel heat treatment process is austenization. In this second step, the steel is heated to a lower-temperature austenitic state and quenched in oil or water. This step is also called the hardening step, where a metastable structure containing high levels of residual stresses known as martensite is formed upon quenching. This step gives the steel extreme strength and hardness but little ductility or toughness [44]. The final step is tempering, where martensitic steels are heated to elevated temperatures so that they become more ductile; this allows the steel to possess both high strength and ductility [44, 45]. Most of the information available on the heat treatment of UHSLA steels is for wrought steels, but the heat treatment processes for the UHSLA cast steels can in general be expected to be similar to those used for the conventional wrought steels. Developing the proper specifications and proper control of each step in the heat treatment process of UHSLA cast steels will be imperative to develop optimal mechanical properties.

2.6.4 Homogenization

In this initial heat treatment step for cast steels, the steel is heated to a high austenization temperature for a prolonged amount of time to obtain a more uniform distribution of the substitutional alloying elements throughout the steel casting. Microsegregation during initial solidification can be homogenized by a homogenization heat treatment step to more evenly distribute the alloying elements throughout the casting [46].

2.6.4.1 The Effect of Homogenization Temperatures on Toughness

In studies on ultrahigh strength low alloy cast steels, a homogenization step in the heat treatment process has been shown to increase the impact toughness of the final, fully heat treated casting product [47, 48]. The literature is mixed on whether or not higher homogenization temperatures, above 1700ºF, improve the impact toughness (CVN) or fracture toughness (K_{IC}) of ultrahigh strength low alloy cast steels. In response to steel foundries reporting better mechanical properties at higher homogenization temperatures in early studies, the study by Eddy

and Marcotte (1947) was carried out by SFSA. They concluded that heat treatments employing high temperature homogenization treatments (above 1650ºF to 2100ºF) are not effective in materially improving the impact and hardenability properties of high strength low alloy cast steels with thin walled sections [49]. A study by Leger (1985) showed that HSLA cast steels, namely 12MDV6-M, when homogenized between 1920ºF and 1980ºF (1050ºC to 1080ºC) develop optimal properties [48]. In his 1977 study of 4340, 15-5PH stainless, and two maraging steels, Floreen (1977) noted that the impact toughness of these cast steels was lower than their wrought counterparts as a result of quai-cleavage fractures when impact tested. He attributed this to the microsegregation that occurs in castings during solidification. Floreen (1977) alluded to the fact that high-temperature "solution anneal" or higher homogenization temperatures could cure microsegregation, decreasing the occurrences of localized brittle regions in the material, and thus improving the charpy impact values of the alloys [50].

Since reduction in microsegregation is the focal point of homogenization and the diffusion of alloying elements is the driving force behind microsegregation reduction, diffusion during homogenization and the important variables associated with diffusion in steel castings need to be discussed.

2.6.4.2 Diffusion During Homogenization

The solute rich interdendritic regions of alloy steels are typically rich in the substitutional alloying elements such as Mo, Cr, W, Ni, and Mn. The diffusion of substitutional atoms is via vacancy diffusion. An atom leaves its current lattice site to fill a nearby vacancy in the lattice [9]. Since substitutional atoms are much larger than the interstitial atoms, such as carbon, vacancy diffusion occurs at a much slower pace than carbon diffusion. This means that a larger amount of thermal energy is required to move substitutional atoms from one lattice site to another when compared to the movement of smaller interstitial atoms. During high temperature homogenization, limited movement or diffusion of substitutional atoms can be expected. The movement of these subtitutional atoms is necessary to reduce the microsegregation of alloying elements occurring between the dendrite cores and the interdendritic regions resulting from initial solidification. To determine how much microsegregation can be mitigated during homogenization, classical diffusion modeling for dendritic steel castings would need to be carried out.

2.6.4.3 Diffusion Models

Much of the casting segregation modeling research that is ongoing today is an extension of the pioneering work by Flemings and co-workers in the 1960s [51]. The literature cites many models for estimating diffusion during homogenization, all of which are based upon Fick's Laws. Fick's Second Law describes dynamic or non-steady state diffusion and is the basis for many diffusion models. In three dimensions, Fick's second law can be stated as:

$$\frac{\partial c}{\partial t} = D\left(\frac{\partial^2 c}{\partial^2 x^2} + \frac{\partial^2 c}{\partial^2 y^2} + \frac{\partial^2 c}{\partial^2 z^2}\right) \qquad \textbf{Equation 2.2}$$

where

c = the concentration,

t = the time,

D = the diffusion coefficient

Solutions of this expression depend on the specific boundary conditions. Askeland [52] suggests one solution to Fick's Second Law which permits the calculation of the concentration profile for one diffusing species into another. The equation allows simple calculation of the concentration profile for one element diffusing into another in a direction normal to the diffusion plane. This solution is dependent upon the diffusion coefficient (D) remaining constant regardless of concentration and can be expressed as [52]:

$$\frac{c_x - c_m}{c_1 - c_m} = \mathrm{erf}\left(\frac{x}{2\sqrt{Dt}}\right) \qquad \textbf{Equation 2.3}$$

where:

c_1 = the concentration of atom A in material 1,

c_m = the average concentration of element A in materials 1 and 2,

c_x = the concentration of element A in material 2 at a distance x from the original interface after time t,

D = the diffusion coefficient of element A in material 2 at a specific temperature.

A simplified and useful solution to Fick's Diffusion Equation is given by [52]:

$$x \approx \sqrt{Dt} \qquad \textbf{Equation 2.4}$$

where:

x = the diffusion distance,

t = the time,

D = the diffusion coefficient of the element of interest in austenite.

The effect of temperature on the diffusion coefficient can be expressed by the Arrhenius equation [10]:

$$D = D_0 * \exp\left(\frac{-Q}{RT}\right) \qquad \textbf{Equation 2.5}$$

where:

Q = the activation energy (usually kJ/mole),

R = the universal gas constant,

T = the absolute temperature (K),

D_0 = the diffusivity coefficient.

A literature review of the diffusivity coefficients (D_0) and activation energies (Q) of the common UHSLA cast steel substitutional alloying elements in austenitic iron (γ) and austenitic iron based alloys are shown in **Tables 2.11 - 2.15**. The literature review shows evidence of what appear to be large differences in both the activation energies and the diffusivity coefficients for the alloying elements. The differences could be attributed to the different techniques and data collection methods used to estimate the parameters.

Table 2.11: Diffusion data for molybdenum in austenitic (γ) iron and iron based alloys.

D_0 (cm^2/sec)	**Q (kJ/mole)**	**Material**	**Reference**
0.043	255.224	Fe	[53]
25.1	323.7	Fe	[54]
0.0684	246.85	Fe	[55]
0.0358	239.8	Fe	[56]
20.4	313.8	Fe-Cr-Mn-Ti-Mo	[53]

Table 2.12: Diffusion data for tungsten in austenitic (γ) iron and austenitic iron based alloys.

D_0 (cm^2/sec)	Q (kJ/mole)	Material	Reference
0.13	267.4	Fe	[57]
0.509	272	Fe	[58]
4400	376.56	Fe	[59]
460	338.9	Fe	[60]
--	261.5	Fe	[61]
0.6	267.357	R9K10 Tool Steel	[62]
13	313.8	U8 Tool Steel	[59]
49	310	R9 Tool Steel	[63]

Table 2.13: Diffusion data for manganese in austenitic (γ) iron and austenitic iron based alloys.

D_0 (cm^2/sec)	Q (kJ/mole)	Material	Reference
0.038	246.85	Fe	[53]
0.16	261.7	Fe	[62],[63]
0.019	240.8	Fe	[62]
0.486	277.8	Fe	[64]
0.23	271.96	Fe+Cr	[53]

Table 2.14: Diffusion data for chromium in austenitic (γ) iron and in austenitic iron based alloys.

D_0 (cm^2/sec)	Q (kJ/mole)	Material	Reference
0.0624	252.3	Fe	[54]
10.8	291.8	Fe	[65],[66]
0.063	243	Stainless Steel	[67]

Table 2.15: Diffusion data for nickel in austenitic (γ) iron and in austenitic iron based alloys.

D_0 (cm^2/sec)	Q (kJ/mole)	Material	Reference
6.92	324.9	Fe	[68]
4.1	267.76	Fe	[69]
3.0	314	Fe	[70],[71]
0.344	282.42	Fe	[72]
0.77	280.5	Fe	[73]

For diffusion models to be developed or adapted for the estimation of the temperature and amount of time required for adequate diffusion of these alloying elements during heat treatment, work would need to be done to select appropriate diffusion parameters (D_0 and Q) along with developing or adapting a model to properly address cast UHSLA microsegregation reduction during homogenization.

Overall, there has not been a large amount of work done on the influence of homogenization temperatures on the microsegregation reduction or impact toughness of cast UHSLA steels. The homogenization for wrought products is not a separate heat treatment step, rather homogenization occurs during the hot rolling or forging of the wrought products prior to heat treatment. The role that austenization plays in the heat treatment of steels and the work that has been carried out on increased austenization temperatures on UHSLA steels will be discussed next.

2.6.5 Austenization

In this second step of heat treatment, the homogenized and air cooled castings are now re-heated to transform the microstructure to austenite [74]. The condition of the austenite (alloy dissolution, grain size, homogeneity of austenite) holds the key to the hardenability of the steel. The other factors that are key to the hardenability of the steel are the carbon content, type and amount of alloying elements, the austenization temperature, and the holding time at a given austenization temperature. When an alloy steel is heated to the austenization temperature, the alloy steel is undergoing a polymorphous phase transformation from α (ferrite) bcc to γ (austenite) fcc. Upon heating to this temperature the dissolution of cementite, carbides, nitrides, and intermetallics within the austenite occurs. Austenite grains are also recrystallized during this heat treatment step. It is very important to limit the growth of the austenite grains during this heat treatment step, because austenite grains that are too large, caused by excessively high austenitizing temperatures can limit hardenability and lead to brittleness upon quenching from the austenization temperature [75]. Large austenite grains correlate to a large ferrite grain size in the final microstructure. The final ferrite grain size is a very important factor in increasing the yield strength and toughness of steels (**Figure 2.13**), therefore controlling the size of the austenite and ferrite grain sizes during casting and heat treatment is important [47].

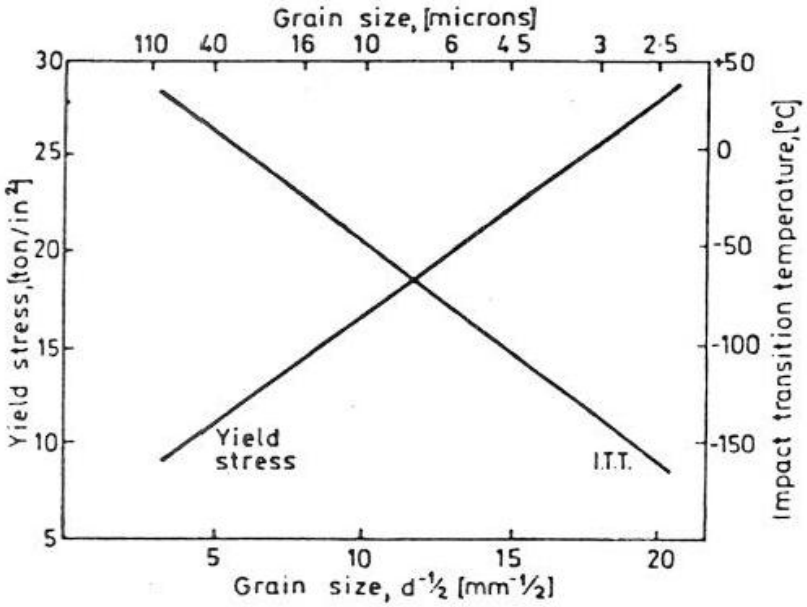

Figure 2.13: Effect of ferrite grain size on yield stress and impact transition temperature (0.1%C, steel) [47].

It is also very important to ensure that the austenization conditions ensure that all of the carbon is put into solution [75]. For the ultrahigh strength low alloy cast steels being studied, it may be critical to increase the austenization temperature to a temperature that allows full solutionizing of all complex carbides and carbonitrides present in the microstructure. Higher austenization temperatures are typically necessary to dissolve special carbides that could impede any growth of austenite grains. Austenite grain growth is impeded by almost all carbide and nitride forming elements. V, Ti, Al, Zr, W, Mo, and Cr slow the growth of austenite grains during austenization, because it generally takes a significant amount of time and energy to solutionize carbides, nitrides, and other intermetallic phases. Experimental studies have shown that Ti, Zr, and V impede austenite grain growth much more strongly than Cr, W, and Mo, because the carbides and nitrides formed by Ti, Zr, and V are more stable and possess lower solubilities in austenite [75].

The enthalpy comparison in **Figure 2.10** above shows that Ti, Zr, and V carbides and nitrides are much more stable than Fe_3C, Cr, W, and Mo carbides and nitrides. In fact, Titanium carbides can be stable in the steel melt. If titanium carbides can form at such high temperatures, they can form and provide grain nucleation sites and they can also continue to grow upon solidification. The problem is that TiC and TiN compounds can cause impact toughness problems in the final steel product if they cannot be dissolved through homogenization and

austenization. **Figure 2.14** below shows that above 1800ºF, V compounds begin to dissolve, while Al compounds may only dissolve above 2000ºF. Nb compounds need processing temperatures above 2100ºF for dissolution. **Figure 2.14** shows that titanium compounds are extremely difficult to dissolve in steels. Above 2200ºF, titanium compounds still do not readily dissolve. This can have serious implications on UHSLA steels containing Ti that are being experimented with for increased impact toughness. The development of increased impact toughness in UHSLA steels can be significantly slowed by undissolved compounds in the microstructure, namely at grain boundaries. Undissolved particles at the grain boundaries serve as crack nuclei, decreasing the impact toughness of UHSLA steels [33,38].

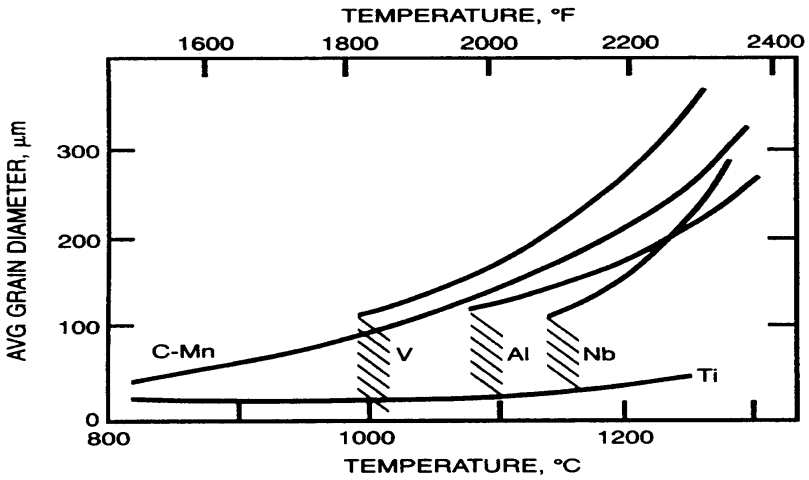

Figure 2.14: Effect of austenization temperature and dissolution of V, Al, Nb, and Ti compounds on average grain diameter (µm) [76].

Being able to dissolve these compounds during austenization is not just dependent on temperature. The carbon content of the steel also plays an important role in carbide solubility in austenite (**Figure 2.15**).

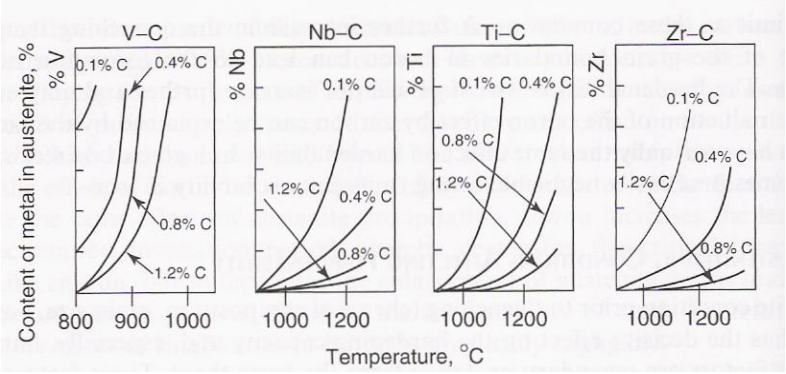

Figure 2.15: The solubility of carbides in austenite at various temperatures vs. steel carbon content for steel alloying elements (a) vanadium; (b) niobium; (c) titanium; (d) zirconium [75].

When C, N, and Al are in the solid solution of austenite and not tied up in carbides or nitrides, they actually help push forward the growth of austenite grains. Hardenability is typically improved in ultrahigh strength steels when carbides are put into solution within the austenite even if there is some cementite grain growth [75]. The alloying elements present and the amounts of each ultimately play the major role in stabilizing austenite and influencing hardenability.

The optimal austenization temperature for ultrahigh strength low alloy steels that will produce optimal mechanical properties is a delicate balancing act. Much experimentation has been carried out on ultrahigh strength low alloy steels to document the effects of austenization temperatures on mechanical properties. The debate on whether or not higher homogenization and austenization temperatures increase the impact toughness or fracture toughness is now discussed.

2.6.5.1 The Effect of Austenization Temperatures on Toughness

Austenization temperatures have been the subject of much study for ultrahigh strength low alloy steels. Again, most of the work carried out was completed on wrought UHSLA and HSLA steels. For the 4340 alloy, the study by Ritchie et al. (1976) concluded that at higher austenization temperatures (1200ºC (2192ºF)) (followed by a step quench to 870ºC (1600ºF)) led to improved fracture toughness, but led to an appreciable decrease in charpy impact energies when compared to conventional austenization at 870ºC (1600ºF) [77]. The Wood (1975) study on UHSLA steels 4130, 4140, 4330, 4340, and 300M showed that the fracture toughness of all these alloys was substantially increased by austenization at 1200ºC (2192ºF) instead of

870ºC(1600ºF). Wood (1975) made it clear that the yield strength level of the alloys tested was substantially independent of the austenization temperature and cooling rate of the material. The results also showed that by employing a faster quenching rate from the 1200ºC (2192ºF) austenization temperature, further increases in the fracture toughness could be achieved for alloys with limited hardenability. Wood (1975) suggested that higher austenization temperatures led to the presence of retained austenite and increased grain size which translated to the significant gains in fracture toughness. In addition, Wood (1975) suggested that faster cooling rates led to the elimination of large amounts of non-martensitic decomposition products, which provided preferential sites for crack initiation [27]. The Youngblood and Raghavan (1977) study on 300M steel showed that when this ultrahigh strength low alloy steel is austenitized at 870ºC (1600ºF), undissolved precipitates could be observed both in the submicrostructure and on fracture surfaces promoting quasi-cleavage failure. When austenitization was increased to between 1700ºF (927ºC) and 1800ºF (982ºC), these precipitates dissolved. A significant increase in fracture toughness occurred when this alloy was austenitized at these higher austenization temperatures. The increase in fracture toughness was attributed to the dissolution of these second phase particles [33]. Lai et al. (1974) made similar claims. They noted that the dispersal of impurities changed the mode of fracture from cleavage to dimple rupture, leading to increased toughness [38].

Higher austenization temperatures can help dissolve carbides and nitrides faster. The higher temperatures also result in a greater supersaturation of the alloying elements in the martensite. The supersaturation of alloying elements in the martensite paves the way for future secondary hardening reactions during subsequent tempering from alloying elements such as Cr, V, W, and Mo that precipitate as very fine alloy carbides [11]. In the Youngblood and Raghavan (1977) study, when the austenization temperature was increased from 1800ºF (982ºC) to 2000ºF (1093ºC) to 2200ºF (1204ºC), the fracture toughness steadily increased with austenization temperature. It was concluded that excessive grain growth occurred at the higher austenization temperatures (2000ºF (1093ºC) to 2200ºF (1204ºC)). The best combination of strength and fracture toughness was found with an 1800ºF (982ºC) austenization step followed by tempering between 400ºF (204ºC) and 600ºF (316ºC). This study also showed that retained austenite was present at the lath and plate martensite boundaries in all samples that were tempered between 400ºF (204ºC) and 600ºF (316ºC). Youngblood and Raghavan (1977) suggest that at higher

tempering temperatures (800ºF (427ºC) and above), the retained austenite decomposed to ferrite and cementite [33]. In a low alloy cast steel study by Shedenov and Lat'eva (1966), when the low alloy cast steels were water quenched at austenization temperatures between 860ºC and 1100ºC, the best impact toughness was found to occur after austenitizing at higher temperatures [78].

The effect of higher austenization temperatures on the impact toughness is much less clear since most of the work has been done on fracture toughness. The consensus seems to be that higher austenization temperatures do in fact improve fracture toughness of UHSLA steels as a result of putting more of the alloying elements into solution in austenite, growing austenite grains, and by presenting the conditions necessary for interlath retained austenite.

2.6.5.2 Retained Austenite in Steels

The role of retained austenite is well documented across the literature especially for high carbon tool steels. When steel with a martensite finish temperature below room temperature is quenched, some austenite will be retained in the microstructure. **Figure 2.16** below shows the amount of martensite that is formed when the temperature of steel is continuously decreased in the martensite formation range (M_s-M_f). The martensite start temperature (M_s) is the temperature at which the transformation from austenite to martensite begins during quenching. The percentage of martensite increases with a decrease in temperature with the end of the martensite transformation at the martensite finish temperature (M_f). If the cooling of the steel is continued immediately to a temperature below the martensite finish temperature (M_f), most, if not all of the austenite that was present at room temperature should now be transformed to martensite. Especially for alloyed steels, at temperatures close to the M_f temperature, an amount of austenite is still retained in the steel because the transformation kinetics become sluggish.

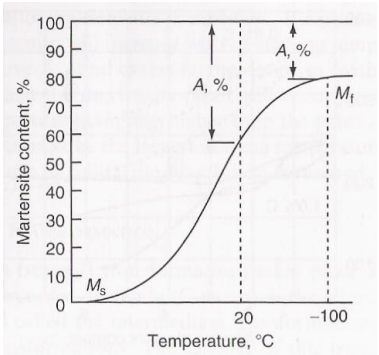

Figure 2.16: % Martensite formation vs. cooling temperature [75].

If a delay exists between quenching to room temperature and the subsequent cooling, austenite can be stabilized, preventing its transformation during further cooling to temperatures below the M_f temperature [75, 79, 80]. Austenite stabilization is associated with stress relaxation and also is thought to be stabilized by interstitial carbon atoms pinning the austenite-martensite interface. The longer the hold time between the M_s and M_f temperatures, the greater the stress relaxation and pinning and the lower the temperature required to accumulate stresses required for martensite transformation to continue [75]. A cold treatment or "cryo" treatment around -120°C is often used in industrial practice after water quenching to fully de stabilize austenite and restart the martensite transformation from prior water quenching [79].

The initial amount of retained austenite (after quenching) is dependent also on the austenization temperature; as austenization temperature is increased and the austenite composition is enriched with carbon and other alloying elements as carbides dissolve, less martensite will be formed upon cooling to room temperature [11, 75]. The austenization temperature must be high enough to ensure the transformation to austenite. Low austenitization temperatures will allow significant amounts of carbon and carbide stabilizing elements to remain tied up in spheroidized carbides, allowing for a higher percentage of martensite transformation and lower amounts of retained austenite in high carbon tool steels **(Figure 2.17)** [11].

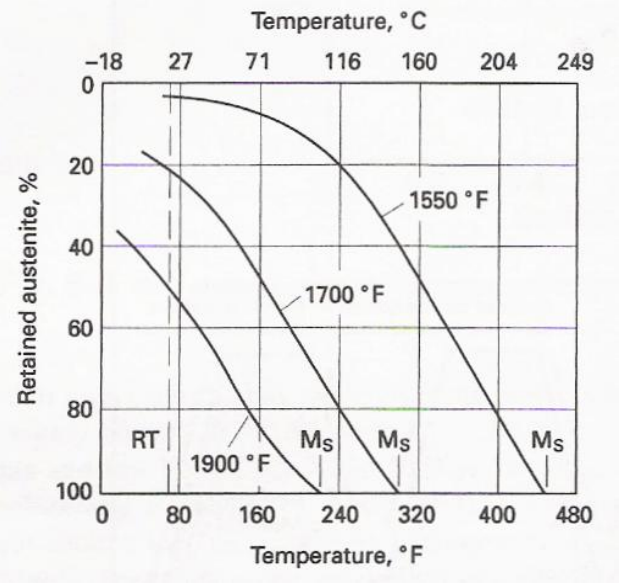

Figure 2.17: The influence of increasing austenization temperature on the martensite transformation kinetics of a wrought tool steel (1.1% C; 2.8% Cr) [81].

As visual evidence of this phenomena demonstrated in **Figure 2.17**, the micrographs shown below in **Figure 2.18** show that the amount of retained austenite increased in wrought 4340 steel when the austenization temperature was increased from 870ºC to 1200ºC.

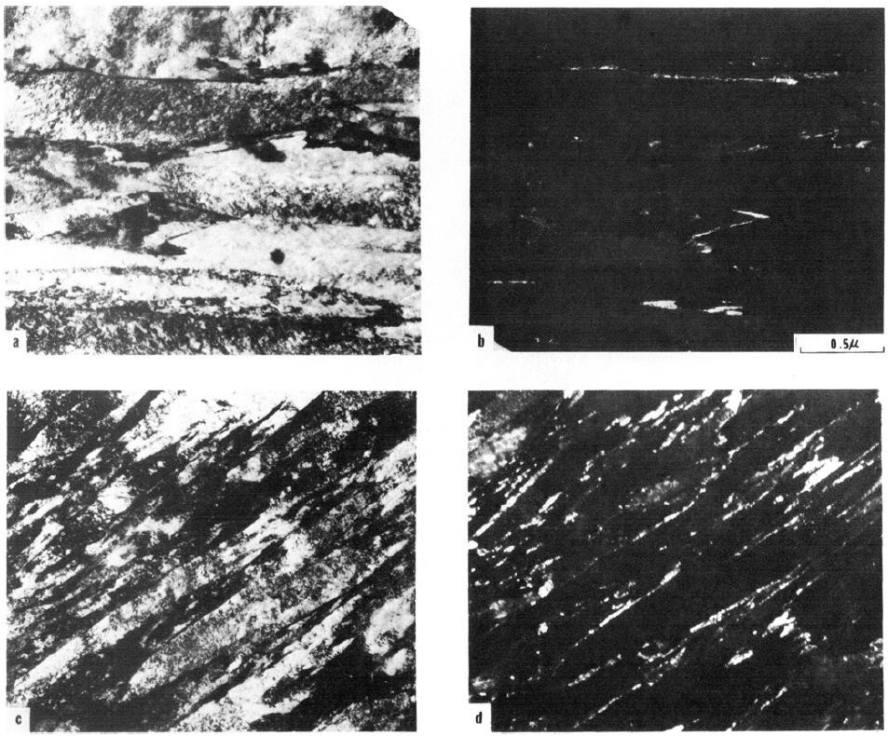

Figure 2.18: Transmission electron micrographs of as-quenched wrought 4340 steel: bright field (a) and dark field of austenite reflection (b) of 870ºC/oil quenched specimen; bright field (c) and dark field of austenite reflection (d) of 1200ºC to 870ºC/oil quenched specimen [38].

2.6.5.2.1 The Effect of Retained Austenite on the Mechanical Properties of Steel

Retained austenite is often thought of as being detrimental to the mechanical properties of steel alloys. Because retained austenite is softer than martensite, retained austenite present after quenching will decrease the hardness of the steel [75]. In tungsten containing tool steels (alloy S1) that also contain large amounts of silicon, Roberts et al. (1998) suggests that the retained austenite caused by the alloy's silicon content accounted for a decrease in impact toughness [5]. However, in some alloy steels, when trying to improve fracture toughness, ductility, and formability, retained austenite is desired [38, 82-86]. The use of higher austenization temperatures in 4340 steel resulted in an increase in the amount of retained austenite and the elimination of twinned martensite. This translated into increased fracture toughness without a decrease in strength. The microstructure of the 4340 steel revealed the presence of retained austenite as thin interlath films in martensite [38]. The presence of this austenite is suggested to

improve fracture toughness by stopping cracks propagating through martensite. Much of the documentation on the stoppage of crack propagation as a result of the presence of interlath retained austenite was first documented by Webster in his work with Cr-Mo-Co stainless steels [87]. When growing cracks intersect a region of retained austenite, additional loading was necessary to cause cracks to branch out and around the austenite regions. When retained austenite arrests crack propagation in steels, the resultant crack branching absorbs more energy than simple straight line crack propagation through martensite, leading to improved impact toughness [1, 38, 87]. In studies on 8620 and 4620 steels (0.20% C), about 20-30% retained austenite led to marked improvements in tensile bending strain values. Improvements in bend ductility were reported for steel samples possessing retained austenite when compared to steels without retained austenite. More plastic strain could be accommodated before crack initiation because the austenite deforms and subsequently transforms to martensite [56]. This idea of austenite deforming and transforming to martensite is well documented in studies by Birat et al. (1971) and Antolovich et al. (1971). In the Gerberlich et al. (1971) study on high-strength metastable austenitic steel and the Antolovich et al. (1971) study on TRIP (transformation induced plasticity) steel, both concluded that when the austenite to martensite phase transformation in these alloys takes place under appropriate conditions it is the major source of fracture toughness. They experimentally showed that the transformation from austenite to martensite alone accounts for about 60 to 85 percent of the fracture toughness in terms of a measured crack extension force [88, 89]. Additional studies on dual phase, transformation induced plasticity steels (TRIP) and TRIP – aided multi-phase sheet steels (TMP) have shown that retained austenite stabilized by silicon and manganese improved the energy absorption characteristics and ductility of these steels [82, 84, 85]. It has also been reported that retained austenite made stable by Si additions to high strength low alloy sheet steels is responsible making press forming easier for high strength steel sheets by improving strength and ductility [83].

As discussed earlier, the retained austenite can be induced by higher austenization temperatures, but the alloying elements present and the amounts ultimately play the major role in stabilizing austenite.

2.6.5.2.2 Alloying Elements and their Impact on Retained Austenite

Each alloying element, depending on its atomic size and electronic structure, may stabilize either the ferrite crystal structure or the austenite crystal structure. **Table 2.16** lists the various ferrite-and-austenite-stabilizing elements found in tool steels.

Table 2.16: Effect of Alloying Elements in Tool Steels [81].

Ferrite-Stabilizing Elements	Austenite-Stabilizing Elements
Chromium	Carbon
Molybdenum	Cobalt
Niobium	Copper
Silicon	Manganese
Tantalum	Nickel
Tungsten	Nitrogen
Vanadium	
Zirconium	

Rao and Thomas [90] studied the influence of the manganese and nickel additions to Fe-C-Cr base steels. One of their main findings was that both fracture toughness and impact toughness increased with Mn and Ni additions. They attributed this to the increased amount and stability of retained austenite. Mn and Ni are fcc austenite stabilizers that promote the retention of austenite. Rao and Thomas [90] found that by adding 2 wt% Mn to Fe-0.3C-4Cr steel, the amount of retained austenite increased from 4 to 5%. They also found that the 5-wt% nickel-modified alloy had between 6 and 8% retained austenite.

Even though silicon is listed as a ferrite-stabilizing element, multiple studies have found that rather than forming brittle interlath cementite, high-silicon-bearing experimental and ultrahigh strength steels such as 4330, 4340, and 300M have retained ductile high-carbon austenite during tempering that resulted in increased ductility and fracture toughness without decreases in tensile strength. These studies were not carried out by conventional austenization and quenching to room temperature in water or oil. The steels were isothermally transformed (i.e. austempered) in the bainitic temperature region [91-94]. Tomita and Okawa (1995) found that the increases in ductility and fracture toughness were attributed to the film form of mechanically stable austenite that separated the individual ferrite plates in the bainitic microstructure. For the austempering treatments, Tomita and Okawa (1995) did not see an increase in charpy impact toughness even though a significant increase in fracture toughness was observed [1, 91-94].

Research continues to understand the actual role that retained austenite plays in ultrahigh strength low-alloy steels. The consensus seems to be that retained austenite has the potential to increase the fracture toughness of ultrahigh strength low-alloy steels. The literature still seems mixed on whether or not retained austenite increases the Charpy impact toughness. Although Eglin steel possesses comparable strength with superior impact toughness when compared to other ultrahigh strength low-alloy steels it is not clear if this is due to retained austenite present in the microstructure after tempering.

Much study still needs to be done to document the effect of higher homogenization and austenization temperatures on UHSLA cast steels. Outside of homogenization and austenization, the Youngblood and Raghavan (1977) study has shed light on the importance of tempering temperature on the mechanical properties of UHSLA steels.

2.6.6 Tempering

After quenching from the austenization temperature, the martensite that is formed contains a high density of dislocations and is very hard and brittle. The final stage of heat treatment of steels is typically tempering. Tempering is a sequence of processes that include the segregation of carbon to lattice defects, the precipitation of carbides, the decomposition of retained austenite, and the recovery and recrystallization of martensite. After tempering, a dispersion of carbides in a ferritic matrix is typically left behind that resembles very little of the martensite that was present prior to tempering. Each of the tempering processes can be affected by alloying elements. As a result the tempering behavior of ultrahigh strength steels is very, very complex [20, 45, 95]. The reactions that occur during tempering are typically broken down into four stages that tend to overlap.

Prior to what is deemed "the first stage of tempering," carbon segregation to lattice defects and pre-precipitation clustering occurs. This can begin to occur during quenching. The first stage of tempering occurs between 100ºC and 250ºC (212ºF and 482ºF). In this stage, iron carbides (Є-carbide, $Fe_{2.3}C$) form and precipitate. The martensite may lose some of its tetragonality, but it remains supersaturated with carbon and will undergo further decomposition upon heating to higher temperatures. The second stage of tempering occurs somewhere between 200ºC and 350ºC (392ºF and 662F) and involves the decomposition of austenite into bainitic ferrite and cementite. The kinetics of this reaction are controlled by carbon diffusion in

austenite. The third stage of tempering occurs between 200ºC and 750ºC (392ºF and 1382ºF). In this stage cementite (Fe_3C) precipitates within the martensite. The cementite nucleation initiates at the prior Є-carbide and can grow as the Є-carbide particles dissolve. Cementite can also nucleate at prior austenite grain boundaries or interlath boundaries. At this stage, most of the carbon in the martensite is removed from solid solution. This leads to the loss of tetragonality of the bct structure. During the initial stages of cementite growth, only carbon diffusion occurs. As the tempering is prolonged, other alloying elements are redistributed between the ferrite and cementite. In addition, the cementite particles may coarsen and spherodize with prolonged tempering. At this fourth stage of tempering between 230ºC and 370ºC (450ºF and 700ºF), Fe_3C particles can now readily nucleate at grain boundaries. The Fe_3C particles nucleate primarily at interlath boundaries and prior austenite grain boundaries as a result of the more rapid diffusion in these areas [20, 45, 95]. This is the point (around 500ºF) at which tempered martensite embrittlement (TME) can occur during tempering. TME can be detrimental to toughness and strength of the steel alloy [96]. During the final stage of tempering above 370ºC (700ºF), the high temperatures lead to the precipitation of preferred alloy carbides such as M_7C_3 and $M_{23}C_6$. In ultrahigh strength low alloy steels, alloying elements such as Cr, Mo, V, and Ti form carbides, giving rise to secondary hardening [20, 45, 95]. The secondary hardening effect in UHSLA steels is very important to developing desired hardness, strength, and toughness. Upon tempering, alloying elements such as chromium, vanadium, tungsten, and molybdenum are able to diffuse and precipitate as fine alloy carbides [11]. The resulting microstructure after this secondary hardening effect is a dispersion of very hard alloy carbides dispersed in a tempered martensite matrix. The alloy carbides have very high hardness relative to martensite and the remaining cementite [81]. Another form of embrittlement, temper embrittlement, can be encountered in the final stage of tempering (700ºF to 1050ºF).

Tempered martensite embrittlement and temper embrittlement can be a major problem when trying to develop ultrahigh strength cast steels with increased toughness because it significantly reduces the toughness of steels tempered in the TME and temper embrittlement temperature range.

2.6.6.1 Temper Embrittlement

High strength Q & T steels are susceptible to a couple different types of embrittlement during tempering. Tempered martensite embrittlement (TME), also referred to as 500ºF embrittlement, occurs after tempering between 500ºF to 700ºF. TME occurs as a result of carbides formed between martensite laths as a result of the transformation of retained austenite to $(Fe, M)_3C$ carbides (**Figure 2.19**) [95, 96]. **Figure 2.20** shows how the carbides form in the martensite laths during tempering, as a result of the transformation of austenite retained in the as-quenched condition for 4340 and 4140 steels.

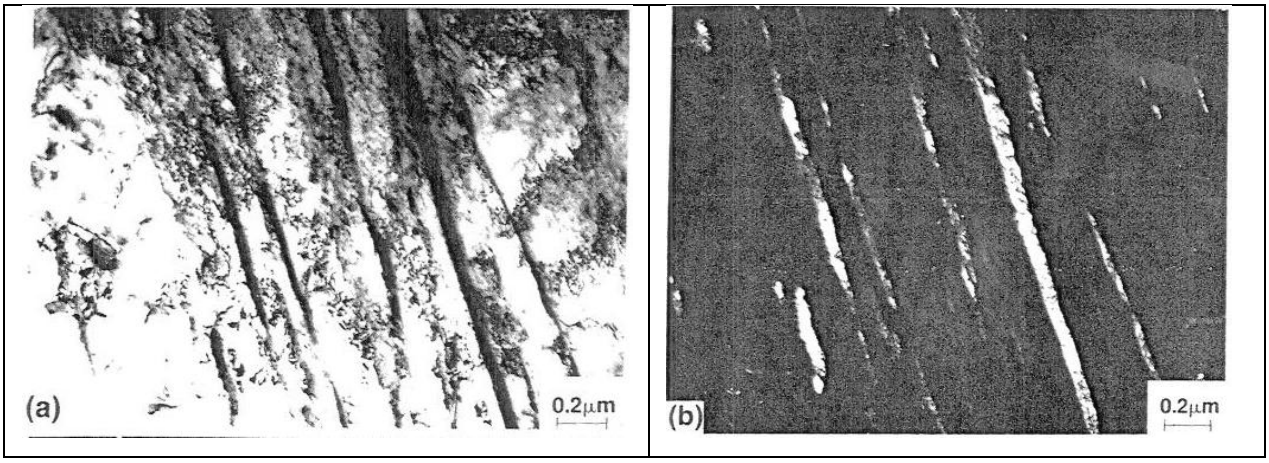

Figure 2.19: Transmission electron micrographs showing interlath carbides formed during tempering of 4340 steel containing 0.003% P at 350ºC (662ºF). (a) Bright-field image and (b) dark-field image using a cementite diffracted beam for illumination [97].

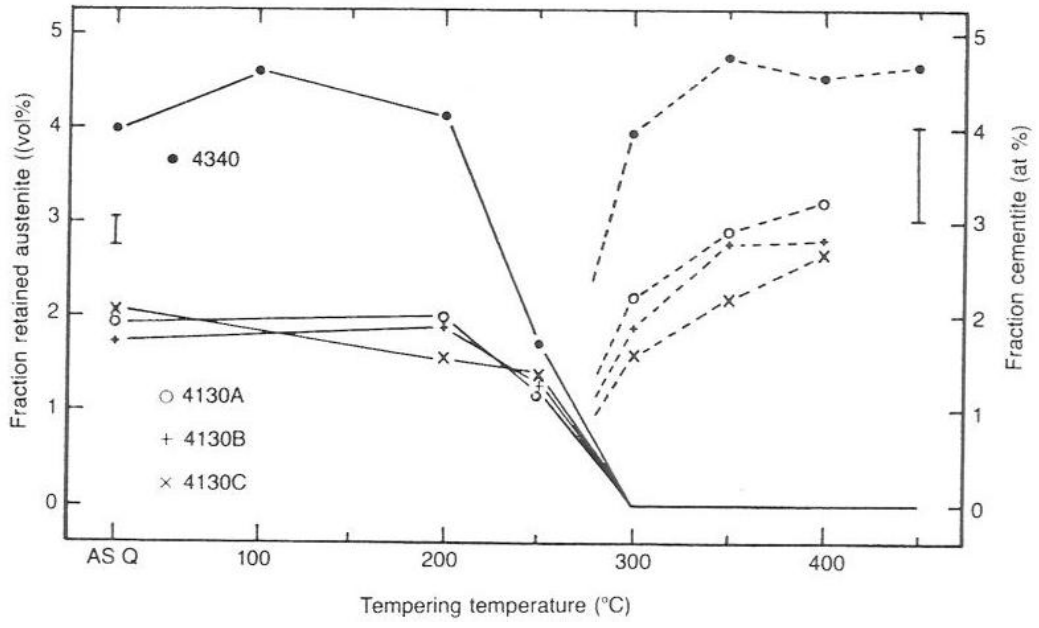

Figure 2.20: Retained austenite and cementite as a function of tempering temperature in 4340 and 4140 steels [97].

In TME fracture, crack initiation and crack growth occur by microvoid coalescence around carbide particles retained after austenitizing and during austenite to carbide transformation in the second stage of tempering. **Figure 2.21** shows the overload or unstable fracture from a CVN specimen of low-phosphorus 4130 steel tempered at 572ºF. The fracture pattern consists mainly of microvoids. These areas of overload fracture of the 4130 steel are preceded by shear initiation and stable crack growth, stages of crack growth accomplished by microvoid coalescence and ductile tearing [97]. It has been reported that the "500ºF" embrittlement problem can be shifted to higher tempering temperature by by adding silicon to low-alloy steel. Silicon inhibits the tempering of martensite by inhibiting the growth of carbide particles and by expanding the range of temperature in which the coherent Є-carbide is stable [45].

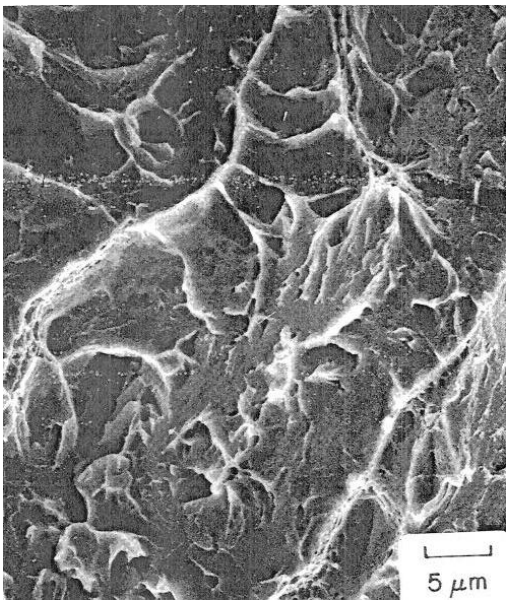

Figure 2.20: SEM fractograph of low-phosphorus 4130 steel tempered at 300ºC (572ºF) [95].

Temper embrittlement (TE), which leads to intergranular fracture (**Figure 2.22**) along former austenite grain boundaries, is said to occur between 700ºF to 1050ºF as a result of the segregation of elements such as antimony and phosphorus to the high-angle, prior austenite grain boundaries, where the cohesion of these boundaries is lowered [96, 98].

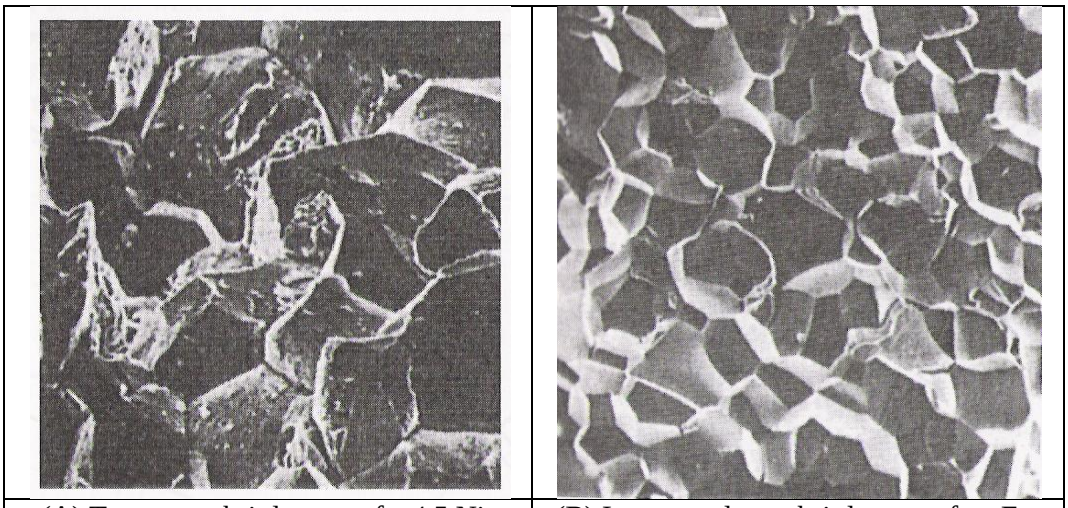

(A) Temper embrittlement of a 4.5 Ni-1.5Cr-0.3C wt% steel fractured at -321ºF.

(B) Intergranular embrittlement of an Fe-0.26P wt% alloy after holding at 932ºF.

Figure 2.22: Temper embrittlement of steel alloys [98].

Larger austenite grain size can increase embrittlement because the size of the dislocation arrays impinging on the grain boundary carbides will be larger and thus will promote intergranular crack nucleation [98].

Tempered martensite embrittlement and temper embrittlement (**Figure 2.23**) are additional phenomena that must be closely monitored when developing quench and temper heat treatment cycles to gain adequate impact toughness in ultrahigh strength low alloy steels.

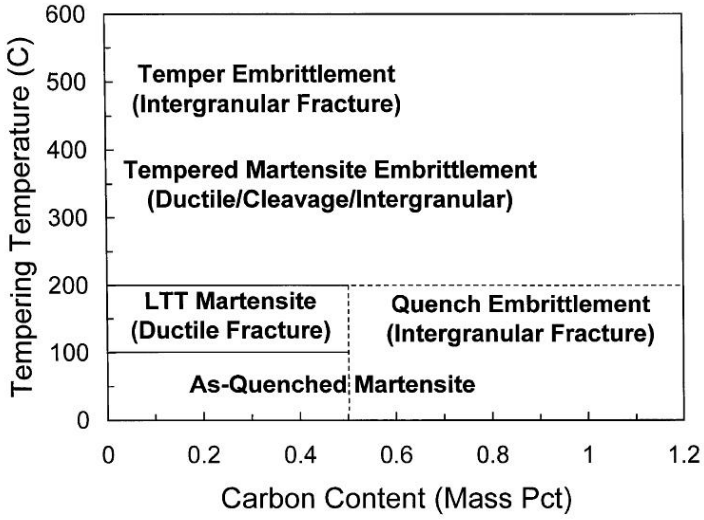

Figure 2.23: Modes of temper embrittlement in carbon and low alloy steels [99].

Temper embrittlement is controlled by both steel composition (alloying) and the tempering time and temperature. Controlling the alloying of the UHSLA steels controls both the tempering kinetics and also the composition of the carbides that form and grow during tempering.

2.6.6.2 Tempering and Carbide Formation in UHSLA and Intermediate Alloy Steels

The development of high toughness in UHSLA and intermediate alloy steels depends on the formation of small coherent or near-coherent carbides homogeneously nucleated throughout the matrix rather than carbide precipitation aligned along heterogeneous nucleation sites in the prior quenched structure. **Table 2.17** summarizes the carbide types typically formed in alloy steel upon tempering. Untempered martensite in medium carbon steels, while strong, suffers from poor ductility and impact toughness. Tempering the martensite at high tempering temperatures above 950°F leads to complete relaxation of the martensitic structure and decomposition of the martensitic structure to ferrite and fine carbides. Both elongation and toughness are increased at the cost of strength. Tempering conventional 4XXX steels at temperatures below 500°F [below the tempered martensite embrittlement (TME) and temper embrittlement (TE) temperature regimes] promotes the formation of fine metastable transition carbides. In UHSLA steels, by preserving these fine, coherent transition carbides (< 10nm) that are formed during the early stages of tempering at low tempering temperatures, **Figure 2.24**, high strength and good toughness can be achieved.

Table 2.17: Common stable carbides found in low and intermediate alloy steels [32],[100].

Carbide	Steel Type	Description
M_3C, Fe_3C	all steels	Found in plain-carbon and alloy steels - stable and often detrimental carbide.
M_6C	tool steels	Detrimental carbide - often Mo/W rich, ubiquitous in tool steels
M_2C	intermediate alloy steels containing Ni-Co-Mo-C.	Balance of Cr/Mo/V and C. Fine interlath and matrix-coherent carbide. Generally desirable.
$M_{2.4}C$, $M_{2.5}C$	Fe-C & Fe-Si-C steels low alloy steels (4340/300M)	Metastable ε/η carbide. Fine structure existing in early tempering and Si-rich steels.
M_7C_3	various low/intermediate alloy steels	Cr, Mo rich carbide, found at interlath and grain boundaries.
$M_{23}C_6$	stainless & high Cr-tool steels	Generally Cr, Mo, Fe rich, preferentially found at grain boundaries. Commonly found in alloys containing > 7% Cr. Generally coarse and undesirable.
MC, M(C,N)	Nb/V/Ti alloyed steels	High-temperature carbides and nitrides. Desirable in wrought formulations, but may coarsen in castings. Difficult or impossible (Ti) to dissolve. Increases YS/TS ratio.

Controlling carbide formation during tempering in UHSLA steels is crucial to developing the necessary mechanical properties. Carbon content and alloying elements play important roles in controlling carbides. As shown in **Figure 2.24**, impact toughness drops dramatically in the tempered specimens where fracture is exclusively ductile, from 45 ft-lbf. in the 0.3% carbon steel to less than 1.5 ft-lbf. in the 1% carbon steel [76, 97].

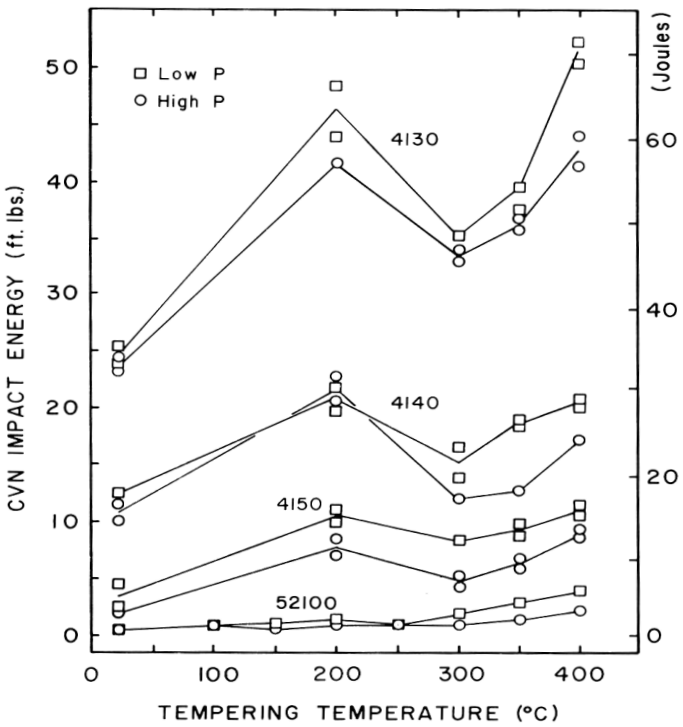

Figure 2.24: Effect of carbon content on the toughness of wrought low alloy steels tempered at low tempering temperatures [77, 97].

Another mode of heat treatment that has seen some exploration to help increase the toughness of ultrahigh strength low alloy steels is austempering, which leads to the formation of a bainitic microstructure.

2.6.7 Austempering

The austempering process (**Figure 2.25**) consists of heating to the austenization temperature, quenching into a molten bath of salt between 260ºC and 450ºC (500ºF and 842ºF) until the bainite transformation is complete. After the transformation is complete, the steel is then cooled to room temperature.

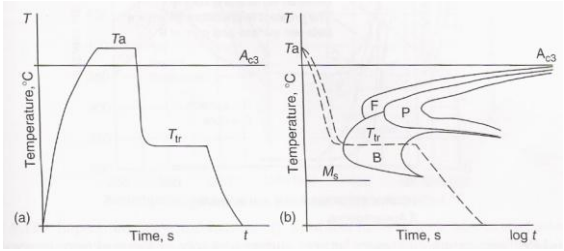

Figure 2.25: The austempering process (a) temperature vs. time graph and (b) isothermal transformation diagram with an austempering cooling cycle [101].

When austempering, there is no austenite-to-martensite transformation. Bainite is instead formed gradually through an isothermal transformation from austenite. After austempering, the steel specimen is air cooled as there is no tempering. The reason researchers have experimented with austempering of ultrahigh strength steels is because bainite gives the steel increased ductility and toughness [100]. Quenching in molten salt and austempering also helps to reduce distortion and cracking. **Figure 2.26** shows a comparison of impact toughness and hardness (HB) of five heats of Cr-Mn-Si steel after conventional quench and tempering and after austempering, as a function of tempering temperature and austempering temperature.

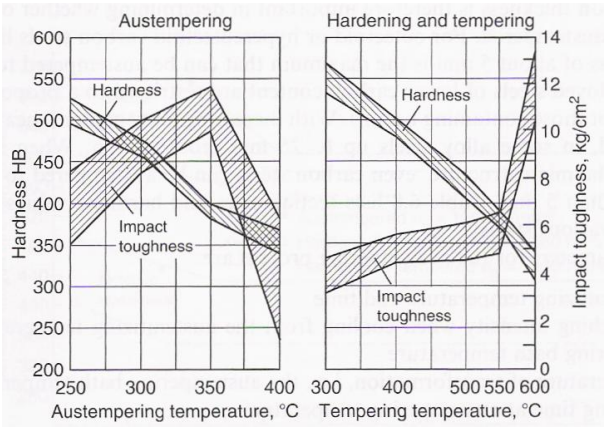

Figure 2.26: Wrought Cr-Mn-Si steel: Impact toughness and hardness after austempering (left) and conventional quench and tempering (right), as a function of austempering temperature and tempering temperature, respectively [101].

The ductility gained by austempering is a result of the final bainitic microstructure of the steel. **Figure 2.27** shows the difference in microstructure between pearlite, bainite, and martensite in a eutectoid steel. Bainite forms in stages from austenite, first through the nucleation and growth of ferrite that is followed by the precipitation of fine carbides.

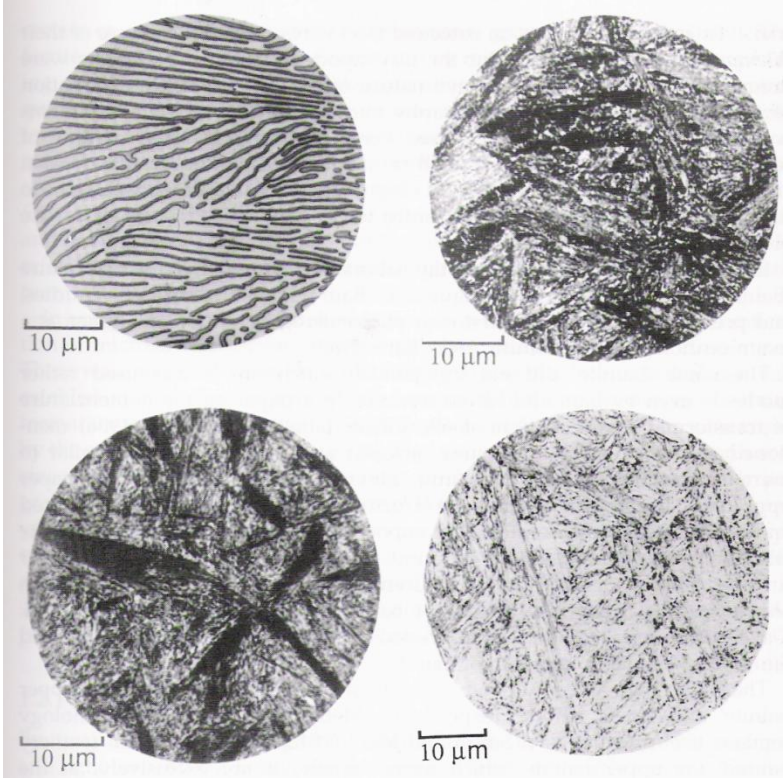

Figure 2.27: Microstructures from a eutectoid steel: Clockwise from top left: (a) pearlite formed at 720ºC (1328ºF); (b) bainite formed at 290ºC (554ºF); (c) bainite formed at 180ºC (356ºF); (d) martensite [100].

Some work on the austempering of select wrought UHSLA steels has been carried out. Mirak and Nili-Ahmadabadi (2004) studied the effects of austempering on 4130 steel. Austempering of 4130 steel at 380ºC (716ºF), 500ºC (932ºF), and 550ºC (1022ºF) led to mixed mechanical property results. Maximum Charpy impact toughness occurred at 550ºC (1022ºF), but the yield strength was low [102]. The most recent austempering work on wrought UHSLA steels was carried out by Tartaglia et al. (2008) on 4340 steel. Tartaglia et al. (2008) compared a typical quench and temper heat treatment (austenitize at 1625ºF, quench in oil at 160ºF, and temper at 425ºF) to samples that were austempered at 594ºF after being austenitized at 1625ºF. **Figure 2.28** shows the Charpy impact energy vs. testing temperature results for the study. The austempered steel that was primarily lower bainite with some martensite had the same yield strength as the Q & T 4340 steel [103]. The austempered steel had a significantly higher charpy impact toughness.

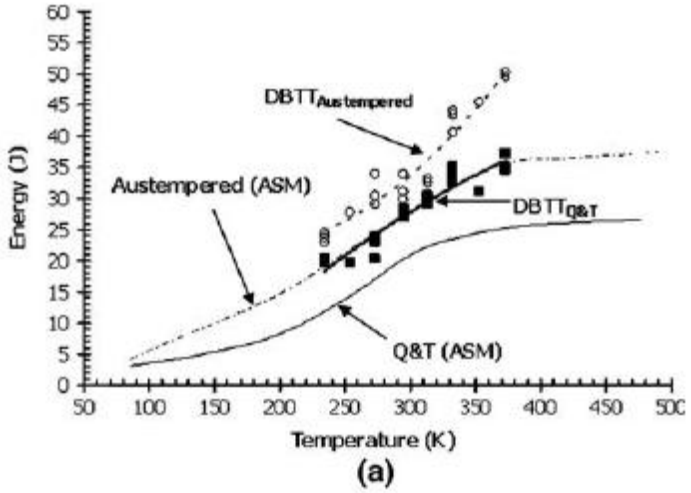

Figure 2.28: Charpy impact toughness vs. testing temperature for austempered and quench and tempered wrought 4340 steel [103].

The recent austempering work carried out on high strength cast steels was carried out on high silicon cast steels. The Lie and Chen (2001) study showed that an ausferrite structure consisting of bainitic ferrite and retained austenite could be obtained by austempering high silicon cast steel in the temperature range of 240ºC - 400ºC (464ºF - 752ºF). Austempering was carried out for 30 minutes. The study also concluded that the best combination of strength, toughness, and hardness could be obtained after austempering between 320ºC and 360ºC (608ºF and 680ºF). Impact toughness increased as austempering temperature increased until 360ºC (680ºF) when the ausferrite structure became coarse (**Figure 2.29(A)**). The increasing silicon content from 1.8 to 3.8% led to a decrease in strength, hardness remained unchanged, and toughness increased to a maximum before decreasing (**Figure 2.29(B)**) [104].

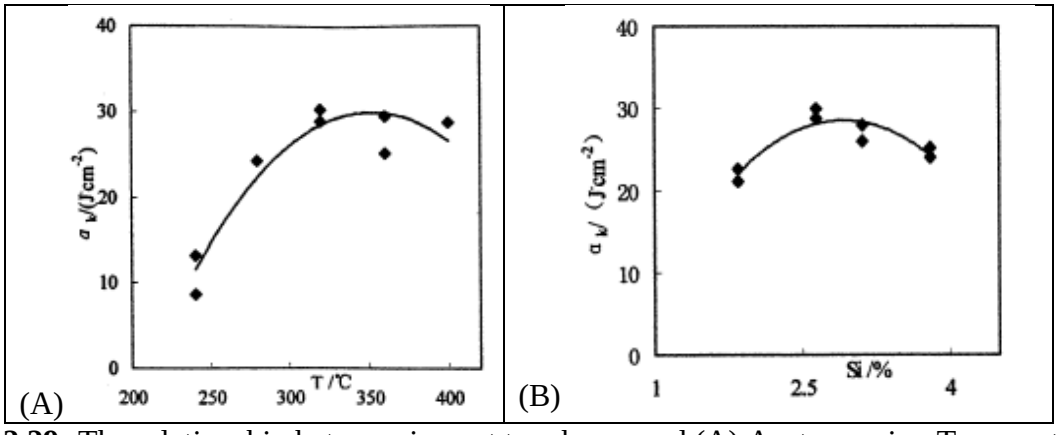

Figure 2.29: The relationship between impact toughness and (A) Austempering Temperature; (B) % Silicon [104].

The second Chen and Li (2006) study on high silicon cast steel examined the effect of Ti, V, and rare earth elements on the mechanical properties of austempered high silicon cast steel. All austempering was carried out for 60 minutes. This study showed that when high silicon cast steel (2.36%) with about 0.77% C was modified with Ti, V, and rare earth elements, the austempering temperature at which the optimum impact toughness is obtained shifts from about 320ºC (608ºF) to 360ºC (680ºF) (**Figure 2.30(A)**). The effect of austempering temperature on impact toughness was very similar to the effect that the volume fraction of retained austenite (%) had on impact toughness (**Figure 2.30(B)**). High impact toughness was obtained in the austempered high silicon cast steel when the retained austenite amount was 15 to 25% for the modified steel and 30 to 30% for the unmodified steel [105].

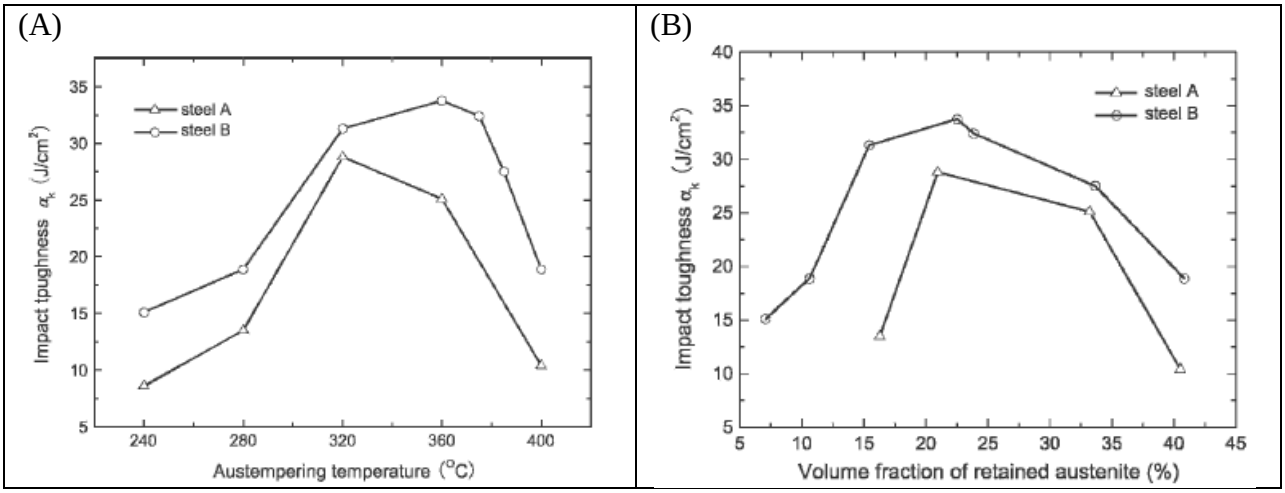

Figure 2.30: The influence of (A) austempering temperature and (B) volume fraction of retained austenite on the impact toughness of high silicon cast steels [105].

The Putatunda (2003) study carried out on a high carbon (1%), high silicon (3%), and high manganese (2%) cast steel displayed the development of a spherodized cast steel with about 85% of the structure being austenitic. Much longer austempering times (6hrs. or more) were needed to carry out the bainitic reaction to completion for this high silicon steel with high manganese. The study showed that the fraction of austenite in the steel increased with increasing austempering temperature up to 343ºC (650ºF) with a drastic decrease in the austenite content at higher temperatures. This drop was the result of the high carbon austenite decomposing to α-ferrite + Ϲ carbide at the higher austempering temperature for longer periods of time. As expected, the high carbon steel properties behaved differently when austempered than the

UHSLA low alloy steels. The yield strength and tensile strength both increased as the austempering temperature increased. Ductility decreased as the austempering temperature increased and fracture toughness was found to be highest at intermediate temperatures of 316ºC and 393ºC (600ºF to 740ºF) (**Figure 2.31**).

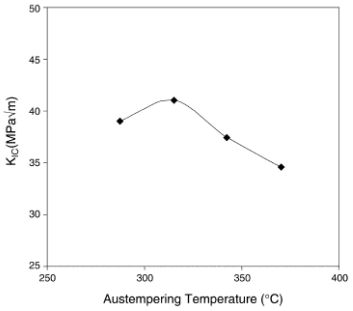

Figure 2.31: The influence of austempering temperature on the fracture toughness of high carbon, high silicon, and high manganese cast steel [106].

The effects of homogenization temperature, austenization temperature, tempering temperatures, and austempering on the toughness of ultrahigh strength steels have been discussed; all have been explored on at least wrought ultrahigh strength steel alloys to some degree. One of the secondary heat treatment processes that can potentially improve the mechanical properties of ultrahigh strength cast steels that has not been discussed in the literature for improving toughness of cast steels is hot isostatic pressing (HIP).

2.7 Secondary Processing of Cast Steels

Multiple heat treatments and other secondary processing steps can be used to further improve the mechanical properties, and particularly the impact toughness of castings. Hot isostatic processing (HIP) or hot isostastic pressing, which is commonly used to compress metal powders during the production of power metal parts, has recently been introduced as a secondary process for upgrading castings when reduction in porosity and microporosity are needed to gain additional strength and toughness for high integrity casting applications. HIPing is well known in powder metallurgy; however, there has been much less study on the influence of HIP cycles on removing porosity from high integrity cast components.

2.7.1 HIP of Cast Steels

Hot isostatic pressing (HIP) is a method that can be used to upgrade castings by the removal of internal porosity. HIPing has the ability to remove both macro and microporosity. Microporosity can have a detrimental effect on strength and in particular the toughness of ultrahigh strength cast steels. For hot isostatic pressing, castings are heated to high temperatures and exposed to high pressure at the same time [107]. Sintering refers to the application of heat to a casting or powder metal to sinter grains together and provide some densification. It is not clear if simple sintering at atmospheric pressure can remove microporosity from castings. If high temperatures alone are applied to castings, grain growth may occur before the process of pore elimination is completed. This can further inhibit pore removal. With the high pressures, HIPing can be done at lower temperatures than sintering to achieve a particular density. At lower temperatures, grain growth can be slowed or inhibited [107, 108]. The HIPing of castings is only documented fairly well in the literature for Al-, Ti-, and Ni-based alloys. Castings can seemingly possess the same properties as forged products when HIP is carried out successfully prior to heat treatment [46]. HIPing can be used to remove porosity while not adversely affecting the microstructure of the casting alloy. **Figure 2.32** shows the reduction of microporosity from HIPing and the effect of microporosity reduction on the impact toughness of a cast steel. **Figure 2.33** shows how the mechanical properties of a cast Ni-Al bronze (AB2) alloy can be improved by HIPing.

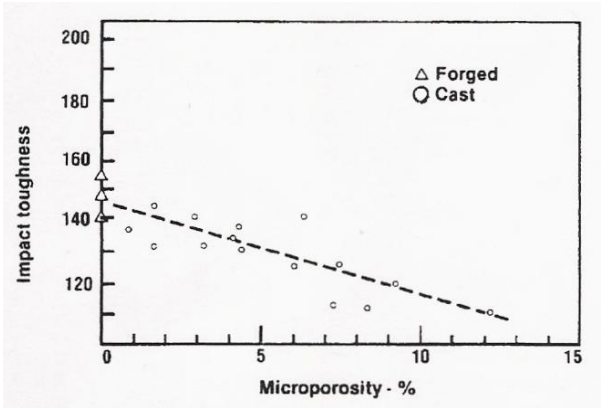

Figure 2.32: The influence of microporosity on impact toughness (J/cm^2) of 1 wt. % Cr-0.25 wt. % Mo cast steel [107].

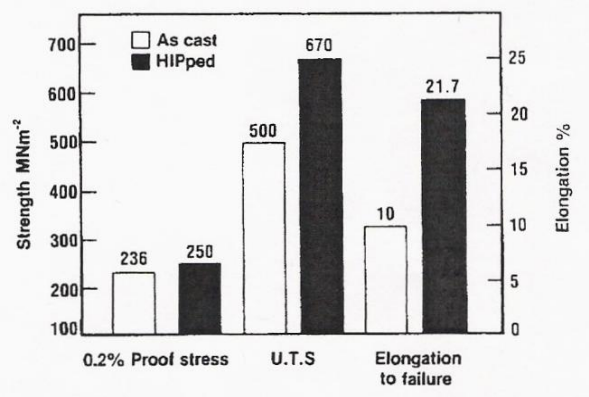

Figure 2.33: The influence of HIP on mechanical properties of Ni-Al bronze (AB2) that contains 10% to 20% porosity [107].

The results of the work on 70/30 cupronickel alloys showed that a two stage densification process occurs during isostatic pressing, involving plastic flow followed by creep and diffusion. The initial densification that takes place during the heating/ pressurization stage of the HIP treatment is thought to take place via plastic flow. It is in this stage that internal pores of up to 16% by volume can be recovered (**Figure 2.34**). Most of the pore closure in both unencapsulated and encapsulated castings occurs within a short period of time (45 minutes) at the sustained temperature and pressure (**Figures 2.34 and 2.35**), after which the additional densification of encapsulated castings continues at a very slow rate (**Figure 2.36**). HIPing has no adverse effects on the mechanical properties of the 70/30 cupronickel alloy; HIPing significantly enhances the ductility and impact toughness (**Figure 2.37**) [109].

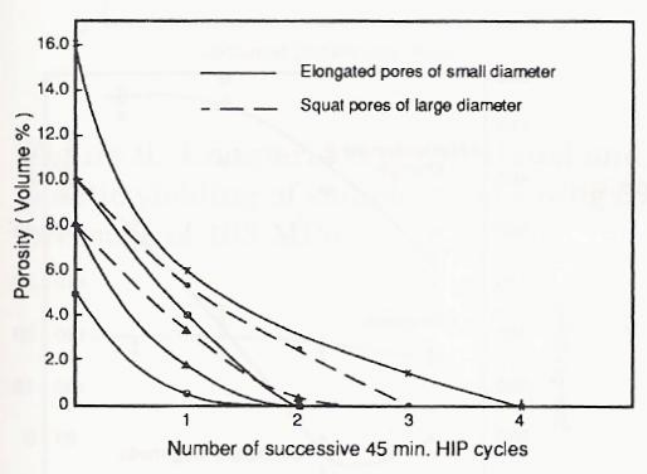

Figure 2.34: The effect of successive 45 minute (Type 1) HIP cycles on the densification of 70/30 cupronickel castings [109].

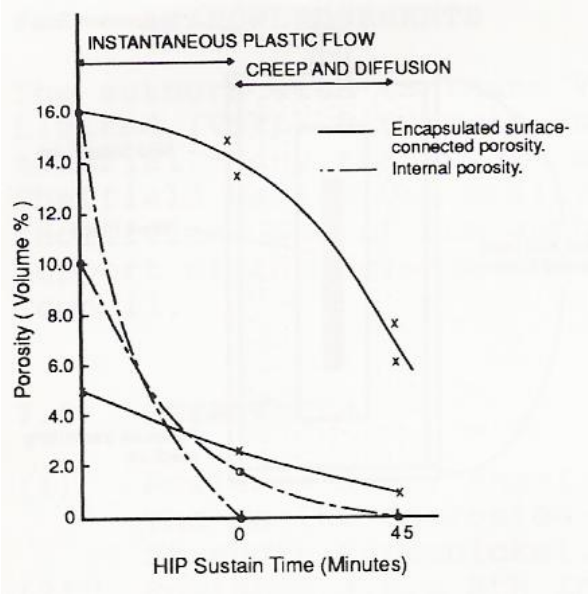

Figure 2.35: The effect of HIP time on the recovery rate and casting densification mechanisms of 70/30 cupronickel castings [109].

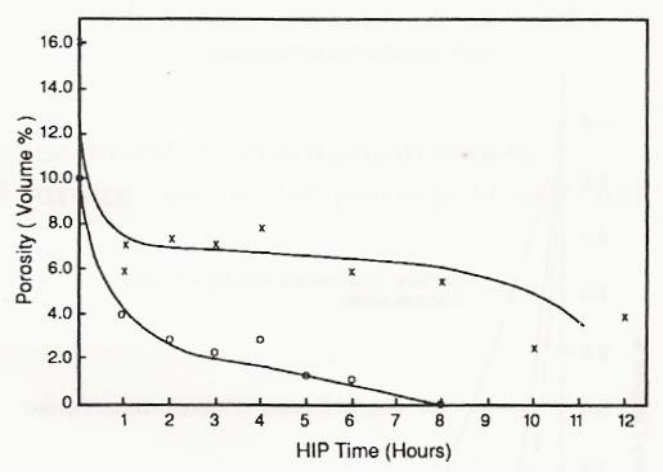

Figure 2.36: The effect of continuous HIP time on the closure of elongated pores in 70/30 cupronickel castings [109].

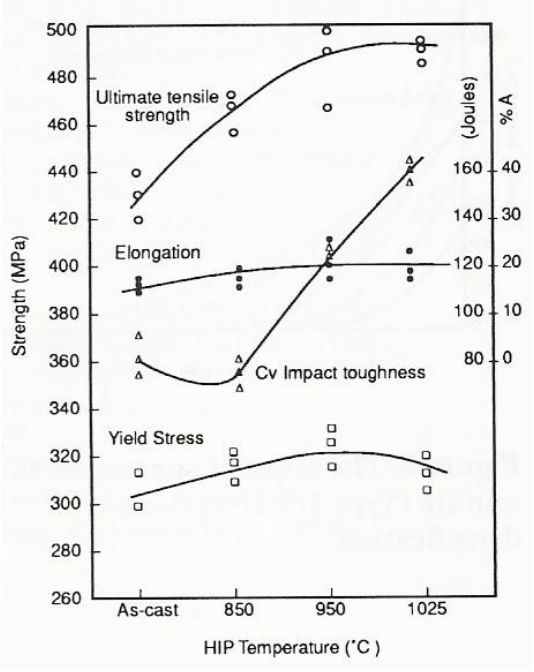

Figure 2.37: The effect of HIP temperature on the mechanical properties of 70/30 cupronickel [109].

Very little work has been carried out on quantifying the effects of HIPing on casting alloys. Although **Table 2.18** shows a typical HIPing pressure and temperature for steel castings, very little, if any, work has been completed to quantify the effects of HIPing on steel castings.

Table 2.18: Typical HIPing pressures and temperatures for various casting alloys [107].

Material	Melting Point T_m (°C)	Yield Stress at Room Temperature (MPa)	Hipping Temperature (°C)	Hipping Pressure (MPa)
Al and its alloys	660 (Al)	100 to 627	500	100
Al/Al_2O_3	—	—	300	350
Cu and its alloys	1083 (Cu)	60 to 960	800 to 950	100
Be and its alloys	1289 (Be)	240	900	103
Nimonic and superalloys	1453 (Ni)	200 to 1600	1100 to 1280	100 to 140
Hydroxyapatite	—	—	1100	200
Mg/Zn ferrite	—	—	1200	100
TiAl	—	—	900 to 1150	35 to 200
Ti_3Al	—	—	925	200
Ceramic superconductors	—	—	900	100
Steels	1536 (Fe)	500 to 1980*	950 to 1160	100
Ti and its alloys	1670 (Ti)	180 to 1320	920	100
Al_2O_3	2050	5000	1500	100
Al_2O_3/glass	—	—	1400	100
Al_2O_3/TiC	—	—	1935	150
Al_2O_3/ZrO_2	—	—	1500	200
SiC	2837	10,000	1850	200
B_4C	—	—	2000	200
WC/Co	2867	6000	1350	100

*Low-alloy steels (water quenched and tempered).

The lone study that can be found in the literature on the influence of HIP on cast steels is a Carpenter technology study on Cast + HIP Aermet 100. The Aermet 100 Cast+HIP steel casting alloy was developed to rival forged parts in strength and fracture toughness. HIP of this cast alloy significantly increased the CVN impact toughness and ductility of the cast Aermet 100 alloy. By using near-net-shape Cast + HIP Aermet 100 alloy parts, cheaper net shape castings can replace expensively machined forgings [110]. A study was performed to evaluate the properties of re-melted and cast AerMet100 with the properties of wrought 300M, 4340, H11, and Marage 250 alloy steels, **Figures 2.38 (A-E)**. **Figure 2.38(A)** shows that the Cast + HIP Aermet 100 alloy has the same yield and tensile strengths as the wrought alloys tested while possessing much greater fracture toughness than wrought alloys of similar strength, **Figure 2.38(B)**. When the ratio of fracture toughness (K_{IC}) to yield strength (Y.S.) is plotted against ultimate tensile strength (**Figure 2.38(C)**), the critical flaw size for the different strength alloys can be evaluated. Since critical flaw size is a measure of the damage tolerance of a part, **Figure 2.38(C)** shows that an AerMet 100 casting can have an ultimate tensile strength of 280ksi and be able to withstand more damage than forgings of the same strength. **Figure 2.38(D)** shows that the Cast + HIP alloy's elongation is superior to the other alloys and its reduction in area is about double that of wrought 4340 or 300M. **Figure 2.38(E)** shows that the Cast + HIP Aermet alloy has excellent impact toughness.

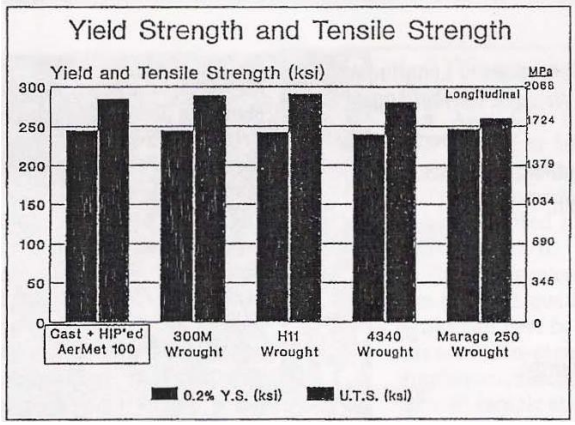

Figure 2.38(A)

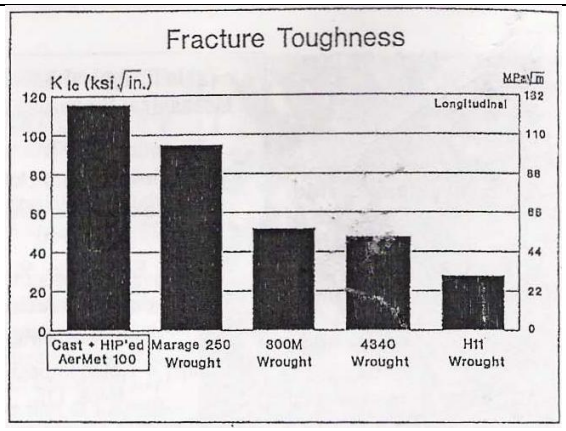

Figure 2.38(B)

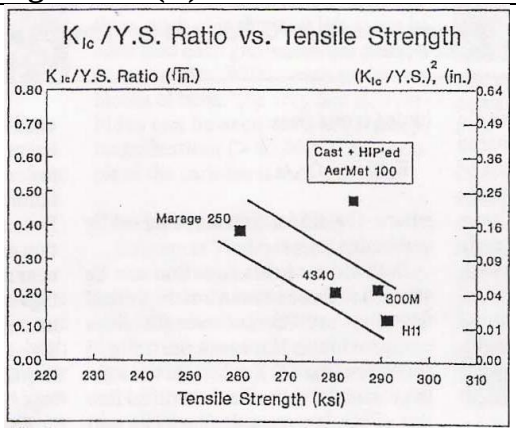

Figure 2.38(C)

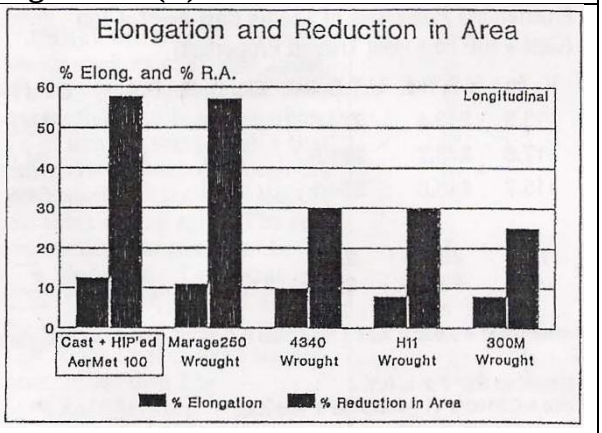

Figure 2.38(D)

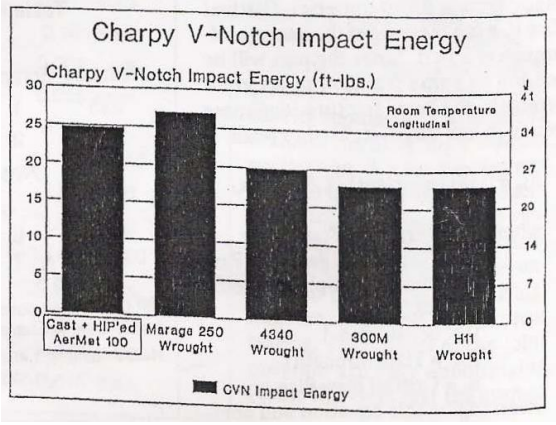

Figure 2.38(E)

Figure 2.38: Properties of cast + HIP intermediate alloy Aermet 100 vs. other wrought high strength steels: (A) yield strength; (B) fracture toughness; (C) fracture toughness (K_{IC})/ yield strength ratio vs. tensile strength; (D) % elongation and reduction in area; (E) Charpy v-notch impact energy [110].

Other than this study of cast Aermet 100, no detailed analyses of the upgrading of steel castings by hot isostatic pressing have been reported. There has not been a thorough quantitative analysis done on the reduction in pore size and estimation of microsegregation reduction during high temperature hot isostatic pressing of steel castings.

2.8 Summary of Chapter 2

The development of ultrahigh strength low alloy cast steels with increased impact toughness depends mainly on controlling the composition or chemistry of the alloys and also on the heat treatment processes used to control microstructure. It is evident that the ultrahigh strength of these alloys is obtained by adding microalloying elements that will contribute to fine dispersion strengthening, secondary hardening, and the control of grain size. Most of the previous research was performed on ultrahigh strength low alloy wrought steels. Limited heat treatment studies have been completed on wrought ultrahigh strength low alloy steels to try to help improve toughness. Researchers have experimented with homogenization temperatures, higher austenization temperatures, tempering temperatures, and also austempering to try to improve the toughness and ductility of ultrahigh strength low alloy wrought steels. One processing study indicated that HIP can potentially improve the impact properties of an intermediate alloy high strength cast alloy. Much work still needs to be completed to improve the toughness of these wrought ultrahigh strength low alloy steels.

During the past 50 years, only a minimal amount of work has been done to develop ultrahigh strength low alloy cast steels. The casting specifications, heat treatment guidelines, and chemistries for the ultrahigh strength low alloy cast steels have not been definitively studied. Alloy and heat treatment guidelines to produce UHSLA castings with optimal strength and impact properties have not been analyzed. The relationships between alloy and heat treatment variables and the resultant microstructural development need to be studied further to gain a fundamental understanding of the development of properties. Researchers have also not done a thorough job of modeling the reduction in microsegregation during homogenization of castings including ultrahigh strength low alloy steel castings. HIPing could potentially replace homogenization step prior to heat treatment, leading to significant gains in toughness without changing strength. There has not been conclusive work documented on the effects of HIPing on the reduction of porosity in ultrahigh strength cast steels. In addition, researchers have not

characterized microsegregation reduction during homogenization and related it to property improvements in steel castings. Much work needs to be done to be able to understand the amount of microsegregation reduction that is possible at existing homogenization temperatures and times along with trying to develop critical homogenization cycles necessary to reduce microsegregation to specific levels necessary for mechanical property development in ultrahigh strength low alloy steel castings.

The following experimental procedures and modeling work will lay the foundation to provide answers and tools to be able to improve the impact toughness of current ultrahigh strength low alloy cast steels. It includes a first study of a low cost ultrahigh strength low alloy cast steel, ES-1, expected to have good low temperature toughness. Along with the development of a heat treatment process for the ES-1 alloy, a thorough analysis of the mechanical properties of the alloy including impact transition behavior, strength, and hardness will be completed. Experimental work to quantify the effects of homogenization and HIP on microsegregation reduction and the effects of HIP on pore size reduction will also be described.

Chapter 3

Experimental Procedures

The underlying experimental procedures were developed and carried out to accomplish the objectives of this ultrahigh strength low alloy cast steel study. The overall objective of the study is to develop affordable ultrahigh strength low alloy (UHSLA) cast steels with improved impact toughness. The primary driving force behind developing affordable ultrahigh strength low alloy cast steels is the significant cost savings possible both in alloy and processing costs. In addition, a full bodied supplier network is available to produce military and commercial components using UHSLA alloy steels. To be able to develop affordable UHSLA cast steels with improved impact toughness, a thorough literature review of the physical metallurgy and processing of wrought and cast UHSLA was necessary. With very little work completed on the development of processing guidelines and conventional quench and temper heat treatments for cast UHSLA steels, work needed to be carried out to develop processing guidelines necessary to achieve acceptable mechanical properties. In order to develop the processing guidelines, work needed to be carried out to understand the physical metallurgy of the cast steels, namely ES-1 (Eglin) steel. Understanding the physical metallurgy principles that influence strength and impact toughness was extremely important. Since the mechanical properties of cast steels are developed and optimized primarily through heat treatment, much experimental work needed to be carried out on the development of traditional and advanced heat treatment processes for UHSLA cast steels. Thus, in addition to understanding the physical metallurgy of the UHSLA alloys, much work needed to be carried out to understand and quantify the effect of hot isostatic processing (HIP), high temperature homogenization, and tempering temperature on the microstructure and mechanical properties of UHSLA cast steels.

To be able to accomplish the overall objective of developing UHSLA cast steels with acceptable mechanical properties to substitute for more expensive intermediate and high alloy steels, the following experimental procedures were carried out to develop the necessary processing guidelines to develop UHSLA cast steels with optimal mechanical properties.

3.1 Approach

From the thorough literature review, it is apparent that little work has been done on trying to develop the next generation of ultrahigh strength low alloy cast steels with improved impact toughness. Malakondaiah et al. (2000) provided a detailed assessment of the work that has been completed to improve the toughness of ultrahigh strength wrought steels since 1960 (**Figure 3.1**). Progress has been made in the development of ultrahigh strength wrought steels with improved toughness. However, current UHSLA cast steel usage indicates that cast 4340 steels developed in the 1960's are still widely used in cast form. Also, the wrought steel progress has been made mainly through the development of very expensive high alloy maraging and secondary hardening steels that contain large amounts of nickel and cobalt [1].

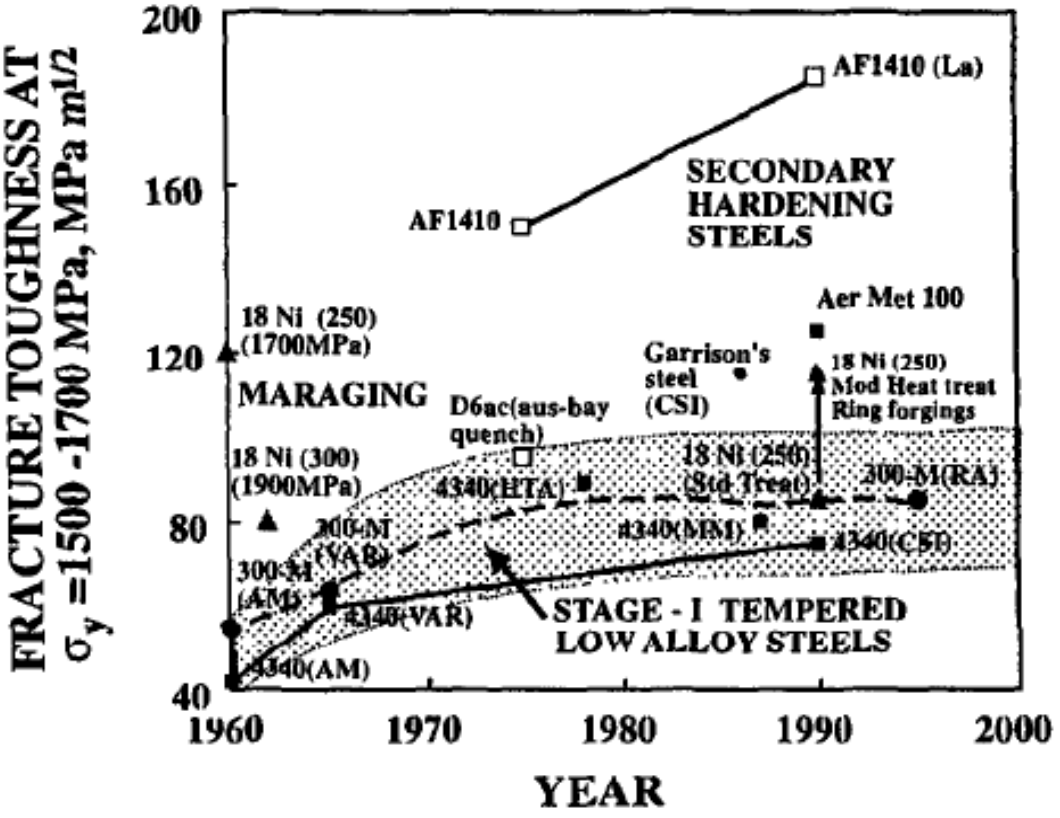

Figure 3.1: A look at the improvements in fracture toughness of wrought ultrahigh strength steels from 1960 to 2000 [1].

The first approach to the development of > 220 ksi yield strength ultrahigh strength low alloy cast steel with increased impact toughness involved the investigation of a silicon alloyed 4340 steel similar to 300M and designated 4340+ cast material. Screening heat treatment studies were carried out to evaluate the effects of heat treatment variables on the strength and impact

toughness of the alloy. Fracture surface characterization, microstructural analysis, and X-ray diffraction studies were also carried out.

The second approach involved investigation of a high toughness ultrahigh strength low alloy cast steel with a yield strength of > 180ksi designated as cast ES-1, an alloy that was not known to have been cast to shape prior to this study. An impact transition study was carried out on ES-1 cast ingot material. The impact transition study also tested the effects of HIP, homogenization, austenization temperatures, and tempering temperatures on the impact toughness of the cast alloy. The impact transition study was followed up by a study to estimate the degree of porosity reduction possible by HIP on the ES-1 cast ingot material. Ingot material was then investment cast to experiment with basic melting, deoxidation, and heat treatment processes for the cast alloy.

The final approach was to model and estimate the extent of microsegregation reduction in ultrahigh strength cast steels, namely ES-1 steel, during heat treatment processes including homogenization, austenization, and HIP. By modeling the extent of microsegregation reduction, steel foundries will have a baseline for the temperatures and times required to achieve varying degrees of microsegregation reduction of the substitutional alloying elements (W, Cr, Mo, Mn, and Ni) in UHSLA steels.

3.2 Materials

To carry out the experimentation needed for this study, multiple heats of material needed to be procured from various steel foundries. A single heat of investment cast 4340+ steel, three heats of investment cast ES-1 material, and a single a heat of ES-1 cast ingot material were procured from commercial producers.

3.2.1 Investment Cast 4340+ Steel

The 4340 + (300M) investment cast material used in this study was obtained from Metal Casting Technologies. One 300 lb. investment cast heat was poured into 0.5 in. diameter X 3.0 in. long sub-sized tensile specimen blanks and also into 0.6 in. X 0.6 in. X 2.25 in. Charpy blanks (**Figure 3.2**).

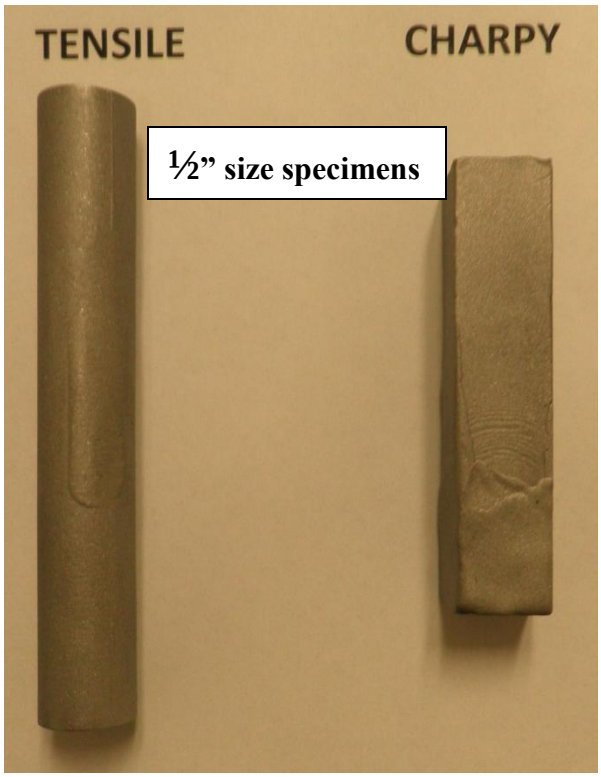

Figure 3.2: Investment cast 4340+: tensile and Charpy blanks.

The investment cast material was melted under an inert gas blanket and cast using the CLA process. The composition of the 4340+ (300M) heat provided by Metal Casting Technologies is given in **Table 3.1**.

Table 3.1 - Composition of 4340+ IC test materials compared to targets.

4340+ (Investment Cast) (wt%)									
element	C	Cr	Ni	V	Mo	Mn	Si	P	S
	0.450	0.831	1.834	0.100	0.397	0.757	1.628	0.008	0.010

3.2.2 Cast Ingot ES-1 Material

The cast ES-1 ingot material was provided by McConway & Torley, LLC (M&T) under USAF CRADA NUMBER 08-157-RW-01. This as-cast ingot material was induction melted and vacuum degassed by North American Hoganus (Heat No. H0490). The as cast ingot was 16.5 inches in diameter. This material was provided in the form of 1" x 1" x 8" machined bars (**Figure 3.3**). Six of the bars shown in **Figure 3.3** were supplied to Penn State for

experimentation. The material ID for the cast ES-1 ingot material was 42008-05. The composition of the ES-1 cast ingot material is shown in **Table 3.2**.

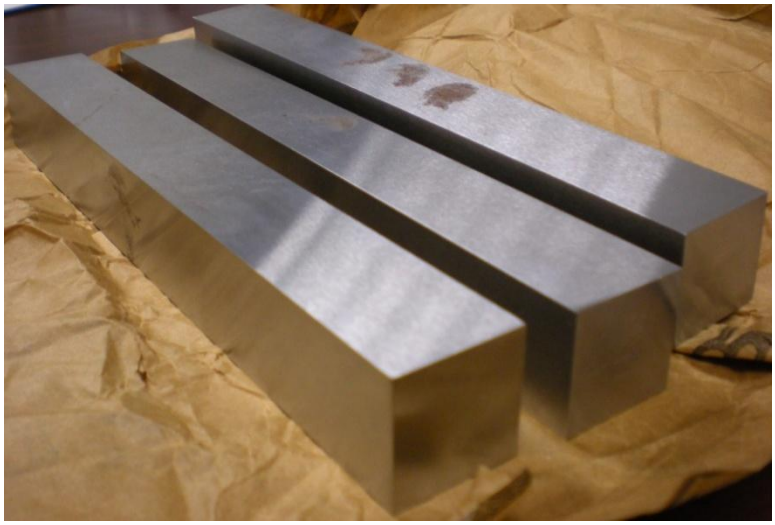

Figure 3.3: 1in. X 1in. X 8in. machined cast ES-1 steel bars.

Table 3.2: Composition (Wt %) of Cast ES-1 ingot material.

C	**Mn**	**P**	**S**	**Si**	**Cr**	**Al**	**V**	**Mo**
0.27	0.78	0.01	0.002	0.98	2.59	0.008	0.11	0.40
Ni	**Cu**	**W**	**N**	**Fe**	**Cb**	**Ti**	**Co**	**O**
1.00	0.07	0.98	0.006	Bal	<.01	<.01	0.01	0.003

3.2.3 Investment Cast ES-1 Material

Three heats of investment cast ES-1 material were poured by Nova Precision Casting. The ES-1 material that was melted and poured by Nova was re-melt material cut from a forged ingot (**Figure 3.4**). The ingot material had been induction melted and vacuum decarburized and degassed before forging at North American Hoganas (Heat No. C7620; 11 in. dia. X 72 in. long). Chemistry data for the ingot provided by Nova Precision Casting are found in **Table 3.3**.

Figure 3.4: Forged ES-1 billet.

Table 3.3: Composition (Wt %) of Forged ES-1 ingot material, used for all investment cast heats.

C	**Mn**	**P**	**S**	**Si**	**Cr**	**Al**	**V**	**Mo**	**Sn**
0.24	0.66	0.025	0.009	0.91	2.47	0.011	0.09	0.43	0.01
Ni	**Cu**	**W**	**N**	**Fe**	**Cb**	**Ti**	**Co**	**O**	
1.19	0.07	1.08	-----	Bal	-----	<0.01	0.01	-----	

The investment cast shell material used to pour ES-1 test bars was conventional fused silica. Each heat weighed 180 lbs. While the ES-1 material was in the electric induction furnace, an argon purge of 4 liters/min. was added to the melt. For deoxidation of heat #1, 0.20lb (0.10 wt %) of aluminum was added to the 180 lb. heat. For deoxidation of heat #2, 0.10 lb (0.05 wt %) of aluminum was added to the 180 lb. heat. Heats 1 and 2 were the first two heats poured from a new crucible. For heat #3, the deoxidation practice was the addition of 0.05% by weight of aluminum cut wire. After the heat was melted and brought to temperature, the power was turned off and the melt was deslagged. The aluminum was added on top of the bare metal and the power was applied at a level to just maintain the pouring temperature. The furnace was tapped with a pouring temperature of 2850°F; pouring was done directly from the furnace into the preheated shells. Each shell produced two test bars measuring 1" diameter X 5.75" length (**Figure 3.5**).

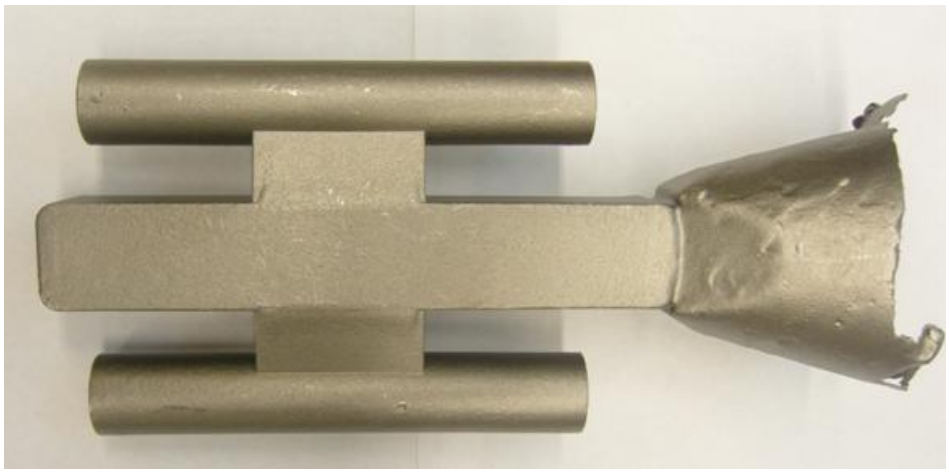

Figure 3.5: Investment cast ES-1 test bars.

To reduce the solidification cooling rate and promote excellent surface finish, the shells were "canned". In this process, the shells were poured in a can which was immediately covered after the shells were poured. Sugar was thrown on the hot shells before closing to consume the oxygen in the atmosphere around the shells while the shells cooled. The chemistries for the investment cast ES-1 alloy heats supplied by Nova Precision Casting are shown in **Tables 3.4 - 3.6**.

Table 3.4: Composition (Wt %) of Heat #1 Investment Cast ES-1.

C	**Mn**	**P**	**S**	**Si**	**Cr**	**Al**	**V**	**Mo**	**Sn**
0.25	0.52	0.027	0.009	0.76	2.47	0.096	0.10	0.46	0.01
Ni	**Cu**	**W**	**N**	**Fe**	**Cb**	**Ti**	**Co**	**O**	
1.23	0.08	1.10	-----	Bal	-----	0.00	0.02	-----	

Table 3.5: Composition (Wt %) of Heat #2 Investment Cast ES-1.

C	**Mn**	**P**	**S**	**Si**	**Cr**	**Al**	**V**	**Mo**	**Sn**
0.24	0.51	0.024	0.009	0.76	2.47	0.064	0.10	0.44	0.01
Ni	**Cu**	**W**	**N**	**Fe**	**Cb**	**Ti**	**Co**	**O**	
1.19	0.07	1.08	-----	Bal	-----	0.00	0.02	-----	

Table 3.6: Composition (Wt%) of Heat #3 Investment Cast ES-1.

C	**Mn**	**P**	**S**	**Si**	**Cr**	**Al**	**V**	**Mo**
0.25	0.47	0.025	0.009	0.70	2.51	0.011	0.10	0.44
Ni	**Cu**	**W**	**N**	**Fe**	**Cb**	**Ti**	**Co**	**O**
1.20	0.07	1.07	-----	Bal	-----	-----	------	-----

3.3 Investment Cast (IC) 4340+ Heat Treatment Studies

With only a single heat of investment cast 4340+ available for heat treatment experimentation, the following set of screening experiments was carried out. All heat treatments were developed based on wrought heat treatment procedures outlined by ASM International [7].

3.3.1 Experimental Heat Treatment Procedures for (IC) 4340+ (300M) Steel

Initial heat treatment screening tests were performed on the tensile and Charpy blanks. Conventional 'standard practice' heat treatment was compared to standard practice with a higher homogenization temperature expected to be more appropriate for a casting alloy, **Table 3.7**. The Youngblood and Raghavan (1977) study on the wrought 300M material suggested that higher austenization temperatures helped to improve toughness. They cited undissolved precipitates seen both in the submicrostructure and fracture surfaces promoting quasi-cleavage fracture [84]. Their austenization study had a constant homogenization temperature of 1675°F (913°C). The idea was to test the effects of higher homogenization temperature on the standard heat treatment practice of 300M to be followed up with a more formal study to hone in on optimal homogenization and austenization temperatures to produce optimal toughness. As shown in **Table 3.7**, samples were austenitized at 1600°F for 1.0 hour, quenched in room temperature water and then double tempered at 400°F with each cycle being 4 hours. Both oil quenching and water quenching have been employed when heat treating the 4340 alloys. Quench cracking of the heat treated samples was not observed in the heat treatment trials.

Table 3.7: Study #1: Heat Treatments for Homogenization Temperature Study of 4340+ (300M) Cast Steel.

	Standard Practice	**Study #1 Practice**
Homogenize	**1675°F / 1.0 hr**	**1800°F or 1950°F / 1.0 hr**
Air Cool	**Air Cool to Room Temperature**	**Air Cool to Room Temperature**
Austenitize	**1600°F / 1.0 hr**	**1600°F / 1.0 hr**
Quenching	**Water Quench at 74°F**	**Water Quench at 74°F**
Temper	**600°F, 4 hours** **Water Quench at 74°F** **600°F, 4 hours** **Water Quench at 74°F**	**600°F, 4 hours** **Water Quench at 74°F** **600°F, 4 hours** **Water Quench at 74°F**

The second set of screening heat treatments on 4340+ (300M) was carried out to test the effects of hot isostatic pressing (HIP) on the mechanical properties of the alloy. The heat treatment plan for the initial HIPing screening study is shown in **Table 3.8**. The HIP cycle replaced the homogenization step in the standard heat treatment plan. All HIP was carried out by Bodycote, Andover, MA, using their recommended HIPing conditions; the remainder of the heat treatment cycles were carried out in the Penn State University FAME lab. The effects of double tempering at 500°F (260°C) versus 600°F (316°C) were also studied.

Table 3.8: Study #2: Heat Treatments for HIP and Tempering Study of 4340+ (300M) Cast Steel.

	Standard Practice	**Study #2 Practice**
HIP	**-**	**1950F for 4 Hours with 15ksi. pressure (slow vessel cool to 700F) (Air Cool to Room from 700F)**
	1675°F / 1.0 hr	**-**
Air Cool	**Air Cool to Room Temperature**	**Air Cool to Room Temperature**
Austenitize	**1600°F / 1.0 hr**	**1600°F / 1.0 hr**
Quenching	**Water Quench at 74°F**	**Water Quench at 74°F**
Temper	**600°F, 4 hours Water Quench at 74°F 600°F, 4 hours Water Quench at 74°F**	**(1A)500°F or (2A)600°F, 4 hr Water Quench at 74°F (1A)500°F or (2A)600°F, 4 hr Water Quench at 74°F**

Subsequent austempering heat treatment trials were conducted in an attempt to reduce ultimate tensile strength and yield strength for improved impact toughness. The experimental results from the Li and Chen (2000) study on austempering high silicon cast steel study showed that an ausferrite structure consisting of bainitic ferrite and retained austenite could be obtained by austempering a high silicon cast steel within a broad range of austempering temperatures (240°C - 400°C) [464°F - 752°F] [104]. A study by Li and Chen (2000) indicated that a full ausferrite structure could be obtained by austempering the steel with silicon content around 2.64%. Their austempering study found that as the silicon content was increased from 1.8% to 3.8%, the strength decreased, hardness stayed unchanged and the toughness increased to a maximum silicon content and then decreased [104]. Some of what was learned in the Putatunda (2003) study carried out on a high carbon (1%), high silicon (3%), and high manganese (2%) steel was also used in this work. Putatunda showed that much longer austempering times (6hrs.

or more) were be needed to carry out the bainitic reaction to completion for this high silicon steel with high manganese [106]. The third set of heat treatments on 4340 + (300M) were completed to test the effects of austempering on the mechanical properties of the investment cast 4340+ (300M) alloy. The heat treatment plan for the initial austempering screening study is shown in **Table 3.9**. The austempering step replaced the double tempering step from the standard heat treatment plan for the alloy.

Table 3.9: Study #3: Heat Treatments for Austempering Study of 4340 + (300M) Cast Steel.

	Standard Practice	**Study #3 Practice**
Homogenize	**1675°F / 1.0 hr**	**1675°F / 1.0 hr**
Air Cool	**Air Cool to Room Temperature**	**Air Cool to Room Temperature**
Austenitize	**1600°F / 1.0 hr**	**1600°F / 1.0 hr**
Quenching	**Water Quench at 74°F**	**Place in Molten Salt Bath at (1) 572°F or (2) 599°F**
Temper	**600°F, 4 hours Water Quench at 74°F 600°F, 4 hours Water Quench at 74°F**	**-**
Austemper	**-**	**(1)572°F or (2) 599°F for (A) 840min. or (B) 480min. Water Quench at 74°F**

Based on the actual composition in **Table 3.1**, the martensite start temperature was estimated using the following empirical relationship due to the Andrews relationship (concentrations in wt %) [111]:

$$M_S(°C)= 539 - 423(\%C) – 30.4(\%Mn) – 17.7(\%Ni) – 12.1(\%Cr) – 7.5(\%Mo). \text{ [111]}$$
$$M_S(°C)= 280°C$$
$$M_S(°F)= 536°F$$

Carbon has a large effect on the temperature range where upper and lower bainite occur. The bainite start temperature was estimated using the following empirical relationship (concentrations in wt% of given elements in solid solution in austenite) [112]:

$$B_S(°C)= 830 - 270(\%C) – 90(\%Mn) – 37(\%Ni) – 70(\%Cr) – 83(\%Mo). \text{ [112]}$$
$$B_S(°C) = 482°C$$
$$B_S(°F) = 900°F$$

The fourth set of heat treatments on 4340+ (300M) were completed to test the effects of austempering combined with HIP on the mechanical properties of the alloy. The heat treatment plan for the initial HIP + austempering screening study is shown in **Table 3.10**. The HIP cycle replaced the homogenization step and the austempering step replaced the double tempering step from the standard heat treatment plan for the alloy.

Table 3.10: Study #4: Heat Treatments for Austempering + HIP Study for 4340+ (300M) material.

	Standard Practice	**Study #4 Practice**
HIP	**-**	**1950°F for 4 Hours with 15ksi. pressure (slow vessel cool to 700°F) (Air Cool to Room from 700°F)**
Homogenize	**1675°F / 1.0 hr**	**-**
Air Cool	**Air Cool to Room Temperature**	**Air Cool to Room Temperature**
Austenitize	**1600°F / 1.0 hr**	**1600°F / 1.0 hr**
Quenching	**Water Quench at 74°F**	**Place in Molten Salt Bath at (1) 572°F or (2) 599°F**
Temper	**600°F, 4 hours Water Quench at 74°F 600°F, 4 hours Water Quench at 74°F**	**-**
Austemper	**-**	**(1)572°F or (2) 599°F for (A) 840min. or (B) 480min. Water Quench at 74°F**

The second approach to developing ultrahigh strength low alloy cast steels with increased impact toughness involves the development of a new ultrahigh strength low alloy steel, Eglin steel. Eglin steel (also denoted as ES-1) is being experimented with as a casting alloy. The lower carbon content of ES-1 steel can be expected to reach somewhat lower yield strength levels (<190 ksi) but with improved impact toughness.

3.4 Cast ES-1 Ingot Heat Treatment Experimentation

The cast ingot material provided, **Figure 3.3**, was supplied to fully characterize the transition behavior for cast + HIP ES-1 alloy under varying heat treatment conditions. The study was followed up by a study on cryo quenching and its effects on impact toughness and possible retained austenite in the cast ES-1 material. Finally, a study was carried out to quantify the effects of HIP on the porosity of the cast ingot material.

3.4.1 Initial Heat Treatment Procedure for Cast ES-1 Ingot

The ES-1 bottom poured cast ingot used in this study was obtained from the North American Hoganas Stony Creek Plant. Six 1" X 1" X 8" machined and lapped bars from this large ingot were supplied to Penn State in the as-cast conditions. Parallel heat treatment studies, not reported in this dissertation, were performed on wrought ES-1 material under contract from SAIC. The cast ingot material was melted in an induction furnace. Secondary melting was done in a vacuum degassing unit. The composition of the cast ingot is given in **Table 3.2**.

A 2^{3-1} heat treatment study, **Table 3.11**, was completed on the ES-1 material to examine the effects of HIP, homogenization, austenization temperature, and tempering temperature on the mechanical properties and impact transition behavior of cast ES-1.

Table 3.11: Study #1: Impact Transition Study for Cast ES-1 Ingot material.

Heat Treatment # 1			
Step	Temperature	Time	Cooling
Step 1A: HIP (@ 15 ksi)	2125°F (1163°C)	240 min.	Slow Vessel Cool to 700°F; Air Cool to Room Temp. from 700°F
Step 1B: Homogenize: **NONE**	-	-	-
Step 2: Austenitize	1800°F (982°C)	60 min.	Room Temp. Water Quench
Step 3: Temper	375°F (191°C)	240 min.	Room Temp. Water Quench
Heat Treatment # 2			
Step	Temperature	Time	Cooling
Step 1A: HIP (@ 15 ksi)	2125°F (1163°C)	240 min.	Slow Vessel Cool to 700°F; Air Cool to Room Temp. from 700°F
Step 1B: Homogenize: **NONE**	-	-	-
Step 2: Austenitize	1900°F (1038°C)	60 min.	Room Temp. Water Quench
Step 3: Temper	450°F (232°C)	240 min.	Room Temp. Water Quench
Heat Treatment # 3			
Step	Temperature	Time	Cooling
Step 1A: HIP	2125°F (1163°C)	4 Hours @ 15ksi.	Slow Vessel Cool to 700°F; Air Cool to Room Temp. from 700°F
Step 1B: Homogenize	2000°F (1093°C)	120 min.	Room Temp. Air Cool
Step 2: Austenitize	1800°F (982°C)	60 min.	Room Temp. Water Quench
Step 3: Temper	450°F (232°C)	240 min.	Room Temp. Water Quench
Heat Treatment # 4			
Step	Temperature	Time	Cooling
Step 1A: HIP (@ 15 ksi)	2125°F (1163°C)	240 min.	Slow Vessel Cool to 700°F; Air Cool to Room Temp. from 700°F
Step 1B: Homogenize	2000°F (1093°C)	120 min.	Room Temp. Air Cool
Step 2: Austenitize	1900°F (1038°C)	60 min.	Room Temp. Water Quench
Step 3: Temper	375°F (191°C)	240 min.	Room Temp. Water Quench

*All Homogenization, Austenization Steps were completed in the presence of Cast Iron Chunks and 4 CF/Hr. Argon.

3.4.2 Microporosity Study Heat Treatment Procedure for Cast ES-1 Ingot

To be able to quantify the effect of HIP and homogenization on microporosity on the cast ES-1 ingot material, an additional heat treatment experiment was carried out, **Table 3.12**. After heat treatment, samples were prepared metallographically and image analysis studies were conducted to quantify the effects of processing on microporosity. The data collected from the samples was pore count, pore size, and the area fraction of porosity (A_A) expressed as % porosity [113].

Table 3.12: Heat Treatments for Microporosity Study on Cast ES-1 Ingot Material.

Sample	Heat Treatment Conditions
A	As – Cast
B	HIP (2125°F, 4 hours, 15ksi.)-slow cool in vessel to 700°F- air cool to room temp. from 700°F
C	Homogenize (2125°F, 4 hours) in presence of cast iron chunks and 4 CF/Hr. argon flow- air cool to room temp.

3.4.3 Cryo Quenching and Retained Austenite Study for Cast ES-1 Ingot Material

The literature suggests that the retained austenite content of silicon-alloyed steels may play an important role in the development of toughness. The following experimental conditions (**Table 3.13**) were laid out to test the effects of cryo quenching on the impact toughness and amount of retained austenite of the cast ES-1 material. The experimental conditions were also designed to study the amount of retained austenite in the cast ES-1 material before and after cryo quenching. The sample sizes for the heat treatment were 1” X 0.5” X 0.5”.

Table 3.13: Heat Treatments for Cryo Quenching and Retained Austenite Study on Cast ES-1 Ingot Material.

Cryo Sample:			
Step	Temperature	Time	Cooling
Step 1A: HIP (@ 15 ksi)	2125°F (1163°C)	240 min.	Slow Vessel Cool to 700°F; Air Cool to Room Temp. from 700°F
Step 1B: Homogenize	2000°F (1093°C)	120 min.	Room Temp. Air Cool
Step 2: Austenitize	1900°F (1038°C)	60 min.	Room Temp. Water Quench
**After Quenching in Room Temp. Water, the samples were submerged in Liquid (N) for 6 hrs. The samples were then wared to Room Temperature in Air prior to tempering.			
Step 3: Temper	375°F (191°C)	240 min.	Room Temp. Water Quench
Non Cryo Sample:			
Step	Temperature	Time	Cooling
Step 1A: HIP (@ 15 ksi)	2125°F (1163°C)	240 min.	Slow Vessel Cool to 700°F; Air Cool to Room Temp. from 700°F
Step 1B: Homogenize	2000°F (1093°C)	120 min.	Room Temp. Air Cool
Step 2: Austenitize	1900°F (1038°C)	60 min.	Room Temp. Water Quench
Step 3: Temper	375°F (191°C)	240 min.	Room Temp. Water Quench

*All Homogenization, Austenization Steps were completed in the presence of Cast Iron Chunks and 4 CF/Hr. Argon.

3.4.4 Transition Carbide Characterization Study for ES-1 Material

The following experimental conditions (**Table 3.14**) were carried out to grow transition carbides into stable, incoherent carbides in forged ES-1 ingot material. After heat treatment, the sample was mounted and polished. Using scanning electron microscopy and EDAX, the incoherent carbides were characterized using scanning electron microscopy and EDAX.

Table 3.14: Heat Treatment for Transition Carbide Characterization Study.

Step	**Temperature**	**Time**	**Cooling**
Step 1: Homogenize	2000°F (1093°C)	120 min.	Room Temp. Air Cool
Step 2: Austenitize	1900°F (1038°C)	60 min.	Room Temp. Water Quench
Step 3: Temper	1112°F (600°C)	60 min.	Room Temp. Water Quench

3.5 Investment Cast ES-1 Screening Experiments

Initially, two 180 pound heats of investment cast ES-1 material described previously were cast for initial screening experimentation of the cast ES-1 alloy. Heat #1 was cast with a 0.10 wt % aluminum addition for deoxidation which resulted in an undesirable high aluminum content of 0.096 wt%. Heat #2 was cast with a 0.05 wt% aluminum addition for deoxidation which resulted in a 0.064 wt% final aluminum retention. Cast steel alloys should typically only possess < 0.06 wt% aluminum to prevent aluminum oxides and nitrides from hampering the mechanical properties of the material. In spite of the high aluminum, the following heat treatments (**Table 3.15**) were only carried out on the bars from heat #2 to screen the very first heat of investment cast ES-1 material for mechanical properties. The heat treatments were also designed to compare the differences in properties of a high temperature HIP cycle and a high temperature homogenization cycle mimicking the high temperature HIP cycle without pressure. In addition, the effect of removing the homogenization step in the heat treatment cycle was also studied.

Table 3.15: Heat #1: Initial Investment Cast ES-1 Screening Experiment Heat Treatments.

Heat Treatment # 1 (HIP, H, Q&T)			
Step	Temperature	Time	Cooling
Step 1A: HIP (@ 15 ksi)	2125°F (1163°C)	240 min.	Vessel Cool to 700F; Air Cool
Step 1B: Homogenize	2000°F(1093°C)	120 min.	Room Temp. Air Cool
Step 2: Austenitize	1900°F(1038°C)	60 min.	Room Temp. Water Quench
Step 3: Temper	375°F(191°C)	240 min.	Room Temp. Water Quench
Heat Treatment # 2 (HIP, Q&T)			
Step	Temp	Time	Cooling
Step 1: HIP (@ 15 ksi)	2125°F (1163°C)	240 min.	Vessel Cool to 700°F; Air Cool to Room Temperature
Step 2: Austenitize	1900°F (1038°C)	60 min.	Room Temp. Water Quench
Step 3: Temper	375°F(191°C)	240 min.	Room Temp. Water Quench
Heat Treatment # 3 (H, H, Q&T)			
Step	Temperature	Time/Cooling	
Step 1A: Homogenize	2125°F (1163°C)	Insert Samples at Room Temperature - Heat up Furnace to 2125°F (1 hour 45 minutes); hold for 240 min.; Furnace Cool to 700°F; Air Cool to Room Temperature	
Step 1B: Homogenize	2000°F(1093°C)	120 min.	Room Temp. Air Cool
Step 2: Austenitize	1900°F (1038°C)	60 min.	Room Temp. Water Quench
Step 3: Temper	375°F(191°C)	240 min.	Room Temp. Water Quench
Heat Treatment # 4 (H, Q&T)			
Step	Temperature	Time/Cooling	
Step 1A: Homogenize	2125°F (1163°C)	Insert Samples at Room Temperature- Heat up Furnace to 2125°F (1 hour 45 minutes); hold for 240 min.; Furnace Cool to 700°F; Air Cool to Room Temperature	
Step 2: Austenitize	1900°F (1038°C)	60 min.	Room Temp. Water Quench
Step 3: Temper	375°F (191°C)	240 min.	Room Temp. Water Quench
Heat Treatment # 5 (H, Q&T)			
Step	Temperature	Time	Cooling
Step 1: Homogenize	2000°F(1093°C)	120 min.	Room Temp. Air Cool
Step 2: Austenitize	1900°F (1038°C)	60 min.	Room Temp. Water Quench
Step 3: Temper	375°F(191°C)	240 min.	Room Temp. Water Quench
Heat Treatment # 6 (Q&T)			
Step	Temperature	Time	Cooling
Step 1: Austenitize	1900°F (1038°C)	60 min.	Room Temp. Water Quench
Step 2: Temper	375°F(191°C)	240 min.	Room Temp. Water Quench

*All Homogenization, Austenization Steps were completed in the presence of Cast Iron Chunks and 4 CF/Hr. Argon.

After the above heat treatments were carried out and tensile + RT & -40°F Charpy properties were tested, it was evident that the mechanical properties likely suffered as a result of

the high aluminum retention. Thus, heat #3 was poured with a tightly controlled deoxidation process. Heat treatments 1-4 from **Table 3.15** were carried out on the bars from heat #3 to screen the mechanical properties of investment cast ES-1with a composition with improved aluminum deoxidation practices.

3.6 Mechanical Testing Procedures

The heat treatment experiments outlined in sections 3.3 through 3.5 for the UHSLA cast steels were followed by mechanical property testing where room temperature tensile properties and impact properties at various temperatures between -100°F and 212°F were gathered for the treatments outlined above. Depending on the amount of material available for heat treatment, between 1 and 3 test specimens for tensile and impact properties were tested for each treatment condition. Tensile properties were evaluated using standard sub-size 0.250 in. round tensile specimens according to ASTM E8 specifications, **Figure 3.6**. Full size Charpy specimens were also machined according to ASTM E23 specifications, **Figure 3.7**. Wire EDM was used to produce the standard Charpy specimen notch.

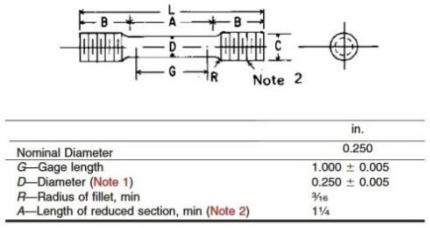

	in.
Nominal Diameter	0.250
G—Gage length	1.000 ± 0.005
D—Diameter (Note 1)	0.250 ± 0.005
R—Radius of fillet, min	3/16
A—Length of reduced section, min (Note 2)	1¼

Figure 3.6: Sub-sized tensile specimen used in testing (ASTM E8).

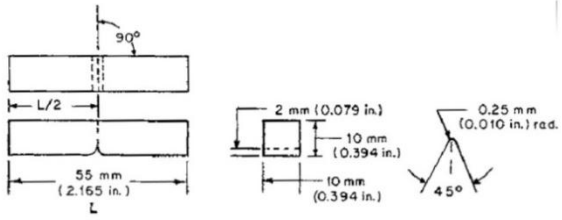

Figure 3.7: Charpy specimen dimensions (ASTM E23).

Westmoreland Mechanical, Testing, and Research, Youngstown, PA, performed both the machining and mechanical testing of the samples. Rockwell C hardness (HRC) values were taken from the Charpy samples. Three Rockwell hardness readings were taken from each sample that was measured.

3.7 Microstructure Evaluation

Metallographic specimens for selected heat treatment schedules for the 4340+ and ES-1 alloys outlined above were prepared by polishing and etching with 2% nital, 6% nital, or picral base etchants (**Table 3.16**). Using a Nikon optical microscope in the Penn State Center for

Innovate Sintered Products (CISP) lab, the unetched and etched microstructures were photographed and evaluated at magnifications ranging from 50X to 1000X.

Table 3.16: Metallographic Reagents for Steel [114].

Etchant	Composition
Nital (2%)	2 mL HNO_3 (Nitric Acid) 98 mL Ethanol
Nital (6%)	6 mL HNO_3 (Nitric Acid) 94 mL Ethanol
Picral	4 g Picric Acid 100 mL Ethanol

3.7.1 Pore Size and Pore Reduction Quantification

Using the Nikon optical microscope in the Penn State CISP lab, the pore size, pore count, and % porosity measurements could be taken with Clemex Vision Professional Edition (PE) image analysis software. The statistics that were tracked by the Clemex Vision PE software were: number of pores per image frame, individual pore size (in microns), and the area fraction of pores (A_A) or % porosity (expressed as a fraction of the frame area) [113]. The methods for expressing the pore size and pore reduction measurements were adopted from similar studies on nickel based superalloys [113, 115]. For each of the 3 samples that were characterized, 9 frames were captured and pore statistics were collected and inputted to Microsoft Excel. The statistics (average and standard deviation) reported in the results section were calculated from the 9 frames captured at 100X from the 0.5" X 0.5" cross sections analyzed for each sample.

3.8 Fractograph Characterization

Fracture surface images were taken with an SEM for selected 4340+ and ES-1 alloy samples. Secondary electron images from a Philips XL30 SEM were used for the analysis. The fracture surface images were taken on samples tested at room temperature for the cast 4340+ alloy; the fracture surface images were taken on samples tested at -40°F for the ES-1 alloy. The fracture surfaces were studied for regions of brittle quasi-cleavage fracture and ductile dimpled

rupture fracture. When particles of interest were located on the fracture surface, SEM-EDAX work was completed to identify the composition of the particles.

3.9 Crystallographic Characterization

Metallographically prepared specimens for selected heat treatment schedules for the 4340+ and ES-1 alloys were screened for retained austenite in the samples. A Panalytical Xpert Pro MPD Theta-Theta Diffractometer at the Penn State Material Characterication Lab (MCL) was used for the analysis. The radiation source for the diffractometer was a copper long fine focus; 60kV, 2.2 kW. The percentages of retained austenite were automatically determined from the resultant x-ray scans based on peak area measurements [116].

3.10 Impact Transition Curves

Charpy impact transition curves (Charpy v-notch impact toughness vs. temperature) were constructed using Charpy v-notch impact data at the following temperatures: -100°F, 65°F, -40°F, 0°F, +32°F, +74°F, +140°F, +212°F. Within Microsoft Excel v. 2007, an order 3 polynomial trendline was used as the curve fit for the data points.

3.11 Modeling Studies

The final experiment that was carried out in this study was the modeling of microsegregation reduction during HIP and homogenization of UHSLA steel castings. Chapter 4 will outline the modeling work and Chapter 5 will display the results of the modeling experimentation and results for all experimental procedures laid out in Chapter 3.

Chapter 4

Modeling Microsegregation Reduction in USHLA Steel Castings

Throughout the literature review, researchers experimented with increased austenization and homogenization temperatures to improve properties degraded by segregation of alloying elements during solidification, but none of the researchers did a comprehensive study to estimate the microsegregation reductions that are possible during experimental heat treatments. This is an area of steel casting research that needed development work for UHSLA cast steels. Initial screening experiments in the current study showed signs of higher homogenization temperatures resulting in additional impact toughness. The following chapter will show how a classical diffusion model from the literature was adapted to estimate both mathematically and visually the microsegregation reduction profiles of substitutional alloying elements during heat treatment of UHSLA cast steels.

4.1 Diffusion in Steel Castings

The substitutional alloying elements studied in this work include the substitutional atoms Mo, Cr, W, Ni, and Mn that are present in UHSLA cast steels. Diffusion of substitutional atoms is via vacancy diffusion (**Figure 4.1**). An atom leaves its current lattice site to fill a nearby vacancy in the lattice [79]. Since substitutional atoms are much larger than the interstitial atoms, such as carbon, vacancy diffusion occurs at a much slower pace than carbon diffusion. A larger amount of thermal activation is required to move substitutional atoms from one lattice site to another when compared to the movement of smaller interstitial atoms (**Figure 4.2**). However, limited movement or diffusion of substitutional atoms can be expected during high temperature homogenization, potentially reducing the microsegregation of alloying elements occurring between the dendrite cores and the interdendritic regions resulting from initial solidification.

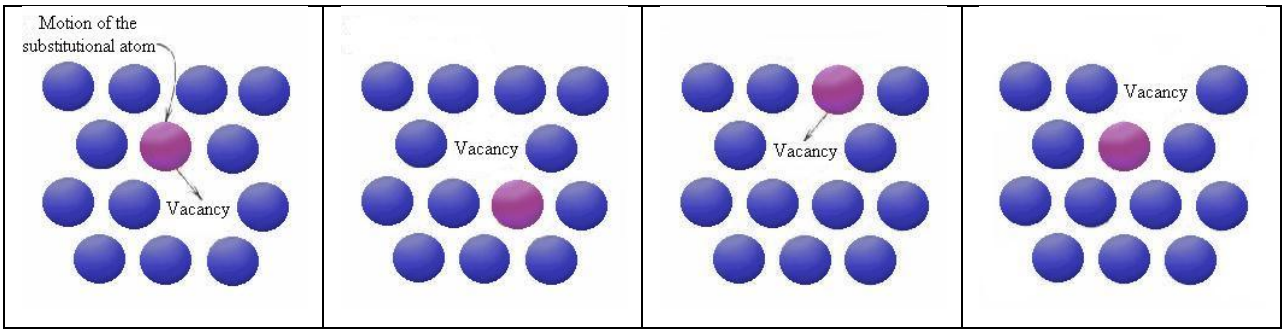

Figure 4.1: The progression (from left to right) of substitutional atom diffusion via vacancy diffusion [117].

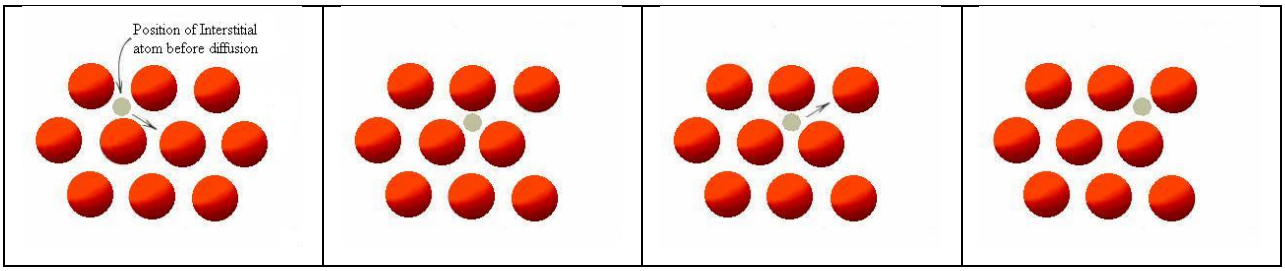

Figure 4.2: The progression (from left to right) of carbon diffusion in steel via interstitial diffusion [117].

Classical diffusion modeling can be further developed and used to estimate the amount of temperature and time required for adequate diffusion of these alloying elements during heat treatment. The initial solidification cooling rate of a casting is expected to play an important role in the development of the initial segregation profiles in the casting during solidification processing. Heavy section castings solidify at slow cooling rates resulting in both coarser dendrite arm spacing and more alloy segregation between the dendrite cores and the interdendritic regions. Thus the required diffusion distances for segregation mitigation are greatly increased in heavy section castings requiring more extensive homogenization or HIP cycles.

4.2 Microsegregation Reduction Modeling

For the case of simple diffusion in single-phase alloys, Flemings [51] developed a simple model of the micro-segregation present in the dendrites. The index he uses to discuss micro-segregation is called the index of residual micro-segregation (δ) :

$$\delta = \frac{C_M - C_m}{C_M^0 - C_m^0} \qquad \textbf{Equation 4.1}$$

Where:
C_M = the maximum solute concentration of the element in inter-dendritic spaces at time t,

C_m = the minimum solute concentration of element in the center of the dendrite arm at time t,

C_M^0 = maximum initial concentration of the element in inter-dendritic spaces,

C_m^0 = minimum initial concentration element in the center of the dendrite arm (both at time zero)

After any thermal cycle resulting in diffusion, δ will have some intermediate value between zero (0%) and one (100%) [118]. If homogenization is sufficient to completely (100%) remove solidification segregation, then $\delta = 0$. To optimize homogenization during heat treatment, it will be important to determine the value of δ needed to develop necessary mechanical properties. In addition, it will be important to know the temperature and time parameters that are necessary to achieve the necessary δ values.

By assuming a sinusoidal distribution of the concentration of the element across the interdendritic and the secondary dendrite arms, Flemings [51] describes the appropriate solution for the index of residual micro-segregation as:

$$\delta = \exp\left(-\pi^2 Dt/l_0^2\right) \qquad \textbf{Equation 4.2}$$

Where:
D = the diffusivity constant,

t = time,

l_0= half of the secondary dendrite arm spacing (DAS)

According to the work done by Flemings, interstitial carbon atoms are completely homogenized by the time a low-alloy steel reaches 900°C (1652°F) for any typical casting dendrite arm spacing. However, Flemings predicted that significantly longer times and higher temperatures are expected to be necessary to mitigate the segregation of other alloying elements. In fact, Flemings speculates that even at a temperature as high as 1100°C (2012°F), it is likely that only carbon is completely homogenized. For the common substitutional elements of concern in steel (Ni, Mn, Cr, Mo), little homogenization has been reported to occur below 1100°C (2012 °F) [51]. Flemings theorizes that at secondary dendrite arm spacings (DAS) ≥ 200 μm, practically no homogenization can be achieved ($\delta \geq 0.9$) even at homogenization temperatures greater than 1300°C (2372°F) for one hour. The Flemings model used only simple

boundary conditions and did not fully estimate the complex microsegregation profiles present in the dendritic areas of steel castings.

The work by Reill et al. [119] allows for estimation of inter-diffusion concentration in amorphous thin films. Instead of looking solely at a single concentration step, the work by Reill et al. is helpful for estimating inter-dendritic microsegregation because it estimates a periodically modulated composition distribution [119, 120]. In this work, the composition estimates are made layer by layer, similar to neighboring interdendritic and dendritic compositions.

For multilayer films, assuming a constant diffusion coefficient, D, the concentration profile (C_a) of element (a) is given by [119]:

$$C_a(z,t) = \alpha + \sum_m \beta_m \exp\left[-(\pi/H)^2 m^2 Dt\right] * \sin(m\pi z/H) \qquad \textbf{Equation 4.3}$$

Where:
H= the layer thickness,

2H= the length of periodicity,

t=the diffusion time,

z= the coordinate normal to the film plane

α and β_m= the Fourier coefficients describing the initial concentration profile of adjacent films prior to diffusion.

Reill et al. explained that during inter-diffusion, the exponential functions with $m > 1$ decay very fast with time. In addition, if an initially square wave is assumed prior to the start of diffusion, the contribution of the terms with $m > 1$ becomes very small for typical diffusion times where $(\pi/H)^2 Dt \geq 0.3$ [119]. Therefore, for most practical cases only the first term of the series expansion from **Eq. 4.3** is important. In a dendritic structure, the inter-diffusion from heat treatments eventually leads to a sinusoidal concentration distribution given by the first term in the series expansion of **Eq. 4.3**. However, the solution of this diffusion expression requires a periodical concentration distribution prior to the start of diffusion. The amplitude of this resultant sinusoidal distribution, ΔC_a, can be expressed as:

$$\Delta C_a = \beta_1 * \exp\left[-(\pi/H)^2 Dt\right] \qquad \textbf{Equation 4.4}$$

Fredriksson and Åkerlind [42] provide a similar approximation to that of **Eq. 4.3**, which can be used to model dendritic segregation of cast materials. They state that while the initial

concentration distribution is much more complicated than a simple sine wave segregation assumption, it is possible to use either a rectangular or a sine wave approximation. This is because after a short diffusion time, only the fundamental tone of the concentration remains, independent of the initial shape, as explained by Fredriksson's solution to Fick's Second Law for Homogenization [118]. Prior to homogenization, the alloy concentration x as a function of an arbitrary distance y can be written as:

$$C_x = x_0 + \left(\frac{x_0^M - x_0^m}{2}\right) * sin\left(\frac{2\pi y}{\lambda_{prim}}\right) \qquad \textbf{Equation 4.5}$$

Where:

x_0 = the average concentration throughout the material,

λ = the secondary dendrite spacing (DAS),

x_0^M = the maximum concentration of solute,

x_0^m is the minimum concentration of solute

This initial concentration then has an amplitude before heat treatment given by:

$$\text{Amplitude} = \left(\frac{x_0^M - x_0^m}{2}\right) \qquad \textbf{Equation 4.6}$$

Frederiksson and Ackerlind [42] showed that by solving the partial differential in Fick's second law (**Eq. 2.2**) and combining it with the concentration equation (**Eq. 4.5**), it is possible to determine the concentration profile for the fundamental wave after homogenization. This final solution can be expressed as [42]:

$$C_x = x_0 + \left(\frac{x_0^M - x_0^m}{2}\right) * exp\left(-\frac{4\pi D}{\lambda_{prim}^2}\right) sin\left(\frac{2\pi y}{\lambda_{prim}}\right) \qquad \textbf{Equation 4.7}$$

Where:

x_0 = the average concentration throughout the material,

x_0^M = the maximum concentration of solute,

x_0^m = the minimum concentration of solute,

λ_{prim} = the secondary dendrite arm spacing (DAS)

It should be noted that this solution describes what happens to each alloy component independently of the others. As reflected in the equation above, the arbitrary sine-shaped concentration profile will remain while the amplitude of the sine curve decreases [42].

Over a dendritic structure, when comparing **Eq. 4.7** to **Eq. 4.3** it becomes apparent that $\alpha = x_0$ and $\beta_m = \left(\frac{x_0^M - x_0^m}{2}\right)$, describing the initial concentration for a dendritic structure. Relating to the current development work on the next generation of UHSLA cast steels, because of this direct agreement between equations **Eq. 4.3** (adapted for thin films) and **Eq. 4.7** (for general dendritic microsegregation), it should be possible to accurately model the concentration profile of microsegregation of alloying elements throughout the heat treatment of UHSLA cast steels. With that said, the selection of accurate diffusivity coefficients (D_0) for alloying elements in UHSLA cast steels will be extremely important for accurate diffusion distance predictions.

4.3 Diffusivity Coefficient Selection

Since the accuracy of the output of any microsegregation model depends on the accuracy of the inputs to the model, it is important to ensure accurate model input data. Similar diffusivity constant and activation energy values in the literature for given alloying elements in iron differ greatly from study to study. In some cases, the diffusivity coefficients differ by orders of magnitude (far beyond the differences between activation energies) (**Tables 2.11-2.15**). Since the diffusion constant will be directly impacted by the diffusivity coefficient that is selected, the diffusion constants were plotted versus temperature to examine the differences in D caused by the differences in the diffusivity coefficients (D_0) for the substitutional alloying elements being studied (Mo, W, Mn, Cr, Ni). **Figure 4.3** shows the plot of tungsten diffusion constants versus temperature; each data series is plotted based on unidirectional diffusivity coefficient (D_0) values for tungsten in fcc iron reported in the literature. From the plots, representative values were chosen as the source for the respective diffusivity coefficient and activation energy values to be inputted to estimate the diffusion constant for each alloying element. The plot of tungsten diffusion constant data shown in **Figure 4.3** shows the characteristic behavior of all of the alloying element plots for D_o and Q values reported in the literature for the diffusion temperature range of interest. To help explain how a "most representative value" was chosen for the diffusivity coefficient, **Figure 4.3** should be examined. The diffusivity coefficient value from source [57] was chosen as the most representative value for tungsten diffusivity as it creates the midpoint curve between the upper and lower bounds on the range of plots of different different diffusivity coefficients and activation energies on the diffusion constant (D) vs. Temperature plot. This selection method was carried out for the remainder of the alloying element diffusivity

coefficients shown in **Tables 2.11 – 2.15**. **Table 4.1** displays the diffusivity coefficient and activation energy values that were selected as the "most representative values" for each of the alloying elements that were modeled.

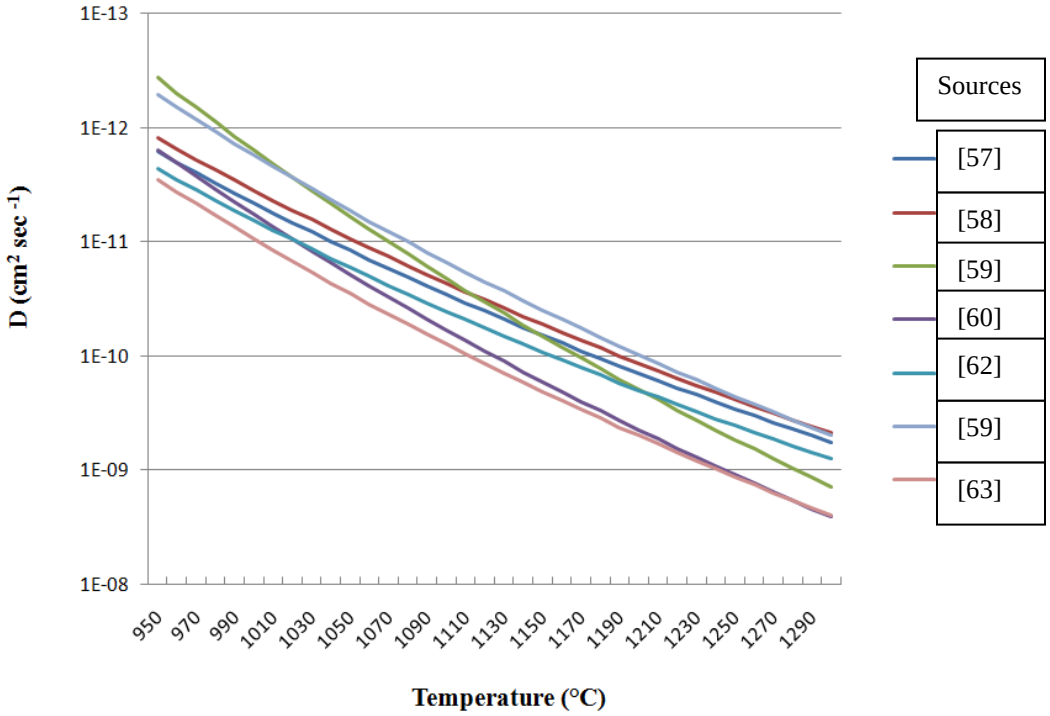

Figure 4.3: Diffusion Constant (D) **vs.** Temperature (°C) showing the dependence of the diffusion constant (D) for different estimates of diffusivity coefficients (D_0) and activation energy (Q) for tungsten diffusion in FCC iron.

Even though D_o values differed by orders of magnitude in the literature, the D values based on both the D_o and corresponding Q estimates were very similar over the temperature range of interest.

Table 4.1: Diffusivity coefficients (D_0) and activation energies (Q) that were selected for use in the diffusion model to estimate the diffusivity constant (D).

Element (in γ-Fe)	D_0 (cm^2/sec)	Q (kJ/mole)	Reference
Mo	0.0684	246.85	[56]
W	0.13	267.4	[57]
Mn	0.038	246.85	[53]
Ni	0.063	243	[67]
Cr	0.77	280.5	[73]

4.4 Model Implementation

Using Microsoft Excel, the diffusion constant (**Eq. 2.5**) was expressed as:

$$D = D_0 * \exp\left(\frac{-Q}{kT}\right) \quad \textbf{Eq.2.5}$$

where:

D_0 = diffusivity coefficient (cm^2/sec)

Q = activation energy per particle (eV)

T = temperature (K)

k = Boltzmann constant 8.614E-5 (eVK^{-1}) [used in place of R for pure particles]

Individual values for the diffusivity constant (D_0) and activation energy (Q) for the elements W, Cr, Mo, Ni, and Mn in fcc iron were inputted. These are the primary alloying elements in the ES-1 and 4340+ steel. The model could easily be adapted in the future to include additional alloying elements. The temperature (T) and time (t) for common heat treatment cycles and cycles for high strength steel castings could readily be inputted to the diffusion model.

The second part of the modeling work consisted of coding the profile for the fundamental wave after heat treatment. Building off of what was learned from Reill et al. [119] and Fredriksson and Ackerlind [42], (**Eq. 4.8**) was coded into Microsoft Excel to estimate dendritic microsegregation reduction in UHSLA steel castings under various heat treatment conditions, while also visually representing the microsegregation as:

$$C_a(z,t) = \alpha + \sum_m \beta_m \exp\left[-(\pi/H)^2 m^2 D t\right] * \sin(m\pi z/H) \quad \textbf{Equation 4.3}$$

$$C_x = x_0 + \left(\frac{x_0^M - x_0^m}{2}\right) * exp\left(-\frac{4\pi D}{\lambda_{prim}^2}\right) sin\left(\frac{2\pi y}{\lambda_{prim}}\right) \quad \textbf{Equation 4.7}$$

$$C_x = \left(\frac{x_0^D + x_0^{ID}}{2}\right) + \left(\frac{x_0^{ID} - x_0^D}{2}\right) * \exp\left[-\left(\frac{\pi}{(\lambda_{prim}/2)}\right)^2 * D * \mathrm{t} * 60\right] * sin\left(\frac{\pi y}{(\lambda_{prim}/2)}\right) \quad \textbf{Equation 4.8}$$

Where:

x_0^D = initial concentration of alloying element in the dendrite of the steel.

x_0^{ID} = initial concentration of alloying element in the inter-dendritic region of the steel.

λ_{prim} = secondary dendrite arm spacing (microns)

D = the diffusivity constant from **Eq. 4.3** at the temperature (T) in **Eq. 4.3**

t = the time (in minutes) spent at the temperature (T) in **Eq. 4.3**

y = the location (arbitrary distance) at which the concentration is determined (microns)

Since quantitative estimates of the initial concentration of alloying elements in the initial dendrite core and in the interdendritic regions are difficult to accurately determine in low alloy steels, an assumption regarding the initial microsegregation profile of the alloying elements in the UHSLA cast steel after solidification had to be made. The assumption made was that the alloying elements in the dendritic and inter-dendritic regions were chosen to be +/- 0.5 wt % from given alloy nominal concentrations. For future experimentation, quantitative results from EPMA or other elemental quantification methods should be inputted to the model. An EPMA validation and verification analysis was initially measured for the cast steel alloys in this study; however only the first of five samples were analyzed (**See Appendix A.1**). The expected micro segregation profile in castings depends not only on the partition ratio of the specific alloying element, but also on the solidification cooling rate which controls the secondary dendrite arm spacing (DAS). Representative DAS values were used in this analysis ranging from 20μm to 200μm representative of the DAS expected for thin section and heavy section steel castings respectively [121].

The model was developed to estimate overall diffusion effects from either single or multi-stage heat treatments (e.g. HIP + homogenization + austenization + tempering). At each stage of the heat treatment process, a fixed temperature (T) and a fixed amount of time at temperature (t) were chosen. It is assumed that the diffusion constant (D) remains the same throughout the heat treatment process, a reasonable assumption. The model also assumes that the width of the interdendritic region between two secondary dendrite arms is equivalent to the thickness of a secondary dendrite arm. The composition of the cast alloy at a distance y can be determined after each stage or after the entire heat treatment by simply summing up the increase or decrease in alloy concentration occurring during each stage of the heat treatment process. This multi stage model can be expressed as a summation of the diffusion occurring at each of the individual steps in the heat treatment process.

Cumulative Concentration (X_{CC})=

$$\sum_{i=1}^{n} D_i t_i$$

Equation 4.9

By simply incorporating the summation into **Eq. 4.8** above, the cumulative concentration, X_{CC}, can be estimated for any area in the dendritic structure after each and all of the heat treatment (diffusion) steps included in an entire heat treatment cycle.

4.5 Model Visualization

The reduction in segregation from heat treatment cycles can be represented with dendritic and inter-dendritic concentration profiles as shown in **Figure 4.4**. **Figure 4.5** illustrates a representative concentration profile after a 4 stage heat treatment cycle for a steel casting.

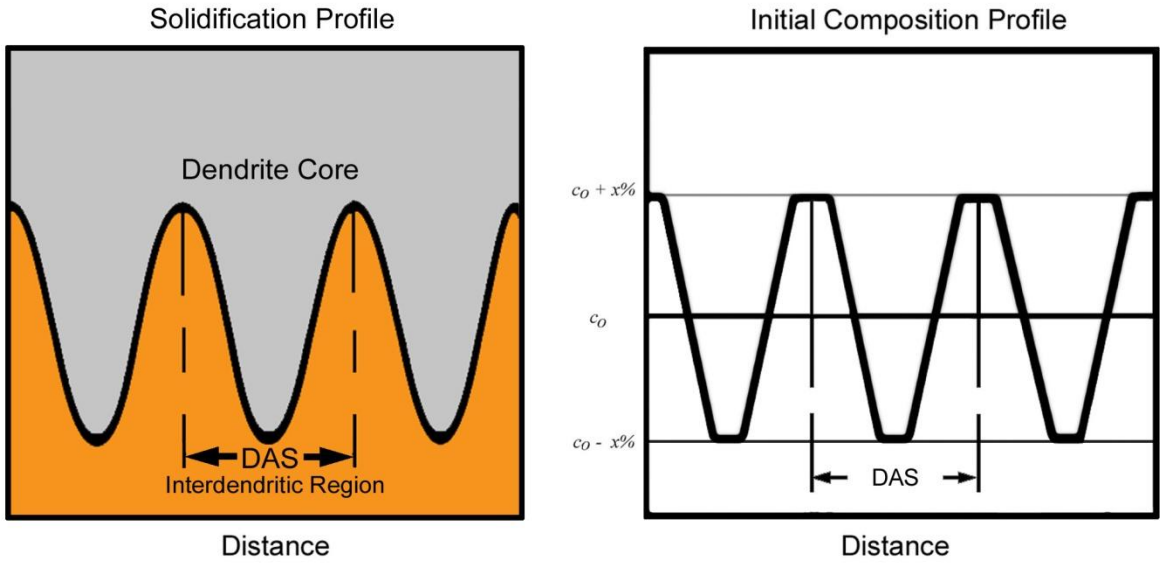

Figure 4.4: Representation of the theoretical concentration profile for the dendritic and interdendritic regions of a steel casting after solidification.

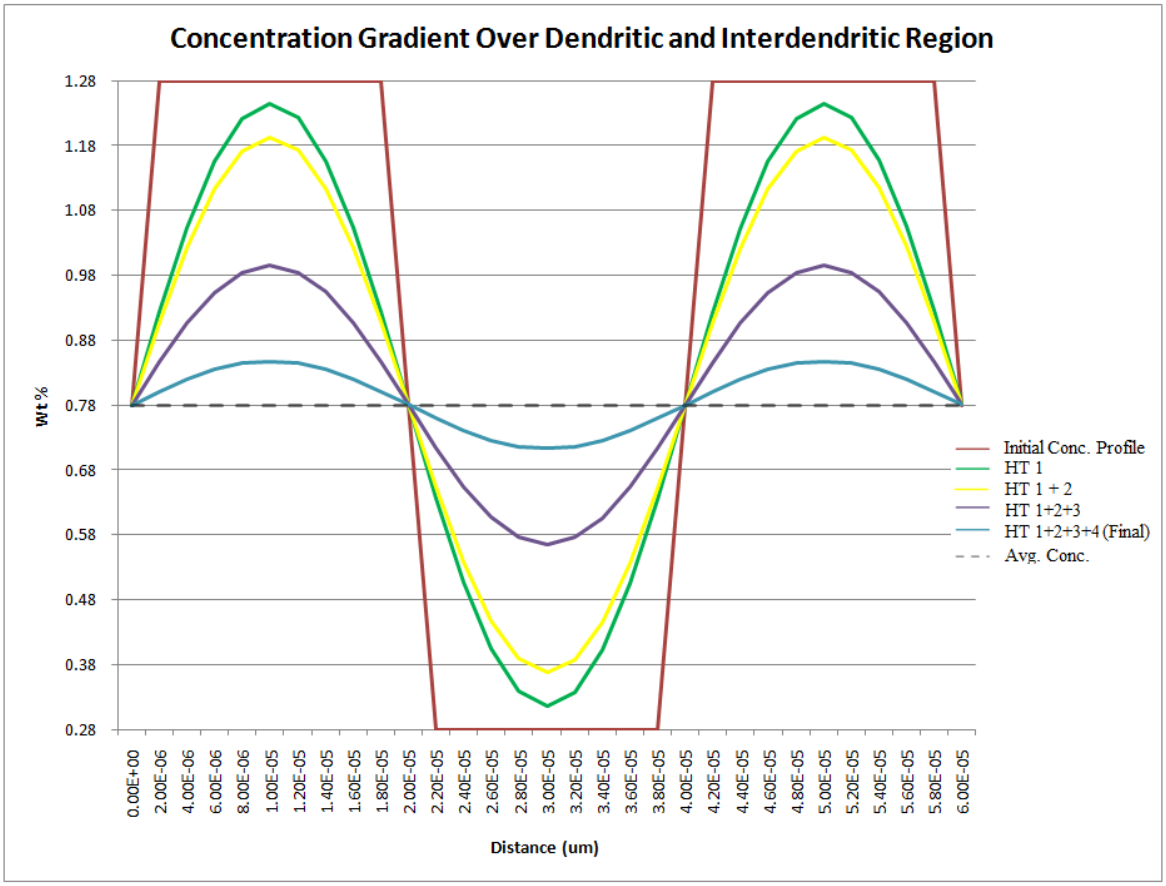

Figure 4.5: Representation of alloy concentration profiles during and after heat treatment of a casting with a given DAS.

4.6 Model Estimation Results

Using **equations 2.5**, **4.8**, and **4.9**, the extent of micro-segregation reduction (% reduction) was estimated for Cr, Mo, Ni, Mn, and W during the heat treatment of ultrahigh strength low alloy cast steels for both simulated and actual heat treatments used in this study. The microsegregation reduction estimates presented in this section are estimates of the % reduction in microsegregation during homogenization and HIP of UHSLA cast steels.

4.6.1 Microsegregation Reduction During Homogenization/ HIP

Using the model, the extent of micro-segregation reduction (% reduction) was estimated for Cr, Mo, Ni, Mn, and W at various DAS (20, 80, 200 µm) during homogenization/HIP temperatures ranging from 1500°F to 2200°F (816°C to 1204°C), and homogenization/HIP times ranging from 2 to 6 hours. A summary of these results of each DAS can be seen in **Tables 4.2 – 4.6**. These percent reductions in segregation are based on the initial concentrations of alloying

elements in the dendritic and inter-dendritic regions of +/- 0.5 wt % from the nominal alloying element concentration unless otherwise noted.

Table 4.2: Summary of Cr Segregation Reduction after Homogenization at various times, temperatures, and DAS.

Time (min.)	Percent Reduction in Cr Segregation							
	$(x_0^D = 2.09wt\%;\ x_0^{ID} = 3.09wt\%;\ x_0 = 2.59wt\%)$							
	20 µm DAS							
	1500°F	1600°F	1700°F	1800°F	1900°F	2000°F	2100°F	2200°F
	816°C	871°C	927°C	982°C	1038°C	1093°C	1149°C	1204°C
120	1%	4%	11%	29%	61%	90%	100%	100%
240	2%	7%	21%	50%	85%	99%	100%	100%
360	3%	10%	30%	65%	94%	100%	100%	100%
Time (min.)	80 µm DAS							
	1500°F	1600°F	1700°F	1800°F	1900°F	2000°F	2100°F	2200°F
	816°C	871°C	927°C	982°C	1038°C	1093°C	1149°C	1204°C
120	< 1%	< 1%	1%	2%	6%	13%	28%	51%
240	< 1%	< 1%	1%	4%	11%	25%	49%	76%
360	< 1%	1%	2%	6%	16%	35%	63%	88%
Time (min.)	200 µm DAS							
	1500°F	1600°F	1700°F	1800°F	1900°F	2000°F	2100°F	2200°F
	816°C	871°C	927°C	982°C	1038°C	1093°C	1149°C	1204°C
120	< 1%	< 1%	< 1%	< 1%	1%	2%	5%	11%
240	< 1%	< 1%	< 1%	1%	2%	4%	10%	21%
360	< 1%	< 1%	< 1%	1%	3%	7%	15%	29%

Table 4.3: Summary of Mo Segregation Reduction after Homogenization at various times, temperatures, and DAS.

Time (min.)	Percent Reduction in Mo Segregation ($x_0^D = 0.00wt\%;\ x_0^{ID} = 0.80wt\%;\ x_0 = 0.40wt\%$)							
	20 μm DAS							
	1500°F	1600°F	1700°F	1800°F	1900°F	2000°F	2100°F	2200°F
	816°C	871°C	927°C	982°C	1038°C	1093°C	1149°C	1204°C
120	1%	3%	8%	23%	51%	83%	99%	100%
240	1%	5%	16%	40%	76%	97%	100%	100%
360	2%	8%	23%	54%	88%	100%	100%	100%
Time (min.)	80 μm DAS							
	1500°F	1600°F	1700°F	1800°F	1900°F	2000°F	2100°F	2200°F
	816°C	871°C	927°C	982°C	1038°C	1093°C	1149°C	1204°C
120	< 1%	< 1%	1%	2%	4%	10%	23%	43%
240	< 1%	< 1%	1%	3%	9%	20%	40%	68%
360	< 1%	< 1%	2%	5%	13%	28%	54%	82%
Time (min.)	200 μm DAS							
	1500°F	1600°F	1700°F	1800°F	1900°F	2000°F	2100°F	2200°F
	816°C	871°C	927°C	982°C	1038°C	1093°C	1149°C	1204°C
120	< 1%	< 1%	< 1%	< 1%	1%	2%	4%	9%
240	< 1%	< 1%	< 1%	1%	1%	3%	8%	17%
360	< 1%	< 1%	< 1%	1%	2%	5%	12%	24%

Table 4.4: Summary of Mn Segregation Reduction after Homogenization at various times, temperatures, and DAS.

Time (min.)	Percent Reduction in Mn Segregation ($x_0^D = 0.28wt\%;\ x_0^{ID} = 1.28wt\%;\ x_0 = 0.78wt\%$)							
	20 μm DAS							
	1500°F	1600°F	1700°F	1800°F	1900°F	2000°F	2100°F	2200°F
	816°C	871°C	927°C	982°C	1038°C	1093°C	1149°C	1204°C
120	< 1%	1%	5%	13%	33%	63%	90%	99%
240	1%	3%	9%	25%	55%	86%	99%	100%
360	1%	4%	14%	35%	70%	95%	100%	100%
Time (min.)	80 μm DAS							
	1500°F	1600°F	1700°F	1800°F	1900°F	2000°F	2100°F	2200°F
	816°C	871°C	927°C	982°C	1038°C	1093°C	1149°C	1204°C
120	< 1%	< 1%	< 1%	1%	2%	6%	13%	27%
240	< 1%	< 1%	1%	2%	5%	12%	25%	47%
360	< 1%	< 1%	1%	3%	7%	17%	35%	61%
Time (min.)	200 μm DAS							
	1500°F	1600°F	1700°F	1800°F	1900°F	2000°F	2100°F	2200°F
	816°C	871°C	927°C	982°C	1038°C	1093°C	1149°C	1204°C
120	< 1%	< 1%	< 1%	< 1%	< 1%	1%	2%	5%
240	< 1%	< 1%	< 1%	< 1%	1%	2%	5%	10%
360	< 1%	< 1%	< 1%	< 1%	1%	3%	7%	14%

Table 4.5: Summary of Ni Segregation Reduction after Homogenization at various times, temperatures, and DAS.

Time (min.)	Percent Reduction in Ni Segregation ($x_0^D = 0.5wt\%;\ x_0^{ID} = 1.5wt\%;\ x_0 = 1.0wt\%$)							
	20 μm DAS							
	1500°F	1600°F	1700°F	1800°F	1900°F	2000°F	2100°F	2200°F
	816°C	871°C	927°C	982°C	1038°C	1093°C	1149°C	1204°C
120	< 1%	1%	3%	11%	31%	65%	94%	100%
240	< 1%	2%	7%	21%	52%	87%	100%	100%
360	1%	3%	10%	30%	67%	96%	100%	100%
Time (min.)	80 μm DAS							
	1500°F	1600°F	1700°F	1800°F	1900°F	2000°F	2100°F	2200°F
	816°C	871°C	927°C	982°C	1038°C	1093°C	1149°C	1204°C
120	< 1%	< 1%	< 1%	< 1%	2%	6%	16%	34%
240	< 1%	< 1%	< 1%	1%	5%	12%	29%	56%
360	< 1%	< 1%	1%	2%	7%	18%	40%	71%
Time (min.)	200 μm DAS							
	1500°F	1600°F	1700°F	1800°F	1900°F	2000°F	2100°F	2200°F
	816°C	871°C	927°C	982°C	1038°C	1093°C	1149°C	1204°C
120	< 1%	< 1%	< 1%	< 1%	< 1%	1%	3%	6%
240	< 1%	< 1%	< 1%	< 1%	1%	2%	5%	12%
360	< 1%	< 1%	< 1%	< 1%	1%	3%	8%	18%

Table 4.6: Summary of W Segregation Reduction after Homogenization at various times, temperatures, and DAS.

Time (min.)	Percent Reduction in W Segregation							
	$(x_0^D = 0.5wt\%;\ x_0^{ID} = 1.5wt\%;\ x_0 = 1.0wt\%)$							
	20 μm DAS							
	1500°F	1600°F	1700°F	1800°F	1900°F	2000°F	2100°F	2200°F
	816°C	871°C	927°C	982°C	1038°C	1093°C	1149°C	1204°C
120	< 1%	< 1%	2%	7%	19%	42%	75%	96%
240	< 1%	1%	4%	13%	34%	67%	94%	100%
360	< 1%	2%	6%	19%	46%	81%	98%	100%
Time (min.)	80 μm DAS							
	1500°F	1600°F	1700°F	1800°F	1900°F	2000°F	2100°F	2200°F
	816°C	871°C	927°C	982°C	1038°C	1093°C	1149°C	1204°C
120	< 1%	< 1%	< 1%	< 1%	1%	3%	8%	18%
240	< 1%	< 1%	< 1%	< 1%	3%	7%	16%	33%
360	< 1%	< 1%	< 1%	2%	4%	10%	23%	45%
Time (min.)	200 μm DAS							
	1500°F	1600°F	1700°F	1800°F	1900°F	2000°F	2100°F	2200°F
	816°C	871°C	927°C	982°C	1038°C	1093°C	1149°C	1204°C
120	< 1%	< 1%	< 1%	< 1%	< 1%	1%	2%	3%
240	< 1%	< 1%	< 1%	< 1%	< 1%	1%	3%	6%
360	< 1%	< 1%	< 1%	< 1%	1%	2%	4%	9%

From **Tables 4.2 – 4.6**, it is evident that at large DAS representative of large casting section sizes (slow solidification cooling rates), it becomes increasingly more difficult to reduce micro-segregation through heat treatment. At very small DAS of 20 μm, it would still take 4 hours at 2100°F (1149°C) to achieve a 90%+ reduction in microsegregation for tungsten. For thicker sections, DAS of 80 μm, it would take 6 hours at 2200°F (1204°C) to achieve just a 45% reduction in W micro-segregation. Even for castings with a smaller section size and faster cooling rate (i.e. DAS of 20-40 μm), homogenization treatments of 2000°F (1093°C) or above for at least 4 hours are necessary to achieve a 90%+ reduction in substitutional alloying element micro-segregation.

4.6.2 Diffusion Model Verification

The results from the diffusion model were verified with the Ni and Mn diffusion work carried out by Flemings [51]. Sprinkle and Keverian [122] also used work by Flemings to verify their Ni diffusion work. To verify their work, Sprinkle and Keverian [122] used plots similar to those shown in **Figures 4.6 and 4.7** below. **Figures 4.6 and 4.7** are plots of the index of

residual micro segregation reduction (1 – (% reduction in micro segregation)) versus temperature for a dendrite arm spacing of 50µm at various temperatures between 1600°F and 2600°F. As shown in **Figure 4.6**, the % of Ni micro segregation reduction predicted by the diffusion model was extremely close to that predicted by Flemings [51]. **Figure 4.7** shows that the % of Mn micro segregation reduction predicted by the diffusion model was also very close to that predicted by Flemings [51].

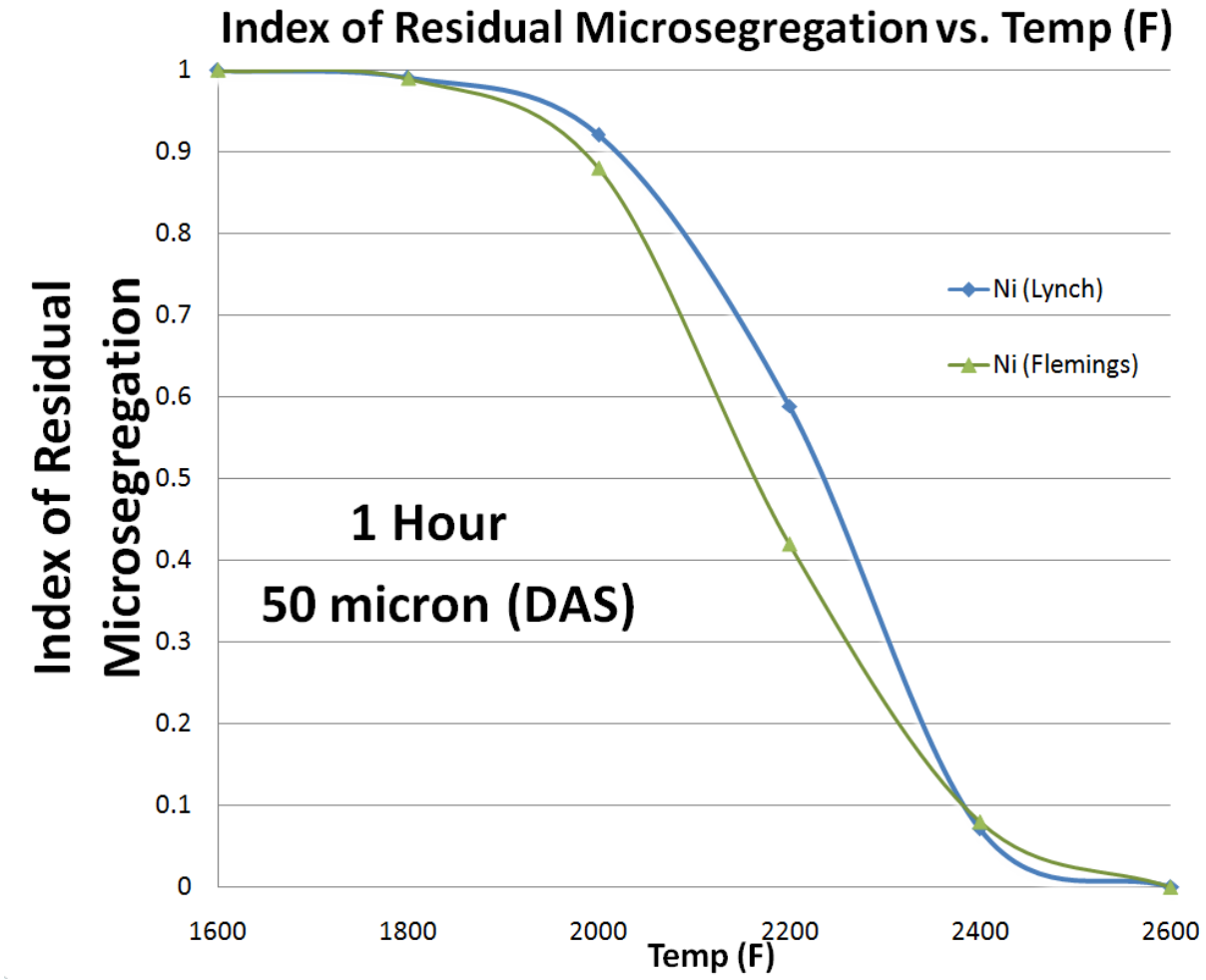

Figure 4.6: The index of residual microsegregation of Ni in a low alloy steel is shown for 1 hour treatments at various temperatures for a 50µm dendrite arm spacing for a comparison between the current model and the Flemings work [51].

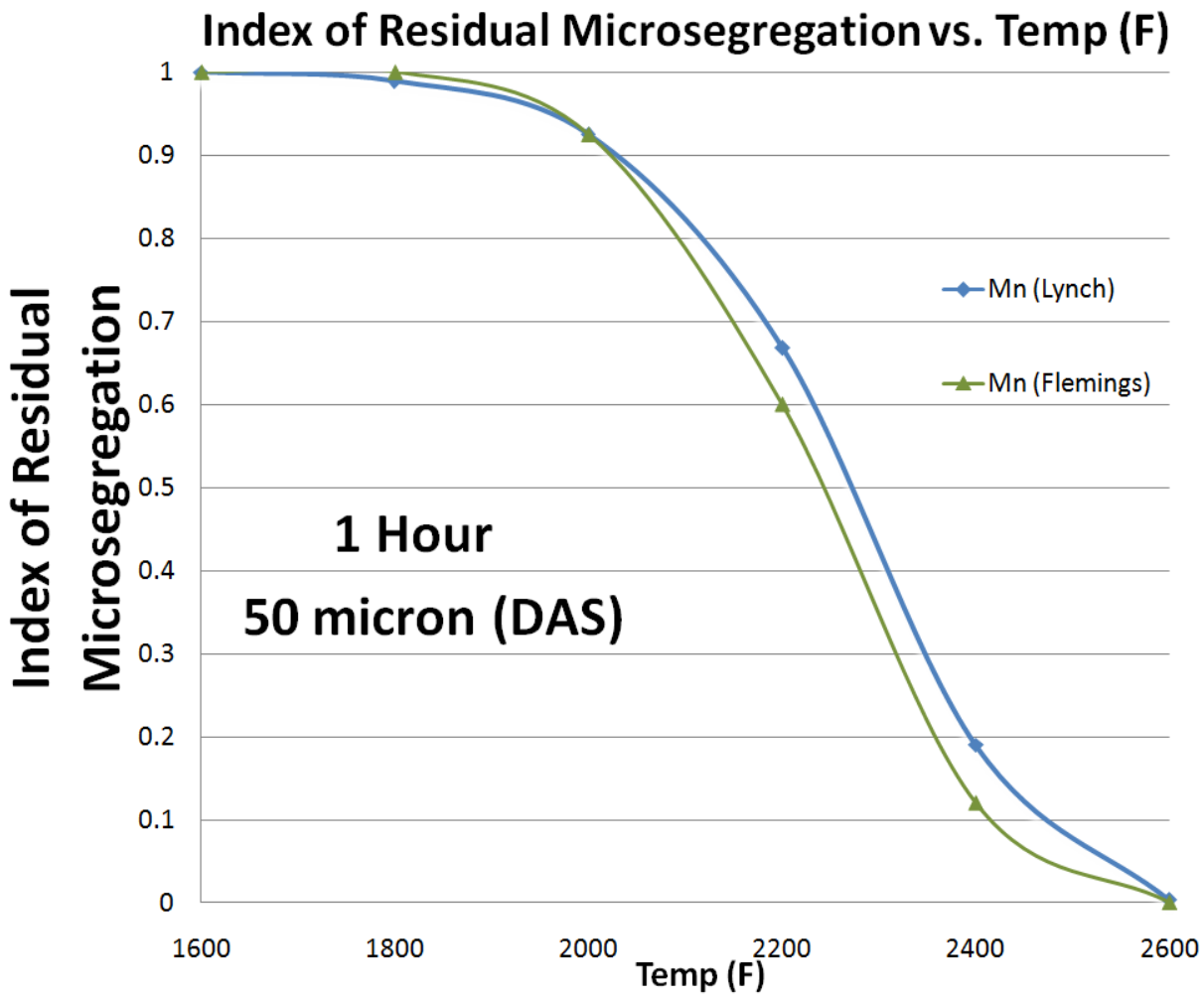

Figure 4.7: The index of residual microsegregation of Mn in a low alloy steel is shown for 1 hour treatments at various temperatures for a 50µm dendrite arm spacing for a comparison between the current model and the Flemings work [51].

After comparing the output of the current model to the output of the Flemings [51] work for Ni and Mn micro segregation reduction shown in **Figure 4.6 and 4.7**, it was apparent that the model was working similarly to the Flemings model. The current model was then applied to the heat treatments carried out in this UHSLA cast steel study.

4.6.3 Microsegregation Reduction During Full Heat Treatment

Throughout Chapter 5, additional estimates of microsegregation reduction during the heat treatments outlined in Chapter 3 will be provided. In addition, estimates of differences in microsegregation reduction in the homogenization temperature study on 4340+ IC steel will be provided.

Chapter 5

Results

The following section will discuss mechanical property, micrograph, fractograph, and X-ray diffraction results for the experimental procedures outlined in Chapter 3. This section will also provide estimates of substitutional alloying element microsegregation reduction that is possible for the respective heat treatments being carried out.

5.1 Results for Investment Cast (IC) 4340+ Cast Steel Screening Experiments

Mechanical test results from all of the initial screening trials and mechanical property trials with the 4340+ (300M) investment cast material are shown in **Table 5.1**. The differences in the individual heat treatments for the studies are presented as the study results are presented sequentially throughout Section 5.1. Throughout Section 5.1, all tensile and yield strength, elongation, and Charpy v-notch impact values reported were reported from a single tensile or Charpy v-notch test specimen while the Rockwell C hardness values reported are given as an average of three readings taken from the finished surface of a Charpy v-notch impact bar. Estimates of % reduction in microsegregation are also reported. The initial concentrations of alloying elements in the dendritic and inter-dendritic regions were chosen to be +/- 0.5 wt % from given alloy nominal concentrations for these calculations unless otherwise noted. For Mo, the nominal composition of Mo is assumed to be 0.4 wt % with the interdendrtic composition assume to be 0.8 wt% Mo and the dendritic composition to be 0.0 wt% Mo. The results in Table 5.1 show that the 4340+ investment cast material is capable of possessing a yield strength of 250 ksi., but the impact toughness and ductility suffer at these strength levels. When the IC 4340+ material is HIP'ed and austempered, 13% elongation and 19 ft-lbs. of impact toughness are achievable, but yield strength suffers.

Table 5.1: Mechanical Properties for screening experiments 1-4 for 4340+ investment cast material.

Study No.	Sample ID	UTS (ksi)	0.2% YS (ksi)	Elong (%)	$CVN_{+72°F}$ (ft-lbs)	Hardness (HRC)
1	1-1950NC	297.6	250.3	4	10	50
1	2-1800NC	299.1	251.5	4	7	52
1	3-1675NC	298.9	251.9	5	6	53
2	1A-HIP	302.2	249.3	8	11	54
2	2A - HIP	298.5	252.0	8	8	52
3	1A- AUS	243.0	183.1	7	13	47
3	1B- AUS	247.8	186.7	10	12	46
3	2A- AUS	234.8	175.8	9	10	45
3	2B- AUS	234.6	173.6	8	9	45
4	1A-HIPAUS	241.4	182.7	13	15	47
4	1B-HIPAUS	240.7	182.0	13	14	45
4	2A-HIPAUS	233.8	178.2	13	19	46
4	2B-HIPAUS	231.8	174.0	13	17	46

5.1.1: Study #1: Effect of Homogenization Temperatures

The initial screening test on the effect of homogenization temperature for the 4340+ (300M) alloy showed that as this temperature was increased from 1675°F to 1950°F, the Charpy impact energy increased from 6 ft-lbs. to 10 ft-lbs. while the UTS, YS, hardness, and percent elongation remained unchanged, **Table 5.2**. The Charpy impact results are plotted in **Figure 5.1**. As the homogenization temperature increased, the impact toughness of the IC 4340+ also increased.

Table 5.2: Mechanical Properties for Increased Homogenization Temperature Study of 4340+ Investment Cast Material.

Study No.	**Sample ID**	**Homogenization**	**Austenitizing**	**Tempering**	**UTS (ksi)**	**0.2% YS (ksi)**	**Elong (%)**	**$CVN_{+72°F}$ (ft-lbs)**	**Tempered Hardness (HRC)**
1	1-1950NC	1950°F, 1 hr. Air Cool	1600°F, 1 hr. Water Quench	600°F, 4 hrs. Water Quench 600°F, 4 hrs. Water Quench	**297.6**	**250.3**	**4**	**10**	**50**
1	2-1800NC	1800°F, 1 hr. Air Cool	1600°F, 1 hr. Water Quench	600°F, 4 hrs. Water Quench 600°F, 4 hrs. Water Quench	**299.1**	**251.5**	**4**	**7**	**52**
1	3-1675NC*	1675°F, 1 hr. Air Cool	1600°F, 1 hr. Water Quench	600°F, 4 hrs. Water Quench 600°F, 4 hrs. Water Quench	**298.9**	**251.9**	**5**	**6**	**53**

* Denotes Standard Heat Treatment for wrought 4340+ 300M alloy.

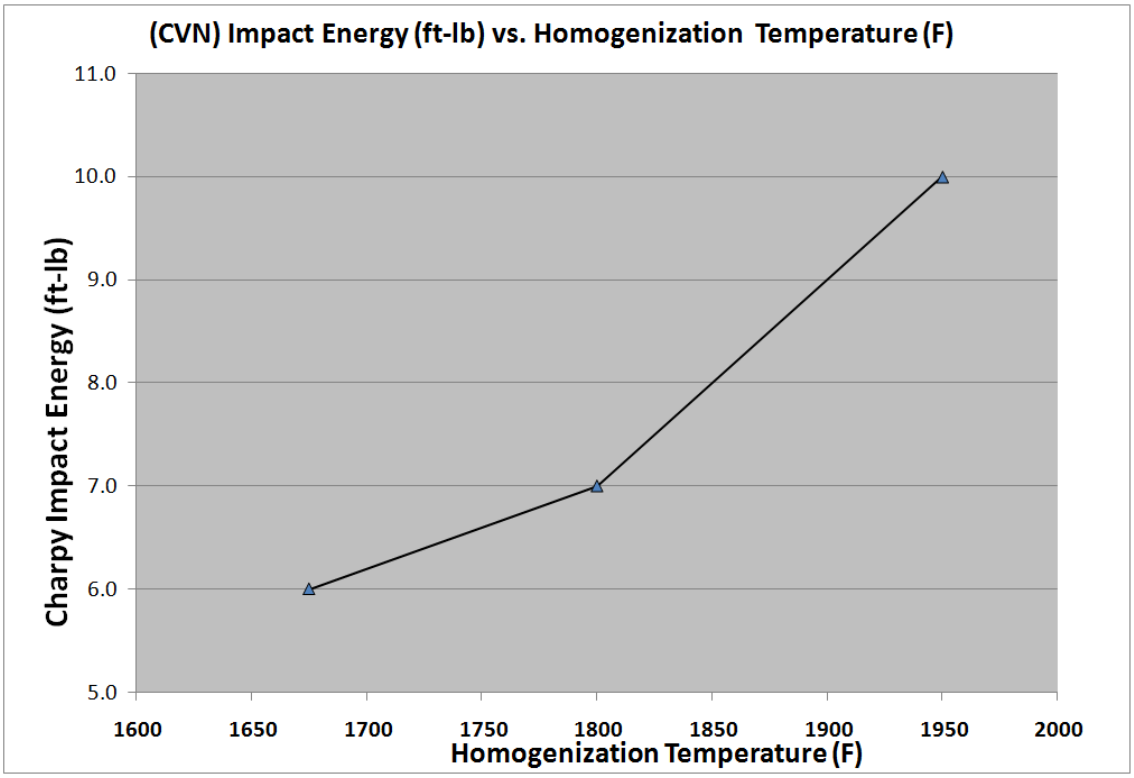

Figure 5.1: The effect of Homogenization Temperature on the Impact Toughness of investment cast 4340+.

The fractographs and etched micrographs of the samples from study #1 are shown below in **Figure 5.2**. The fracture surface shown in **Figure 5.2** (C) shows slightly more dimple rupture than the fracture surface shown in **Figure 5.2** (A). This shows that higher homogenization temperatures resulted in slightly more dimple rupture and less quasi-cleavage fracture on the fracture surfaces of the Charpy specimens impacted at +72°F.

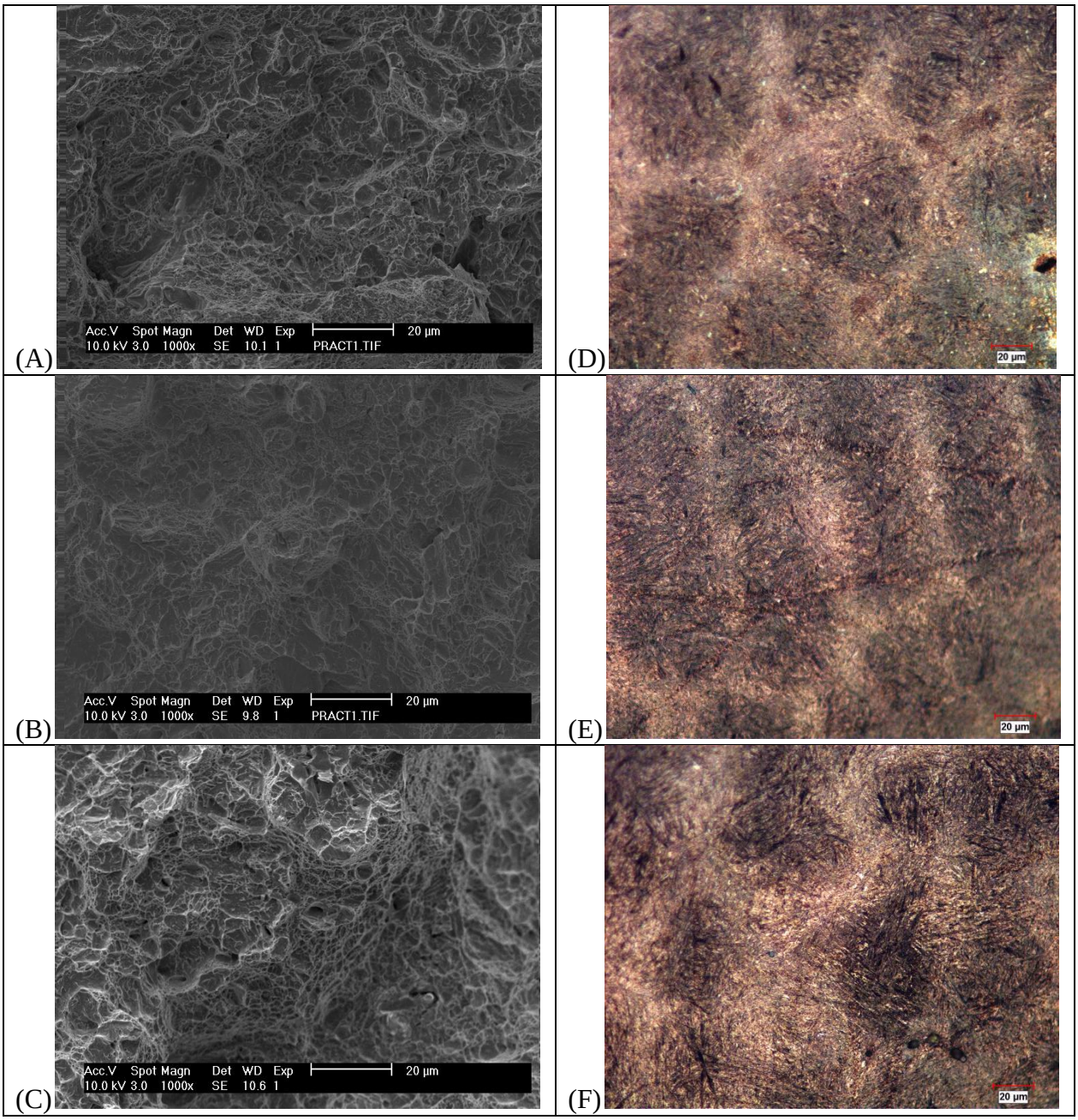

Figure 5.2: Fracture surface images for 4340+ homogenized at various temperatures, SEM 1000X: (A) 1675°F, (B)1800°F, and (C)1950°F. Micrographs in the etched condition for 4340+ alloy homogenized at various temperatures; etched, 500X: (D) 1675°F, (E) 1800°F, and (F) 1950°F.

Using the diffusion model presented in Chapter 4, the extent of microsegregation reduction (% reduction) was estimated for Cr, Ni, and Mo at small dendrite arm spacings (DAS) (20, 40 µm) representative of small investment casting section sizes (0.5 in) at the various homogenization temperatures used during heat treatment experiments. The microsegregation

reduction estimates are reported after each of the three steps that make up the full heat treatments outlined in **Table 3.7**. Because tempering cycles are performed at very low temperatures, the diffusion occurring during tempering can be ignored. A summary of the segregation reduction estimates for both DAS can be seen in **Table 5.3**.

Table 5.3: Estimates of Percent Reduction in Segregation for Cr, Ni, and Mo for the Investment Cast 4340+ alloy.

Homogenization Temp. (°F) / Time (hrs.)	**Percent Reduction in Segregation**								
	Cr: ($x_0^D = 0.33wt\%;\ x_0^{ID} = 1.33wt\%;\ x_0 = 0.83wt\%$)								
	Ni: ($x_0^D = 1.35wt\%;\ x_0^{ID} = 2.35wt\%;\ x_0 = 1.85wt\%$)								
	Mo: ($x_0^D = 0.0wt\%;\ x_0^{ID} = 0.8wt\%;\ x_0 = 0.4wt\%$)								
	20 μm DAS								
	Homogenize			Homo. + Austenitize*			Full Heat Treatment		
	Cr	Ni	Mo	Cr	Ni	Mo	Cr	Ni	Mo
1675°F / 4 hrs.	4%	1%	3%	6%	2%	4%	6%	2%	4%
1800°F / 4 hrs.	16%	6%	12%	17%	6%	13%	17%	6%	13%
1950°F / 4 hrs.	53%	23%	44%	53%	23%	44%	53%	23%	44%
Homogenization Temp. (°F)	40 μm DAS								
	Homogenize			Homo. + Austenitize*			Full Heat Treatment		
	Cr	Ni	Mo	Cr	Ni	Mo	Cr	Ni	Mo
1675°F / 4 hrs.	1%	<1%	1%	2%	<1%	1%	2%	<1%	1%
1800°F / 4 hrs.	4%	1%	3%	5%	2%	4%	5%	2%	4%
1950°F / 4 hrs.	17%	8%	13%	17%	8%	14%	17%	8%	14%

* Austenitized at 1600°F for 1 hour.

As shown in **Table 5.3**, for a DAS of 20 μm, significant differences in microsegregation reduction exist between the three homogenization temperatures for Cr, Ni, and Mo. For Cr, the model estimates that 53% of the microsegregation is removed after homogenization at 1950°F (1066°C) for 1 hour while the percent reductions are estimated to be just 16% and 4% when homogenization is at 1800°F (982°C) and 1675°F (913°C) respectively. Even at a homogenization temperature of 1950°F (1066°C) for a DAS of 20 μm, the maximum reductions in microsegregation after homogenization are less than 50% for Cr, Ni, and Mo. When the DAS is increased to 40 μm, the extent of microsegregation reduction at 1950°F (1066°C) is estimated to be less than 20% for Cr, Ni, and Mo. For temperatures at or below 1800°F (982°C), the microsegregation reduction is estimated to be at most 5% for Cr, Ni, and Mo at a 40 μm DAS.

5.1.2: Study #2: HIP of Investment Cast 4340+ (300M) Steel

Table 5.4 shows that replacing the one hour homogenization step for the standard heat treatment with a 4 hour high temperature HIP cycle led to increased Charpy v-notch impact toughness (up to 11 ft-lbs.) and percent elongation (8%) while the UTS, YS, and hardness remained about the same as the baseline heat treatment in study #1 (1675°F) for the 4340+ (IC) alloy.

Table 5.4: Mechanical properties for 4340+ (IC) HIP and Tempering Temperature Study.

Study No.	Sample ID	HIP Homogenization	Austenitizing	Tempering	UTS (ksi)	0.2% YS (ksi)	Elong (%)	$CVN_{+72°F}$ (ft-lbs)	Tempered Hardness (HRC)
1	1A-HIP	1950°F, 4 hrs., 15ksi., slow vessel cool to 700°F- Air Cool to Room Temp.	1600°F, 1 hr. Water Quench	500°F, 4 hrs. Water Quench 500°F, 4 hrs. Water Quench	**302.2**	**249.3**	**8**	**11**	**54**
1	2A-HIP	1950°F, 4 hrs., 15ksi., slow vessel cool to 700°F- Air Cool to Room Temp.	1600°F, 1 hr. Water Quench	600°F, 4 hrs. Water Quench 600°F, 4 hrs. Water Quench	**298.5**	**252.0**	**8**	**8**	**52**

Figure 5.3 shows the effect of HIP and tempering temperature on the Charpy impact toughness of the investment cast 4340+ alloy. Similarly, **Figure 5.4** shows the effect of HIP and tempering temperature on the percent elongation. At a tempering temperature of 600°F, impact toughness and % elongation both lagged behind the sample that was tempered at 500°F.

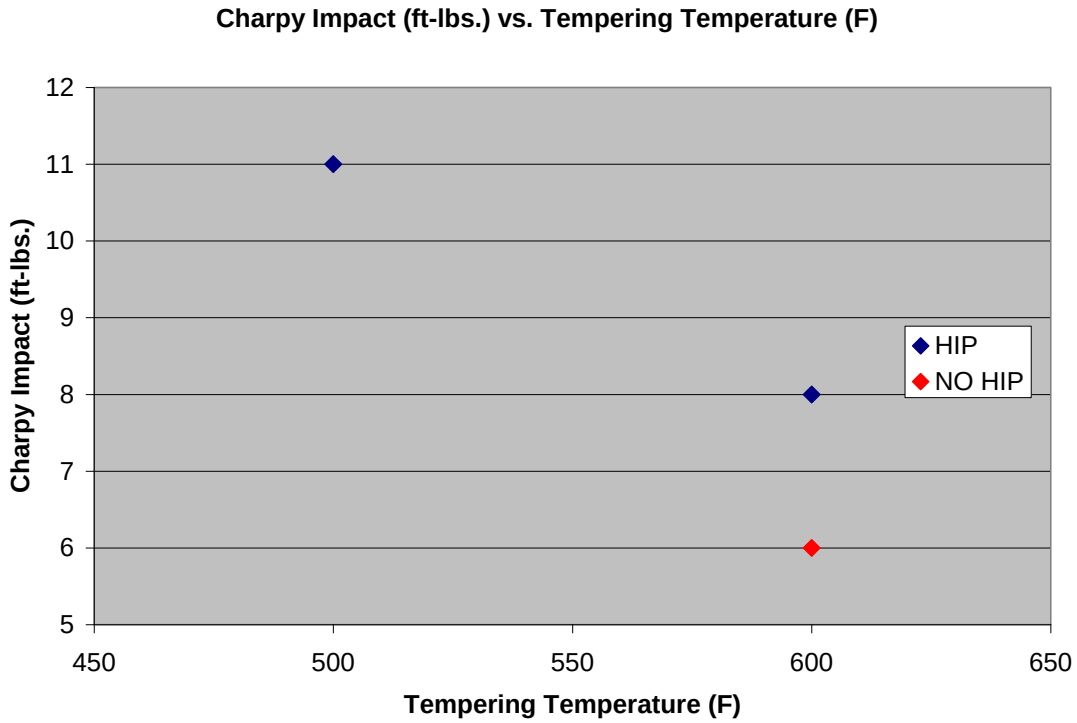

Figure 5.3: The effect of HIP and tempering temperature on the room temperature Charpy impact toughness of the cast 4340+ alloy.

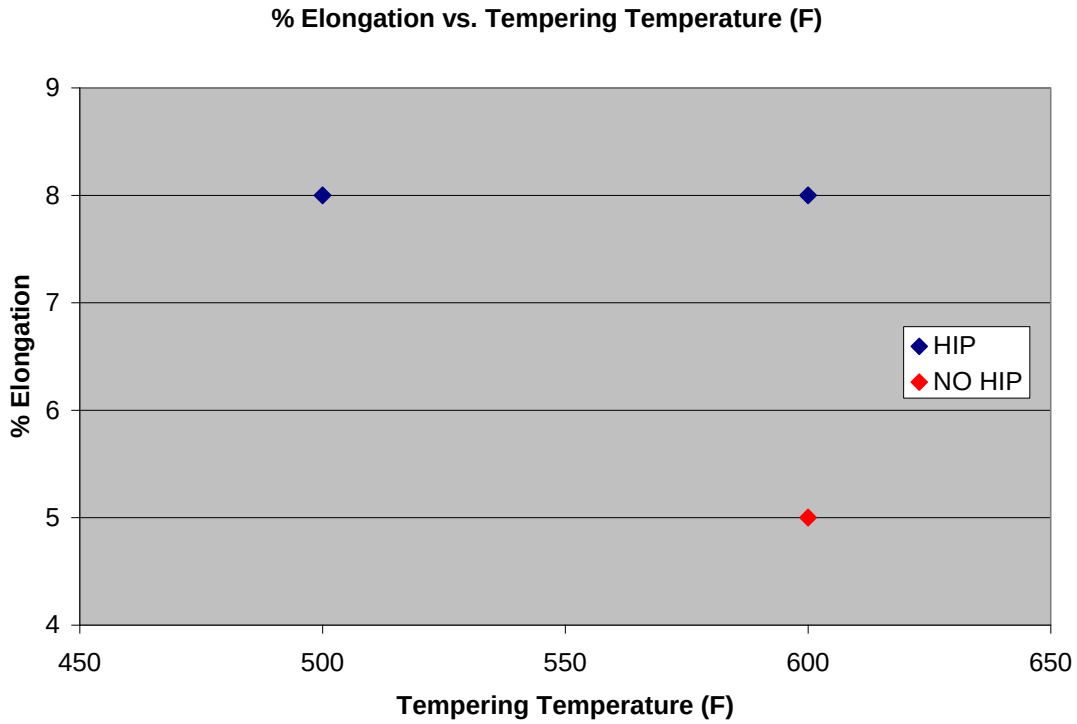

Figure 5.4: The effect of HIP and tempering temperature on the % elongation of the cast 4340+ alloy.

The fractographs and etched micrographs of the samples from this HIP study are shown in **Figure 5.5**. The fractographs for the HIP material in study #2 have significantly less microporosity when compared to the standard heat treatment, unHIP samples in study #1.

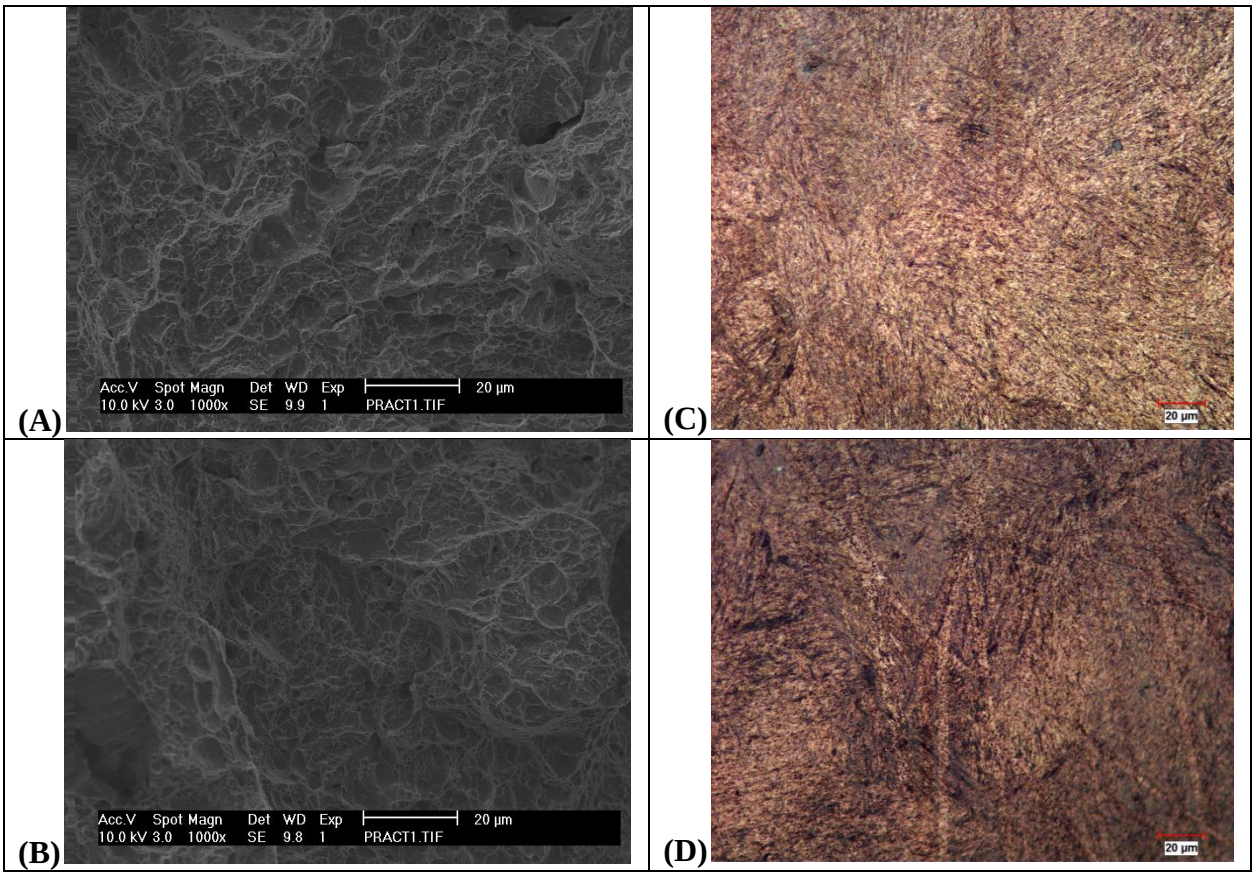

Figure 5.5: Fracture surface images for 4340+ HIPed and double tempered at various temperatures, SEM 1000X: (A) 500°F, (B) 600°F. Micrographs in the etched condition for the 4340+ alloy double tempered at various temperatures; etched, 500X: (C) 500°F, (D) 600°F.

A summary of the segregation reduction estimates can be seen in **Table 5.5**. For the same heat treatment, significant differences exist in estimated microsegregation reduction between the 20 and 40 µm DAS for Cr, Ni, and Mo. For Cr, the model estimates that 95% of the microsegregation is removed after HIP homogenization at 2125°F (1163°C) for 4 hours at a DAS of 20 µm while the percent reduction in microsegregation is estimated to be just 53% at a DAS of 40 µm. For Ni, the model estimates that 72% of the microsegregation is removed after HIP homogenization at 2125°F (1163°C) for 4 hours at a DAS of 20 µm while the percent reduction in microsegregation is estimated to be just 27% at a DAS of 40 µm.

Table 5.5: Estimates of Percent Reduction in Segregation for Cr, Ni, Mo, and Mn for the Investment Cast 4340+ alloy.

Secondary Dendrite Arm Spacing (DAS)	**Percent Reduction in Segregation**								
	Cr: ($x_0^D = 0.33wt\%;\ x_0^{ID} = 1.33wt\%;\ x_0 = 0.83wt\%$)								
	Ni: ($x_0^D = 1.35wt\%;\ x_0^{ID} = 2.35wt\%;\ x_0 = 1.85wt\%$)								
	Mo: ($x_0^D = 0.0wt\%;\ x_0^{ID} = 0.8wt\%;\ x_0 = 0.4wt\%$)								
	Mn: ($x_0^D = 0.26wt\%;\ x_0^{ID} = 1.26wt\%;\ x_0 = 0.76wt\%$)								
	HIP Homogenization					HIP Homogenization + Austenization			
	Cr	Mo	Mn	Ni		Cr	Mo	Mn	Ni
20 µm	95%	90%	72%	72%		95%	90%	72%	72%
40 µm	53%	44%	27%	27%		53%	44%	27%	27%

5.1.3: Study #3: Austempering of Investment Cast 4340+ (300M)

The initial screening test on the effect of austempering on the 4340+ (300M) cast alloy showed that austempering significantly increased the Charpy impact energy (up to 13 ft-lbs.) and percent elongation (up to 10%) while the UTS, YS, and hardness all decreased from the conventionally heat treated quench and tempered sample in study #1 (**Table 5.6**).

Table 5.6: Mechanical properties for 4340+ (IC) Austempering Study.

Study No.	Sample ID	Homogenization	Austenitizing	AUS Tempering	UTS (ksi)	0.2% YS (ksi)	Elong (%)	$CVN_{+72°F}$ (ft-lbs)	Tempered Hardness (HRC)
3	1A- AUS	1675°F, 1 hr. Air Cool	1600°F, 1 hr. Quench in salt bath	572°F, 14 hrs. Water Quench	**243**	**183.1**	**7**	**13**	**47**
3	1B- AUS	1675°F, 1 hr. Air Cool	1600°F, 1 hr. Quench in salt bath	572°F, 8 hrs. Water Quench	**247.8**	**186.7**	**10**	**12**	**46**
3	2A- AUS	1675°F, 1 hr. Air Cool	1600°F, 1 hr. Quench in salt bath	599°F, 14 hrs. Water Quench	**234.8**	**175.8**	**9**	**10**	**45**
3	2B- AUS	1675°F, 1 hr. Air Cool	1600°F, 1 hr. Quench in salt bath	599°F, 8 hrs. Water Quench	**234.6**	**173.6**	**8**	**9**	**45**

Figures 5.6 and 5.7 show the effects of austempering temperature and time on the toughness and yield strength of the investment cast 4340 + respectively. When compared to the properties at the lower austempering temperature, the higher austempering temperature (600°F) resulted in a significant drop in room temperature impact toughness and yield strength. The impact toughness and yield strength did not change significantly between the 480 minute (8 hour) and 840 minute (14 hour) austempering treatments. Impact toughness values only changed by 1 ft-lb. and the yield strength values only differed by 2 to 3 ksi.

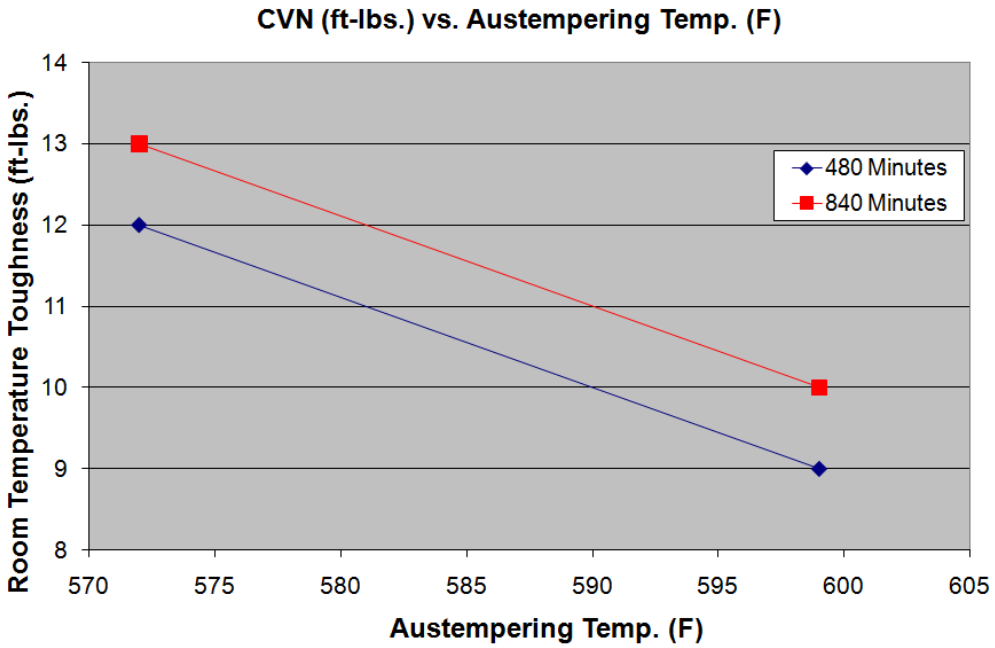

Figure 5.6: The effects of Austempering Temperature and Time on the Charpy impact toughness of the investment cast 4340+ alloy.

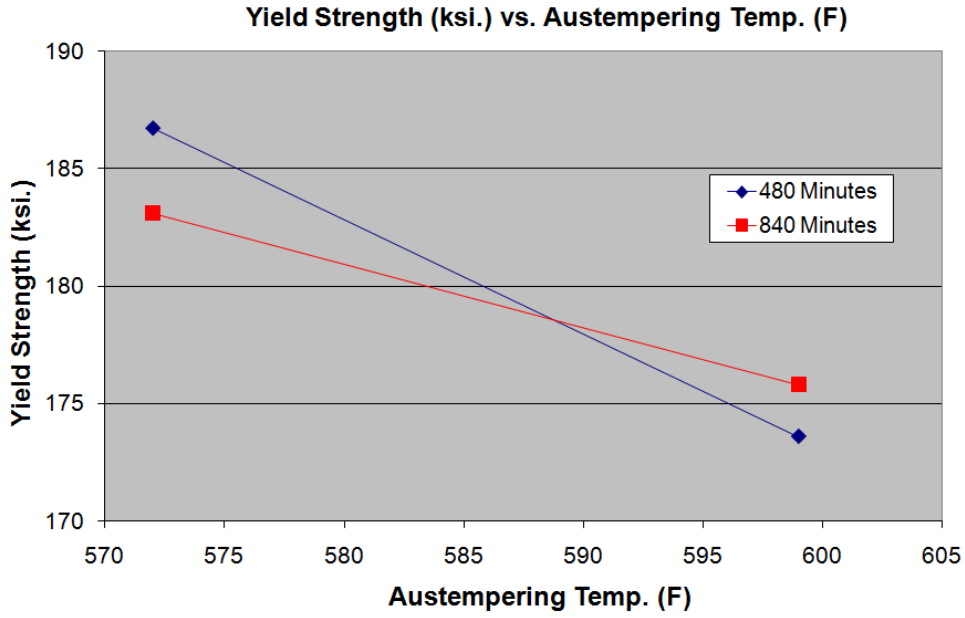

Figure 5.7: The effects of Austempering Temperature and Time on the yield strength of the investment cast 4340+ alloy.

The fractographs and the bainitic micrographs of the samples from study #3 are shown in **Figures 5.8 and 5.9**. An increased amount of dimple rupture is present on the HIPed fractographs in **Figure 5.8** when compared with the unHIPed fractographs in **Figures 5.2 and 5.5**.

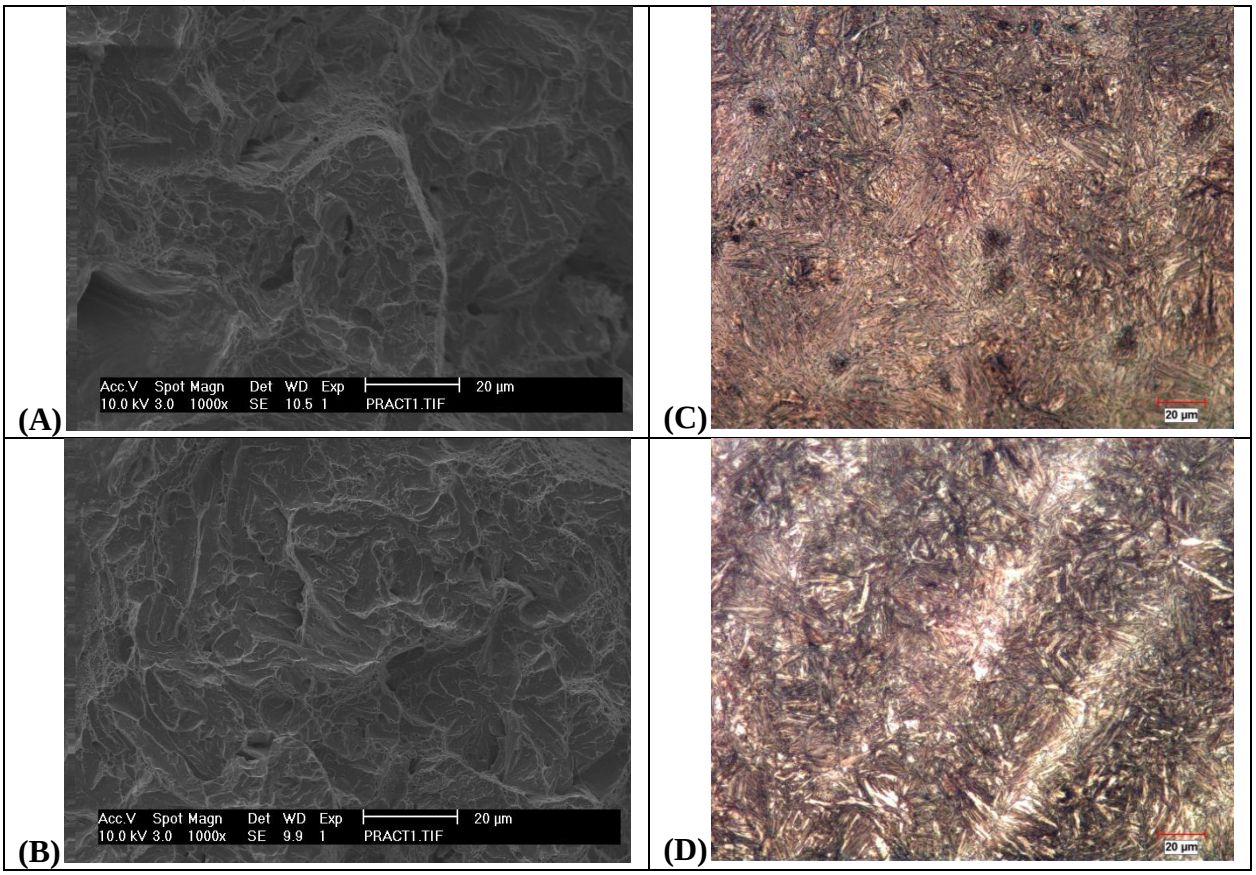

Figure 5.8: Fracture surface images for 4340+ austempered at 572°F for various times, SEM 1000X: (A) 840 mins., (B) 480 mins. Micrographs in the etched condition for the 4340+ alloy austempered at 572°F for various times; etched, 500X: (C) 840 mins. or (D) 480 mins.

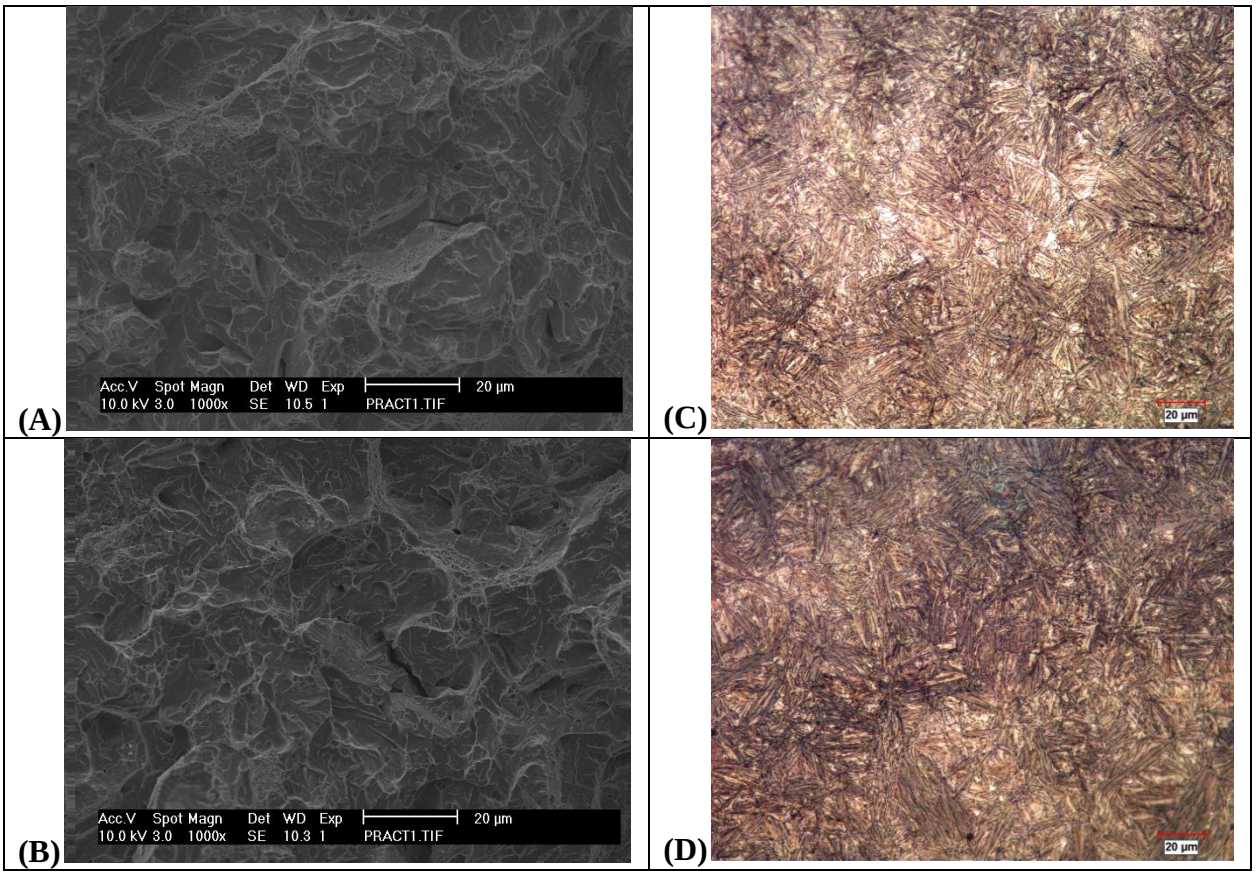

Figure 5.9: Fracture surface images for 4340+ austempered at 599°F for various times, SEM 1000X: (A) 840 mins., (B) 480 mins. Micrographs in the etched condition for the 4340+ alloy austempered at 599°F for various times; etched, 500X: (C) 840 mins. or (D) 480 mins.

5.1.4: Study #4: Austempering + HIP of Investment Cast 4340+

Since the initial screening tests on austempering and HIP on investment cast 4340+ showed that both HIP and austempering had the potential to significantly increase the Charpy impact energy, the last screening test was completed to examine the effects of the combination of austempering and HIP on the mechanical properties of the investment cast 4340+ alloy. The mechanical property results for study #4 on HIP + austempering are shown in **Table 5.7**. When the IC 4340+ material is both HIP'ed and austempered, 13% elongation and 19 ft-lbs. of impact toughness are achievable, but yield strength is only 180ksi.

Table 5.7: Mechanical properties for the 4340+ (IC) HIP + Austempering Study.

Study No.	Sample ID	HIP	Austenitizing	AUS Tempering	UTS (ksi)	0.2% YS (ksi)	Elong (%)	$CVN_{+72°F}$ (ft-lbs)	Tempered Hardness (HRC)
4	1A-HIPAUS	1950°F, 4 hrs., 15ksi., slow vessel cool to 700°F- Air Cool to Room Temp.	1600°F, 1 hr. Quench in salt bath	572°F, 14 hrs. Water Quench	**241.4**	**182.7**	**13**	**15**	**47**
4	1B-HIPAUS	1950°F, 4 hrs., 15ksi., slow vessel cool to 700°F- Air Cool to Room Temp.	1600°F, 1 hr. Quench in salt bath	572°F, 8 hrs. Water Quench	**240.7**	**182**	**13**	**14**	**45**
4	2A-HIPAUS	1950°F, 4 hrs., 15ksi., slow vessel cool to 700°F- Air Cool to Room Temp.	1600°F, 1 hr. Quench in salt bath	599°F, 14 hrs. Water Quench	**233.8**	**178.2**	**13**	**19**	**46**
4	2B-HIPAUS	1950°F, 4 hrs., 15ksi., slow vessel cool to 700°F- Air Cool to Room Temp.	1600°F, 1 hr. Quench in salt bath	599°F, 8 hrs. Water Quench	**231.8**	**174**	**13**	**17**	**46**

Figures 5.10 and 5.11 show the effects of austempering temperature and time on the room temperature toughness and yield strength of the investment cast 4340+ respectively. UTS and yield strength properties similar to the austempered specimens in study #3 were observed in the HIP + austempered samples. When compared to the first three screening studies, significant increases in both the impact toughness and % elongation were observed in the HIP + austempered samples. HIP is expected to decrease porosity in the cast 4340+ alloy while austempering is expected to form a bainitic microstructure, both of which are expected to lead to increased impact toughness and % elongation. While the yield strength decreased from the low austempering temperature (572°F or 300°C) to the high austempering temperature (599°F or 315°C), impact toughness significantly increased from the lower austempering temperature (572°F or 300°C) to the higher austempering temperature (599°F or 315°C). As was the case in study #3, the austempering time did not significantly affect the room temperature Charpy impact toughness and yield strength of 4340+.

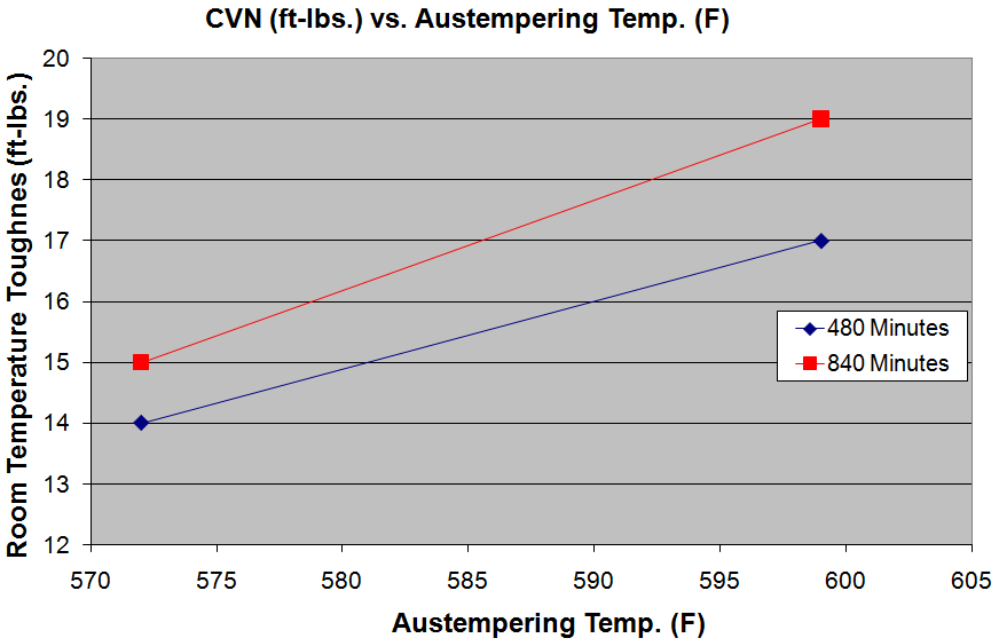

Figure 5.10: The effects of Austempering Temperature (°F) and Time (mins.) on the Charpy impact toughness of the HIPed investment cast 4340+.

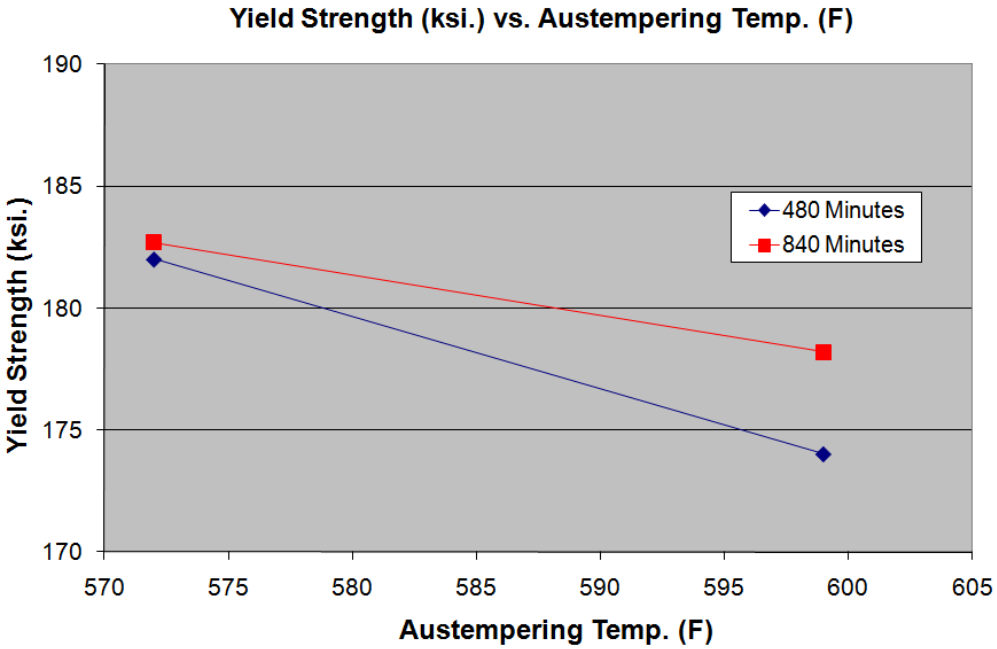

Figure 5.11: The effects of Austempering Temperature (°F) and Time (mins.) on the yield strength of HIPed cast 4340+.

The fractographs and bainitic etched micrographs of the samples from study #4 are shown in **Figures 5.12 and 5.13** below. **In Figure 5.13**, fracture surfaces A&B show evidence of significant amounts of dimple rupture characteristic of tougher materials.

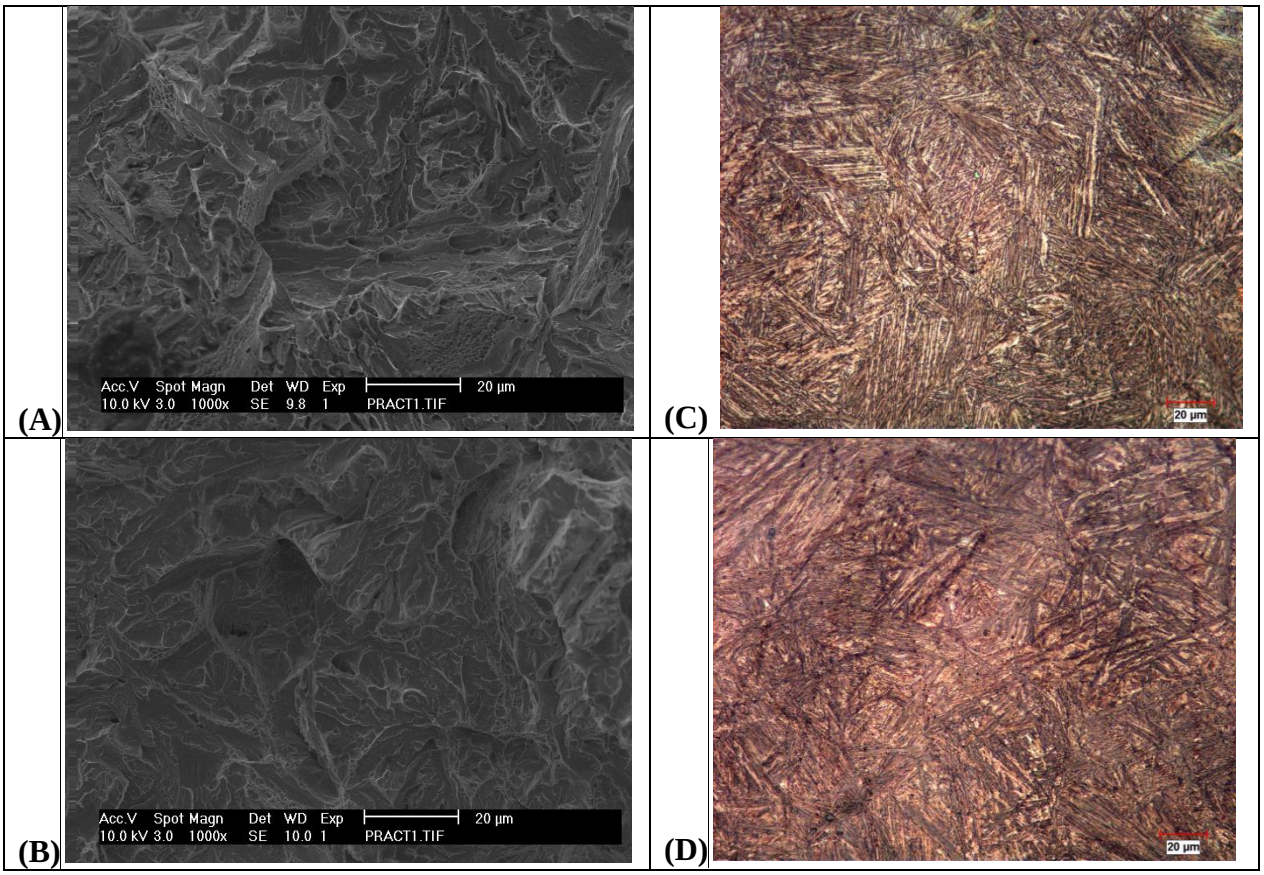

Figure 5.12: Fracture surface images for 4340+ HIP and austempered at 572°F for various times, SEM 1000X: (A) 840 mins., (B) 480 mins. Micrographs in the etched condition for the 4340+ alloy HIP and austempered at 599°F for various times; etched, 500X: (C) 840 mins. or (D) 480 mins.

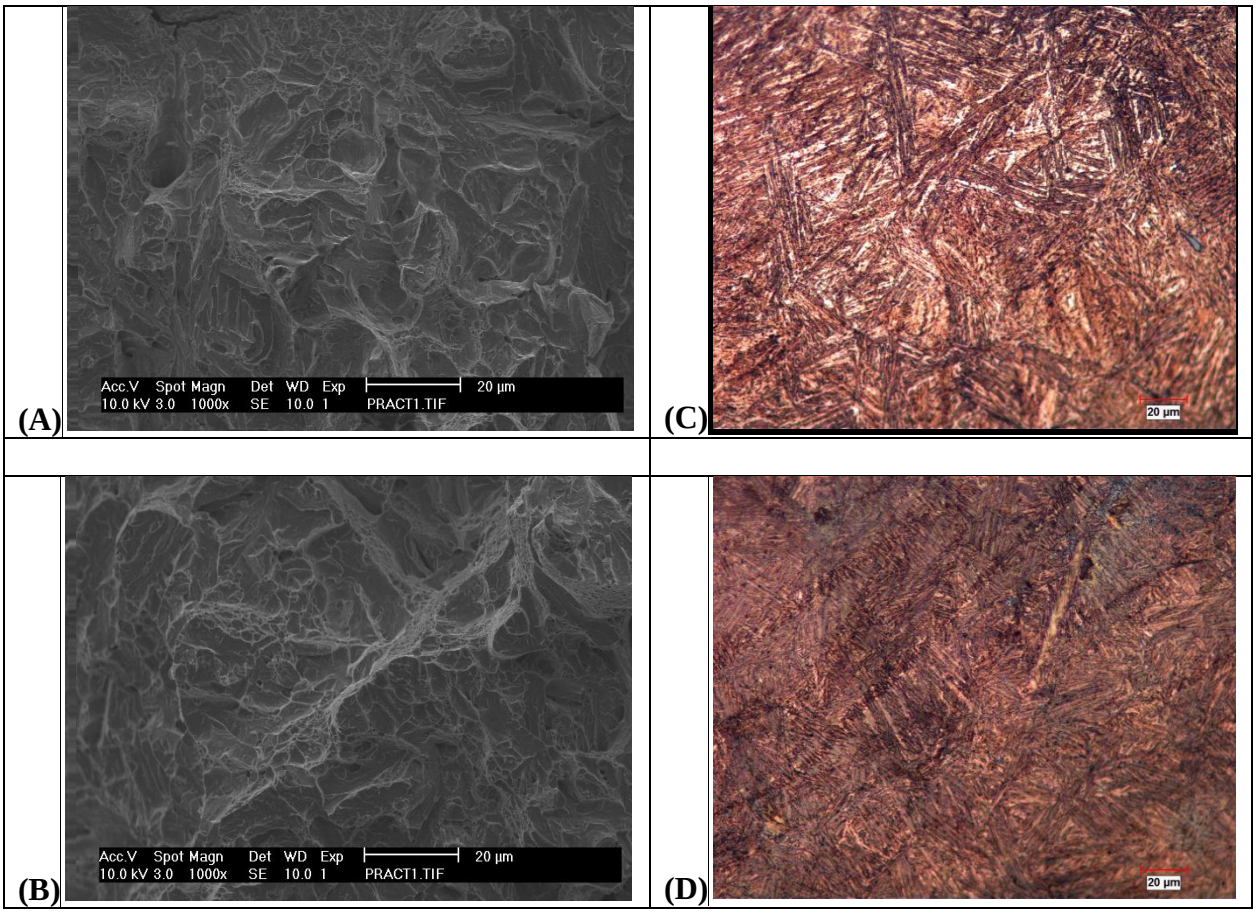

Figure 5.13: Fracture surface images for 4340+ HIP and austempered at 599°F for various times, SEM 1000X: (A) 840 mins., (B) 480 mins. Micrographs in the etched condition for the 4340+ alloy HIP and austempered at 599°F for various times; etched, 500X: (C) 840 mins. or (D) 480 mins.

5.1.5 Summary of the Initial Experimentation of 4340+ Cast Steel

The initial screening experiments completed with the cast 4340+ (300M) alloy have shown that replacing the conventional homogenization step with a high temperature homogenization or high temperature HIP homogenization step in the conventional heat treatment procedure can increase impact toughness without changing the ultimate tensile strength (UTS) or yield strength (YS) of the cast material. Austempering the material improves toughness at the expense of tensile and yield strength. By combining HIP and austempering on the material, significant gains can be made in impact toughness and ductility at the 180ksi yield strength level. For future work, the idea would be to take results from past research on austenization temperatures and austempering and combine it with the current results on increased homogenization temperatures, HIP, and austempering to develop heat treatment procedures that would give optimal toughness and elongation values at yield strength values up to 250 ksi. Since

only a single heat of material could be procured for this study, additional 4340+ material is needed to continue with this study.

The second approach to developing ultrahigh strength low alloy cast steels with increased impact toughness involves the development of a new ultrahigh strength low alloy steel, Eglin steel. This study will display the very first property results for cast Eglin steel (also denoted as ES-1).

5.2 Results for Cast ES-1 Ingot Experiments

The 2^{3-1} factorial experimental design was used to determine the effects of homogenization, austenization temperature, and tempering temperature on the mechanical properties of the cast ES-1 material while also studying the effects of a HIP cycle prior to heat treatment. The results of a Charpy impact energy transition behavior study of the cast ES-1 ingot steel subject to HIP and various heat treatments are presented along with the corresponding tensile properties and hardness. The microstructure and fracture surfaces were also characterized and the results are presented. Estimates of the % reduction in microsegregation of substitutional alloying elements are also presented. For the estimates, the initial concentrations of alloying elements in the dendritic and inter-dendritic regions were chosen to be +/- 0.5 wt % from given alloy nominal concentrations unless otherwise noted (**See Table 3.2**). A summary of the average mechanical property results from the Charpy impact energy transition study of the cast ES-1 + HIP ingot material are shown in **Table 5.8**.

Table 5.8: Summary of the mechanical property results for Cast + HIP ES-1 Ingot Impact Transition Study.

Heat Treatment	HIP	Homogenization	Austenitizing/ Tempering	UTS (ksi)	0.2% YS (ksi)	Elong (%)	CVN -40°F/+72°F (ft-lbs)	Tempered Hardness (HRC)
1	2125°F, 4 hrs., 15ksi., slow vessel cool to 700°F- Air Cool to Room Temp.	None	1800°F, 1 hr. Water Quench/ 375°F, 4 hrs. Water Quench	**237.6**	**190.7**	**15**	**38 / 50**	**46**
2	2125°F, 4 hrs., 15ksi., slow vessel cool to 700°F- Air Cool to Room Temp.	None	1900°F, 1 hr. Water Quench/ 450°F, 4 hrs. Water Quench	**239.3**	**183.5**	**15**	**37 / 51**	**48**
3	2125°F, 4 hrs., 15ksi., slow vessel cool to 700°F- Air Cool to Room Temp.	2000°F, 2 hrs. Air Cool to Room Temp.	1800°F, 1 hr. Water Quench/ 450°F, 4 hrs. Water Quench	**244.0**	**187.5**	**15**	**38 / 51**	**47**
4	2125°F, 4 hrs., 15ksi., slow vessel cool to 700°F- Air Cool to Room Temp.	2000°F, 2 hrs. Air Cool to Room Temp.	1900°F, 1 hr. Water Quench/ 375°F, 4 hrs. Water Quench	**253.1**	**193.3**	**15**	**40 / 51**	**49**

**Note: -40°F impact value is an average of (2) Charpy values; +72°F impact value is from a single Charpy specimen; all tensile data is an average of (2) tensile specimens; all hardness data is an average of (3) measurements from a single Charpy specimen.

The table above shows that heat treatment #4 which includes a HIP cycle followed by a high temperature homogenization treatment, high temperature austenization treatment, and a low temperature tempering step produces superior tensile and impact properties when compared to the other three heat treatments. Yield strength values in excess of 190 ksi. were achieved, along with ultimate tensile strength values of 250 ksi., 15% elongation and 40 ft-lbs. of CVN impact energy at -40°F.

5.2.1 Impact Transition Curves and Mechanical Properties

The completed Charpy impact transition curves are shown in **Figure 5.14.** The corresponding complete mechanical property results are shown in **Appendix A.2**. The lower shelf energy for the cast + HIP ES-1 alloy could not be estimated from the impact toughness vs. temperature data, because the lower shelf energy for this alloy occurs at a temperature below -100°F, the lowest impact testing temperature in this study.

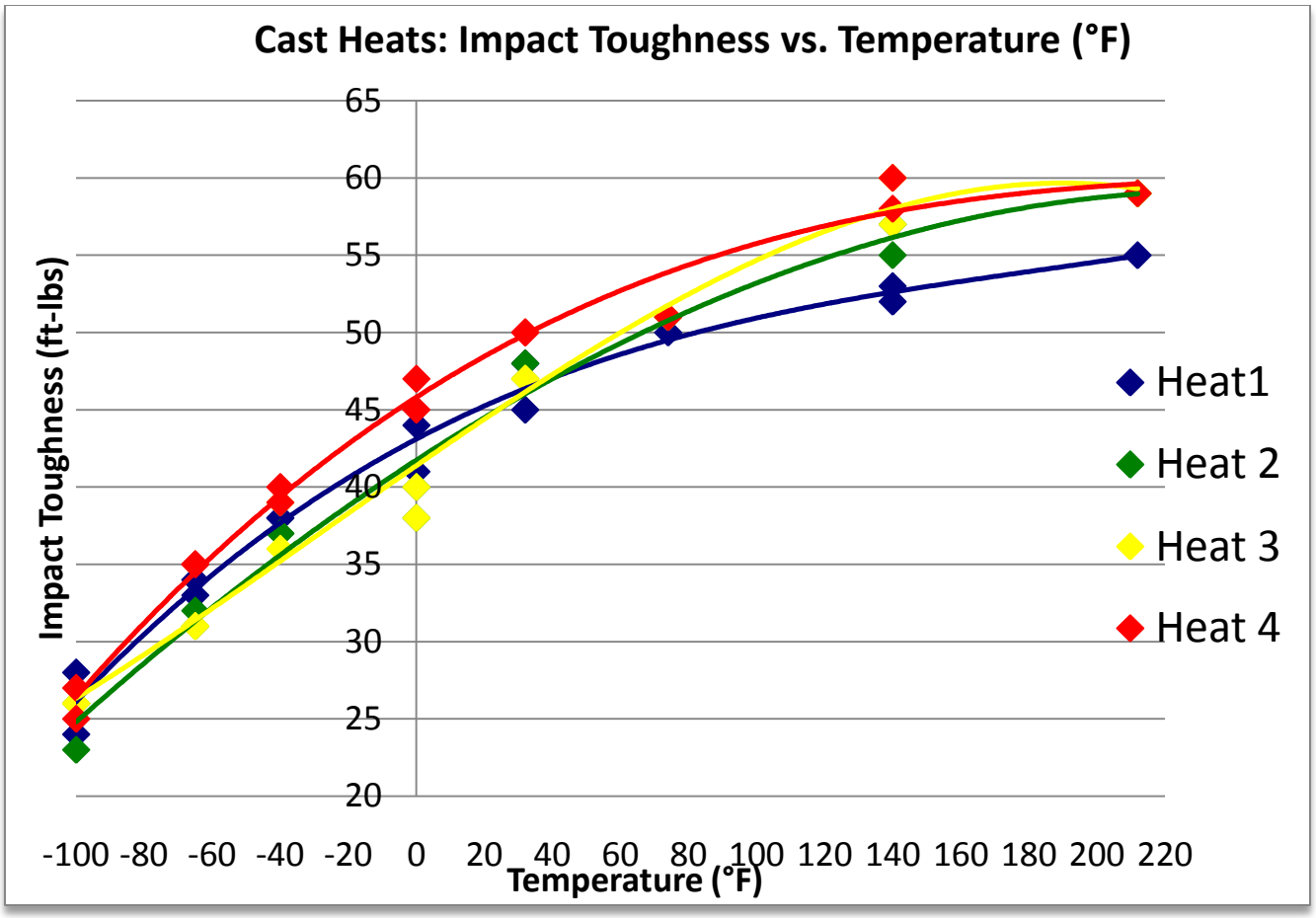

Figure 5.14: Impact transition curves for the cast + HIP ES-1 ingot material.

At -40°F, the cast+ HIP material had impact energies between 36 and 40 ft-lbs. At room temperature, the impact energies of the cast + HIP material were between 50 and 51 ft-lbs. The best heat treatment procedure for this study was heat treatment #4 (homogenization at 2000°F, high temperature austenization at 1900°F, and low temperature tempering at 375°F). This heat treatment procedure produced superior mechanical properties when compared to the remainder of the heat treatments in the 2^{3-1} study.

5.2.2 Micrographs and Fractographs

Micrographs for the cast + HIP ES-1 material are shown in **Figures 5.15 and 5.16** while fractographs of the Charpy impact specimens are shown in **Figures 5.17 and 5.18**. Examination of the etched micrograph did not indicate significant differences in microsegregation for the various heat treatments. Examination of the fractographs did not show significant differences in the -40°F modes of fracture between Charpy specimens for the various heat treatments. When

compared to all the fractographs for the cast 4340+ material shown in Section 5.1 at +70°F, the cast ES-1 fractographs at -40°F had significantly more dimpled rupture on the fracture surfaces.

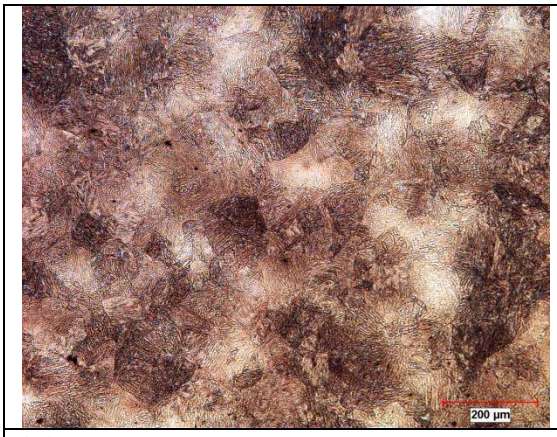

(A) Cast: Heat Treatment # 1: HIP + Austenitize (1800°F) 1 Hour + Temper (375°F) 4 Hours

(B) Cast: Heat Treatment #2: HIP + Austenitize (1900°F) 1 Hour + Temper (450°F) 4 Hours

(C) Cast: Heat Treatment #3: HIP + Homogenize (2000°F) 2 Hours + Austenitize (1800°F) 1 Hour + Temper (450°F) 4 Hours

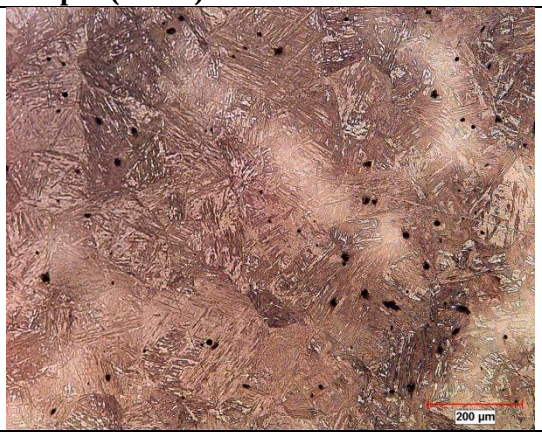

(D) Cast: Heat Treatment #4: HIP + Homogenize (2000°F) 2 Hours + Austenitize (1900°F) 1 Hour + Temper (375°F) 4 Hours

Figure 5.15: Micrographs for the ES-1 alloy HIP and heat treated with various conditions; etched, 100X.

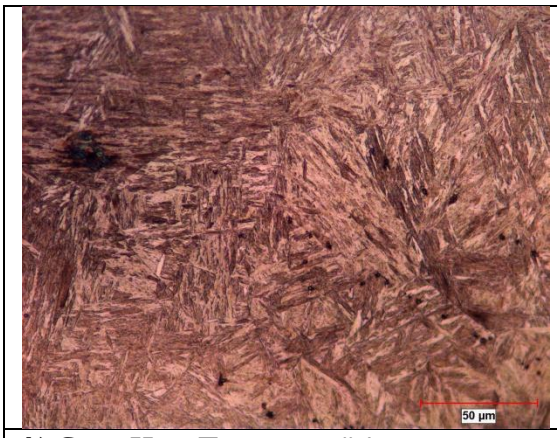	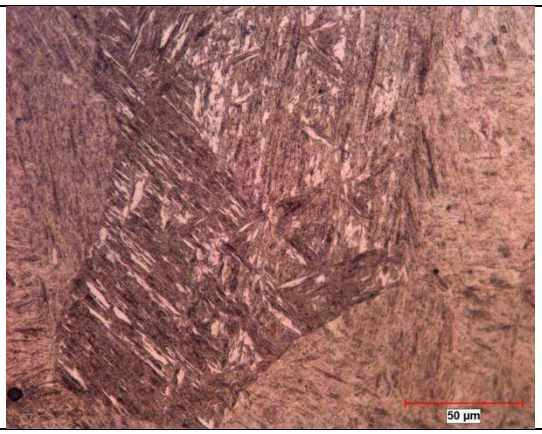
A) Cast: Heat Treatment # 1: HIP + Austenitize (1800°F) 1 Hour + Temper (375°F) 4 Hours	**(B) Cast: Heat Treatment #2: HIP + Austenitize (1900°F) 1 Hour + Temper (450°F) 4 Hours**
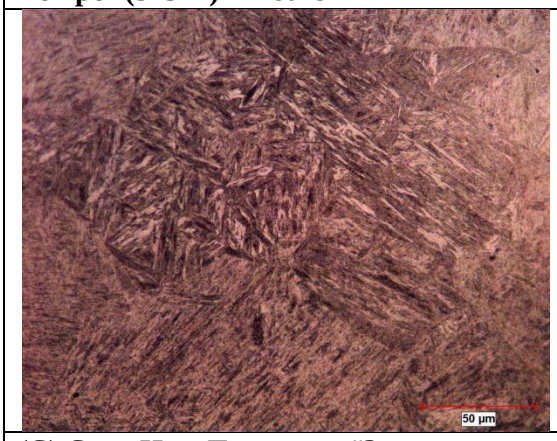	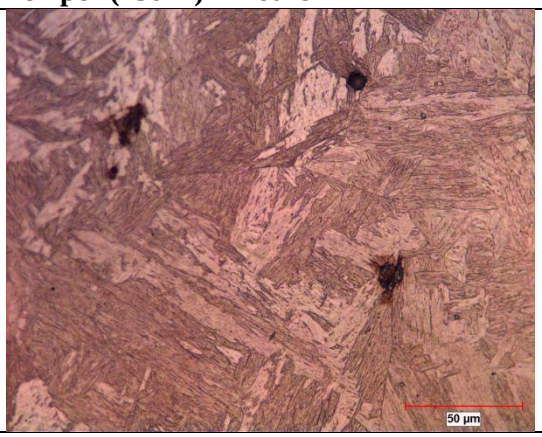
(C) Cast: Heat Treatment #3: HIP + Homogenize (2000°F) 2 Hours + Austenitize (1800°F) 1 Hour + Temper (450°F) 4 Hours	**(D) Cast: Heat Treatment #4: HIP + Homogenize (2000°F) 2 Hours + Austenitize (1900°F) 1 Hour + Temper (375°F) 4 Hours**

Figure 5.16: Micrographs for the ES-1 alloy HIP and heat treated with various conditions; etched, 500X.

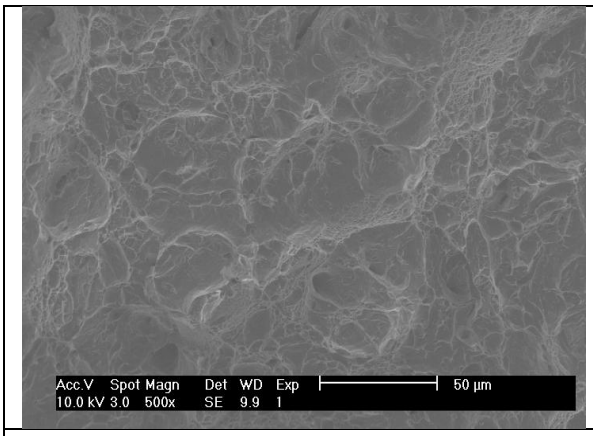

(A) Cast: Heat Treatment # 1:
HIP + Austenitize (1800°F) 1 Hour + Temper (375°F) 4 Hours

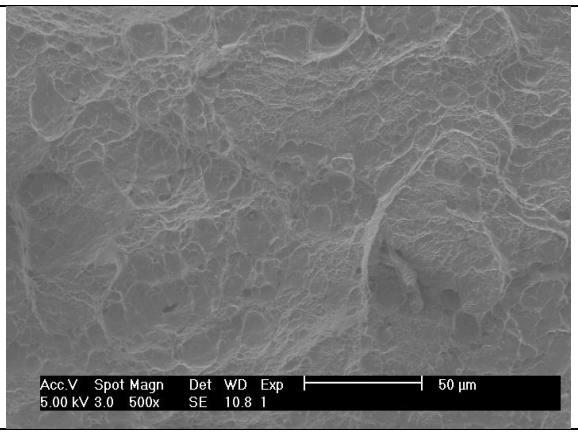

(B) Cast: Heat Treatment #2:
HIP + Austenitize (1900°F) 1 Hour + Temper (450°F) 4 Hours

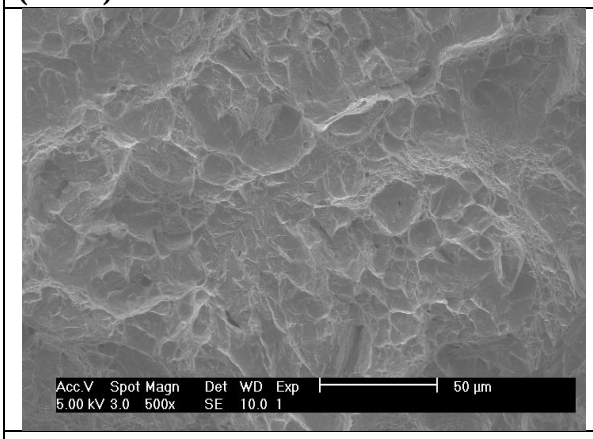

(C) Cast: Heat Treatment #3:
HIP + Homogenize (2000°F) 2 Hours + Austenitize (1800°F) 1 Hour + Temper (450°F) 4 Hours

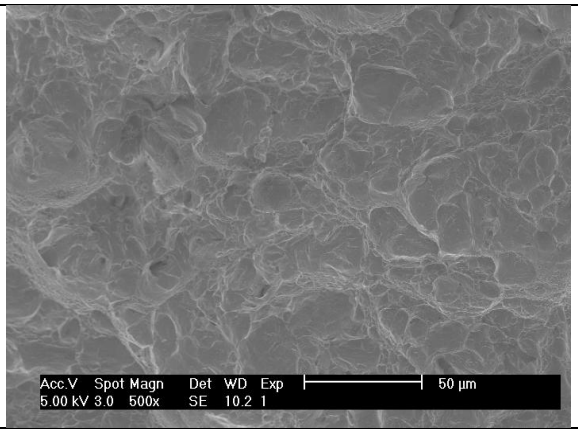

(D) Cast: Heat Treatment #4:
HIP + Homogenize (2000°F) 2 Hours + Austenitize (1900°F) 1 Hour + Temper (375°F) 4 Hours

Figure 5.17: Fracture surface images for ES-1 HIP and heat treated with various conditions, SEM 500X.

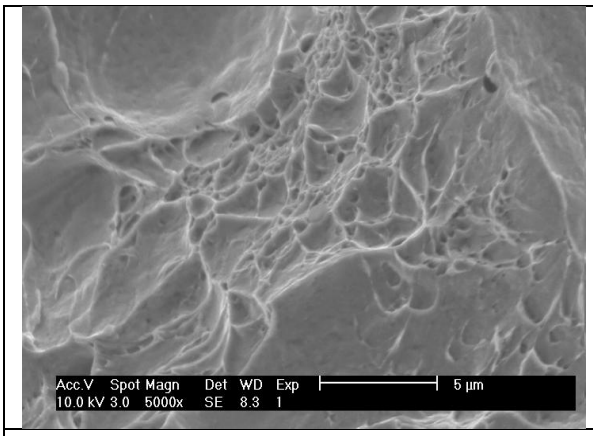

A) Cast: Heat Treatment # 1:
HIP + Austenitize (1800°F) 1 Hour + Temper (375°F) 4 Hours

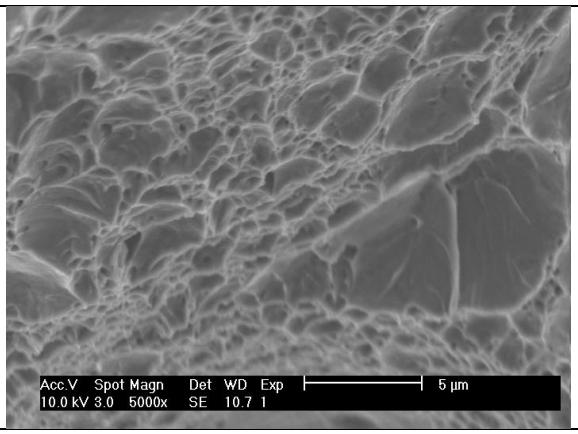

(B) Cast: Heat Treatment #2:
HIP + Austenitize (1900F) 1 Hour + Temper (450F) 4 Hours

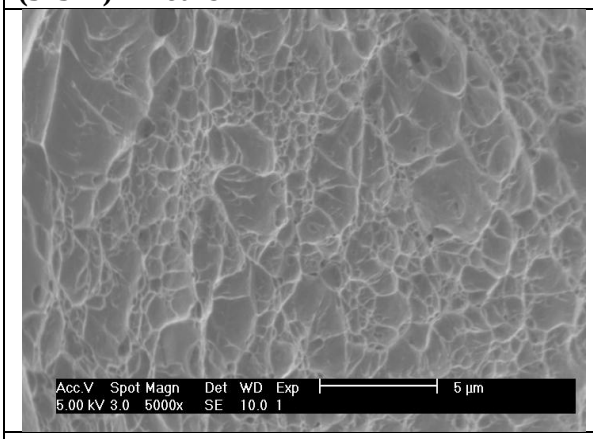

(C) Cast: Heat Treatment #3:
HIP + Homogenize (2000°F) 2 Hours + Austenitize (1800°F) 1 Hour + Temper (450°F) 4 Hours

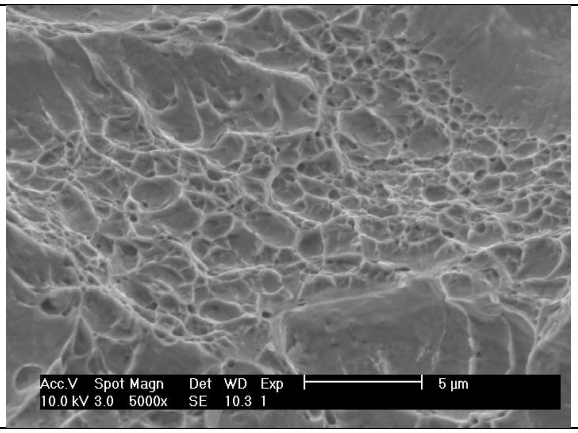

(D) Cast: Heat Treatment #4:
HIP + Homogenize (2000°F) 2 Hours + Austenitize (1900°F) 1 Hour + Temper (375°F) 4 Hours

Figure 5.18: Fracture surface images for ES-1 HIP and heat treated with various conditions, SEM 5000X.

5.2.3 Estimation of Microsegregation Reduction

Since the cast ES-1 ingot material was taken from a large cast ingot, the DAS is expected to be much larger than the DAS in the investment cast 4340+ study. The DAS is expected to be in the 80 to120 µm range rather than the 20 to 40 µm range. **Table 5.9** shows estimates of the microsegregation reductions of the substitutional alloying elements in the cast eglin steel during heat treatments 1 and 2. Heat treatments 1 and 2 both consisted of a 4 hour HIP cycle at 2125°F followed by a 1 hour austenization treatment at either 1900°F (treatment #1) or 1800°F (treatment #2). Looking at **Table 5.9**, it is evident that very few differences are expected in microsegregation reduction between the two heat treatments. As was the case with the

microsegregation reduction estimates for the investment cast 4340+ material, significant differences in microsegregation reduction are seen both between alloying elements and between the DAS sizes for the same alloying elements. For the ES-1 alloy, at a DAS of 80μm, the microsegregation reduction is estimated to be 56% for Cr after the HIP homogenization cycle while it is estimated to be just 20% for W after the same cycle. When the assumed DAS is increased to 200μm, the microsegregation reduction during long time, high temperature HIPing estimates decreases to just 30% and 9% for Cr and W respectively.

Table 5.9: Estimation of Percent Microsegregation Reduction for the Cast ES-1 alloy for Heat Treatments 1 and 2.

DAS (μm)	Heat Treatment #1									
	HIP (2125°F / 4 hrs.)					HIP + Austenitize (1900°F / 1 hr.)				
	Cr	Mo	Mn	Ni	W	Cr	Mo	Mn	Ni	W
20	100%	100%	100%	100%	97%	100%	100%	100%	100%	97%
40	96%	92%	76%	82%	58%	96%	92%	76%	82%	58%
80	56%	47%	30%	35%	20%	56%	48%	30%	35%	20%
120	30%	25%	15%	17%	9%	31%	25%	15%	18%	9%
200	12%	10%	6%	7%	3%	12%	10%	6%	7%	3%
DAS (μm)	**Heat Treatment #2**									
	HIP (2125°F / 4 hrs.)					HIP + Austenitize (1800°F / 1 hr.)				
	Cr	Mo	Mn	Ni	W	Cr	Mo	Mn	Ni	W
20	100%	100%	100%	100%	97%	100%	100%	100%	100%	97%
40	96%	92%	76%	82%	58%	97%	93%	77%	83%	59%
80	56%	47%	30%	35%	20%	47%	48%	31%	36%	20%
120	30%	25%	15%	17%	9%	31%	25%	15%	18%	9%
200	12%	10%	6%	7%	3%	13%	10%	6%	7%	4%

Table 5.10 displays estimates for the microsegregation reduction expected for the cast ES-1 material after heat treatments 3 and 4. Heat treatments 3 and 4 consist of the same steps in heat treatments 1 and 2 respectively, with the addition of a 2 hour, 2000°F homogenization step carried out after the HIP homogenization treatment. Again, the diffusion estimates show that very little, if any differences in microsegregation are expected between heat treatments 3 and 4. When comparing the estimates of microsegregation reduction for heat treatments 1 and 2 with heat treatments 3 and 4, some slight differences do exist as a result of the addition of the 2000°F homogenization step. For instance, at a DAS of 80μm, the microsegregation reduction for Mo is expected to be just 48% after full heat treatment 1 or 2. The microsegregation reduction for Mo is expected to be 54% after full heat treatment 3 or 4. Again, the differences in the expected

microsegregation reductions are due to the differences in DAS and alloying elements being considered.

Table 5.10: Estimation of Percent Microsegregation Reduction for Cast ES-1 Material after Heat Treatments 3 and 4.

DAS (μm)	Heat Treatment #3														
	HIP (2125F / 4 hrs.)					HIP + Homo. (2000F / 2 hrs.)					HIP + Homo.+ Aus. (1800F / 1 hr.)				
	Cr	Mo	Mn	Ni	W	Cr	Mo	Mn	Ni	W	Cr	Mo	Mn	Ni	W
20	100%	100%	100%	100%	97%	100%	100%	100%	100%	98%	100%	100	100	100%	98%
40	96%	92%	76%	82%	58%	98%	95%	81%	86%	63%	98%	95%	81%	86%	64%
80	56%	47%	30%	35%	20%	62%	53%	34%	39%	22%	62%	53%	34%	39%	22%
120	30%	25%	15%	17%	9%	35%	28%	17%	20%	11%	35%	29%	17%	20%	11%
200	12%	10%	6%	7%	3%	14%	11%	6%	8%	4%	14%	11%	7%	8%	4%
DAS (μm)	**Heat Treatment #4**														
	HIP (2125F / 4 hrs.)					HIP + Homo. (2000F / 2 hrs.)					HIP + Homo.+ Aus. (1900F / 1 hr.)				
	Cr	Mo	Mn	Ni	W	Cr	Mo	Mn	Ni	W	Cr	Mo	Mn	Ni	W
20	100%	100%	100%	100%	97%	100%	100%	100%	100%	98%	100%	100	100	100%	98%
40	96%	92%	76%	82%	58%	98%	95%	81%	86%	63%	98%	95%	82%	82%	64%
80	56%	47%	30%	35%	20%	62%	53%	34%	39%	22%	63%	54%	35%	35%	23%
120	30%	25%	15%	17%	9%	35%	28%	17%	20%	11%	35%	29%	17%	17%	11%
200	12%	10%	6%	7%	3%	14%	11%	6%	8%	4%	15%	12%	7%	7%	4%

5.3 Results for Cast ES-1 Ingot Porosity Reduction Study

The results for the microporosity study carried out on the cast ES-1 ingot material are displayed in **Tables 5.11**. **Figure 5.19** shows representative unetched micrographs from all three samples included in the study. The results show that the addition of a HIP cycle to the processing of the ES-1 cast ingot material significantly reduced both the average number of pores and the average percent porosity. The average number of pores / mm^2 across the 9 images taken for samples A (as cast), sample B (as cast + HIP), and sample C (as cast + homogenize) are 87, 57, and 154 pores/ mm^2 respectively. The average area pore fraction or average percent porosity across the 9 images for samples A, B, and C was 0.21%, 0.11%, and 0.29% respectively. The results suggest that high temperature homogenization treatment increasing the average number and average area fraction (% porosity) of the cast ES-1 material. The average pore size (μm^2) and pore size distribution do not show significant differences between samples. Average pore size (μm^2) across the 9 images for samples A, B, and C was 23.9 μm^2, 21.5 μm^2, and 18.4 μm^2 respectively. The distribution of the pore sizes remained about the same for each of the samples. About 85% of the pores in all three of samples were between 0 and 20 μm^2 in

size. Breaking it down further, 67 to 68% of the pores in all three of the samples were between 0 and 10 μm^2 while another 15 to 20% of the pores in all three of the samples were between 10 and 20 μm^2.

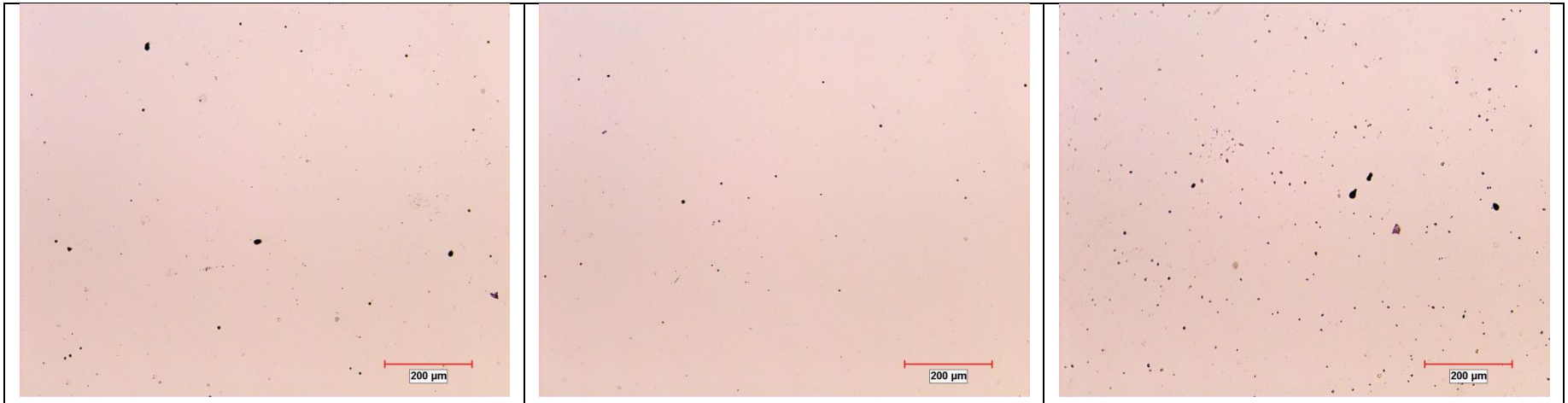

Figure 5.19: Representative micrograph frames used for Cast ES-1 Microporosity Reduction Study. (Polished, Unetched, 100X)

Table 5.11: Summary of HIP microporosity reduction study on cast ES-1.

Sample	A (As Cast)		B (2125°F HIP)		C (2000°F Homogenization)	
	Average	**Std. Deviation**	**Average**	**Std. Deviation**	**Average**	**Std. Deviation**
Number of Pores / mm^2	**87**	**23.0**	**57**	**22.0**	**154**	**66.8**
Minimum Pore Size(µm^2)	1.4	1.0	1.3	0.9	1.5	1.2
Maximum Pore Size(µm^2)	649.3	623.0	426.8	468.3	633.6	828.3
Area of Pores (µm^2)	1933	779.9	1045	613.5	2732	1472.2
Area Pore Fraction	0.00206	0.00083	0.00111	0.00065	0.00291	0.00157
% Porosity	**0.21%**	**0.08%**	**0.11%**	**0.07%**	**0.29%**	**0.16%**
% Pores (0 - 10 µm^2)	68.44%	10.27%	66.89%	11.61%	67.26%	15.49%
% Pores (10 - 20 µm^2)	15.94%	6.26%	20.18%	7.45%	19.80%	11.78%
% Pores (20-30 µm^2)	6.28%	4.36%	6.74%	3.07%	5.05%	4.14%
% Pores (30 - 100 µm^2)	5.85%	2.51%	3.75%	3.06%	5.63%	1.95%
% Pores (> 100 µm^2)	3.96%	2.17%	2.44%	2.39%	2.26%	2.12%
Average Pore Size(µm^2)	**23.9**	**10.9**	**21.5**	**16.7**	**18.4**	**8.2**

5.4 Results for Cryo Quenching Study for Cast ES-1 Ingot Material

The results from the experimental cryo-treatment carried out on the cast-ES-1 ingot material (**Table 5.12**) showed that cryogenic quenching results in a small improvement in hardness with corresponding decreases in -40°F impact toughness. The micrographs (**Figure 5.20**) did not appear significantly different from the non-cryo treated sample in **Figure 5.22**. The optical micrographs at low magnification (**Figure 5.20**) and SEM etched micrographs at high magnifications (**Figure 5.21**) both appeared to be free of large inclusions and appeared to possess only a small amount of microporosity.

Table 5.12: Cryo Quenching Study Mechanical Properties.

Heat Treatment	HIP Homogenization	Homogenization	Austenitizing/ CRYO Quench/ Tempering	UTS (ksi)	0.2% YS (ksi)	Elong (%)	CVN -40°F (ft-lbs)	Tempered Hardness (HRC)
CRYO	2125°F, 4 hrs., 15ksi., slow vessel cool to 700°F- Air Cool to Room Temp.	2000°F, 2 hrs. Air Cool to Room Temp.	1900°F, 1 hr. Water Quench/ Submerge in Liquid Nitrogen for 6 hrs./ 375°F, 4 hrs. Water Quench	**243.0**	**196.0**	**14**	**34**	**53**
NON-CRYO*	2125°F, 4 hrs., 15ksi., slow vessel cool to 700°F- Air Cool to Room Temp.	2000°F, 2 hrs. Air Cool to Room Temp.	1900°F, 1 hr. Water Quench/ 375°F, 4 hrs. Water Quench	**253.1**	**193.3**	**15**	**40**	**49**

* The NON-CRYO treated sample is heat treatment #4 from cast + HIP ES-1 (heat treatment #4) study.

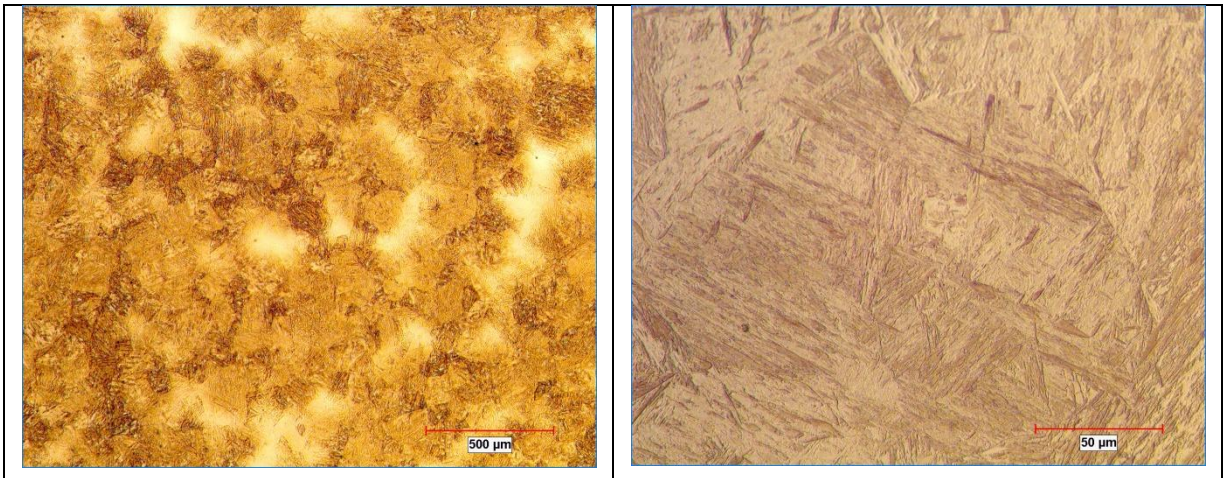

(A) CRYO Treated (50X) (B) CRYO Treated (500X)

Figure 5.20: Micrographs for CRYO treated ES-1; etched, (A) 50X, (B) 500X.

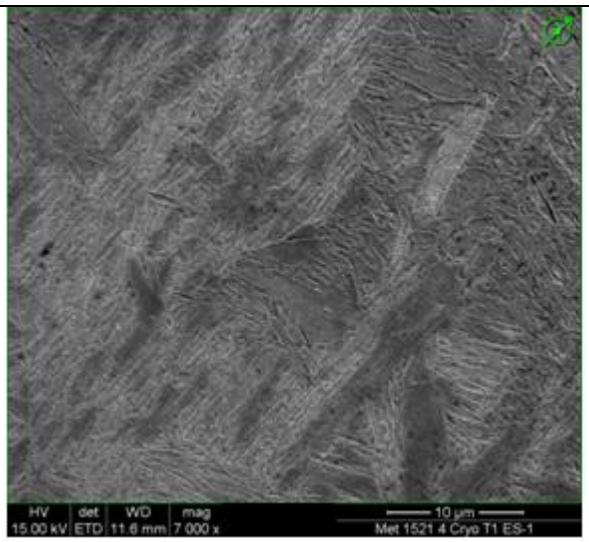

(A) CRYO Treated (7000X)

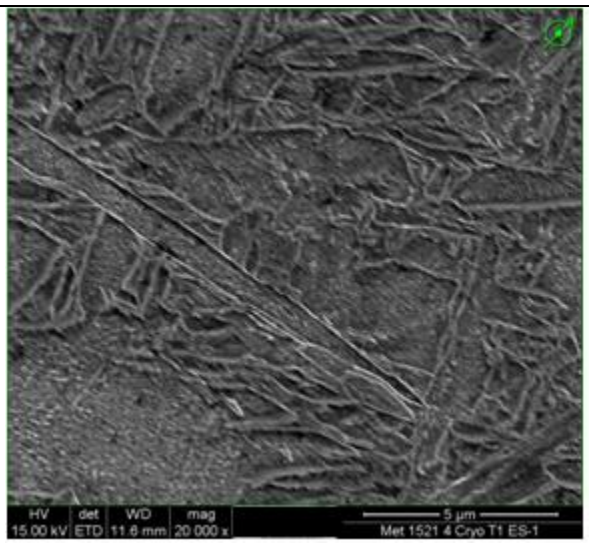

(B) CRYO Treated (20000X)

Figure 5.21: SEM micrographs for CRYO treated ES-1; SEM, (A) 7000X, (B) 20000X.

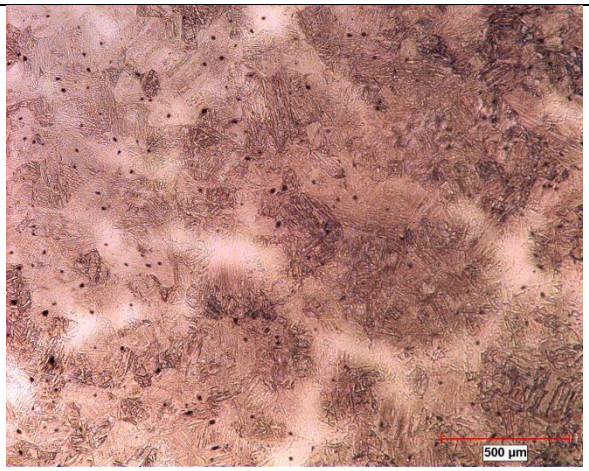

(A) Non-CRYO Treated (50X)

(B) Non-CRYO Treated (500X)

Figure 5.22: Micrographs for the non-CRYO treated ES-1; etched, (A) 50X, (B) 500X.

5.5 XRD Retained Austenite (RA) Study Results for Cast ES-1 Ingot Material

The quantitative results for the XRD study carried out on cast ES-1 ingot material are shown in **Table 5.13.** No retained austenite was found in any of the three cast ES-1 samples that were analyzed using XRD analysis.

Table 5.13: % Retained Austenite Results for XRD Analysis of Cast ES-1 Ingot Material

Sample No.	HIP Homogenization	Homogenization	Austenitizing	Tempering	% RA
1	2125°F, 4 hrs., 15ksi., slow vessel cool to 700°F- Air Cool to Room Temp.	2000°F, 2 hrs. Air Cool to Room Temp.	1900°F, 1 hr. Water Quench	375°F, 4 hrs. Water Quench	**0%**
2	2125°F, 4 hrs., 15ksi., slow vessel cool to 700°F- Air Cool to Room Temp.	2000°F, 2 hrs. Air Cool to Room Temp.	1900°F, 1 hr. Water Quench	None	**0%**
3	None	2000°F, 2 hrs. Air Cool to Room Temp.	1900°F, 1 hr. Water Quench	None	**0%**

The ASTM E975 standard for austenite measurement is commonly used to measure the amount of retained austenite in steels. The standard assumes the steel has a nearly random orientation and has few carbides. As shown in **Figure 5.23**, the method compares the 200 Martensite (M200) peak with the Austenite 200 and 220 peaks (A200 & A220, respectively). If austenite A200 and A220 peaks exist in the XRD diffraction pattern plot along with the M200 peak, a correction factor must be used to account for the differences in the scattering power of the austenite and martensite phases in order to quantify the percent of retained austenite in the samples [115]. In this study, the percent of retained austenite could not be quantified because the A200 and A220 peaks did not exist on any of the diffraction pattern plots shown in **Figures 5.24 – 5.26**. Because of the detection limit of retained austenite x-ray diffraction measurements, the austenite percentage in these samples should be considered to be less than 2% retained austenite.

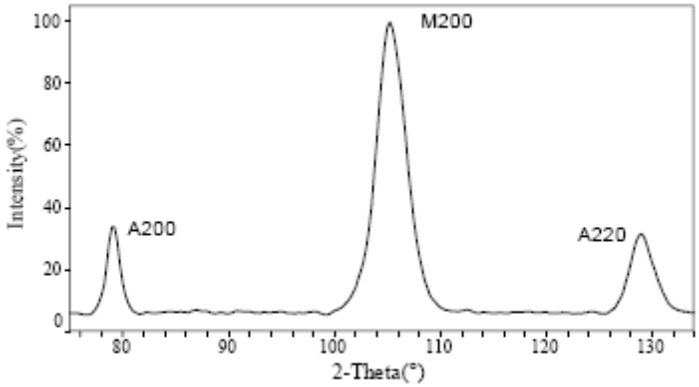

Figure 5.23: Example x-ray diffraction pattern of a steel containing a significant amount of retained austenite.

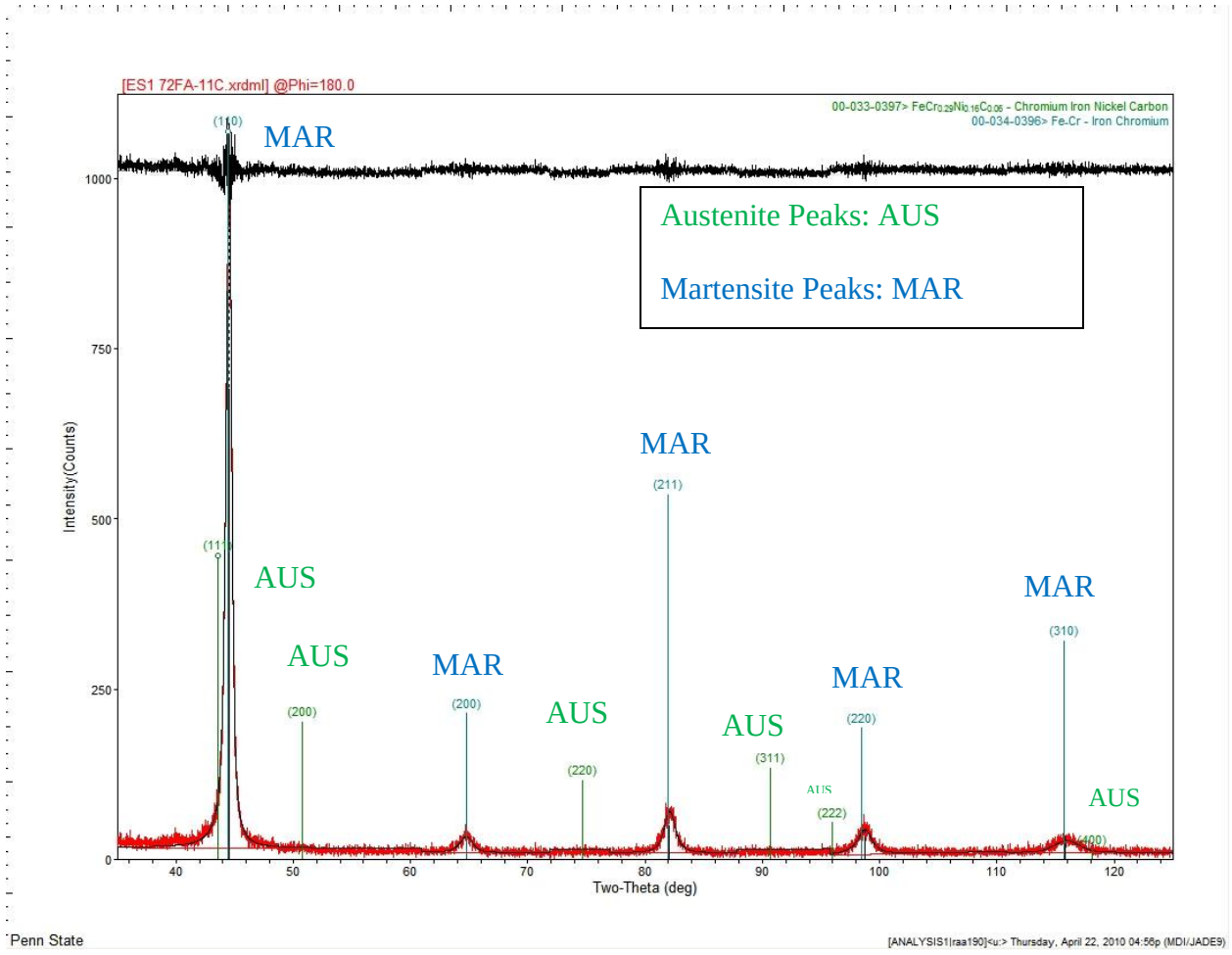

Figure 5.24: XRD Diffraction Pattern Plot for Sample 1.

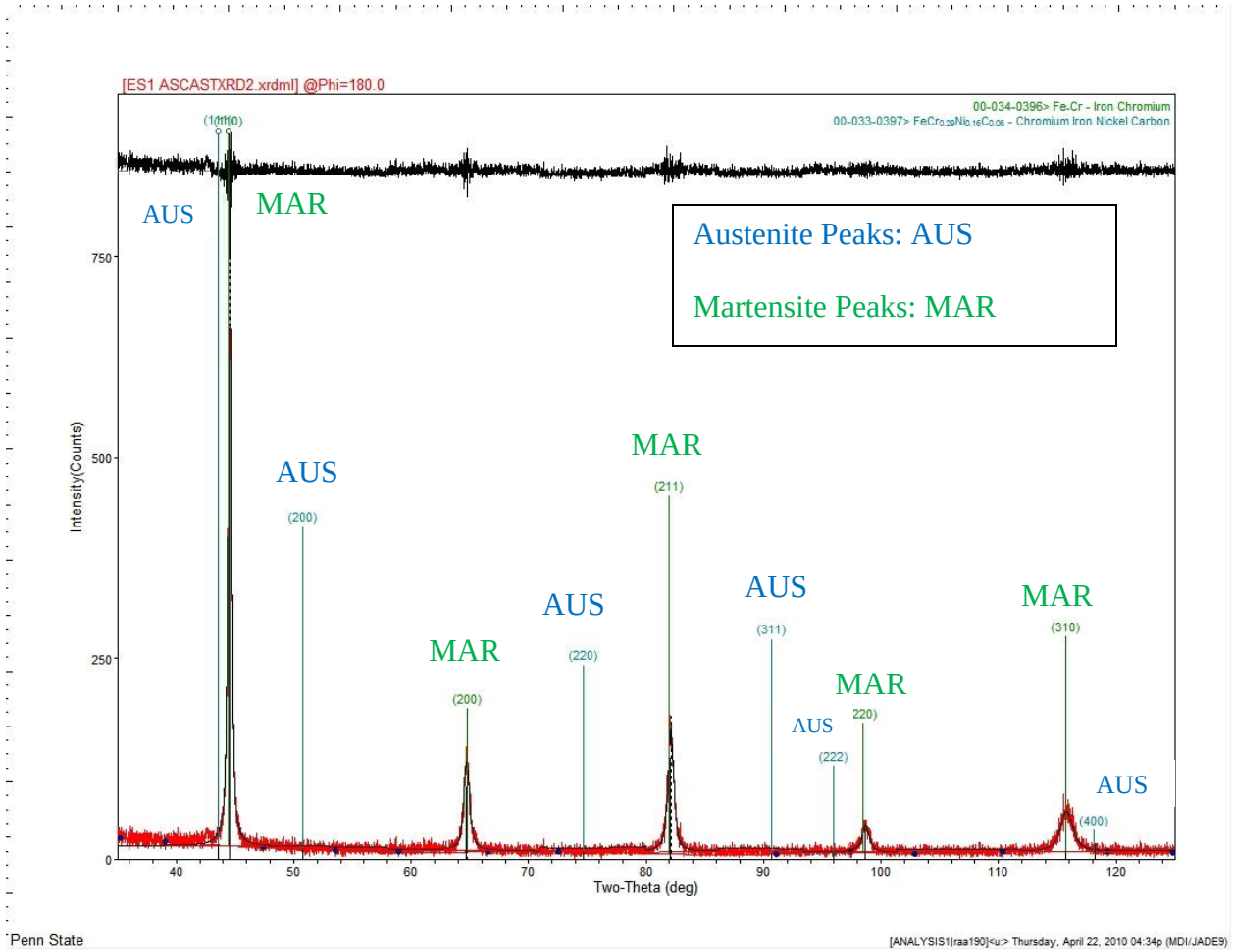

Figure 5.25: XRD Diffraction Pattern Plot for Sample 2.

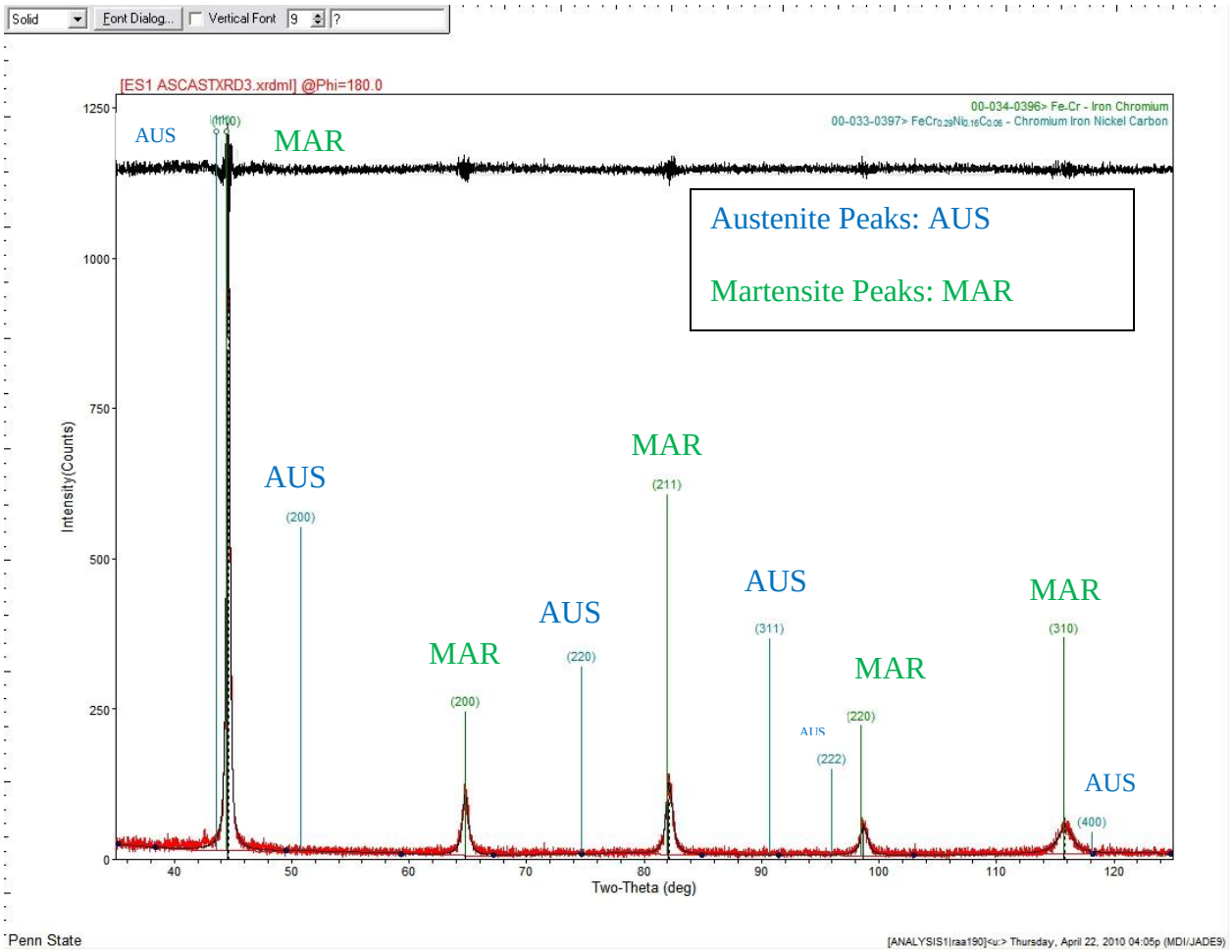

Figure 5.26: XRD Diffraction Pattern Plot for Sample 3.

5.6 Results for Transition Carbide Characterization Study for ES-1 Material

The results of the heat treatment study, outlined in section 3.4.4, carried out to characterize the transition carbides present in the ES-1 material are shown in **Figure 5.27** below. The SEM results show that after a high temperature tempering step, small (less than 1 micron) alloy carbides are present along lath and martensite packet boundaries. The EDAX work results show these alloy carbides are rich in chromium, molybdenum, and tungsten.

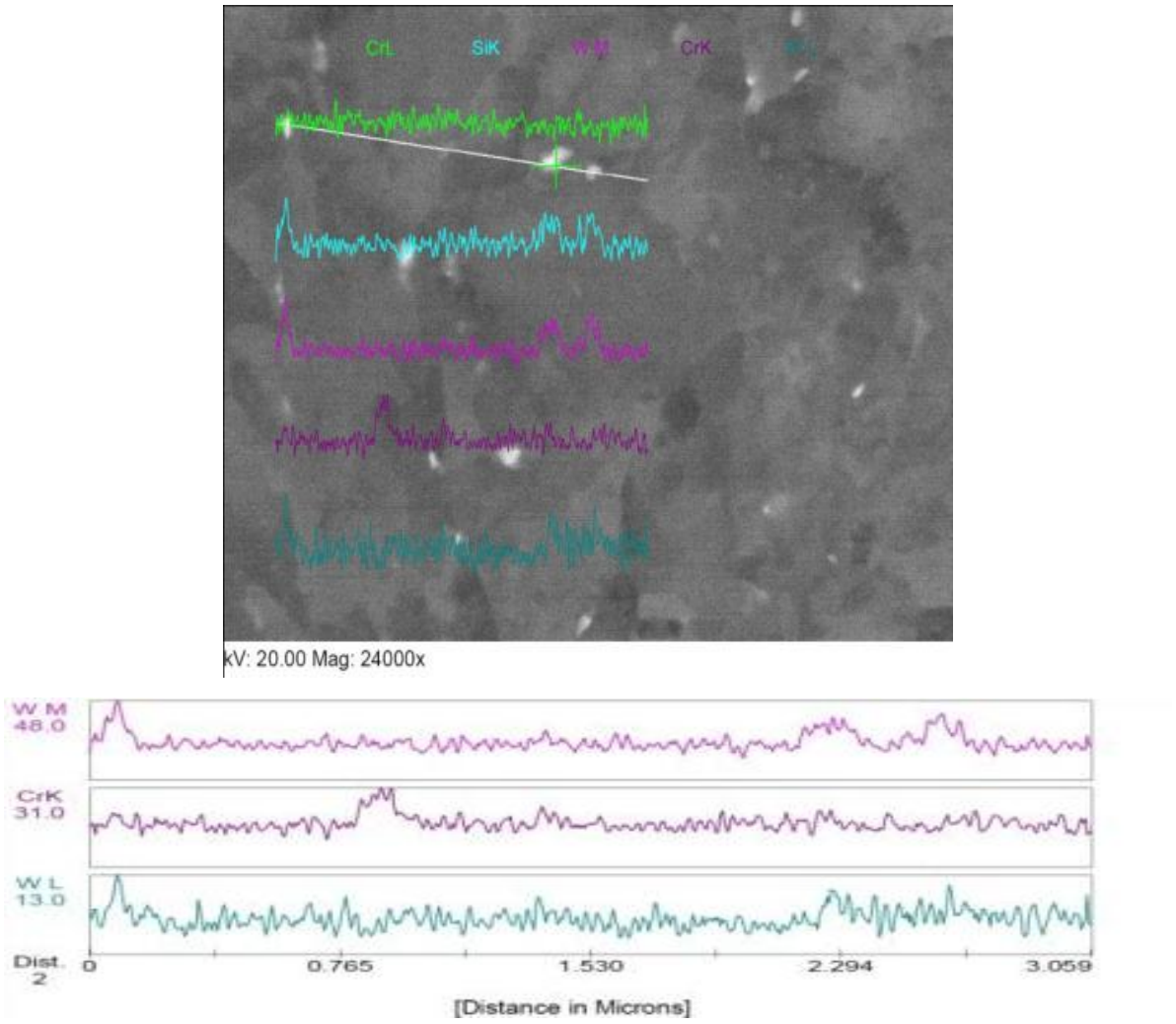

Figure 5.27: SEM image at 24,000X of forged ES-1 Material Quenched and Tempered at 1112°F (600°C) showing evidence of carbides rich in chromium, molybdenum, and tungsten.

5.7 Results for Investment Cast ES-1 Screening Experiments (Heats 1 & 2)

The first experiment with investment ES-1 re-melt material, including heats 1 and 2, was carried out to evaluate the mechanical properties achievable with the previously determined best heat treatment cycle. In addition, the effects of a homogenization cycle that mimicked a HIP cycle (without pressure) was also carried out. Finally, the effects of removing the homogenization and austenization steps from the heat treatment process were studied. Because of the undesirable high aluminum content in heats 1 (0.09%) and 2 (0.06%), the mechanical properties were only screened for heat 2, which possessed the lower aluminum content. A summary of the mechanical property results for the six different heat treatment cycles carried out

on heat #2 of the investment cast material are shown in **Table 5.14**. The microstructure and fracture surfaces were characterized and are presented. Estimates of the percent reduction in microsegregation are also presented for each heat treatment cycle. As for previous modeling estimates of percent reduction in microsegregation are reported, the initial concentrations of alloying elements in the dendritic and inter-dendritic regions were chosen to be +/- 0.5 wt % from given alloy nominal concentrations. For this analysis, the nominal composition of Mo is assumed to be 0.4 wt % with the interdendrtic composition assume to be 0.8 wt% and the dendritic composition to be 0.0wt%. The mechanical property results show that both the average -40°F and +72°F impact toughness of the fully heat treated investment cast + HIP ES-1 material (**Table 5.14**) is somewhat lower than that of the cast + HIP ES-1 ingot material (**Table 5.8**). At -40°F, for identical treatments, the average impact energy for heat treatment #1 in the investment cast study was 27 ft-lbs. while the average impact energy for heat treatment #4 in the cast ES-1 ingot study above was 40 ft-lbs. The results for the investment cast study show that the 4 hour, high temperature (2125°F) HIP cycle significantly increases the average impact toughness and % elongation when compared to its 4 hour, high temperature (2125°F) homogenization cycle counterpart. When both the high temperature HIP cycle and the high temperature homogenization cycle are left out of the heat treatment cycle, the average impact toughness of the alloy degrades even further. The average UTS and YS values remain relatively unchanged throughout the heat treatments for the investment cast study.

Table 5.14: Summary of the mechanical property results for heat #2 of the Investment Cast Study.

Heat Treatment	HIP Homogenization	Homogenization	Austenitizing/ Tempering	UTS (ksi)	0.2% YS (ksi)	Elong (%)	CVN -40°F/+72°F (ft-lbs)	Tempered Hardness (HRC)
1	2125°F, 4 hrs., 15ksi., slow vessel cool to 700°F- Air Cool to Room Temp.	2000°F, 2 hrs. Air Cool to Room Temp.	1900°F, 1 hr. Water Quench/ 375°F, 4 hrs. Water Quench	**234**	**180**	**12**	**27 / 31**	**49**
2	2125°F, 4 hrs., 15ksi., slow vessel cool to 700°F- Air Cool to Room Temp.	None	1900°F, 1 hr. Water Quench/ 375°F, 4 hrs. Water Quench	**230**	**176**	**14**	**24 / 30**	**50**
Heat Treatment	**Homogenization (No HIP)**	**Homogenization**	**Austenitizing/ Tempering**	**UTS (ksi)**	**0.2% YS (ksi)**	**Elong (%)**	**CVN -40°F/+72°F (ft-lbs)**	**Tempered Hardness (HRC)**
3	Heat up in Furnace from Room Temp. to 2125°F (2 hrs.)/hold 4 hrs. at 2125°F /slow cool in furnace to 700°F- Air Cool to Room Temp.	2000°F, 2 hrs. Air Cool to Room Temp.	1900°F, 1 hr. Water Quench/ 375°F, 4 hrs. Water Quench	**228**	**179**	**5**	**22 / 22**	**50**
4	Heat up in Furnace from Room Temp. to 2125°F (2 hrs.)/hold 4 hrs. at 2125°F /slow cool in furnace to 700°F- Air Cool to Room Temp.	None	1900°F, 1 hr. Water Quench/ 375°F, 4 hrs. Water Quench	**226**	**178**	**7**	**21 / 23**	**49**
Heat Treatment	**HIP Homogenization**	**Homogenization**	**Austenitizing/ Tempering**	**UTS (ksi)**	**0.2% YS (ksi)**	**Elong (%)**	**CVN -40°F/+72°F (ft-lbs)**	**Tempered Hardness (HRC)**
5	None	2000°F, 2 hrs. Air Cool to Room Temp.	1900°F, 1 hr. Water Quench/ 375°F, 4 hrs. Water Quench	**231**	**177**	**10**	**18 / 22**	**49**
6	None	None	1900°F, 1 hr. Water Quench/ 375°F, 4 hrs. Water Quench	**228**	**174**	**7**	**17 / 25**	**50**

**Note: All impact and tensile values shown are an average of (2) Charpy or tensile values; all hardness data is an average of (3) measurements from a single Charpy specimen.

5.7.1 Mechanical Property Results

In addition to the average values reported, the complete mechanical property results are shown in **Appendix A.4**.

5.7.2 Micrographs and Fractographs

The etched **(Figures 5.28 & 5.29)** and unetched **(Figure 5.30)** micrographs for the investment cast ES-1 material are shown below. The samples homogenized at 2125°F for 4

hours (Samples A – D) seem to differ in terms of the contrast between the dendritic and inter dendritic areas when compared to those samples not homogenized at 2125°F for 4 hours (Samples D & E). The representative unetched micrographs in **Figure 5.30** show further evidence of the results reported for the cast ES-1 ingot material in **Figure 5.19 and Table 5.11.** The samples that received a HIP treatment, **Figures 5.30 (A) and (B)**, possess smaller and less pores when compared with **Figures 5.30 (C) through (F)** that did not receive a HIP treatment. The complete microporosity study results can be found in **Appendix A.2**. From the picture and the porosity analysis, HIP appears to reduce the area fraction and number of pores in the cast ES-1 material.

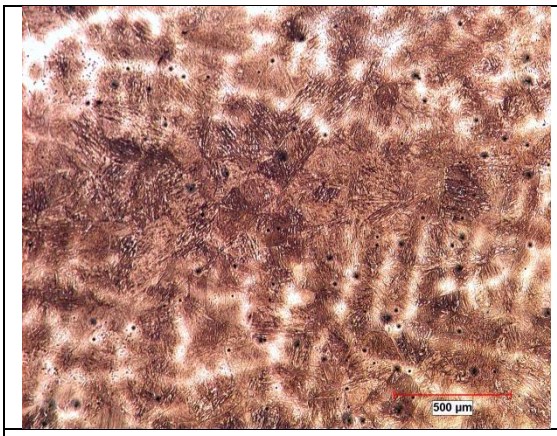

(A) Investment Cast: Heat Treatment # 1
HIP: 2125°F / 4 hrs; Homo: 2000°F / 2 hrs

(B) Investment Cast: Heat Treatment #2
HIP: 2125°F / 4 hrs; No Homo.

(C) Investment Cast: Heat Treatment #3
No HIP; Homo: 2125°F / 4 hrs;
Homo: 2000°F / 2 hrs

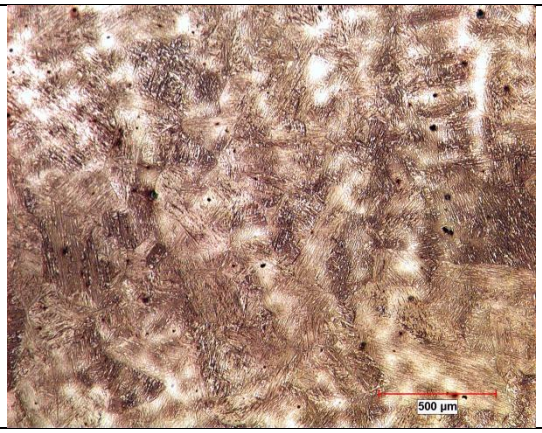

(D) Investment Cast: Heat Treatment #4
No HIP; Homo: 2125°F / 4 hrs

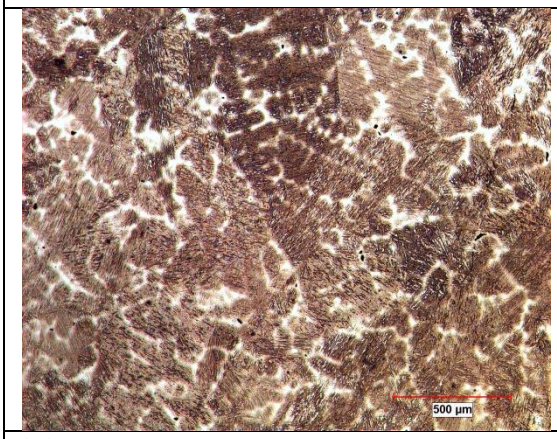

(E) Investment Cast: Heat Treatment #5
No HIP; Homo: 2000°F / 4 hrs

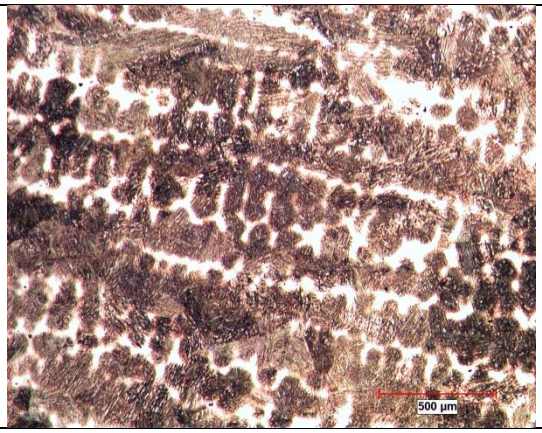

(F) Investment Cast: Heat Treatment #6
No HIP; No Homo

Figure 5.28: Micrographs for the investment cast ES-1 alloy heat treated with various conditions; etched, 50X.

(A) Investment Cast: Heat Treatment # 1
HIP: 2125°F / 4 hrs; Homo: 2000°F / 2 hrs

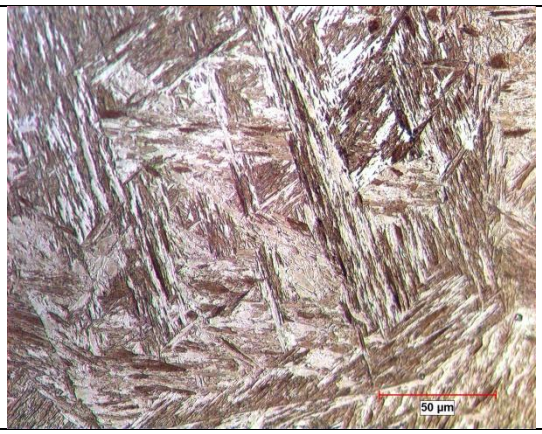

(B) Investment Cast: Heat Treatment #2
HIP: 2125°F / 4 hrs; No Homo.

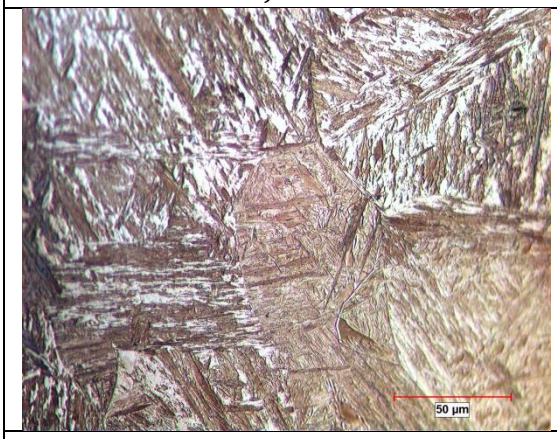

(C) Investment Cast: Heat Treatment #3
No HIP; Homo: 2125°F / 4 hrs;
Homo: 2000°F / 2 hrs

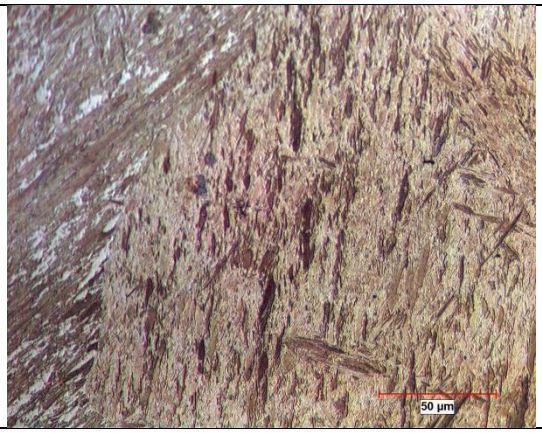

(D) Investment Cast: Heat Treatment #4
No HIP; Homo: 2125°F / 4 hrs

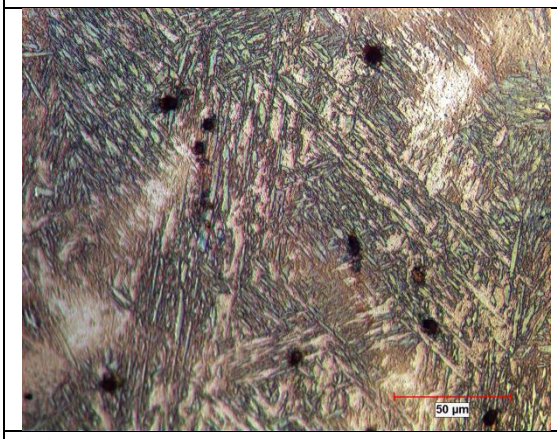

(E) Investment Cast: Heat Treatment #5
No HIP; Homo: 2000°F / 4 hrs

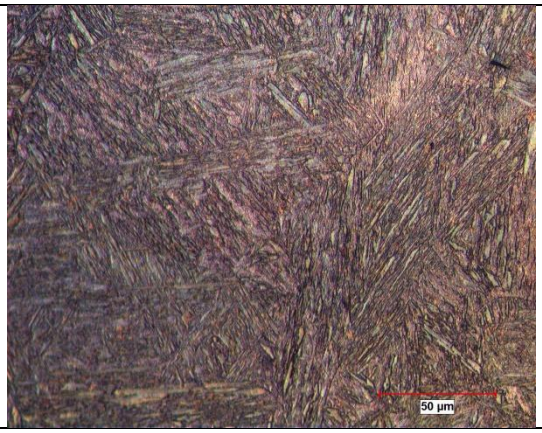

(F) Investment Cast: Heat Treatment #6
No HIP; No Homo

Figure 5.29: Micrographs for the investment cast ES-1 alloy heat treated with various conditions; etched, 500X.

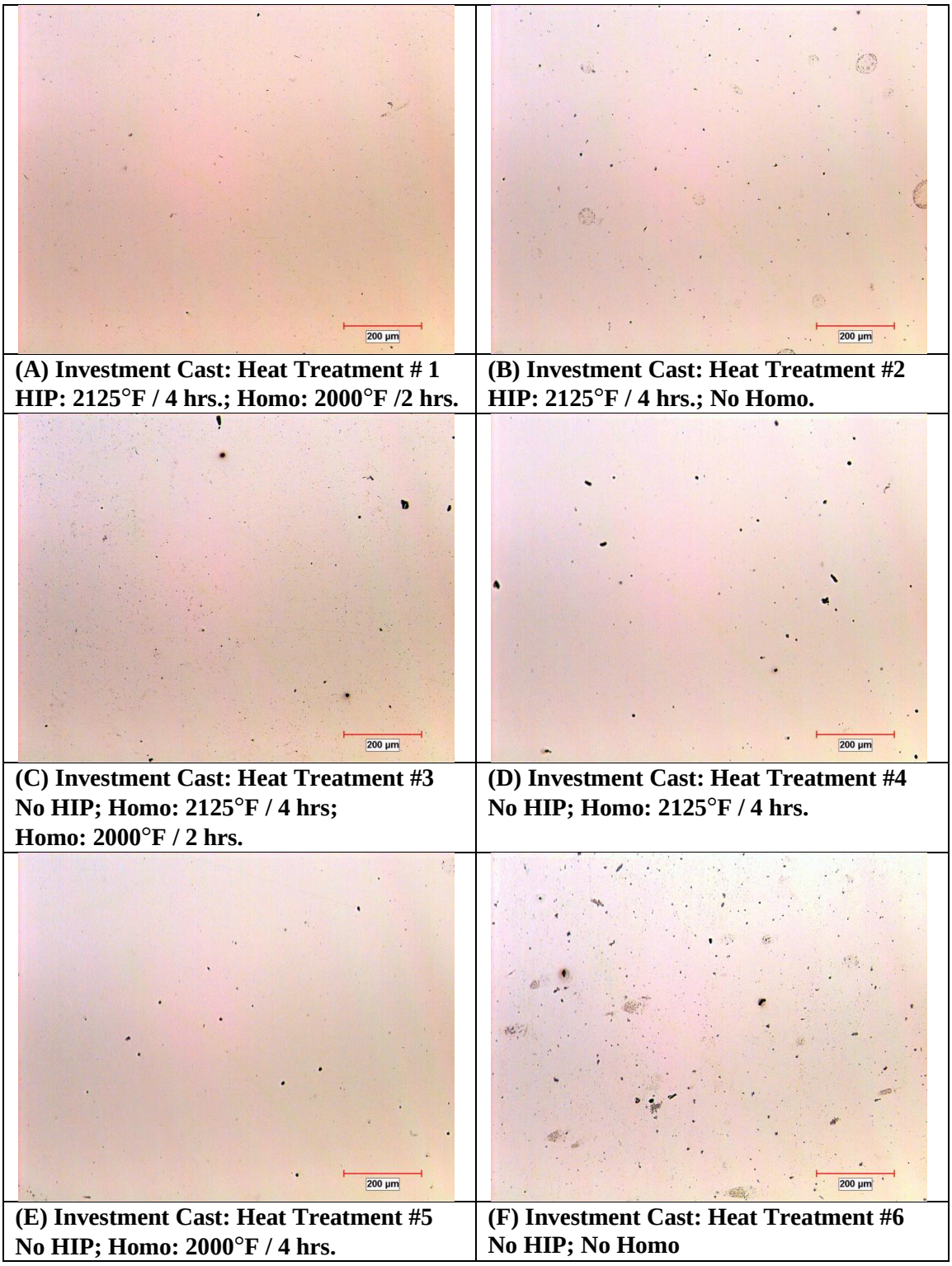

(A) Investment Cast: Heat Treatment # 1 HIP: 2125°F / 4 hrs.; Homo: 2000°F /2 hrs.	**(B) Investment Cast: Heat Treatment #2 HIP: 2125°F / 4 hrs.; No Homo.**
(C) Investment Cast: Heat Treatment #3 No HIP; Homo: 2125°F / 4 hrs; Homo: 2000°F / 2 hrs.	**(D) Investment Cast: Heat Treatment #4 No HIP; Homo: 2125°F / 4 hrs.**
(E) Investment Cast: Heat Treatment #5 No HIP; Homo: 2000°F / 4 hrs.	**(F) Investment Cast: Heat Treatment #6 No HIP; No Homo**

Figure 5.30: Micrographs for the investment cast ES-1 alloy heat treated with various conditions; unetched, 100X.

The results of the SEM fractograph analysis showed that a large amount of inclusions were present across all six of the investment cast samples. The spherical shape of the particles in

Figure 5.31A along with EDAX scans showing high concentrations of manganese and sulfur (**Figure 5.31B**) were proof that MnS sulfide inclusions were serving as crack initiation sites along the fracture surfaces of the investment cast ES-1 material. The cubic shape of the particles in **Figure 5.32A** along with EDAX scans (**Figure 5.32B**) showing high concentrations of aluminum and oxygen were proof that aluminum deoxidation products were serving as crack initiation sites along the fracture surfaces of the investment cast ES-1 material. The fracture surface results showed that the material was not near as "clean" as the cast ingot material studied previously.

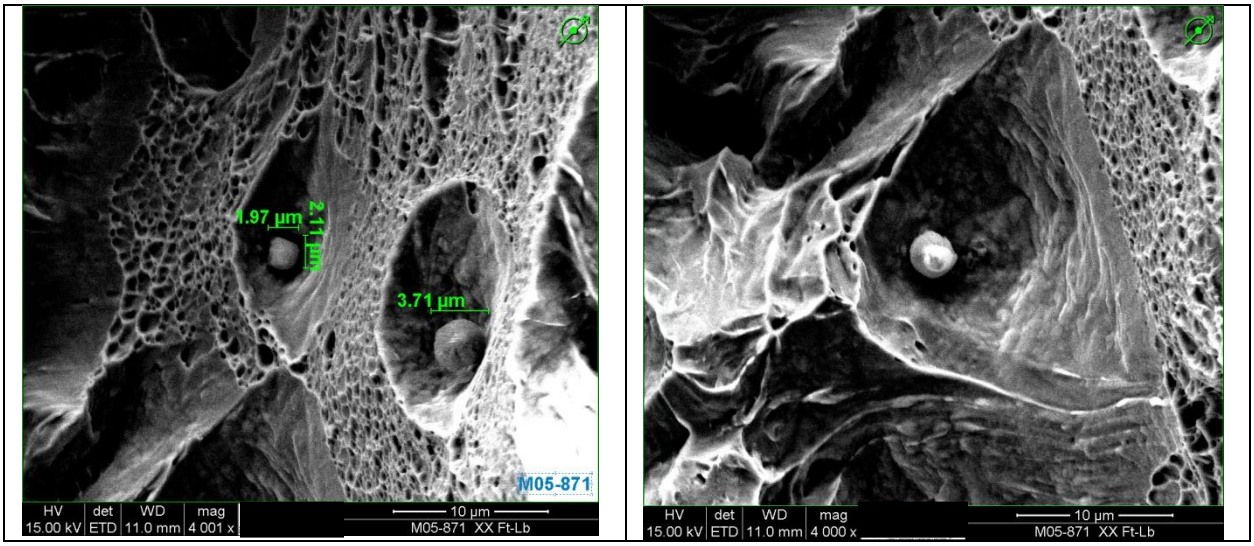

Figure 5.31A: Fractographs show evidence of MnS inclusions along the fracture surface of investment cast ES-1 material; SEM, 4000X.

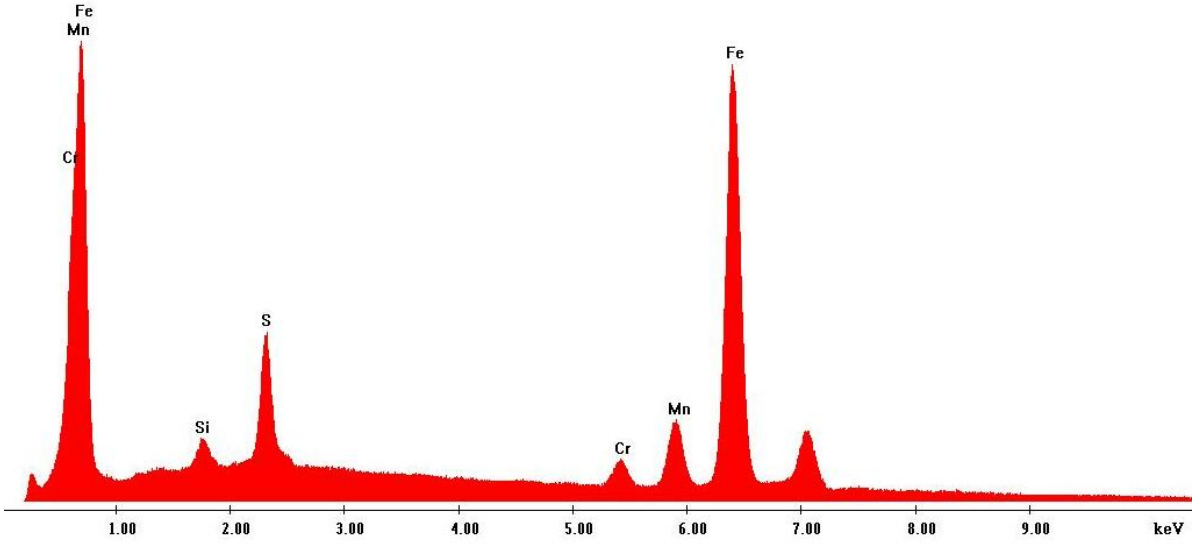

Figure 5.31B: EDS spectrum of the MnS inclusions on the fracture surface of the investment cast ES-1 material.

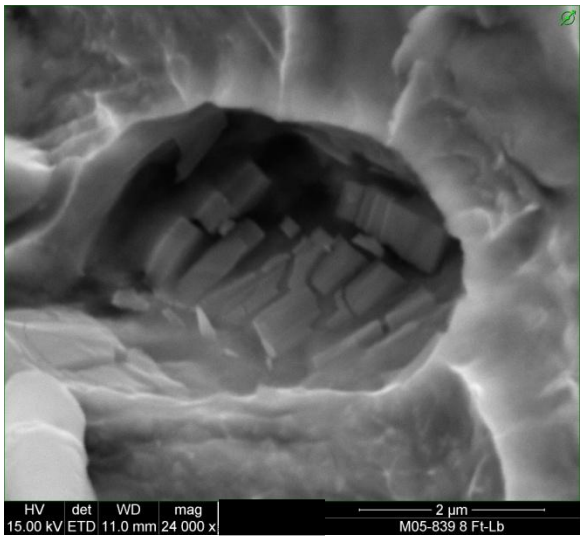

Figure 5.32A: Fractograph showing evidence of an aluminum deoxidation product inclusion along the fracture surface of investment cast ES-1 material; SEM, 24000X.

kV : 20.00 Tilt: 0.10 Take-off:19.65 AmpT : 3.2
Detector Type:SDD Apollo 40 Resolution:143.78 Lsec 56

EDAX ZAF Quantification (Standardless)
Element Normalized
SEC Table : Default

Element	Wt %	At %	K-Ratio	Z	A	F
O K	21.81	38.45	0.0571	1.0821	0.2415	1.0012
AlK	30.38	31.76	0.1293	1.0071	0.4215	1.0023
S K	14.38	12.65	0.0847	1.0277	0.5721	1.0018
TiK	1.43	0.84	0.0124	0.9219	0.9154	1.0322
V K	0.33	0.18	0.0029	0.9026	0.9445	1.0508
MnK	13.74	7.06	0.1209	0.9021	0.9751	1.0000
FeK	17.94	9.06	0.1626	0.9189	0.9867	1.0000
Total	100.00	100.00				

Element	Net Inte.	Bkgd Inte.	Inte. Error	P/B
O K	3187.16	156.04	0.25	20.43
AlK	11553.34	529.77	0.13	21.81
S K	6511.94	697.53	0.18	9.34
TiK	563.03	510.61	0.94	1.10
V K	117.86	521.15	3.85	0.23
MnK	3690.84	467.80	0.25	7.89
FeK	4271.38	471.03	0.22	9.07

Figure 5.32B: EDAX spectra analysis of aluminum oxide particles on the fracture surface of the investment cast ES-1 material.

5.7.3 Microsegregation Reduction Estimation for Heat Treatments 1 – 6

An estimate of the expected percent reduction in microsegregation for each of the six heat treatments carried out on the investment cast ES-1 material are shown in **Tables 5.15 – 5.20** below. The results are similar to those presented previously for microsegregation reduction in the cast ES-1 ingot material. In addition to the microsegregation reduction trends discussed for the cast + HIP ingot study, the microsegregation reduction estimates for the investment cast study show results that confirm the differences shown visually in **Figure 5.28**. From the etched micrographs, it is reasonable to assume an average DAS of about 80 μm for the investment cast alloy. Removing the 4-hour, 2125°F homogenization treatment from the heat treatment process drastically reduces the estimate of microsegregation reduction for the alloy. After full heat treatment, at a DAS of 80μm, the estimated percent reduction in microsegregation for Cr and Ni are 63% and 35% (heat treatment #1). When the initial 4 hour homogenization treatment is removed, those microsegregation reduction estimates reduce to 16% and 7% (heat treatment #5).

Table 5.15: Estimation of percent microsegregation reduction for (IC) cast ES-1 material for heat treatment # 1.

DAS (μm)	**Heat Treatment #1**														
	HIP Homogenization					HIP Homo. + Homo. Austenitize					HIP Homo. + Homo.+ Aus. Aus.				
	Cr	Mo	Mn	Ni	W	Cr	Mo	Mn	Ni	W	Cr	Mo	Mn	Ni	W
20	100%	100%	100%	100%	97%	100%	100%	100%	100%	98%	100%	100	100	100%	98%
40	96%	92%	76%	82%	58%	98%	95%	81%	86%	63%	98%	95%	82%	82%	64%
80	56%	47%	30%	35%	20%	62%	53%	34%	39%	22%	63%	54%	35%	35%	23%
120	30%	25%	15%	17%	9%	35%	28%	17%	20%	11%	35%	29%	17%	17%	11%
200	12%	10%	6%	7%	3%	14%	11%	6%	8%	4%	15%	12%	7%	7%	4%

Table 5.16: Estimation of percent microsegregation reduction for (IC) ES-1 material for heat treatment # 2.

DAS (μm)	**Heat Treatment #2**									
	HIP Homogenization					HIP Homogenization + Austenization				
	Cr	Mo	Mn	Ni	W	Cr	Mo	Mn	Ni	W
20	100%	100%	100%	100%	97%	100%	100%	100%	100%	97%
40	96%	92%	76%	82%	58%	97%	93%	77%	83%	59%
80	56%	47%	30%	35%	20%	47%	48%	31%	36%	20%
120	30%	25%	15%	17%	9%	31%	25%	15%	18%	9%
200	12%	10%	6%	7%	3%	13%	10%	6%	7%	4%

Table 5.17: Estimation of percent microsegregation reduction for (IC) ES-1 material for heat treatment # 3.

DAS (µm)	Heat Treatment #3														
	Mimic HIP Homogenization					HIP Homo. + Homo.					HIP Homo. + Homo.+ Aus.				
	Cr	Mo	Mn	Ni	W	Cr	Mo	Mn	Ni	W	Cr	Mo	Mn	Ni	W
20	100%	100%	100%	100%	97%	100%	100%	100%	100%	98%	100%	100	100	100%	98%
40	96%	92%	76%	82%	58%	98%	95%	81%	86%	63%	98%	95%	82%	82%	64%
80	56%	47%	30%	35%	20%	62%	53%	34%	39%	22%	63%	54%	35%	35%	23%
120	30%	25%	15%	17%	9%	35%	28%	17%	20%	11%	35%	29%	17%	17%	11%
200	12%	10%	6%	7%	3%	14%	11%	6%	8%	4%	15%	12%	7%	7%	4%

Table 5.18: Estimation of percent microsegregation reduction for (IC) ES-1 material for heat treatment # 4.

DAS (µm)	Heat Treatment #4									
	Mimic HIP Homogenization					HIP Homogenization + Austenization				
	Cr	Mo	Mn	Ni	W	Cr	Mo	Mn	Ni	W
20	100%	100%	100%	100%	97%	100%	100%	100%	100%	97%
40	96%	92%	76%	82%	58%	97%	93%	77%	83%	59%
80	56%	47%	30%	35%	20%	47%	48%	31%	36%	20%
120	30%	25%	15%	17%	9%	31%	25%	15%	18%	9%
200	12%	10%	6%	7%	3%	13%	10%	6%	7%	4%

Table 5.19: Estimation of percent microsegregation reduction for (IC) ES-1 material for heat treatment # 5.

DAS (µm)	Heat Treatment #5									
	Homogenization					Homogenization + Austenization				
	Cr	Mo	Mn	Ni	W	Cr	Mo	Mn	Ni	W
20	90%	83%	63%	65%	42%	94%	88%	69%	70%	48%
40	44%	36%	22%	23%	13%	50%	41%	26%	26%	15%
80	13%	10%	6%	6%	3%	16%	12%	7%	7%	4%
120	6%	5%	3%	3%	2%	7%	6%	3%	3%	2%
200	2%	2%	1%	1%	<1%	3%	2%	1%	1%	<1%

Table 5.20: Estimation of percent microsegregation reduction for (IC) ES-1 material for heat treatment # 6.

DAS (µm)	Heat Treatment #6					
	Austenization					
		Cr	Mo	Mn	Ni	W
20		37%	30%	18%	17%	10%
40		11%	9%	5%	4%	3%
80		3%	2%	1%	1%	1%
120		1%	1%	1%	1%	<1%
200		<1%	<1%	<1%	<1%	<1%

5.8 Results for Investment Cast ES-1 Screening Experiments (Heat 3)

As a result of high aluminum retention and the presence of inclusions on the fracture surfaces of the impact specimens in heats 1 & 2, a third heat of investment cast ES-1 material was produced. During the production of this heat of material, much care was taken by the steel foundry to ensure proper aluminum retention levels in the final casting. Again, 0.05 wt% of aluminum was added to deoxidize the steel. However, the amount of aluminum measured in the investment cast material after pouring and shakeout was just 0.01 wt%. The specific heat treatments were set up to test the effect of HIP on the mechanical properties of the investment cast ES-1 material. The effect of a second homogenization step was also experimented with. **Table 5.21** summarizes the mechanical property results for heat #3 of the investment cast ES-1 material.

Table 5.21: Summary of the Mechanical Property results for Heat #3 Investment Cast ES-1 Material.

Heat Treatment	HIP Homogenization	Homogenization	Austenitizing/ Tempering	UTS (ksi)	0.2% YS (ksi)	Elong (%)	Energy -40°F/+72°F (ft-lbs)	Tempered Hardness (HRC)
1	2125°F, 4 hrs., 15ksi., slow vessel cool to 700°F- Air Cool to Room Temp.	2000°F, 2 hrs. Air Cool to Room Temp.	1900°F, 1 hr. Water Quench/ 375°F, 4 hrs. Water Quench	**237**	**180**	**12**	**26 / 30**	**49**
2	2125°F, 4 hrs., 15ksi., slow vessel cool to 700°F- Air Cool to Room Temp.	None	1900°F, 1 hr. Water Quench/ 375°F, 4 hrs. Water Quench	**234**	**178**	**12**	**23 / 28**	**50**
Heat Treatment	**Homogenization (No HIP)**	**Homogenization**	**Austenitizing/ Tempering**	**UTS (ksi)**	**0.2% YS (ksi)**	**Elong (%)**	**Energy -40°F/+72°F (ft-lbs)**	**Tempered Hardness (HRC)**
3	Heat up in Furnace from Room Temp. to 2125°F (2 hrs.)/hold 4 hrs. at 2125°F /slow cool in furnace to 700°F- Air Cool to Room Temp.	2000°F, 2 hrs. Air Cool to Room Temp.	1900°F, 1 hr. Water Quench/ 375°F, 4 hrs. Water Quench	**223**	**180**	**7**	**21 / 27**	**50**
4	Heat up in Furnace from Room Temp. to 2125°F (2 hrs.)/hold 4 hrs. at 2125°F /slow cool in furnace to 700°F- Air Cool to Room Temp.	None	1900°F, 1 hr. Water Quench/ 375°F, 4 hrs. Water Quench	**235**	**179**	**10**	**21 / 25**	**49**

* All mechanical property results reported are from an average of two Charpy or two tensile samples.

The tensile and impact results in **Table 5.21** do not show improvement over the experimental results displayed in **Table 5.14**. However, the results in **Table 5.21** show further evidence of the impact of HIP on the impact toughness of the investment cast ES-1 material. Heat treatments 1 & 3 are identical heat treatments except for the pressure applied during the 4 hour HIP homogenization cycle. When the 4 – hour HIP cycle was carried out in heat treatment #1, average -40°F impact values of 26 ft-lbs. were achieved; when the 4 – hour HIP cycle was replaced with a 4 – hour homogenization cycle (i.e. no pressure), an average impact toughness of 21 ft-lbs. was achieved. As shown in **Appendix A.4**, much variability existed in the tensile data for the specimens in heat treatments 3 & 4. The report supplied by WMT&R noted possible tensile testing problems for the specimens from heat treatment 3 & 4.

The complete set of Charpy impact and tensile results are displayed in **Appendix A.4**. The microsegregation reduction estimates for the four heats of material are shown in **Tables 5.15 – 5.20** above.

5.9 Summary of the Initial Experimentation with ES-1 Cast Steel

The results represent a study on cast ES-1 ingot material which demonstrated excellent impact and tensile properties. The results showed that a high temperature HIP homogenization cycle following by a second high temperature homogenization cycle, a high temperature austenization cycle, and a low temperature tempering step had the potential to produce cast ES-1 ingot material with 40ft-lbs of CVN impact toughness at -40°F with 15% elongation, a yield strength of 190 ksi, and an ultimate tensile strength of 250 ksi. The impact transition behavior of this material showed evidence of the ductile fracture exhibited across a wide range of temperatures (-100°F to +212°F). The lower shelf energy for the cast + HIP ES-1 alloy could not be estimated from the impact toughness vs. temperature curves shown, because the lower shelf energy for this alloy occurs at a temperature below -100°F, the lowest impact testing temperature that is generally achievable with acceptable testing equipment.

The results of a porosity study on the cast + HIP ingot material showed that a high temperature HIP homogenization treatment of cast ES-1 ingot material significantly reduces both the average number of pores and the average area fraction or average % porosity. The results also showed that a high temperature homogenization treatment (without pressure) increases the average number and average area fraction (% porosity) of the cast ES-1 material.

The results of a cryo-treatment study on the cast ES-1 ingot material resulted in a small improvement in hardness at the expense of -40°F impact toughness, possibly due to a further reduction of remaining retained austenite films. No retained austenite was found in the as cast, as quenched, or fully heat treated ES-1 ingot samples that were analyzed using XRD analysis.

An initial heat of induction melted, aluminum deoxidized investment cast ES-1 with 0.06 wt % of aluminum showed that the average -40°F and +72°F impact toughness, % elongation, and UTS and YS of the fully heat treated investment cast + HIP ES-1 material lagged significantly behind that of the cast + HIP ES-1 ingot material. Even though the % elongation and impact toughness of the investment cast ES-1 material changed between heat treatment conditions, the average UTS and YS values remain relatively unchanged throughout the heat treatments for the investment cast study. Etched micrographs revealed evidence of potential eductions of microsegregation in samples homogenized at 2125°F for 4 hrs as compared to those which were not subjected to the homogenization treatment. SEM fracture surface work performed on the investment cast material clearly showed that the induction melted investment cast material contained impurities that were not present in the vacuum degassed cast ingot material. The estimation of microsegregation reduction performed for the heat treatments in this study showed that the removal of a 4-hour, 2125°F homogenization treatment would drastically reduce the amount of microsegregation removed from the alloy.

Lastly, the results of a third heat of induction melted, aluminum deoxidized investment cast ES-1 material possessing just 0.01wt% of aluminum showed that the decrease in aluminum content from the first experimental heat did not improve the mechanical properties of the investment cast material. The heat treatment study carried out on this final heat of investment cast ES-1 showed further evidence of HIP significantly increasing the CVN impact toughness of the investment cast ES-1 material.

Throughout all the of cast ES-1 studies, estimates of microsegregation reduction pointed to the following underlying trends: significant microsegregation reduction differences occur between DAS sizes for the same alloying elements and significant microsegregation reduction differences occur between alloying elements for the same DAS.

The following section, Chapter 6, will discuss and explain in detail the results presented in Chapter 5.

Chapter 6

Discussion

The results displayed in Chapter 5 have shown that the development of ultrahigh yield strength cast steels with improved impact toughness is very complex. At higher carbon contents (0.40 wt % C), with yield strengths > 250ksi, increasing ductility and impact toughness is a challenge. At lower carbon contents (0.25 wt% C), impact toughness and elongation can be significantly increased over the higher carbon content low alloy steels and yield strength values > 180ksi. can be achieved. Although at the present time cast steels are rarely used at yield strengths > 130 ksi., this work suggests that higher strength levels with adequate toughness can be achieved through careful control of composition and processing. It is expected that melting practices must also be tightly controlled to ensure both acceptable tensile and impact properties in these UHSLA cast steels. This section will first discuss the melting practices used throughout this study and their effects on the resultant mechanical properties. This section will provide a detailed discussion of the heat treatment variables studied in this research and their effects on the resultant mechanical properties. The results of the cast ES-1 ingot porosity reduction study will also be discussed as well as an interpretation of the microsegregation reduction estimates that were obtained by diffusion modeling.

6.1 Steel Melting and Pouring Practices

Throughout the study on ultrahigh strength low alloy steels, variability in properties can be expected to be limited to variations in steel melting and pouring practices. Limiting the amount of inclusions and controlling their morphology is widely known to control tensile properties, and especially the toughness, of UHSLA steels. Toughness can be significantly reduced when undissolved second phases or inclusions are present in the material. In steel castings, it has been shown that 83% of the macroinclusions present in carbon and low-alloy steel castings are a result of reoxidation of the steel during pouring, **Figure 6.1**. Thus, pouring and gating practices as well as melting practice must be adequately controlled. The initial heat of material that was experimented with, investment cast 4340+ (300M) steel, was melted using clean charge material under an inert gas blanket and was cast using the Hitchiner CLA process. Since the investment cast 4340+ material was produced using the CLA process, these castings

were poured with far less turbulence than the investment cast ES-1 heats, which were gravity poured. Recent studies of UHS high alloy cast steels have clearly demonstrated the benefits of CLA processing compared to conventional investment casting, **Figure 6.2** [123]. The investment cast 4340+ material would be expected to resemble the material in micrograph A while the investment cast ES-1 material would be expected to more closely resemble the material in micrograph B. The investment cast ES-1 material was produced using high quality VIM-VDG ingot materials. This material was re-melted in an electric induction furnace with argon bubbled through the crucible. The re-melt investment cast material was deoxidezed with 0.05 wt% of aluminum addition just before conventional gravity pouring.

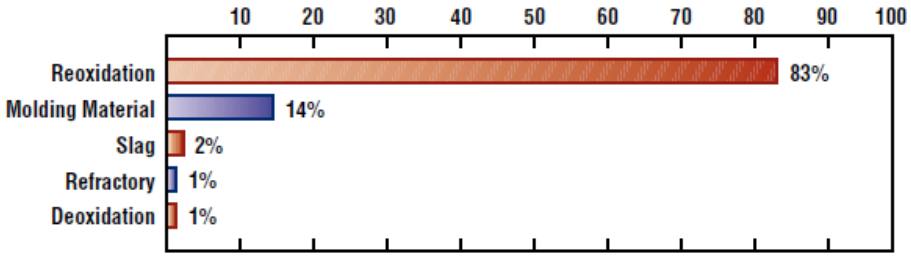

Figure 6.1: Distribution of macroinclusion sources in carbon and low-alloy steel castings [123].

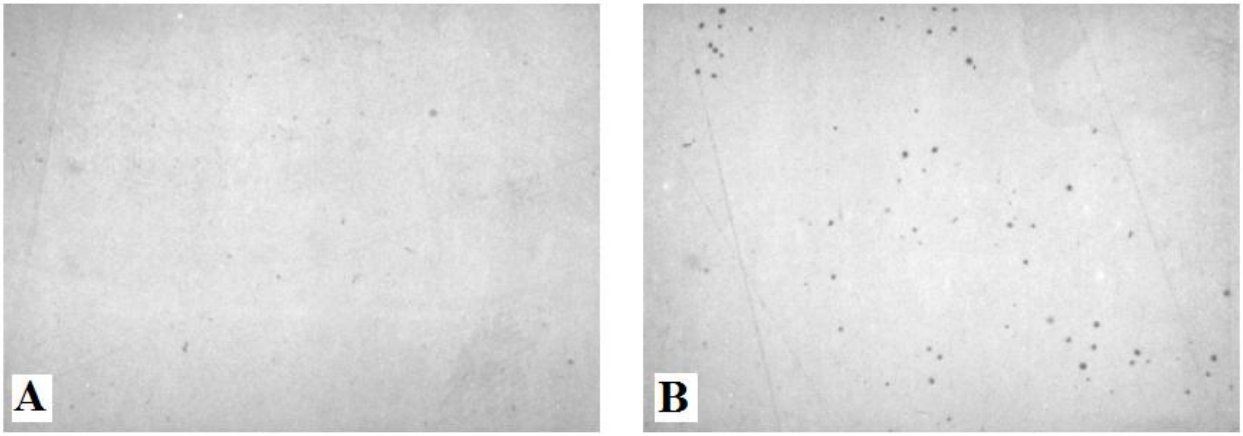

Figure 6.2: Internal microinclusions in typical 17-4PH cast steel are greatly reduced when the metal is counter-gravity cast (A) versus gravity cast (B) [121].

The cast ES-1 ingot material was induction melted and then vacuum degassed to produce low O, S, and P levels in the melt. After vacuum degassing, the cast steel was gravity poured into a bottom poured cast ingot to minimize re-oxidation from pouring.

After close examination of all of the fracture surface images that were examined, the investment cast ES-1 material was the only material that showed evidence of significant amounts

of manganese sulfide and deoxidation product inclusions (**Figures 5.31(A) and 5.32(A))**. For identical heat treatments, the impact toughness of the cast ES-1 ingot material was far superior to the investment cast ES-1 material **(Tables 5.8, 5.14, 5.21)**.

As mentioned earlier, because inclusions such as manganese sulfides and aluminum nitrides act as crack nuclei it is extremely important to control the amount of inclusions in the steel to produce UHSLA steels with high impact properties [1, 39, 41]. Minimizing sulfide inclusions in cast steels begins with the melting and pouring practices used during the production of steel castings. As a result of this study, it is evident that advanced melting techniques such as vacuum degassing and AOD should be used whenever possible to reduce melt O, S, and P levels to minimize microinclusion formation during solidification that serve as crack nuclei that can significantly decrease impact toughness. Minimizing aluminum nitride inclusions is dependent on the deoxidation practice. For alloys with high silicon contents, such as the cast ES-1 alloy, melt dissolved oxygen levels are expected to be low requiring smaller aluminum addition for deoxidation. Excess aluminum retention in the melt can be expected to form aluminum nitride inclusions that serve as crack nuclei that can significantly decrease the impact toughness of these UHSLA steels. A study completed on the cast + HIP AerMet 100 Navy fighter castings showed similar results for mechanical properties. Novotny and Macguire (1993) concluded that the alloy's excellent properties were due to an extremely clean structure along with HIP. They suggested that only foundries that vacuum melt and vacuum cast will be able to take advantage of these outstanding properties [110].

If steel foundries can produce clean steel by closely controlling melting, deoxidation, and pouring practices, heat treatment processing can further enhance tensile and impact properties of USHLA cast steels to desirable levels.

6.2 Heat Treatment

Various heat treatments were applied to the UHSLA cast compositions studied; the various heat treatments produced a wide range of properties. Compared to the conventional Q & T heat treatments that were provided by ASM for the 4340+ (300M) alloy, the heat treatments experimented with in this study significantly improved the impact toughness of the alloy while maintaining acceptable yield strength levels. The heat treatments carried out on the cast ES-1 ingot material produced impact and tensile property results that were far superior to the single

cast ingot study carried out prior to this study. Although the heat treatment processes developed in this study provide improved mechanical properties for both the investment cast 4340+ and cast ingot material, additional work still needs to be completed to select the proper heat treatment times and temperatures to develop optimal mechanical properties. This is true for all stages of the heat treatment processes, including HIP homogenization, homogenization, austenization, and tempering. The effects of the individual heat treatment steps and variables will be discussed separately.

6.2.1 Homogenization

A homogenization step is important in the development of UHSLA cast steels with improved impact toughness as the homogenization step is used to reduce the microsegregation that occurs during solidification of the UHSLA cast steel. Effective homogenization can be achieved during a separate heat treatment step prior to austenitizing or during a HIPing operation prior to austenitizing. In previous studies on ultrahigh strength low alloy cast steels, a homogenization step in the heat treatment process was shown to significantly increase the impact toughness of the end, fully heat treated product [47, 48]. When developing heat treatment procedures for UHSLA cast steels, it is extremely important to understand that most heat treatment guidelines in the literature were developed for forged or hot rolled wrought steel products. For wrought products, initial forging or hot rolling operations during conventional mill processing occur at temperatures that are typically above 2000°F. During these thermomechanical processing steps, significant microsegregation reduction can be expected from solid state diffusion. In fact, it is not uncommon for the widely published wrought heat treatment guidelines to leave out a homogenization step completely. However, heat treatment guidelines developed for wrought UHSLA steels cannot be expected to produce optimal mechanical property results in cast UHSLA steels. Looking at the conventional wrought heat treatment guidelines for 4340+ (300M) steel, the homogenization step is 1675°F for 1 hour. Modeling results clearly show that for the 4340 + (300M) alloy, virtually no microsegregation reduction is occurring for the substitutional alloying elements present at these low homogenization treatment temperatures (**Table 5.3**). In addition, **Figure 2.14** clearly shows that any V, Al, Nb, or Ti compounds that may exist in the cast steel alloy will not dissolve when homogenized at 1675°F. The work carried out on the 4340+ IC alloy in this study showed that by simply increasing the

homogenization temperature to temperatures at which significant alloy diffusion can occur, the impact toughness could be significantly increased. **Figure 6.3** shows how impact toughness increases for 4340+ together with the corresponding reductions in microsegregation expected (modeling result) as the homogenization temperature increases. Even though the estimates of microsegregation reduction are only 14% and 17% respectively for Mo and Cr, significant increases in charpy impact energy were observed. Clearly only some microsegregation mitigation has to occur before improvements in toughness are observed. In addition to the microsegregation reductions occurring, increased dissolution of second phase particles or compounds would be expected to be occurring.

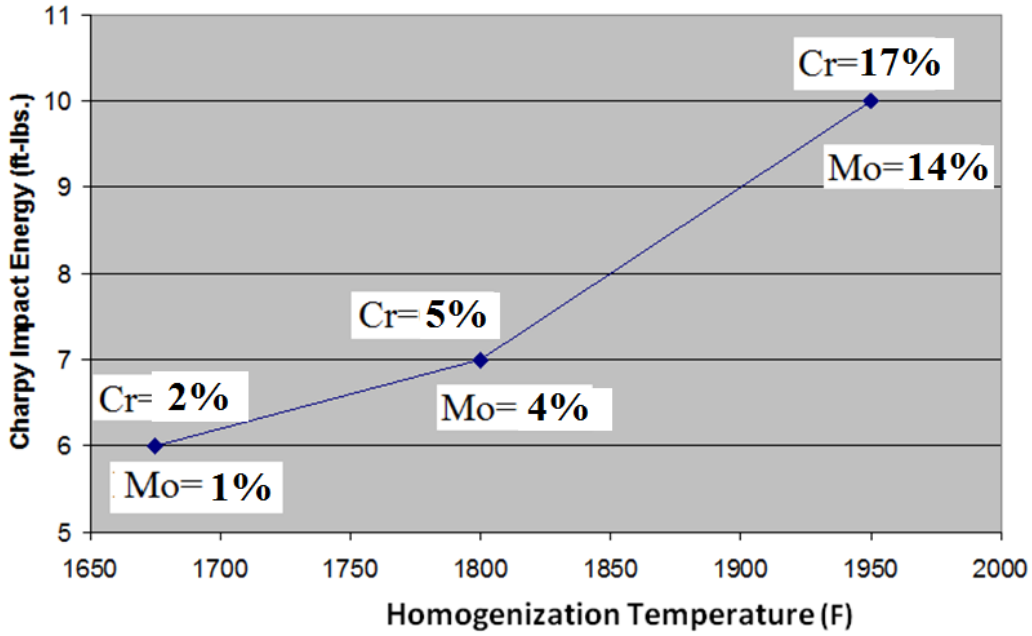

Figure 6.3: The figure above displays estimates of % microsegregation reduction for Cr and Mo expected after the 1 hour homogenization treatments at the temperatures displayed on the graph of Charpy impact Energy vs. Homogenization Temperature for IC 4340+ (300M) steel.

The literature is contradictory on whether or not increased homogenization temperatures translated to increased toughness of UHSLA steels. Outside of the Eddy and Marcotte (1947) [49] study on thin wall sections, the consensus seems to be that increasing the homogenization temperature does increase the toughness of USHLA steels. The study by Eddy and Marcotte (1947) concluded that heat treatments employing high temperature homogenization treatments (above 1650°F to 2100°F) are not effective in materially improving the impact and hardenability properties of high strength low alloy cast steel with **thin walled sections and smaller DAS** [49].

When looking at segregation, if casting section sizes are very small, the cooling rate is expected to be escalated, which would translate into smaller DAS and less microsegregation. When the DAS is small, much less diffusional energy (i.e. temperature and time) is needed to achieve the same % microsegregation reduction when compared to the amount of energy (temperature and time) needed for larger DAS. Thus, because the DAS can be expected to be small in the thin sections studied by Eddy and Marcotte, the necessary amount of diffusion and microsegregation reduction to produce acceptable impact properties could have occurred at lower homogenization temperatures used. If the amount of microsegregation was limited and the DAS was extremely small, the high temperature homogenization treatments may not have had a significant effect on toughness.

The Leger (1985) study showed that microalloyed HSLA cast steels, namely 12MDV6-M, are typically homogenized between 1920°F and 1980°F (1050°C to 1080°C) to develop optimal properties [48]. In his 1977 study of 4340 steel, Floreen noted that the impact toughness of these cast steels was lower than their wrought counterparts as a result of quai-cleavage fractures when impact tested. He attributed this to the microsegregation that occurs in the castings during solidification. Floreen discussed the influence that high-temperature "solution anneal" or homogenization experiments had on the cast structures of these cast steel alloys. In this work, Floreen (1977) alluded to the fact that high-temperature "solution anneal" or higher homogenization temperatures could cure microsegregation, decreasing the occurrences of localized brittle regions in the material, and thus improving the Charpy impact values of the alloys [50].

From the current study, it is evident that high homogenization temperatures (greater than 1950°F) can result in charpy impact toughness improvements in thin-section steel castings where the DAS is less than 120μm. However for heavy section castings, with larger DAS significantly higher homogenization temperatures and times are required to mitigate the segregation enough to cause toughness improvements. Typically these toughness improvements are achieved without corresponding changes in tensile properties.

6.2.2 HIP Homogenization

The benefit observed for HIP processing of cast UHSLA steels can be expected to be due to both the healing of microporosity that occurs and the homogenization effects of this long-time

high-tempered processing cycle. The results of the work carried out on the investment cast 4340+ material showed that by carrying out a high temperature HIP homogenization step prior to the experimental heat treatment, impact toughness and % elongation increased without affecting the UTS or YS. Similarly the cast ES-1 ingot material showed that a high temperature (2125°F), 15 ksi. Pressure, HIP homogenization treatment led to excellent impact, % elongation, and tensile properties **(Table 5.8, Figure 5.4)**. Heats of investment cast ES-1 material that were put through the high temperature (2125°F) HIP homogenization treatment showed superior impact and elongation properties when compared to the samples that were not subject to HIP **(Tables 5.14 & 5.21)**.

As shown in **Tables 6.1** and **6.2**, the results from the Novotny and Macguire (1993) study of Aermet 100 showed that by putting the alloy through a high temperature HIP cycle, the cast + HIP alloy could possess tensile and impact properties similar to the wrought alloy [110].

Table 6.1: Typical Room Temperature Longitudinal Mechanical Properties of Wrought AerMet 100 Alloy [110].

Table II. Typical Room Temperature Longitudinal Mechanical Properties of Wrought AerMet 100 Alloy

Property	AerMet 100*
0.2% Yield Strength, ksi (MPa)	250 (1724)
Ultimate Tensile Strength, ksi (MPa)	285 (1965)
Elongation, %	14
Reduction in Area, %	65
Hardness, HRC	53.5
Charpy V-Notch Impact Energy, ft-lbs. (J)	30 (41)
Fracture Toughness, K_{Ic}, ksi/in. (MPa/m)	115 (126)

* - Heat treatment: 1,625°F (885°C) (1h)/air Cool/-100°F (-73°C) (1h) air Warm/900°F (482°C) (5h) air cool

Table 6.2: Typical Room Temperature Mechanical Properties of Cast + HIP'ed AerMet 100 Alloy [110].

Table III. Mechanical Properties of Sandia Cast AerMet 100
(Cast + HIP'ed + Heat Treated Properties)

Heat/I.D.	Sample	K_{Ic}/in	Y.S. ksi	U.T.S. ksi	Elong. %	R.A. %	CVN ft-lb
225	1	113.3	242.4	276.6	12.4	57.2	25.5
	2	117.6	248.7	291.5	12.8	57.9	24.0
	Avg.	115.7	245.6	284.1	12.6	57.6	24.8

HIP Cycle: Argon atmosphere preheat to 1,550°F, hold 1 hour, heat to 2,250°F, hold for 6.5 hours at 30 ksi pressure, furnace cool.

Heat Treatment: 1,250° F (16h)/Cool 600° F /h to R.T. +
1,625° F (1h) A.C./-100° F (1h) A.W./900° F (5h) A.C.

Previous work by Kittyhawk Products (1998) [124] and Atkinson and Davies (2000) [107] helps to explain the mechanisms responsible for the upgrading of properties found in the current study. Barre (1998) explained that the application of heat and pressure provides the ideal mechanism for the application of a driving force to collapse micro-voids or porosity by creep mechanisms and plastic deformation to "heal" the material by diffusion bonding void surfaces together. Barre (1998) explained that the isostatic nature of HIP is well suited for defect reduction in castings; the void closure occurs with very little, if any distortion. In addition to reducing voids and porosity, Barre (1998) also hypothesized that high temperature HIP could also reduce alloy microsegregation [124]. Barre (1998) and Atkinson and Davies (2000) also explained another interesting finding regarding HIP and casting mechanical property data; HIP significantly reduces the spread or scatter in mechanical property data typically associated with castings [107, 124]. This, along with alloy cleanliness can also help to explain the small amount of variability in the data for the cast + HIP ES-1 ingot material properties **(Appendix A.2)**. After HIP, not only are the average mechanical properties improved, but steel foundries can now achieve minimum specified properties with a higher degree of confidence [107].

Atkinson and Davies (2000) discussed the science and effects of both high temperature sintering (no pressure HIP) and HIP. During HIP in a vessel, the pressure is applied with a gas (typically argon) and is thus isostatic; Atkinson and Davies (2000) explain that under these pressure conditions, internal pores or defects within a casting collapse and diffusion bond. They also reported that HIPing of steels should be carried out between 1750°F and 2120°F; these high temperatures are needed to both lower the yield strength and to raise the diffusivity of vacancies and alloying elements in the material sufficiently for pore closure to occur in a reasonable time

[107]. Kittyhawk recommends a HIP cycle of 2125°F for 3 to 4 hours at 15 ksi. for UHSLA cast steels [125]. After an initial HIP trial with the 4340+ alloy at 1950°F for 4 hours at 15ksi, Bodycote also recommended a HIP cycle of 2125°F for 4 hours at 15 ksi for future trials with this UHSLA cast steel. Interestingly, the HIP temperature and times recommended by Kittyhawk and Bodycote for these steels are the ranges in which the diffusion model predicts significant diffusion to occur which suggests that significant reductions in microsegregation for the UHSLA steels are expected during recommended HIPing cycles.

Atkinson and Davies (2000) concluded that HIPing is a far more dynamic process than sintering. The plastic flow during HIPing can be expected to accelerate the simple diffusion process that occurs in sintering [107]. The modeling work done by Coble and Flemings (1971) showed that sintering alone can lead to a reduction in microporosity in castings. However, their model, which was dependent on the solid diffusivity, pore size, and pore spacing relative to grain size in the casting showed that it could take 10 to 20 hours to close micropores in castings simply by high temperature homogenization [108].

It is evident that the toughness improvements due to HIPing of UHSLA cast steels in this study are likely coming from significant microporosity reductions coupled with increased dissolution of second phase particles and significant microsegregation reductions.

6.2.2.1 Microporosity Reduction During HIP and Homogenization

Reduction in casting microporosity during HIPing can be expected. However, the influence of high temperature homogenizing (i.e. sintering) on the microporosity has not been previously reported. The average size and the size distribution of the microporosity remained relatively unchanged across the cast, cast + HIP, and cast + homogenize samples. However, HIPing significantly decreased the percent porosity (**Figure 6.4**) and the average number of pores (**Figure 6.5**) across the images for the cast ES-1 ingot material.

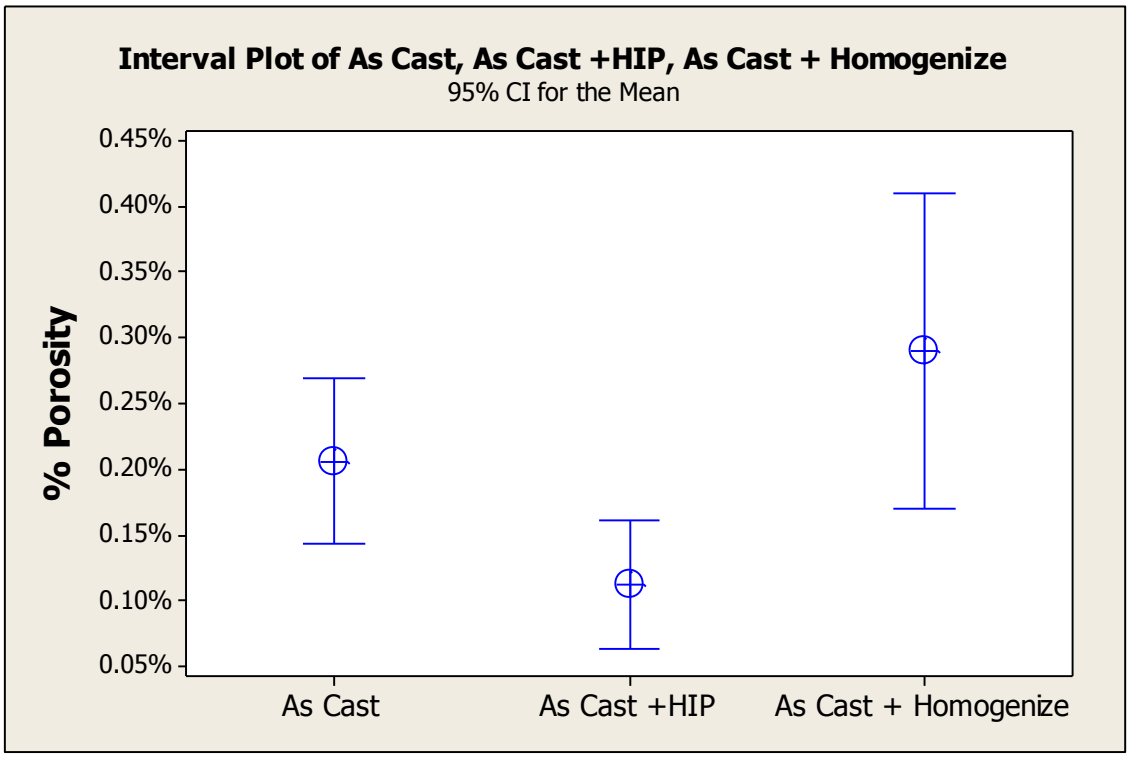

Figure 6.4: Interval Plot for the % porosity of as cast, as cast + HIP, and as cast + homogenize ES-1 cast ingot material.

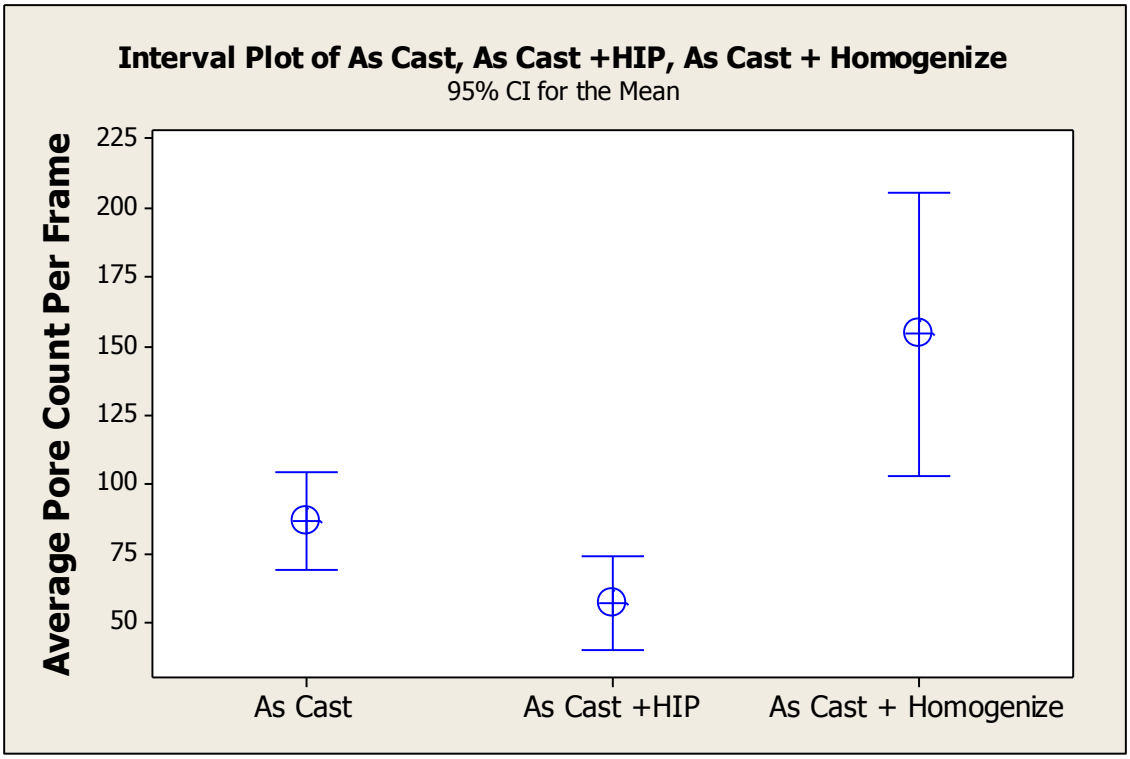

Figure 6.5: Interval Plot for the average pore count of as cast, as cast + HIP, and as cast + homogenize ES-1 cast ingot material.

From the published work by Atkinson and Davies (2000) and Barre (1998), it was expected that HIP would decrease the number of pores and percent porosity of the cast steel. From **Figure 2.32**, it can be observed that the significant increase in impact properties found in all HIPing studies has been attributed to a significant decrease in the percent microporosity in UHSLA steels.

The increase in percent porosity and in the average pore count due to high temperature homogenization (i.e. HIP without pressure) was intriguing. However, the Anton and Giamei (1985) study on microporosity distribution and growth during homogenization of a nickel-base superalloy found a similar result (**Table 6.3, Figures 6.6 & 6.7**). They found that [115]:

(1) Micropores that were associated with casting and homogenization are essentially spherical.

(2) Porosity occurs exclusively within the interdendritic regions of the crystal.

(3) The volume fraction of measureable porosity increased rapidly on initial heating and gradually declined at extended homogenization times.

(4) Initially the average pore radius increased at 2400°F (1315°C) but on continued homogenization a leveling-off in pore growth occurred while no change in pore radius took place at 2368°F (1298°C).

(5) In the as-cast condition the spread in the pore size distribution is narrow and becomes larger with homogenization time [115].

Table 6.3: Summary of homogenization times, temperatures, and metallographic microporosity results for the volume fraction of porosity, the mean linear intercept (L) of the pores as measured and the calculated average pore radius (r) [115].

Homogenization temperature (°C)	*Time* (h)	*Volume porosity* (%)	$\bar{L}$ (μm)	$\bar{r}$ (μm)
As cast	—	0.082	10.66	8.00 ± 0.35
1298	0.5	0.132	11.31	8.48 ± 0.49
1298	2.0	0.143	11.63	8.72 ± 0.49
1298	4.0	0.153	11.28	8.46 ± 0.50
1298	8.0	0.135	10.84	8.13 ± 0.42
1315	0.25	0.156	12.10	9.08 ± 0.49
1315	1.0	0.159	13.29	9.97 ± 0.64
1315	4.0	0.223	15.08	11.31 ± 0.77
1315	16.0	0.213	15.79	11.84 ± 0.81

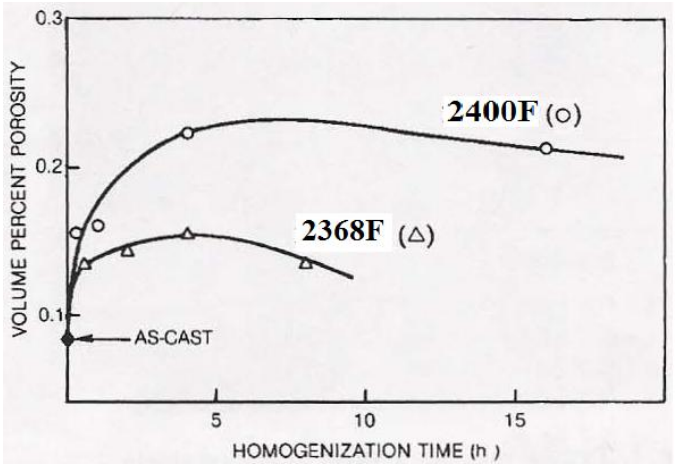

Figure 6.6: The change in porosity volume with homogenization for homogenization temperatures of 2368°F and 2400°F [115].

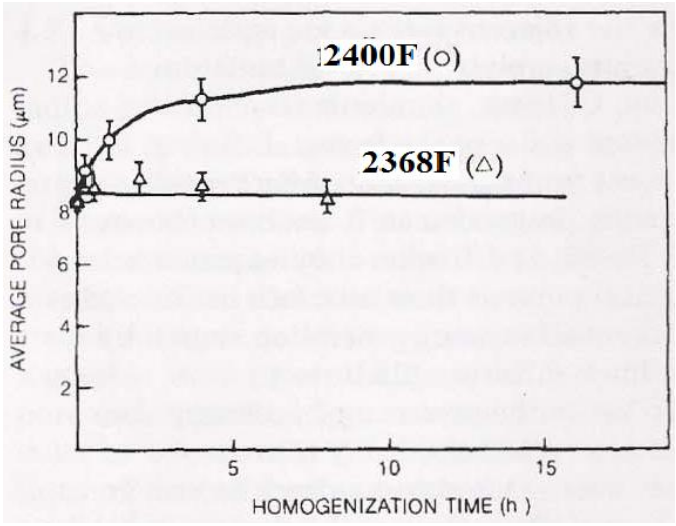

Figure 6.7: The change in average pore radii with homogenization for homogenization temperatures of 2368°F and 2400°F [115].

Anton and Giamei (1985) did not fully interpret their result, but they hypothesized that the increase in percent porosity was attributed to a mechanism of diffusional growth of pores through the accumulation of vacancies. This vacancy generation mechanism, known as the Kirkendall mechanism, occurs if a concentration gradient exists in the material where one of the diffusing elements is much more mobile than the other. An imbalance in the atomic flux produces spherical pores in the gradient region as a result of the accumulation of vacancies. In the nickel superalloy study, significant concentration gradients were present when microprobe analysis was carried out between the dendrite cores (i.e. Ni rich areas) and the low melting interdendritic eutectic phase (i.e. Al, Mo, and Ta solute enriched areas). The authors

hypothesized that of the solute elements present in the interdendritic regions, Al was likely the culprit, because it was the most abundant and also the fastest diffusion element. The authors suggested that by extending the homogenization time at high homogenization temperatures, induced microporosity caused by the Kirkendall effect would not be a contributing factor [115]. Interestingly, the sintering model work by Coble and Flemings (1971) showed that it is only after about 10 to 20 hours of high temperature homogenization that closure of micropores in castings could be accomplished by high temperature homogenization alone [108].

For the ES-1 alloy, the interdendritic regions are expected to be rich with substitutional alloying elements such as Mo, Cr, and W. This suggests that a Kirkendall mechanism could be responsible for the significant increase in percent porosity and an increase in the average number of pores after homogenizing for 4 hours at 2125°F (compared to the as cast and HIP samples).

6.2.2.2 Microsegregation Reduction During Homogenization and HIP Homogenization

This study has demonstrated that high temperature homogenization is a key processing step in the development of UHSLA cast steels with adequate toughness. In addition, high temperature HIP treatment has the potential to both remove significant amounts of microsegregation and microporosity to develop improved toughness at high yield strength levels. Multiple researchers [50, 57, 108, 124] have speculated that high temperature homogenization and high temperature HIP homogenization should significantly reduce microsegregation in steel castings. Flemings (1974) first attempted to model and quantify the expected reduction in microsegregation during high temperature processing [51]. According to the work done by Flemings [51, 126], interstitital carbon atoms are completely homogenized by the time a low-alloy steel reaches 900°C (1652°F) for any typical casting dendrite arm spacing. The approximation model in Chapter 4 also shows that carbon atoms are completely homogenized by the time a steel reaches 900°C (1652°F) for the range of DAS (20 - 200μm) studied in the model.

Flemings predicted that significantly longer times and higher temperatures are expected to be necessary to mitigate the segregation of other alloying elements such as Ni, Mn, Cr, and Mo. In fact, Flemings reported that at 1100°C (2012°F), it is likely that only carbon is completely homogenized. Flemings theorizes that at a secondary dendrite arm spacings (DAS) ≥ 200μm, practically no homogenization can be achieved ($\delta \geq 0.9$) even at homogenization temperatures greater than 1300°C (2372°F) for one hour [51, 126]. The results of this study,

Tables 4.2-4.6, are in agreement with the predictions made by Flemings. For moderate dendrite arm spacings (around 80μm), it is not until homogenization is carried out above 1900°F or 2000°F for at least 4 hours that a significant (>10% reduction) in micro segregation of the subtitutional alloying elements Cr, Mn, Mo, W, Ni is expected to occur. **Figures 6.8** through **6.10** are graphs of the index of micro segregation reduction versus time. The index of micro segregation reduction is simply (1 – (% reduction in micro segregation)). These graphs were constructed using the diffusion model presented in Chapter 4 to estimate the % reduction in micro segregation at various temperatures and times for a fixed DAS. From **Figures 6.8 to 6.13,** it is clear that for a moderate DAS (80μm), it will take an impractical long homogenization time at 2100°F to get close to 100% homogenization of Cr, Mo, or W when the initial segregation is approximately +/- 0.5 wt % of these elements. **Figure 6.11 and 6.12** show that even after 8 hours of a high temperature (2100°F) homogenization treatment, none of the alloying elements undergo complete homogenization. **Figure 6.13** shows that it is only after 20 hours of a 2200°F homogenization treatment that complete homogenization can be achieved for Cr, Mo, and W. It is only at about 2500°F that a typical 2 hour homogenization treatment can be expected to completely homogenize microsegregation of the substitutional alloying elements present in UHSLA cast steels. However, these high homogenization temperatures are impractical and cannot be reached with commonly available heat treatment or HIPing equipment. The cost of carrying out these very long heat treatments at high temperatures will be extremely expensive. Also excessive amounts of oxide and surface decarburization can be expected at these extreme atmosphere unless furnace atmospheres are strictly controlled.

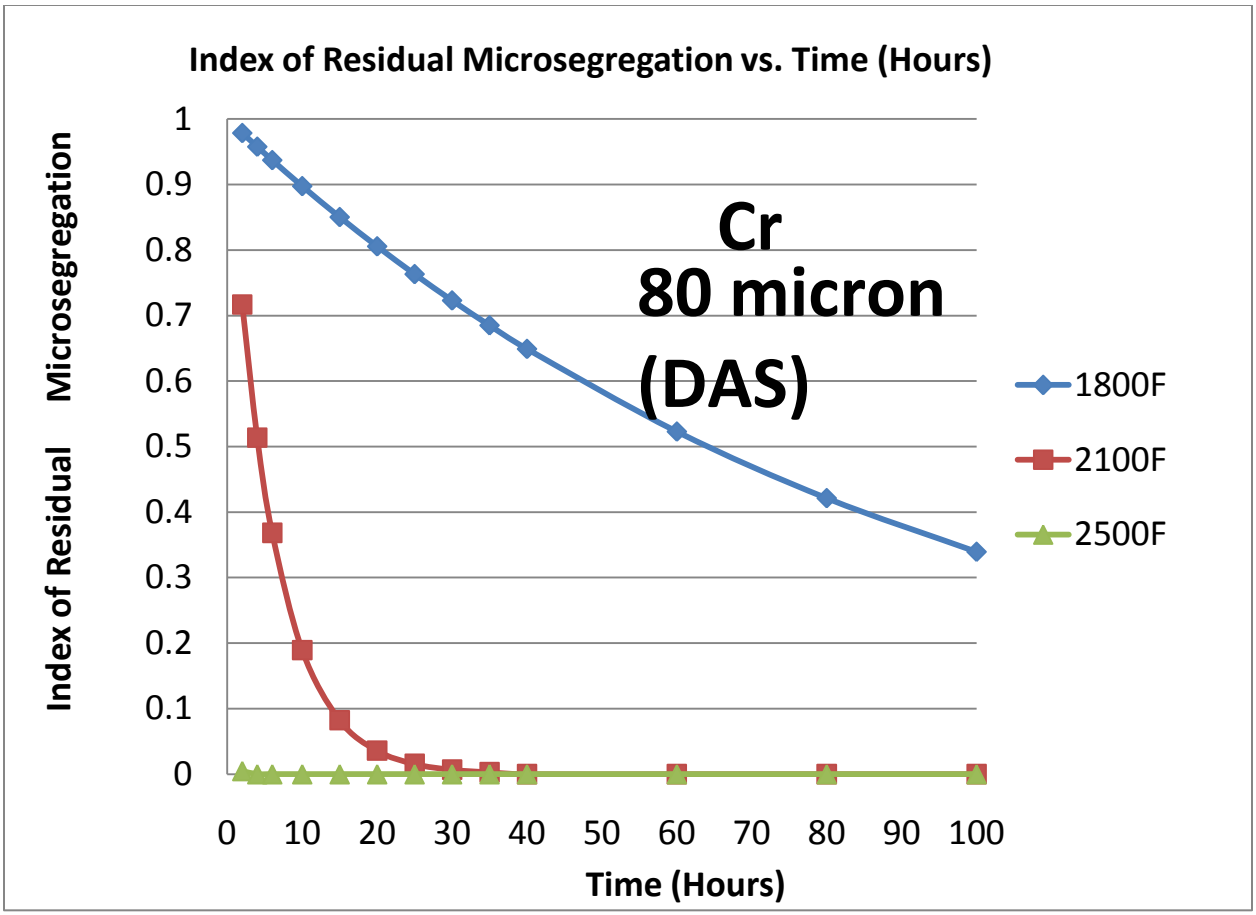

Figure 6.8: The index of Residual Microsegregation Reduction (δ) versus Time for Cr at a DAS of 80μm.

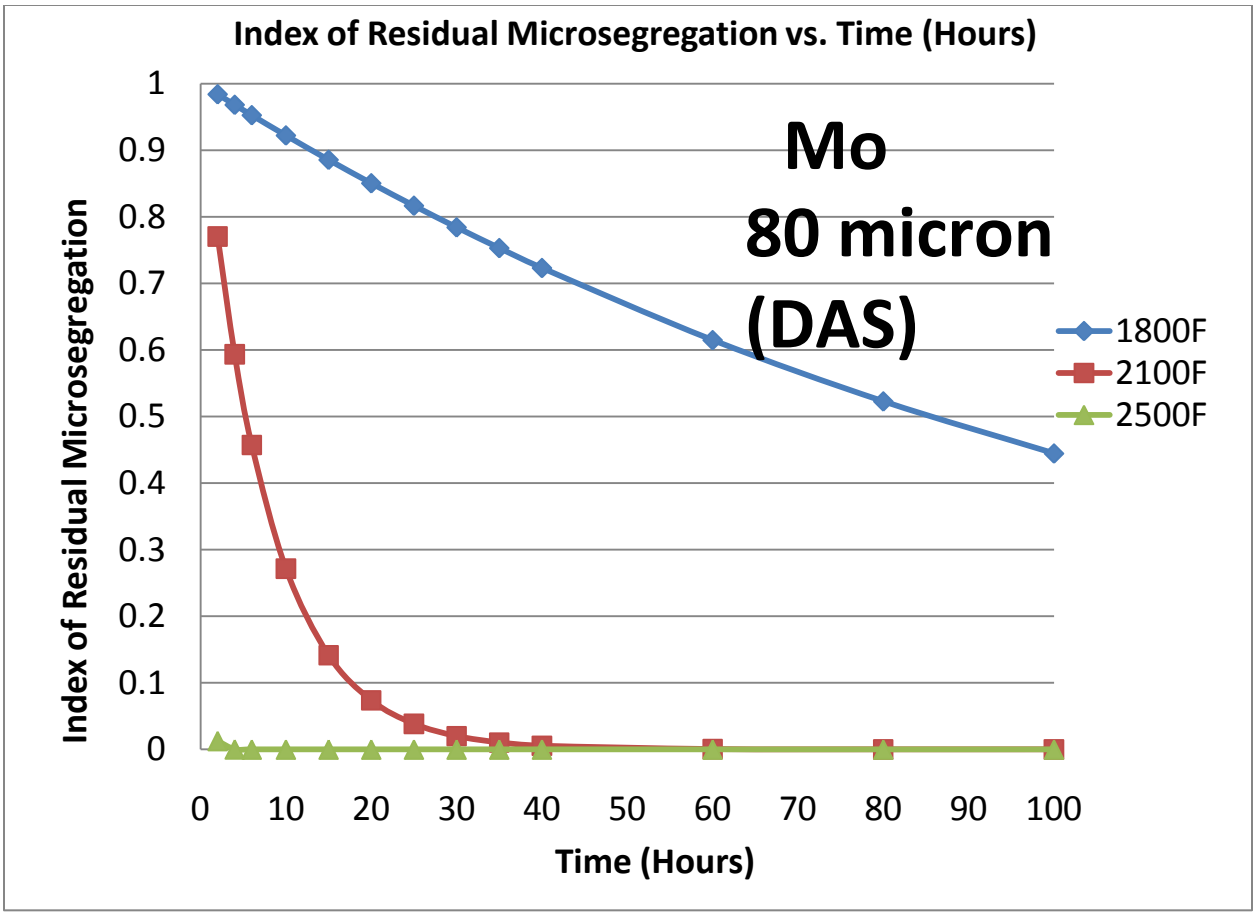

Figure 6.9: The Index of Residual Microsegregation Reduction (δ) versus Time for Mo at a DAS of 80μm.

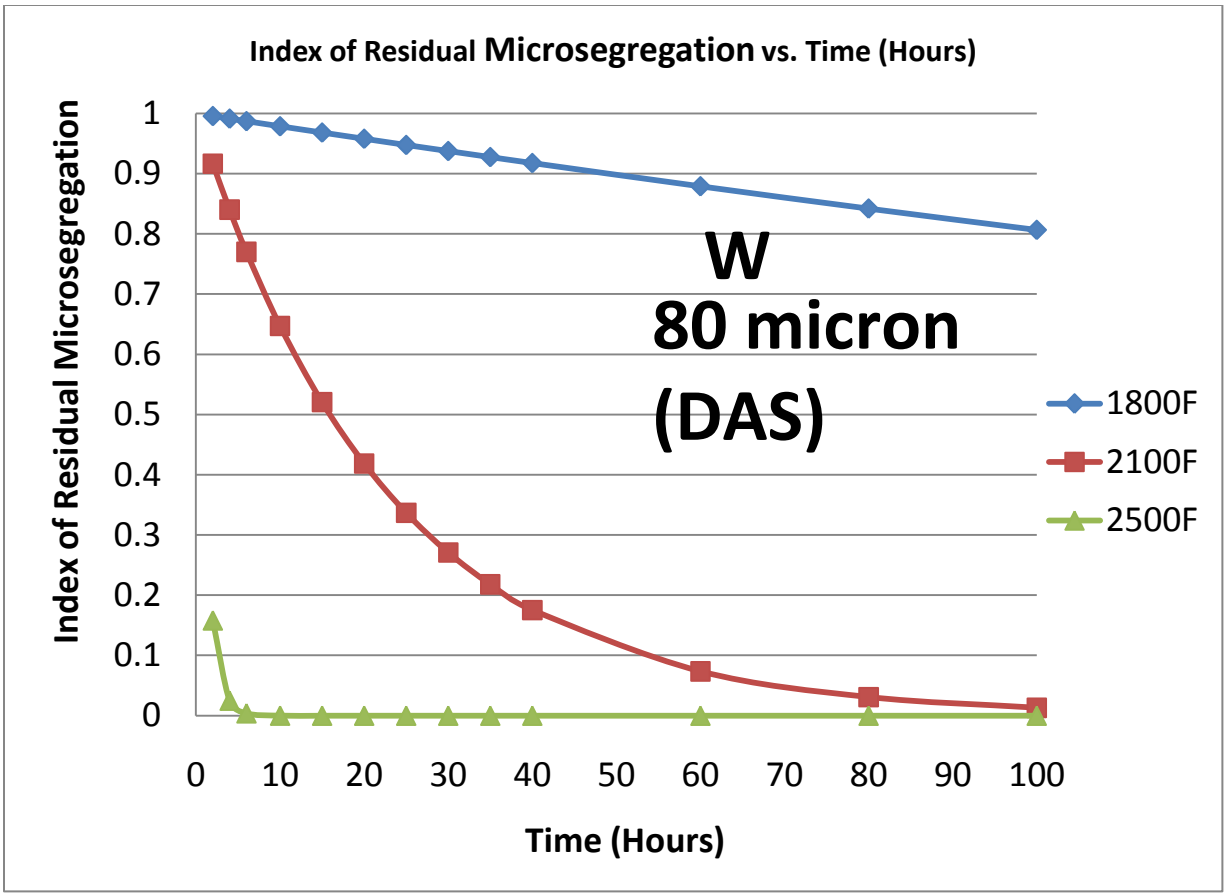

Figure 6.10: The Index of Residual Microsegregation Reduction (δ) versus Time for W at a DAS of 80μm.

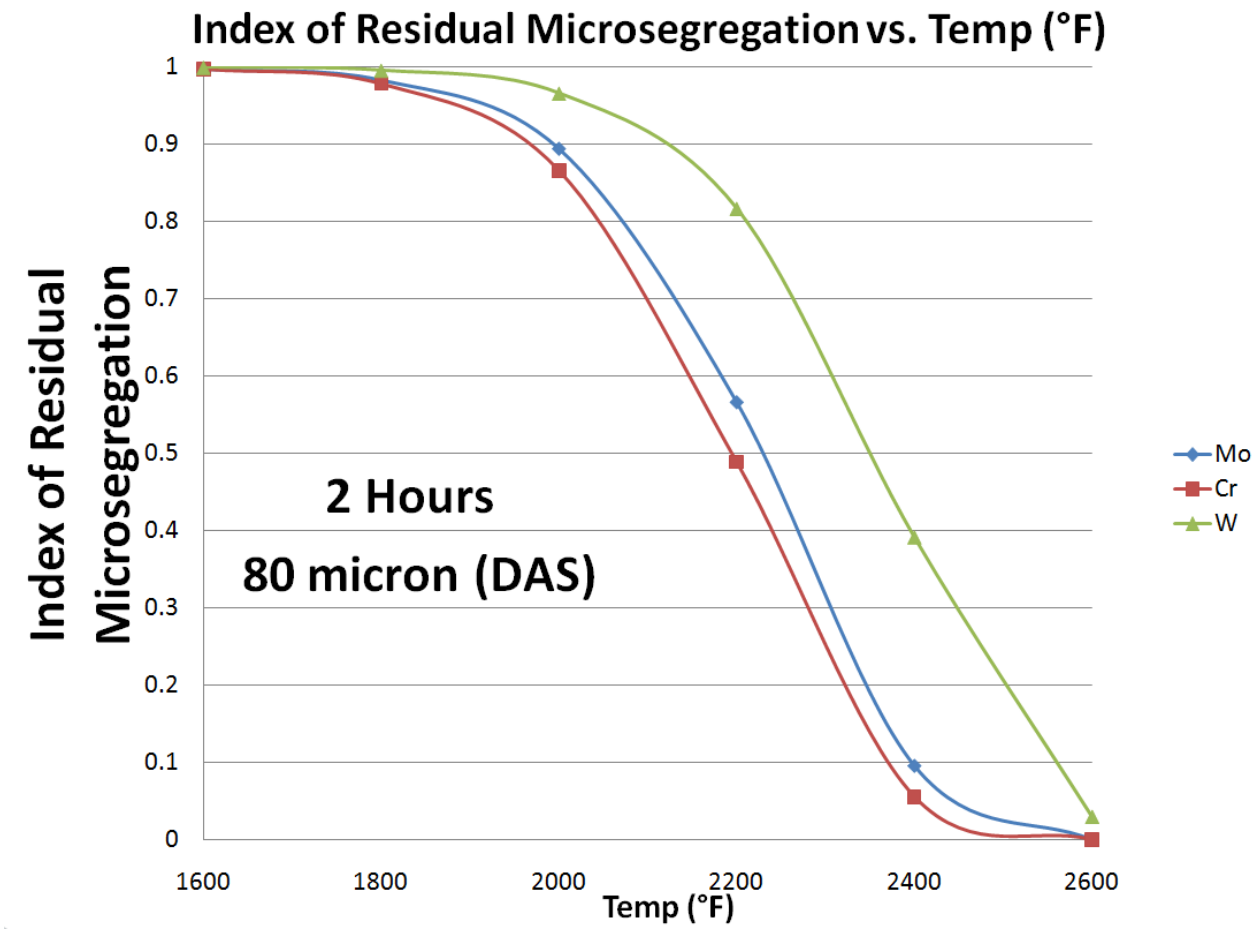

Figure 6.11: The Index of Residual Microsegregation Reduction (δ) for Cr, Mo, and W versus Temperature for a 2 Hour Homogenization Treatment at a DAS of 80µm.

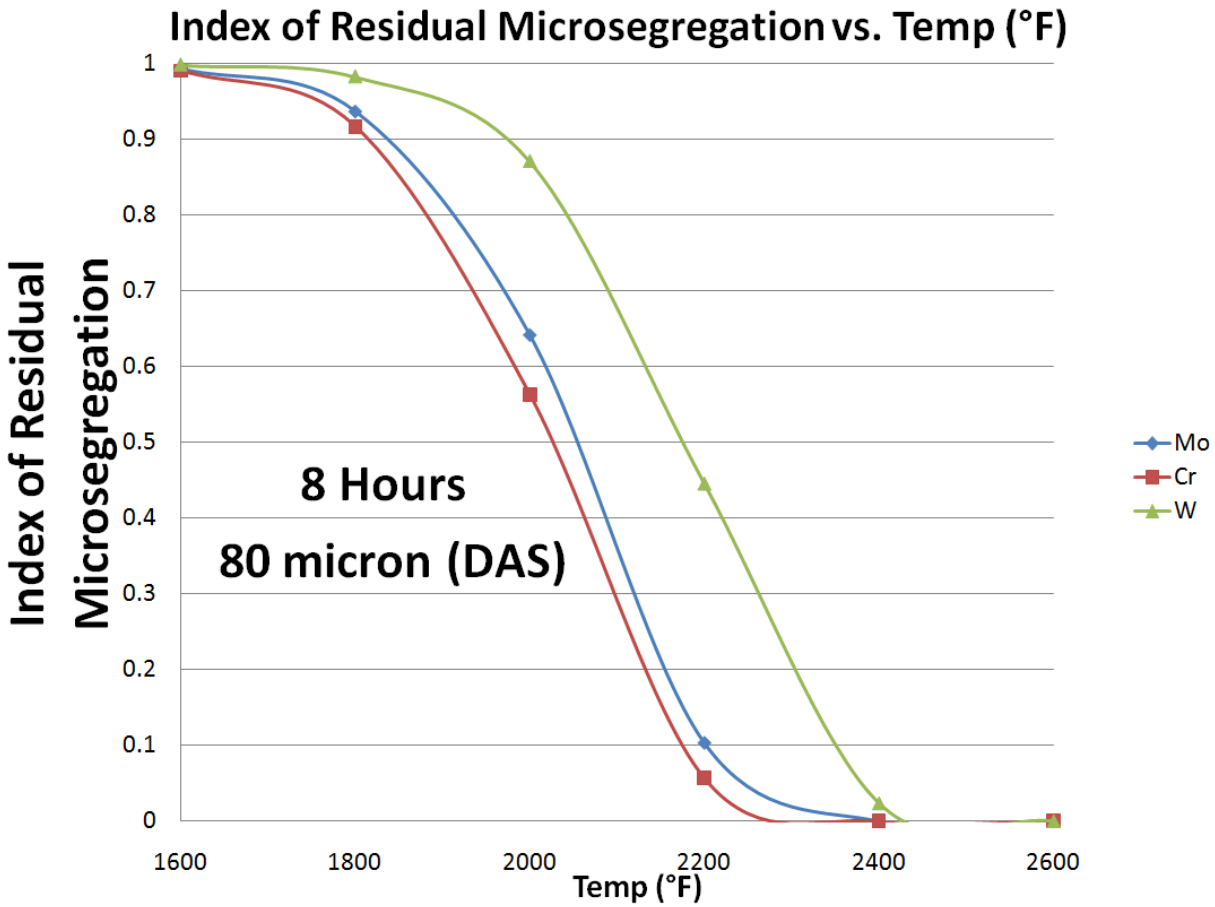

Figure 6.12: The Index of Residual Microsegregation Reduction (δ) for Cr, Mo, and W versus Temperature for an 8 Hour Homogenization Treatment at a DAS of 80µm.

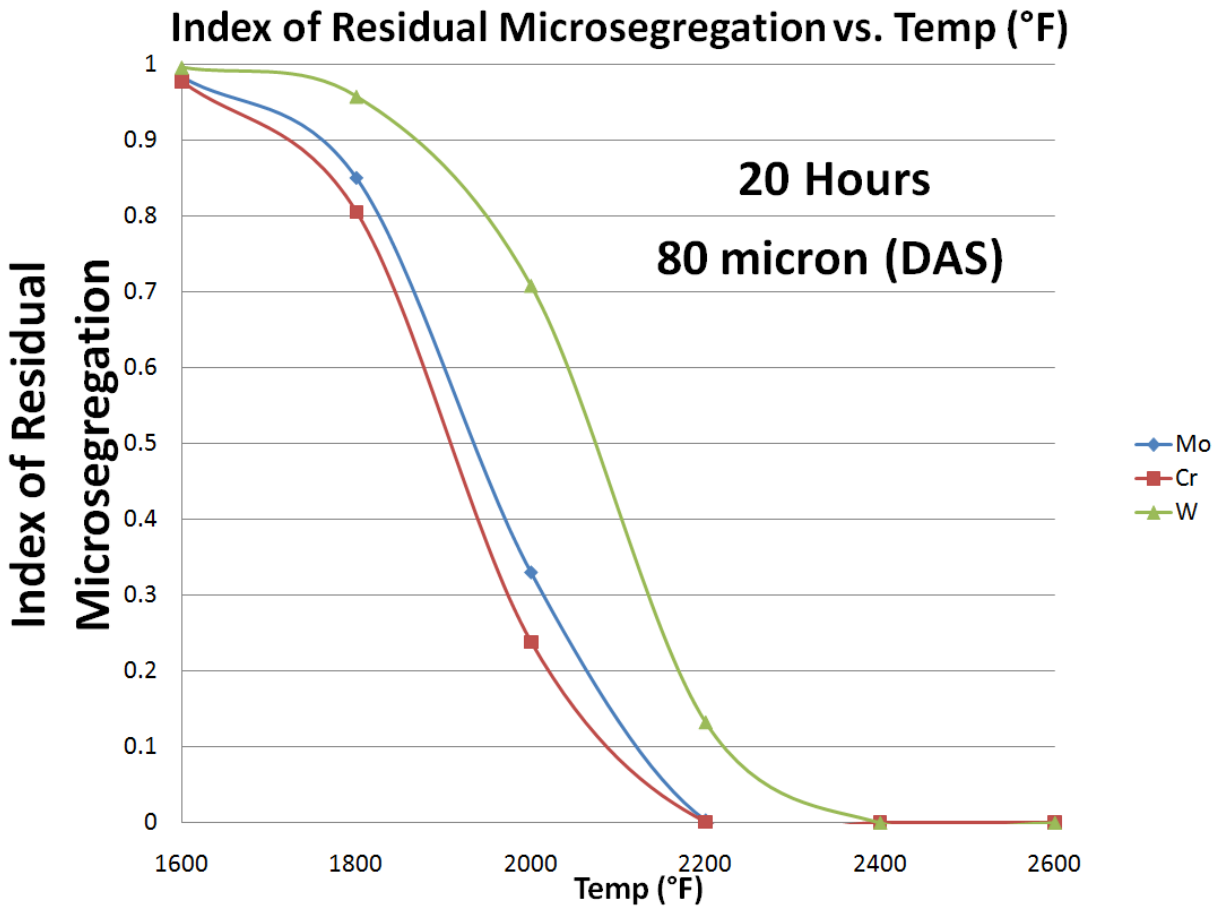

Figure 6.13: The Index of Residual Microsegregation Reduction (δ) for Cr, Mo, and W versus Temperature for a 20 Hour Homogenization Treatment at a DAS of 80µm.

Mechanical property results from this study suggest that significant toughness increases can be achieved for less severe homogenization/HIP treatments that only partially remove segregation. It will be very important for foundries to have knowledge of how much microsegregation reduction will be needed to develop the necessary mechanical properties desired in UHSLA steel castings.

6.2.3 Austenization

In UHSLA cast steels, the austenization temperature must be high enough to ensure the dissolution of coarse carbide and intermetallic phase that form upon solidification. At the same time, excessively high austenitizing temperatures can lead to undesirable austenite grain growth. As shown in Chapter 2, there has been frequent debate over the use of high austenization temperatures for HSLA steels, to fully solutionize V and particularly Nb carbides to achieve full

strength levels. As shown in **Figure 2.14**, Titanium compounds are stable at high temperatures and are extremely difficult to dissolve, even at temperatures above 2200°F. A balance must be achieved in terms of effective dissolution of detrimental coarse alloy carbides and limiting grain growth. Results of some of the investigations into UHSLA steels are detailed in **Table 6.4**.

Table 6.4: The reported Effects of Austenization Temperatures on the Fracture and Impact Toughness of Low Alloy Steels.

Reference	Alloy	Effect of Increased Austenization Temperature	
		Fracture Toughness K_{IC}	CVN Impact
Carlson et. al. [127]	Fe-4Cr-0.30C	Increase	Small Decrease
	Fe-4Cr-0.35C	Increase	Little/No Change
	Fe-4Cr-0.27C-0.2Ti	Little/No Change	Peak at 1832°F, then Decrease
Ritchie et. al. [77]	AISI 4340	Increase	Decrease
Wood [27]	AISI 4130, 4140, 4330 4340, 300M	Increase	N/A
Lai et. al. [38]	AISI 4340/300M	Increase	Slight Decrease
Youngblood/Raghavan [33]	300M	Increase	N/A

During the study on the investment cast 4340+ alloy, austenization temperature was kept at 1600°F, the prescribed temperature for the alloy given by ASM International. As shown in the literature review, the common theme for designing a proper austenization cycle during heat treatment is assuring dissolution of second phase particles, namely alloy carbides in UHSLA steels. Out of the studies above, the most comprehensive study was the Youngblood and Raghavan (1977) study that showed that by increasing the austenization temperature of the 300M alloy from 1600°F to 1800°F, second phase particles, namely alloy carbides were fully dissolved and optimum strength and impact toughness were developed [33]. In the current study, when the ES-1 cast ingot material was experimented with, the material was austenitized at 1800°F and 1900°F. Excellent properties were found for both heat treatments, with optimal yield strength, CVN, and % elongation at an austenization temperature of 1900°F. This suggests that the tungsten carbides in this tungsten alloyed material require higher than usual austenitizing temperatures for complete dissolution. High temperature homogenization treatments carried out on UHSLA cast steels can help to put second phase particles into solution, but upon slow cooling, the second phase particles can re-precipitate. In future heat treatment trials with the cast 4340+ alloy, austenization temperatures at or above 1800°F should be evaluated in an effort to try to increase impact toughness by dissolving alloy carbides (**Figure 6.14 (A)**), taking away

crack nucleation sites (**Figure 6.14 (B)**) to promote higher toughness. With increased austenization temperatures, the fracture surfaces for the investment cast material shown in **Figure 5.2** should begin to resemble the fracture surfaces in **Figures 5.5, 5.8, and 5.9**, moving from a low energy absorbed quasi cleavage fracture to a high energy absorbed dimpled rupture mode.

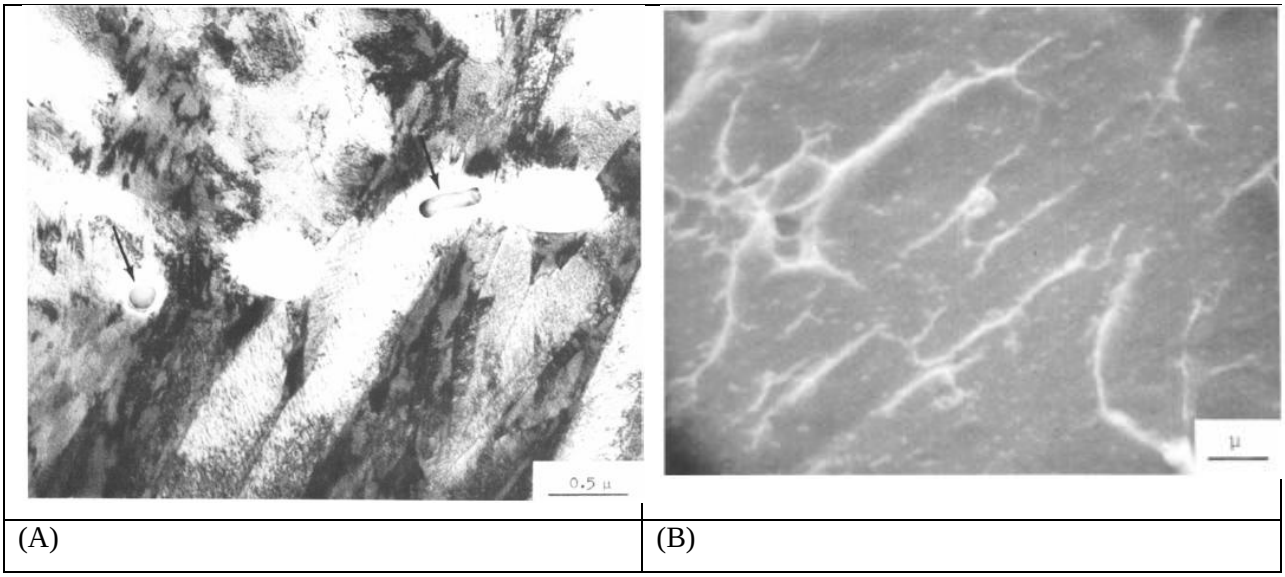

(A)	(B)

Figure 6.14: (A) 300M steel specimen austenitized at 1600°F and quenched to room temperature where the arrows are pointed to undissolved second particles; (B) high resolution fractograph showing concentration of undissolved particles on quasi-cleavage region of the fracture surface of a 300M specimen austenitized at 1600°F [17].

Fully dissolving second phase particles is an important task for austenization treatment of UHSLA steels, but as shown in Section 2.6.5.2, the austenization temperature also plays a role in the amount of retained austenite found in UHSLA steels upon quenching as well. The amount and morphology of the retained austenite is also expected to impact the mechanical properties of UHSLA steels.

6.2.3.1 Retained Austenite in UHSLA Cast Steels

In many of the UHSLA steels, there remains a small fraction of untransformed austenite that remain as thin films between lath structures from the parent martensite upon quenching. The fraction of untransformed austenite is highly dependent on composition; large amounts of FCC stabilizing alloying elements will increase the proportion of retained austenite in UHSLA steels. The presence of trace amounts of retained austenite and its effects on the

strength and toughness of UHSLA steels is the subject of much debate in the literature. For the compositions of the steels in this study, the main composition difference is the percentage of carbon in the investment cast 4340+ alloy (0.40 wt%) versus the amount in the cast ES-1 alloy (0.28 wt%). As reported in the literature, with the higher carbon content, the 4340+ alloy would be expected to possess a detectable amount of retained austenite [38, 128, 129]. Based on the work by Krauss (1997) on 4140 steel, the interlath retained austenite present in the 4340+ alloy can be expected to be less than 4%. No data is available in the literature on retained austenite measurements in ES-1 steels. In this study, to characterize the retained austenite present after heat treatment, x-ray diffraction work was carried out on the cast ES-1 material. The results in **Table 5.13** and **Figures 5.24 - 5.26** showed that X-ray diffraction could not detect retained austenite in either the fully heat treated or as quenched conditions. If retained austenite exists in the ES-1 material, it is of the interlath variety (**Figure 2.17**) that may only be detectable by transmission electron microscopy [38]. Likely, the retained austenite would be less than 2%, as was the case in the 4130 alloy in the Krauss (1997) study. Future work on the cast ES-1 material should include TEM work to characterize any retained austenite that may be present in the material.

The effects of this retained austenite on the final properties after tempering is a subject of controversy. Investigators have reported that intermediate temperature tempering promotes embrittling carbide particle alignment along the prior austenite films causing low toughness upon tempering. As shown in the literature review, silicon additions to 4330, 4340, and 300M wrought steels have slowed this embrittling phenomenon, allowing the low alloy steels to retain ductile high-carbon austenite during tempering or austempering for increased ductility and fracture toughness in the fully heat treated steel[91-94] . Also, at low tempering temperatures (< 500°F), it is expected that thermal activation is not high enough to promote austenite decomposition into ferrite and brittle alloy carbides/ cementite. Furthermore, it is suggested that the retained austenite may be further enriched in carbon and stabilized during low temperature tempering through localized carbon diffusion [128]. In these cases, thermodynamically stable retained austenite may be beneficial to impact and fracture toughness of some UHSLA steels depending on the mechanical stability of the austenite under stress (i.e. possible transformation induced plasticity (TRIP) behavior) [88, 89, 129].

The low temperature tempering that was carried out throughout the cast ES-1 studies was carried out as a result of previous work on wrought material that experienced degraded impact properties above 450°F. Optimal impact, elongation, and tensile properties were found when the tempering temperature was 375°F. The degrading of the impact properties was likely due to the decomposition of any potential austenite films that were undetectable in the x-ray diffraction study or due to classic tempered martensite embrittlement (**Figure 2.18**). Since significant amounts of retained austenite are expected in the 4340+ alloy, the decrease in impact toughness witnessed when the tempering temperature was increased from 500°F to 600°F could be a result of retained austenite decomposition into ferrite and brittle alloy carbides/cementite or to classic tempered martensite embrittlement. Further study is needed to clarify the role of retained austenite and its decomposition during low temperature tempering on the strength and toughness of UHSLA steels.

Although retained austenite levels are too low to be detected directly, the role of small amounts of retained austenite on properties can possibly be inferred from cryo-quenching studies.

6.2.3.2 Cryo Quenching of cast ES-1 Steel

Cryotreatment and/or subzero cooling can be used to complete the martensitic transformation, eliminating any remaining stabilized retained austenite. Most cryotreatment is performed after quenching from austenite conditioning, though some benefit has been realized from treatment after tempering [130, 131]. The cryotreatment on the cast ES-1 ingot material was carried out directly after quenching. Any retained austenite present upon quenching is likely transformed fully to martensite. Other researchers have reported full transformation of the retained interlath austenite to martensite at both subzero (>0°C) and cryogenic (>-100°C) temperatures [130, 131]. However, subzero cooled and cryo treated (very high carbon content) tool steels can still contain significant amounts of retained austenite but have improved wear resistance [131]. The mechanism as to why cryotreated held for long times steels have better wear resistance as compared to subzero treated steels remains a subject of debate. Some investigations suggest that cryo treatment favors a finer distribution of η-carbide over the slightly more coarsely distributed ε-carbide in terms of transition-carbide that is formed upon tempering. It is important to note that cryo treatment and/or cold treatment does not work with all materials;

low-carbon martensitic materials and austenitic stainless steels either have too little retained austenite and/or austenite that is too stable to be influenced by cryo-quenching [132]. The current study showed that even though no detectable amounts of retained austenite were found in the as-quenched or fully heat treated cast ES- material (**Table 5.20**), CRYO-treatment increased the hardness of the cast ES-1 ingot material somewhat while decreasing the -40°F impact toughness. This suggests that small amounts of interlath retained austenite are indeed present in ES-1 steels and that the retained austenite, even in these small "undetectable" amounts, can influence strength and toughness. A TEM study comparing the cryo and non-cryo treated samples outlined in **Table 5.13** is needed to confirm this explanation.

6.2.4 Austempering

Although very high strength levels were achieved in the quenched and tempered 4340+ steels, the corresponding room temperature impact toughness was low. Austempering heat treatments were carried out on the alloy in an attempt to improve the toughness of the alloy (**Figures 2.26 & 2.28**) [101, 103]. It was expected that austempering of the 4340+ alloy would create a fine lower-bainite structure with somewhat lower strengths, but with improved toughness and ductility. As shown in **Table 5.6** and **Table 5.7**, austempering heat treatments were evaluated both with and without prior HIPing. The austempering treatments were designed to include two different austempering temperatures and times. The long austempering time durations chosen were based on the results of the Putatunda (2003) study on high carbon (1%), high silicon (3%), and high manganese (2%) cast steel. Much longer austempering times (6h or more) were said to be needed to carry out the bainitic reaction to completion for steel with high silicon [69]. However, the Putatunda (2003) study was completed on a high carbon (1wt% C) steel.

As expected, the austempered samples experienced significant gains in CVN and percent elongation, accompanied by significant decreases in hardness and yield strength when compared to the Q & T heat treatments. Austempered specimens achieved about a 50% increase in both impact toughness and elongation on average over quench and tempered specimens. However, both yield and tensile strengths were reduced by 50-70 ksi. as compared to the Q & T specimens, **Tables 5.6 and 5.7**. Similar to the Q & T study, the cast + HIP material that was austempered experienced much less variability in mechanical properties than the as cast + austempered

material. Increasing the austempering temperature from 572°F to 599°F had a significant effect on both the strength and room temperature CVN of the steel. For the non-HIPed samples, CVN and YS both decreased when the austempering temperature increased from 572°F to 599°F. For the HIPed samples, CVN increased and YS decreased when austempering temperature increased from 572°F to 599°F while hardness and percent elongation remained about the same. For all treatments, the mechanical properties did not change significantly between the 8 hour and 14 hour treatments. More testing is needed to clarify the influences of austempering condition on the strength/toughness/ductility relationships for these materials.

Although the microstructure showed signs of successful austempering and gains in impact toughness were accomplished by austempering, the optimal austempering time may have been eclipsed for this high silicon content steel. By austempering for such long times, the high carbon stabilized austenite that is thought to give the bainite and thus these steels their superior impact properties, likely decomposed to carbide, leading to a decrease in strength and sub optimal impact properties. In the future, austempering treatments should be carried out at much shorter austempering times which high retained autenite metastable structures can be achieved. Comparisons between austempered 4340+ and quenched and tempered ES-1 steels (similar yield strength levels) suggest that the ES-1 steels have superior toughness.

6.2.5 Tempering and Temper Embrittlement

As documented in Section 2.6.6, the mechanical properties of UHSLA steels are strongly controlled by tempering time and temperature. The tempering temperature in particular controls both the specific tempering reactions occurring as well as the tempering reaction rates. Alloying elements also have a major influence on tempering kinetics and carbide composition. The development of high toughness in UHSLA steels tempered at low temperatures depends on the formation of small coherent or semi-coherent transition carbides homogeneously nucleated throughout the matrix rather than heterogeneous carbide precipitation aligned along specific nucleation sites in the prior quenched structure. Untempered martensite in these medium carbon steels, while strong, suffers from poor ductility and impact toughness. Tempering the martensite at high tempering temperatures above 950°F leads to complete relaxation of the martensitic structure and complete decomposition of the martensite structure to ferrite and fine carbides. Both elongation and toughness are increased at the cost of strength. Tempering conventional

4XXX steels at temperatures below 500°F promotes the formation of fine metastable transition carbides. Although this tempering temperature regime [below the temper embrittlement (TE) and tempered martensite embrittlement (TME) temperature regimes (**Figure 2.23**) is rarely used, it can result in a fine distribution of these small coherent transition carbides (>10nm) leading to high hardness with reasonable toughness. The TME phenomenon is displayed in **Figure 5.3 and Table 5.4**. In this study, the toughness and hardness of the investment cast 4340+ alloy both decreased when the tempering temperature was increased from 500°F to 600°F. This drop in toughness is not due to tempering reactions in the bulk of the material, but rather to the formation of aligned carbides from the decomposition of the trace retained austenite present in the martensite lath.

In UHSLA steels, high strength and good toughness can be achieved by preserving coherent carbides that are formed during the early stages of tempering at low tempering temperatures. The silicon alloyed UHSLA steels in this study, 4340+ and ES-1 steel, effectively use silicon to stabilize and preserve coherent carbides at low tempering temperatures [133]. Silicon additions to 4340+ and ES-1 can stabilize the ε – carbide (**Table 2.17**) to an extent that it may still be present in the microstructure after tempering at temperatures up to 750°F in steels with 1-2 wt% Si. The nucleation and metastable transition is slowed and silicon enters into the ε – carbide structure. In addition, the transformation of ε – iron carbide to cementite is delayed considerably, promoting both high strength and toughness. As a result of the work on 4130, 4140, and 4150 steels discussed by Krauss (1997), it is evident that the ε – transition carbide densities of the transition carbide clusters are expected to be larger in the 4340+ alloy when compared to the ES-1 alloy. Thus, the dislocation density of the higher carbon 4340+ alloy would be assumed to be larger than the dislocation density in the ES-1 alloy [97].

In lower carbon content martensites in particular, good combinations of strength and toughness have been achieved at low tempering temperatures. The limited carbon diffusion to dislocation tangles within the lath and/or localized prior martensite lath boundaries at low tempering temperatures can be expected to become preferred sites for nucleation and growth of extremely fine transition carbide particles that promote both high strength and toughness [20, 97].

Temper embrittlement phenomena that must be avoided in the UHSLA steels, are controlled by both steel composition and tempering temperature. The 43XX steels tend to embrittle as tempering temperatures reach the 500°F range [77]. Tempering steels in this range leads to both a decrease in hardness as well as CVN impact toughness. The fracture mode changes from ductile to intergranular fracture nucleated at prior austenite grain boundaries. In addition to solute atom segregation to these boundaries, alloy carbide or cementite formation can form, providing the sites for intergranular crack nuclei [98]. Banerji et al. (1978) found that ultra-low residual (P + S) steels without Si and Mn did not suffer TME; however, Si appeared to blunt and widen the range of the TME curve [134]. It has been suggested that Mn and Si additions promote P segregation leading to TME. This is of concern for UHSLA cast alloys, such as 4340+ and ES-1, because these alloys contain Si for castability and preferential carbide formation while Mn is added for solid solution strengthening and as a sulfide getter. The P levels in these steels may need to be very low to exploit success at low tempering temperatures.

It is important to note that at increasing carbon levels, embrittlement phenomena becomes much more difficult to avoid, even at low tempering temperatures. Classical intergranular temper embrittlement (quench embrittlement) is observed in steels with carbon levels above 0.5 wt% C when tempering at low tempering temperatures [98]. The embrittlement of these higher carbon steels occurs even with ultra-low levels of P and S and other residuals at low tempering temperatures. Similarly hydrogen embrittlement can be a problem in a nickel-alloyed UHSLA steels (such as 4340+ and ES-1), particularly when residual phosphorous levels are high. Tempering at low tempering temperatures can cause hydrogen to remain trapped in the matrix. It has been reported that interactions between Mn and P promote segregation of phosphorus during austenization, causing intergranular cracking, even at P levels < 0.005 [134]. Sulfur also contributes to low toughness, particularly when elongated sulfide particles are distributed in the matrix. Attempts to change the morphology of sulfides with rare earth and calcium additions have met with different levels of success in both wrought and cast steels. Adding Ca to 4340 steel favors CaS at the expense of MnS [135]. As the results demonstrated in this study, for UHSLA cast steels, it will be extremely important to produce extremely clean steel, steel with low residual levels of O, S, and P. Moderate increases in upper shelf impart toughness have been reported for low-sulphur materials in particular [135].

Controlling carbide formation during tempering in UHSLA steels is undoubtedly important to developing the necessary mechanical properties. This low temperature tempering regime has not been widely studied in the literature. More research is needed to fully exploit the benefits of tempering lower carbon content UHSLA cast and wrought steels in this tempering temperature regime.

6.3 Low Temperature Tempering of Lower Carbon Content UHSLA Steels

Conventional 43XX based steels can achieve very high yield strength levels (>250ksi.) when tempered at low tempering temperatures; however their toughness is limited. These lower tempering temperatures however can be effectively used in the lower carbon content ES-1 steel to produce high yield strength levels (>180ksi.) with excellent toughness. The results showing superior elongation and impact properties in the lower % carbon containing cast ES-1 were expected. As carbon content increases, the density of carbide clusters increases and the spacing of these carbide clusters decreases. The major portion of strain hardening and carbon-dependent strengthening is accomplished by dislocation interactions in the fine structure of the tempered lath martensite [97]. Carbide coherency, size, and distribution influences the amount of strain on the tempered martensite lattice. The superior impact properties of the ES-1 material could be a result of a fine, coherent or semi-coherent carbide distribution. The results of the carbide characterization study showed that very small (less than 1 micron) carbides rich in chromium, molybdenum, and tungsten are present at the lath and martensite packet boundaries of the ES-1 material when tempered at 600°C (1112°F) (**Figure 5.27**). This study shows that even at a very high tempering temperature, 600°C (1112°F), the carbides formed in the ES-1 material are much smaller than the carbides found its carbon and low alloy steel counterparts at high tempering temperatures. These results suggest that these high temperature carbides originated from very small, coherent transition carbides rich in chromium, molybdenum, and tungsten. At lower carbon contents (0.28 wt% C), the martensite trapped carbon creates a lower amount of lattice strain when compared to its higher carbon content counterparts (0.40wt %C). The ES-1 material, with a lower carbon content, and a presumed favorable $M_{2.4}C$ transition carbide distribution (epsilon carbide) throughout the tempered lath martensite possesses superior impact properties with acceptable strength levels.

ES-1 steel is capable of a high degree of strain hardening, as indicated by a yield strength/ tensile strength ratio (YS/TS) of 0.8, while the more highly alloyed steels and higher

carbon steels exhibit YS/TS ratios of 0.9. The low temperature tempered ES-1 material, with low YS/TS ratios, performs well under high strain rate tensile testing and thus under impact-like strain rates [136]. When increased tempering temperatures and times are used, less coherent carbides are formed and coarsening of both the dislocation substructure and carbide distributions occurs, reducing toughness.

Carbon content, alloying element composition, and heat treatment are all important when designing for specific tensile and yield strength targets. There exists a large area for exploration of UHSLA materials with carbon contents between 0.28% and 0.40%. With a strong research effort, "intermediate toughness and yield strength" materials should be able to be designed that possess carbon contents, impact properties, and yield strengths somewhere between ES-1 steel (CVN: 50 ft-lbs. @ RT; YS> 180ksi.) and 4340+ (CVN: 10ft-lbs. @ RT; YS: 250 ksi.). It is evident that additional study is needed to further optimize the processing of these Fe-0.28%C-Si-W alloys and to determine if other commonly used medium carbon content alloys based on the 43XX and 86XX alloys can also develop excellent properties at low tempering temperatures.

6.4 Eglin Steel (ES-1) Alloy Cost Analysis

The development of the ES-1 alloy (eglin steel) was carried out not only for the potential mechanical performance demonstrated in Chapter 5 but also for the cost effectiveness of the alloy. The Aermet 100 alloy, which is currently used for applications requiring high yield strength and high impact toughness, comes with a high price tag. **Table 6.5** shows a detailed alloy cost analysis that compares the ES-1 alloy to Aermet 100. The cost analysis was completed using the London Metal Exchange real time element cost estimator. The raw material cost quotes are current as of March 22, 2011. The costs do not include raw material supplier sales margins or melting and processing costs of each of the alloys. The raw material supplier sales margins are assumed to be constant for all raw materials being considered**. Table 6.5** shows that the development of the ES-1 alloy and the necessary processing steps has the potential to deliver a material that has significantly higher mechanical performance than earlier USHLA steels and whose cost is approximately 18% of Aermet 100.

Table 6.5: Raw material cost analysis comparison of the ES-1 steel and AerMet 100 alloys [36, 137].

Composition	% of Total	Cost ($/lb.)	Composition	% of Total	Cost ($/lb.)
ES-1			**AerMet 100**		
Fe-C-Mn			Fe-C-Mn		
(Steel Scrap)	93.63	0.33	(Steel Scrap)	69.50	0.33
Si	1.00	1.12	Co	14.00	17.01
Cr	2.75	1.32	Ni	12.00	11.85
Ni	1.03	11.85	Cr	3.30	1.32
Mo	0.36	16.58	Mo	1.20	16.58
W	1.17	18.50			
V	0.06	13.63			
	Total	$0.76		**Total**	$4.27

In addition to providing significant alloy cost savings, the cast ES-1 alloy development has also shown the potential for a cast + HIP ES-1 alloy exhibiting equal or potentially better mechanical properties when compared to the forged ES-1 alloy.

6.5 Cast + HIP vs. Forged ES-1 Routing Summary

To this point in time, all penetrator components manufactured using the ES-1 steel alloy for high yield strength and impact loading conditions necessary for penetrator applications have been forged to develop the necessary mechanical properties. The results displayed in Chapter 5 for the cast + HIP ES-1 alloy show that the potential exists for the ES-1 alloy to be cast to shape while exhibiting mechanical properties characteristic of the forged alloy. **Figure 6.15** shows the current steps being carried out to produce forged components using the ES-1 alloy. **Figure 6.16** shows the steps that would need to be carried out to produce the components using centrifugal casting and HIP. The centrifugal casting method offers the ability to cast near net shape components in a leaner production process. By casting near net shape components, the components will no longer undergo open die forging; the cast components offer a significant decrease in the amount of material needed to cast each component and also a significant decrease in the amount of machining needed for each component.

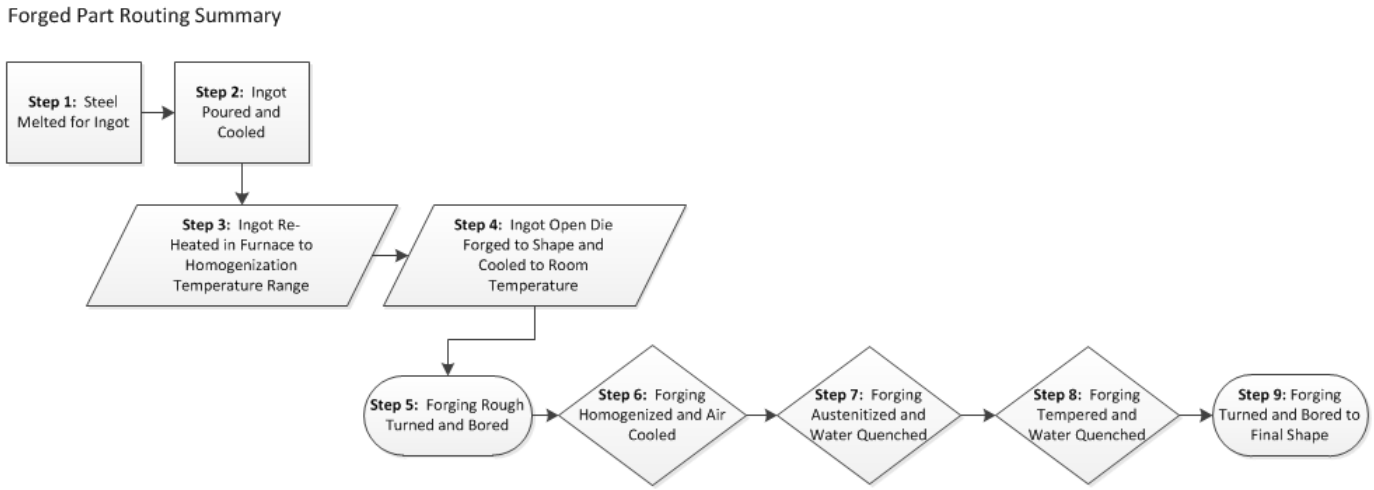

Figure 6.15: Manufacturing routing summary showing the current steps carried out to manufacture forged ES-1 components.

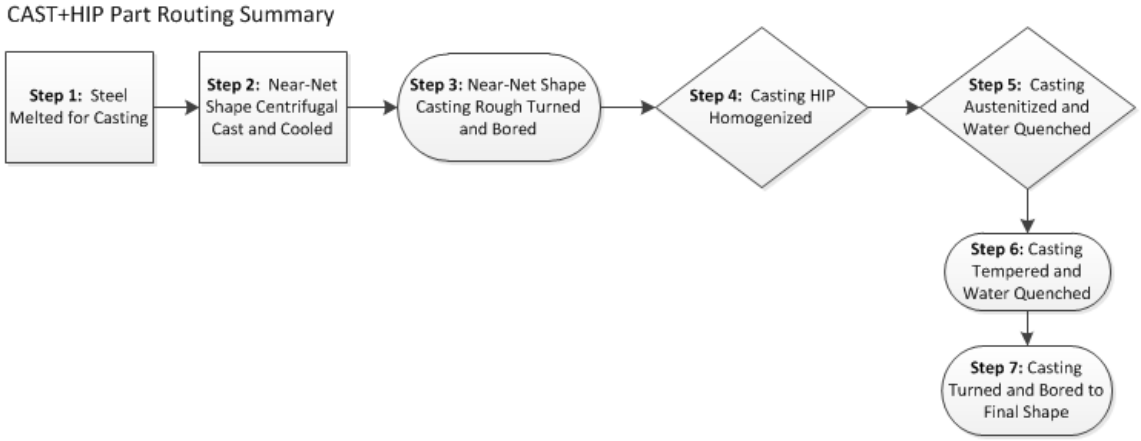

Figure 6.16: Manufacturing routing summary showing the basic steps needed to manufacture ES-1 components using the proposed centrifugal cast + HIP method.

The development of a cost effective UHSLA casting alloy with improved impact toughness not only offers the military a potential alternative for penetrator manufacturing, but also a cost effective UHSLA steel casting alloy for components across all branches of the military. The ES-1 alloy promises to be an important steel casting alloy for both military and commercial applications.

Chapter 7

Conclusions

The results from this study of UHSLA cast steels have helped to clarify the affect of composition, heat treatment parameters, and secondary processing on microstructure and mechanical properties, of the cast 4340+ and ES-1 alloys. Although significant progress was made in the development of these casting alloys, it is clear that additional study is needed to optimize melting, deoxidation, pouring, heat treatment parameters, and secondary processing techniques for these new alloys to develop optimal mechanical properties. From the underlying work that was completed, the following conclusions can be made:

(1) The cast ES-1 alloy promises to be an important new member of the UHSLA cast steel family (YS>180ski) because of its excellent combination of castability, strength, toughness, and ductility. The cast ES-1 alloy possesses properties comparable to its high alloy counterparts without large amounts of expensive alloying elements such as nickel and cobalt. The cast 4340+ alloy also promises to be an important new member of the UHSLA cast steel family (YS>250ksi) as a result of its excellent combination of castability and strength when high toughness is not required.

(2) A diffusion model verified with previous diffusion work has been developed to estimate the percent reduction of microsegregation of alloying elements between the dendritic and inter-dendritic sections of steel castings during subsequent thermal processing.

(3) Casting section size (cooling rate) will directly influence the amount of segregation reduction possible during HIP or homogenization treatments of UHSLA steel castings. The segregation reduction possible depends not only on the alloys present and the homogenization time and temperature, but also on the DAS of cast steels. Model estimates show that little, if any diffusion of substitutional alloying elements will occur during the homogenization of steels castings with DAS $\geq$ 200 μm regardless of the homogenization temperature. The model presented demonstrates the importance of higher homogenization temperatures in particular for UHSLA

steel castings containing significant amounts of substutional alloying elements. Segregation modeling has shown that for typical casting section sizes (DAS > 40μm) it is only above 2000°F (1093°C) that a significant amount of microsegregation reduction of substitutional alloying elements can be achieved. The alloying element, W, in particular is very difficult to solutionize during homogenization treatment.

(4) The initial HIP or homogenization step during the heat treatment of cast steels is critical to reducing microsegregation; very little, if any reduction in segregation occurs during subsequent austenization and tempering that take place at lower temperatures.

(5) High temperature (1950°F - 2125°F) HIP cycles as well as high temperature homogenization cycles have been shown to improve the impact toughness and ductility of UHSLA cast steels. Diffusion modeling suggests that high temperature HIP cycle can significantly reduce the microsegregation of subtitutional alloying elements and can therefore replace the homogenization step in the heat treatment of UHSLA cast steels. HIP processing also significantly reduces microporosity formed during solidification. High temperature HIP and homogenization cycles can also be expected to more readily solutionize second phase particles that may be present in the cast alloy. These are additional ways that high temperature HIPing improves toughness.

(6) The deoxidation, melting, and pouring practices greatly influence the microinclusion content and thus the impact properties of the cast UHSLA steels. Proper oxidation, countergravity pouring, and vacuum degassing of the melt can significantly reduce the number of inclusions in the alloys, leading to better impact properties. High residual levels of Al, O, S, and P result in poor impact properties for the ES-1 alloy in all heat treatment conditions. Foundries producing UHSLA steel castings should consider the use of premium melting practices such as AO refining to insure alloy performance.

(7) The higher carbon content 4340+ alloy experiences tempered martensite embrittlement (TME) when tempered above 500°F leading to both decreased hardness and impact toughness. Austempering heat treatments can alternatively be used to increase the impact toughness and ductility of the 4340+ alloy, but strength decreases in the austempered alloy.

(8) X-Ray diffraction measurements did not indicate that ES-1 steel had measurable amounts of retained austenite present in the structure after quenching. This suggests that less than 2% retained austenite is present. Cryogenic quenching of the ES-1 alloy prior to tempering increased the hardness and decreased the impact properties of the alloy. This strongly suggests that the ES-1 alloy contains a very small amount of retained austenite (less than 2%) and that this retained austenite is influential in controlling properties.

Recommendations for Future Study

This initial study of 4340+ and ES-1 UHSLA cast steels has also indicated areas where further study is needed to fully develop the potential of this new class of materials. The heat treatment response of these materials is complex and has not been well-studied in similar wrought materials. Much more work needs to be done to fully develop the necessary deoxidation procedures, melting procedures, pouring procedures, and secondary processing parameters to produce optimal mechanical properties for the cast 4340+ and ES-1 alloys. Recommendations for further study include:

(1) Additional study is needed to link the predicted amount of micro-segregation reduction to the expected mechanical properties so that heat treatment process guidelines for optimal mechanical properties can be developed. If these relationships can be quantitatively developed, heat treaters can effectively develop heat treatment cycles that will meet the required property specifications and minimize heat treatment cost.

(2) Modeling and electron probe microanalysis (EPMA) work is needed to estimate the extent of microsegregation present before solidification of the cast UHSLA steels and to characterize the extent of microsegregation reduction after heat treatment to fully validate models.

(3) Transmission electron microscopy (TEM) work is needed to further understand the possible role of interlath retained austenite in the cast UHSLA steels and the complex carbide precipitate sequence during tempering. In particular this will clarify the role of silicon and tungsten in the development of high toughness microstructures.

(4) A more complete mechanical property study of the 43XX+ alloy should be carried out with heat treatment processes designed based on the knowledge that was gained in this study on HIP homogenization, homogenization, austenization temperatures, tempering temperatures, and austempering times. Alloys with various carbon contents can be the basis for targeted alloys with good properties at the 200 ksi and 220 ksi yield strength levels and improved toughness at the 250 ksi YS level.

(5) Additional study is necessary to fully characterize the effects of HIP on cast steels and to develop optimal HIP cycles (temperature, pressure, and time) to develop optimal mechanical properties in cast steels. HIP cycles that eliminate the extra homogenization step during heat treatment can also be developed.

Appendix A.1

Cast ES-1 Ingot EPMA Study

EPMA Operating Conditions: 15 kev, 12 nA

Spectrometry: WAVELENGTH dispersive spectrometry.

Study Design: (5 Samples)

Sample ID: EGLIN-EPMA-1 EPMA Sample- Prepared (4/21/2010)

AS CAST – (No Heat Treatment)

Sample ID: EGLIN-EPMA-2 EPMA Sample- Prepared (5/17/2010)

Step 1-HIP 4 hrs. at 2125F, 15ksi.

Sample ID: EGLIN-EPMA-3 EPMA Sample- Prepared (5/17/2010)

AS CAST + HIP + Full Heat Treatment
Step 1-HIP 4 hrs. at 2125F, 15ksi.
Step 2-2000F Homogenize 2 hrs. in Argon; Air Cool to Room Temp.
Step 3-1900F Austenitize 1 hr. in Argon ; Quench in Room Temp. Water
Step 4-375F Temper 4 hrs.; Quench in Room Temp. Water

Sample ID: EGLIN-EPMA-4 EPMA Sample- Prepared (6/5/2010)

AS CAST + Homogenize (Mimic HIP cycle- no pressure)

Step 1-Homogenize 4 Hours at 2125F in Argon- Air Cool to Room Temp.

Sample ID: EGLIN-EPMA-5 EPMA Sample- Prepared (6/5/2010)

AS CAST + Homogenize (Mimic HIP cycle- no pressure) + Full Heat Treatment

Step 1-Homogenize 4 hrs. at 2125F in Argon; Air Cool to Room Temp.
Step 2-2000F Homogenize 2 hrs. in Argon; Air Cool to Room Temp.
Step 3-1900F Austenitize 1 hr. in Argon; Quench in Room Temp. Water
Step 4- 375 F Temper 4 hrs.; Quench in Room Temp. Water

*****The only sample that EPMA analysis was attempted on was EGLIN-EPMA-1**

Notes From Technician on EPMA for the Analysis on EGLIN-EPMA-1 Sample:

The profiles are 126 points (2um steps), 40 points (1um steps), 101 points (1um steps). It clearly shows some non-uniform composition, especially correlation between high W, Cr and Mo. However, the variation is spikes, not zones, indicating very short range composition changes (mostly only one point at a time). The magnitude of these changes is not typical of experimental noise; the technique is much more precise than that. The technician wanted to interrogate these differences so he set up the 40 point profile with shorter step size (1 um) and better counting precision. The 40 points cover the same span as points 85-105 of the 126 point scan except just adjacent to the longer scan rather than right on top of it (it is parallel but about 5 um distant). It doesn't correlate with the data in the longer scan so they are not crossing the same features as in crossing a long dendritic zone. Again, the indication is compositional variation in micron or sub-micron domains, probably in both dimensions such as spots rather than micron wide long features. The third profile is the tight spacing, high precision scan 100 microns long in a completely different area of the sample. It indicates the same spiked variation. The technician felt as though we were seeing submicron mixed carbides. The compositions don't look like carbides because we never really analyze them cleanly, they are smaller than the beam size and so numerous that we often analyze them only partially exposed at the surface or even buried just beneath. The next step in the study (prior to the EPMA equipment failing) was to try to map an area to see what turned up. The problem with mapping would have been that the map times would've needed to be long to see minor compositional differences.

Compositional Notes:

The table below shows the measured (nominal) composition for the cast ingot material. The 3 profile compositional numbers are simply averages of all the data points taken from the scans seen in Figures **A.1.2 – A.1.4**. The W composition measured by EPMA was significantly less than the actual cast ingot composition. The Cr composition seemed high in the EPM analysis.

	Si	Ni	W	Mo	Mn	Cr
Nominal Composition	0.98	1	0.98	0.4	0.78	2.59
EPMA Profile 1	1.052	1.085	0.607	0.459	0.743	2.935
EPMA Profile 2	1.032	1.093	0.530	0.417	0.732	2.851
EPMA Profile 3	0.89	0.995	0.492	0.331	0.626	2.643

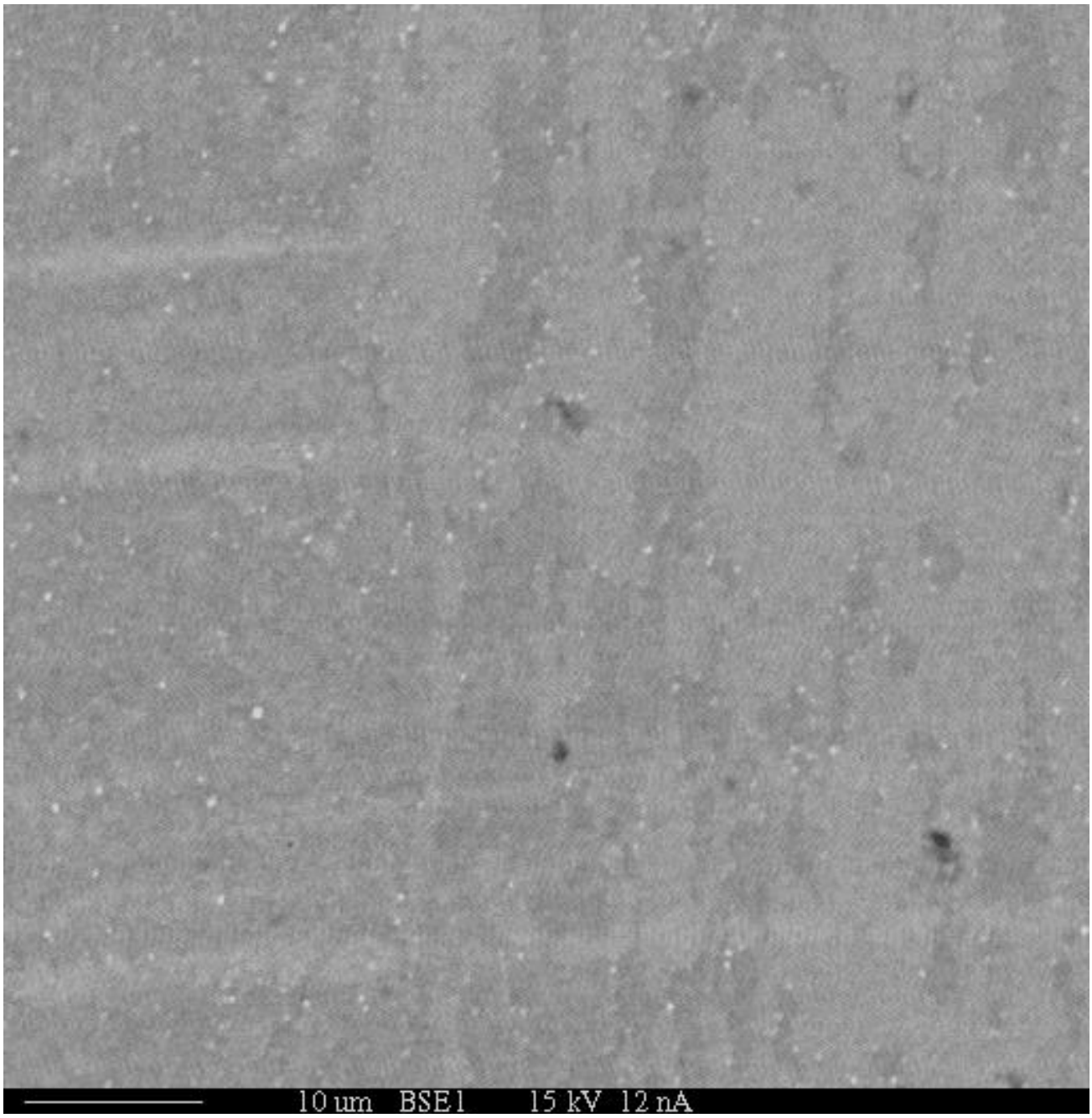

Figure A.1.1: Backscatter Image of Eglin As Cast ES-1 Ingot Sample from EPMA analysis.

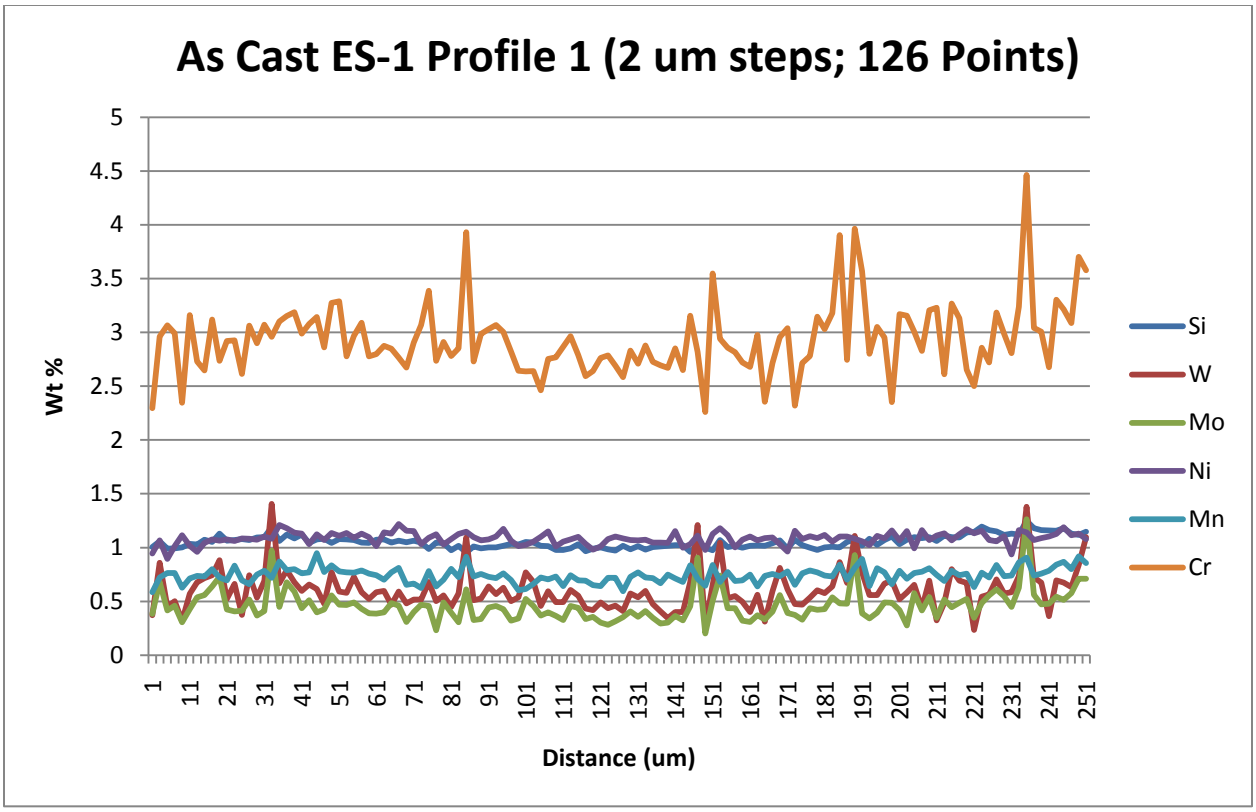

Figure A.1.2: EPMA Analysis (Wt% Alloying Elements vs. Distance) in 2 micron increments.

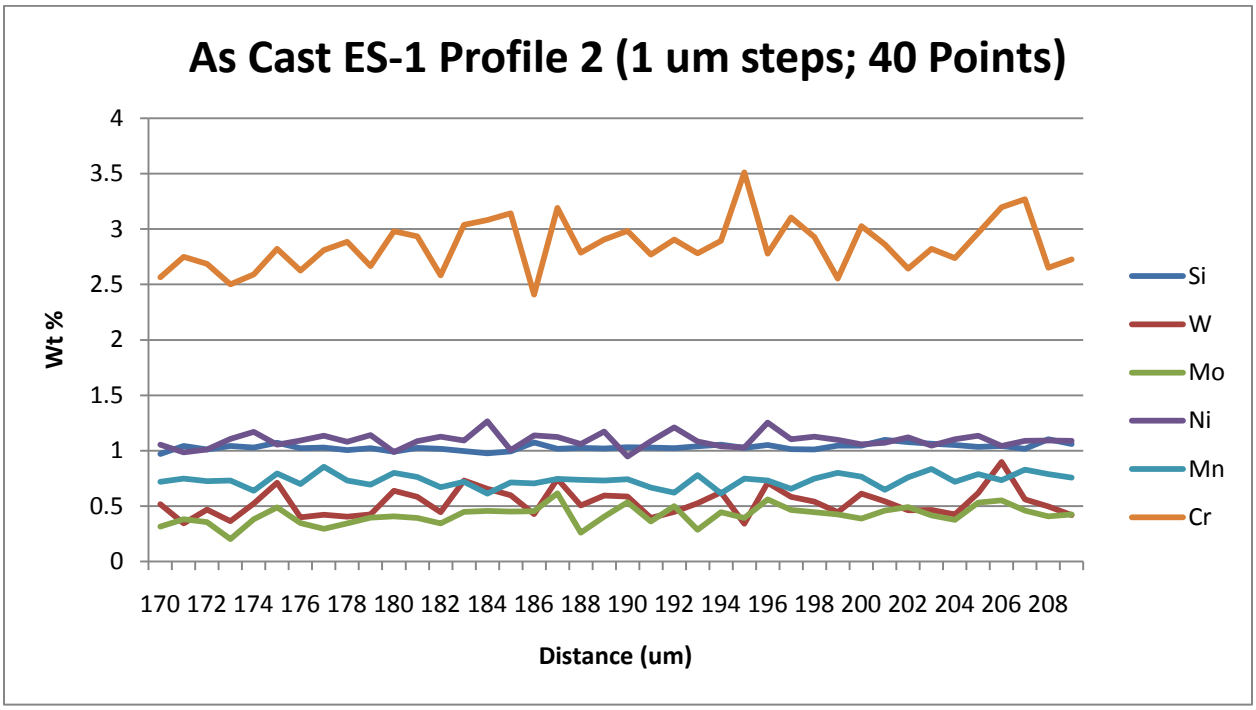

Figure A.1.3: EPMA Analysis (Wt% Alloying Elements vs. Distance) in 1 micron increments.

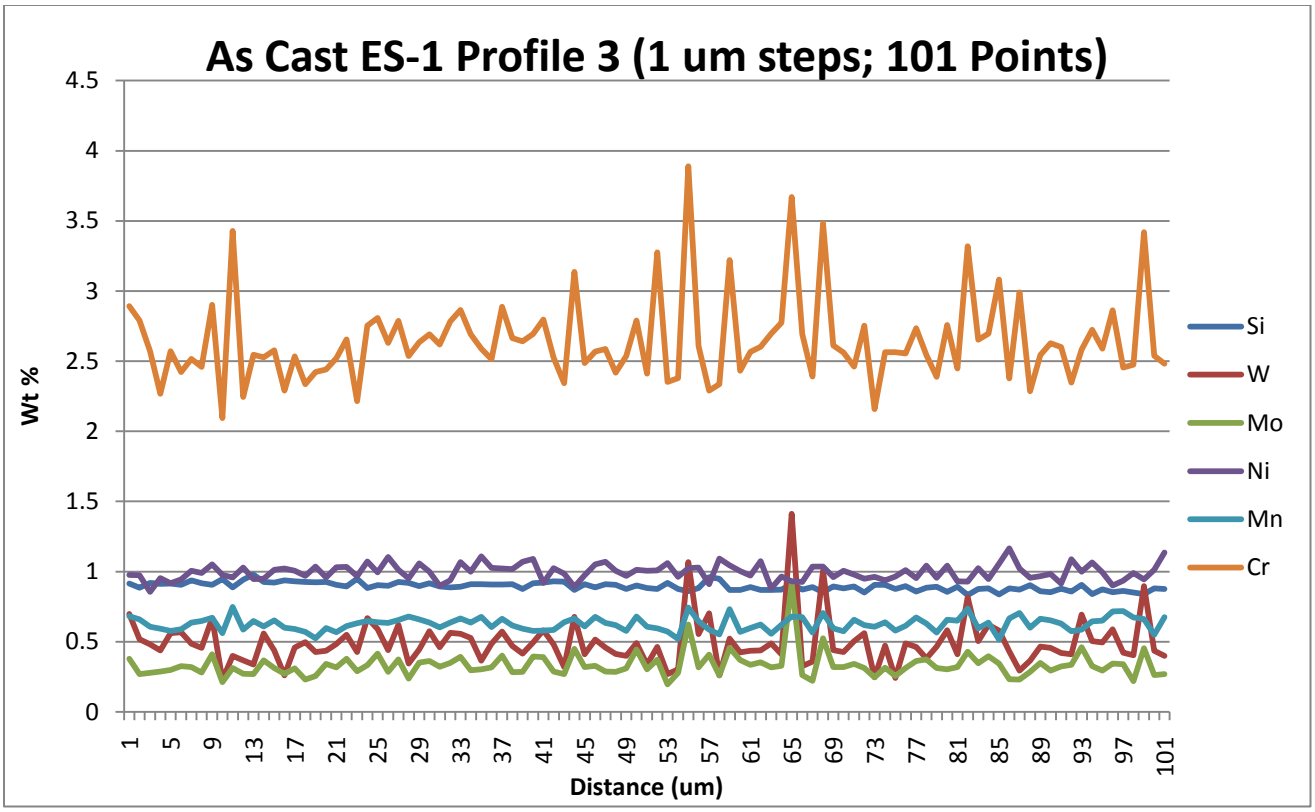

Figure A.1.4: EPMA Analysis (Wt% Alloying Elements vs. Distance) in 1 micron increments.

Search

PENN STATE SEARCH

Contact MCL

Techniques and Services

Facility Locations

News & Events

Personnel

MCL on Facebook

Getting Started

- - Internal Users

- - External Users

Online Sign-Ups

- - UFIS

- - RIMS (Portal)

ELECTRON PROBE MICROANALYSIS (EPMA)

Description

Incident electrons ionize an atom in a sample producing an inner shell vacancy. The atom decays from excited state ultimately producing either a characteristic photon (x-ray fluorescence) or electron (the Auger electron). X-rays are separated by wavelength dispersion in EPMA which results in narrower peak widths and, consequently, a much more quantitative and sensitive analytical tool compared to energy dispersive spectroscopy. Finely focused electron beam and moderate spreading in sample allow analysis in 1-2 μm3 volumes.

Rates

Click here to view current pricing rates

Technique Advantages

- rapid high magnification images of any solid sample
- qualitative (quantitative with standards) elemental analysis in areas down to 1 μm (EDS)
- 2-dimensional elemental mapping

Typical Applications

- quantitative chemical analyses of individual phases in multiphase materials.
- chemical diffusion studies at materials interfaces.
- chemical interaction of components in composites.
- studies of chemical attack by corrosion, weathering, slag penetration and other processes.

Sample Requirements

- Solid samples up to 1 inch in diameter and up to 5/8 inches thick.
- Samples must be flat and polished (preparation area equipped with various polishing media).
- Sample should be conducting (carbon coater available for non-conducting samples).
- Samples should be free of oil and/or other materials which would degas in a high vacuum environment.

EPMA Related Links

- Instrumentation
- EDS - Energy Dispersive X-Ray Spectroscopy
- OIM - Orientation Imaging Microscopy
- SEM - Scanning Electron Microscopy
- TEM - Transmission Electron Microscopy

Contact Info:
Mark Angelone
310 Hosler Bldg
Email: Validate to view contact info
Ph: 814-883-9350

Appendix A.2

Cast + HIP ES-1 Ingot Study Results

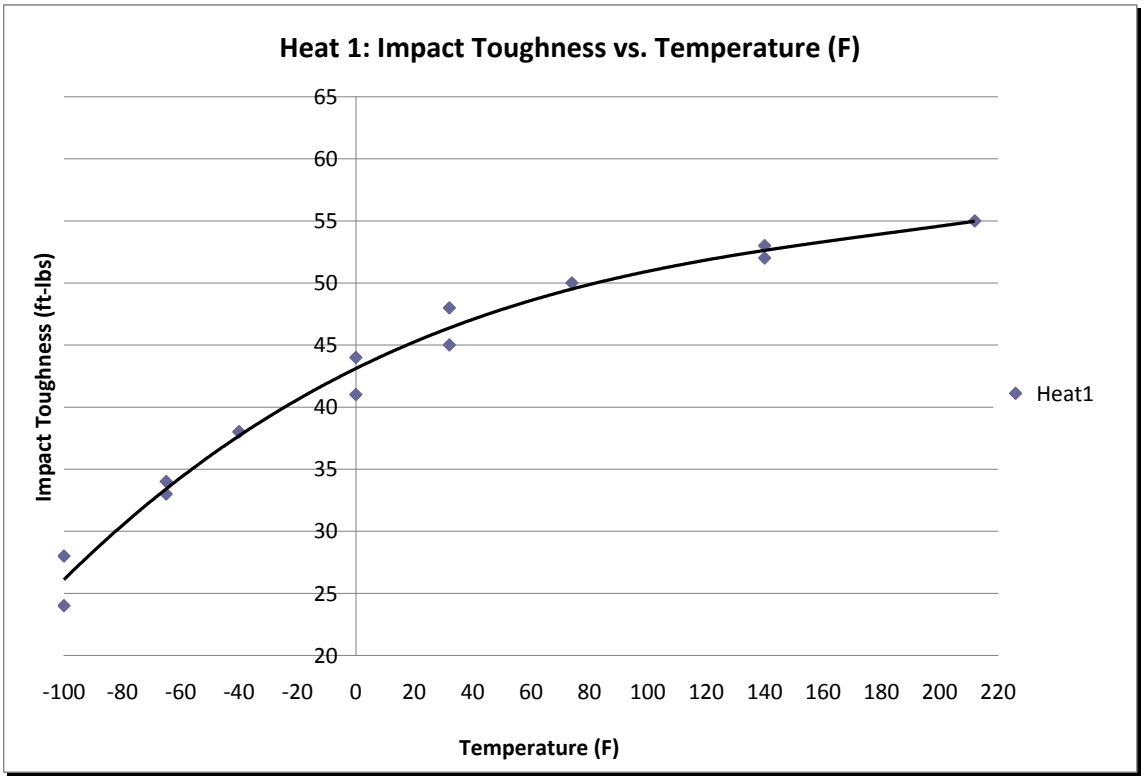

Figure A.2.1: Impact Toughness Transition Curve for Cast ES-1 Heat Treatment 1.

Table A.2.1: Complete Impact Results for Cast ES-1 Heat Treatment 1.

Sample ID	Temp. °F	Energy (ft-lbs)
1Heat-100FA-5C	-100	28
1Heat-100FB-5C	-100	24
1Heat-65FA-5C	-65	33
1Heat-65FB-5C	-65	34
1Heat-40FA-5C	-40	38
1Heat-40FB-5C	-40	38
1Heat0FA-3C	0	44
1Heat0FB-3C	0	41
1Heat-32FA-5C	32	45
1Heat-32FB-5C	32	48
1Heat-72FA-5C	74	50
1Heat-140FA-5C	140	53
1Heat-140FB-5C	140	52
1Heat-212FA-5C	212	55

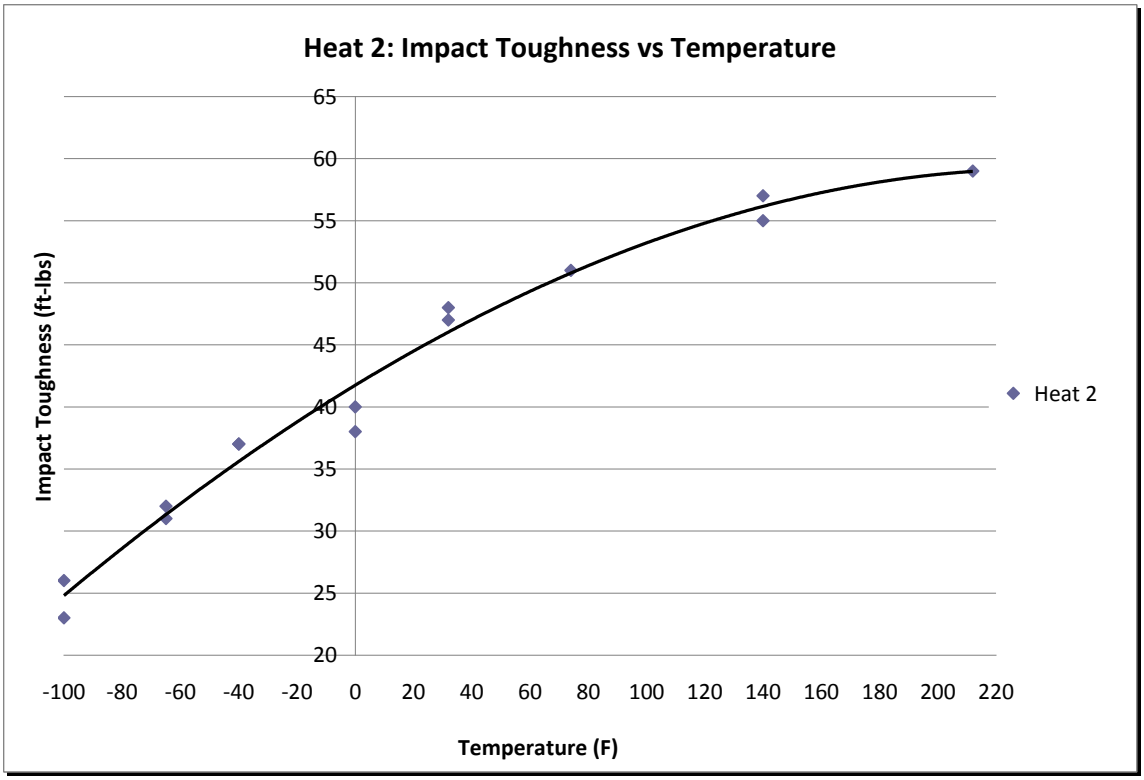

Figure A.2.2: Impact Toughness Transition Curve for Cast ES-1 Heat Treatment 2.

Table A.2.2: Complete Impact Results for Cast ES-1 Heat Treatment 2.

Sample ID	Temp. °F	Energy ft-lbs
2Heat-100FA-7C	-100	23
2Heat-100FB-7C	-100	26
2Heat-65FA-7C	-65	32
2Heat-65FB-7C	-65	31
2Heat-40FA-7C	-40	37
2Heat-40FB-7C	-40	37
2Heat0FA-3C	0	40
2Heat0FB-3C	0	38
2Heat-32FA-7C	32	48
2Heat-32FB-7C	32	47
2Heat-72FA-7C	74	51
2Heat-140FA-7C	140	57
2Heat-140FB-7C	140	55
2Heat-212FA-7C	212	59

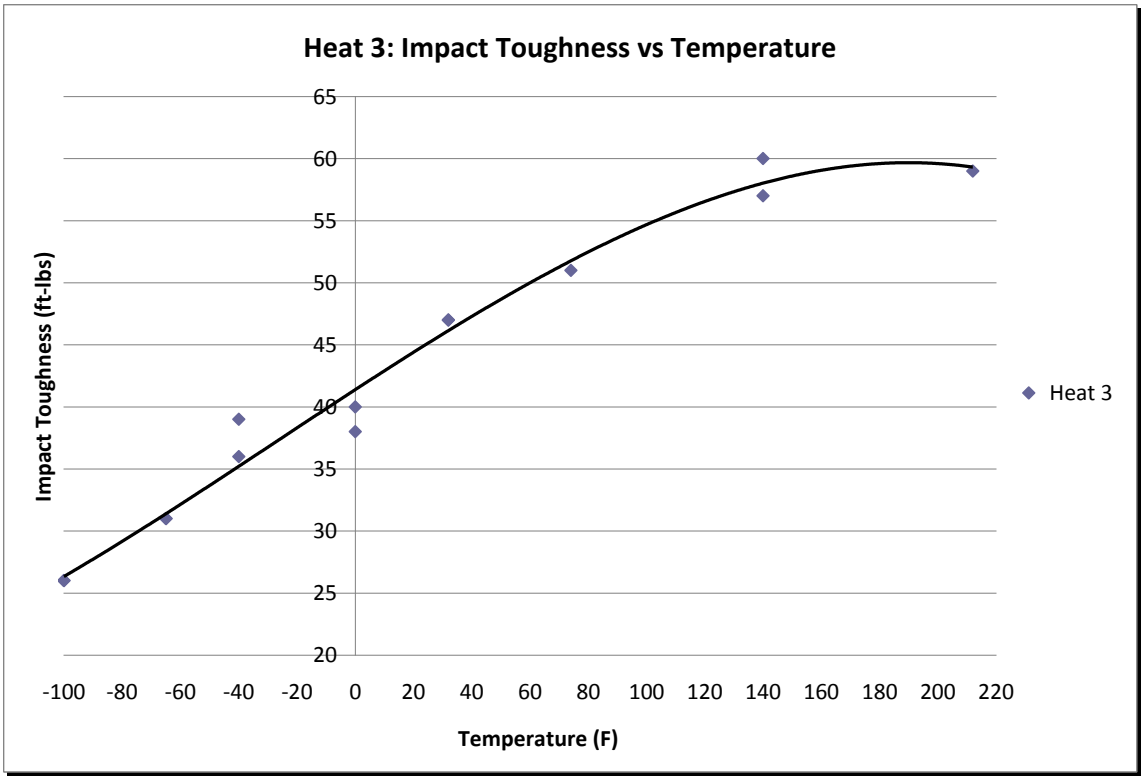

Figure A.2.3: Impact Toughness Transition Curve for Cast ES-1 Heat Treatment 3.

Table A.2.3: Complete Impact Results for Cast ES-1 Heat Treatment 3.

Sample ID	Temp. °F	Energy (ft-lbs)
3Heat-100FA-9C	-100	26
3Heat-100FB-9C	-100	26
3Heat-65FA-9C	-65	31
3Heat-65FB-9C	-65	31
3Heat-40FA-9C	-40	36
3Heat-40FB-9C	-40	39
3Heat0FA-3C	0	38
3Heat0FB-3C	0	40
3Heat-32FA-9C	32	47
3Heat-32FB-9C	32	47
3Heat-72FA-9C	74	51
3Heat-140FA-9C	140	57
3Heat-140FB-9C	140	60
3Heat-212FA-9C	212	59

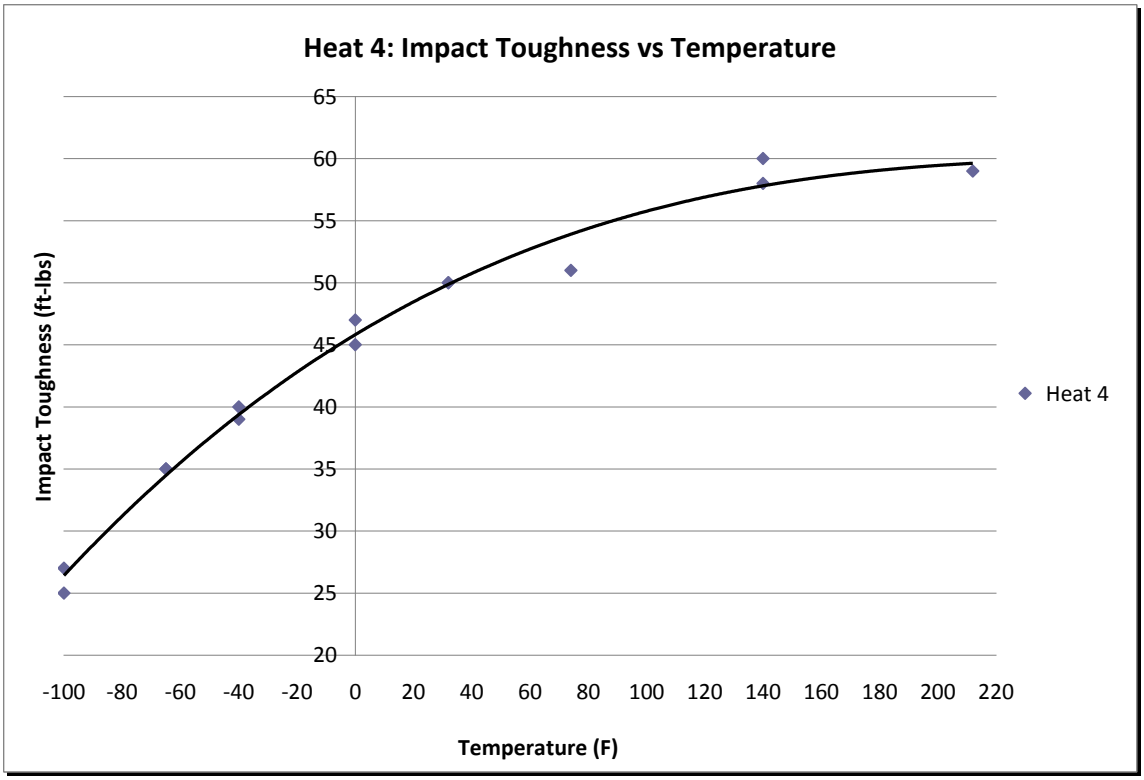

Figure A.2.4: Impact Toughness Transition Curve for Cast ES-1 Heat Treatment 4.

Table A.2.4: Complete Impact Results for Cast ES-1 Heat Treatment 4.

Sample ID	Temp. °F	Energy (ft-lbs)
4Heat-100FA-11C	-100	25
4Heat-100FB-11C	-100	27
4Heat-65FA-11C	-65	35
4Heat-65FB-11C	-65	35
4Heat-40FA-11C	-40	40
4Heat-40FB-11C	-40	39
4Heat0FA-3C	0	47
4Heat0FB-3C	0	45
4Heat-32FA-11C	32	50
4Heat-32FB-11C	32	50
4Heat-72FA-11C	74	51
4Heat-140FA-11C	140	58
4Heat-140FB-11C	140	60
4Heat-212FA-11C	212	59

Table A.2.5: Complete Tensile Results for Cast ES-1 Heat Treatments 1-4.

Heat Treatment	Sample ID	Temp.	UTS ksi	0.2% YS ksi	Elong %
1	1HeatT1-1C	Room	228.7	192.1	15
	1HeatT2-1C	Room	246.5	189.2	14
2	2HeatT1-1C	Room	238.3	182.9	14
	2HeatT2-1C	Room	240.3	184.1	15
3	3HeatT1-1C	Room	243.7	187.6	14
	3HeatT2-1C	Room	244.2	187.4	16
4	4HeatT1-1C	Room	254.6	194.0	14
	4HeatT2-1C	Room	251.6	192.5	15

Appendix A.3

Cast + HIP ES-1 Ingot Microporosity Study Results

Table A.3.1: Sample A (As-Cast) Porosity Reduction Study Results.

Frame	**1**	**2**	**3**	**4**	**5**	**6**	**7**	**8**	**9**	**Average**	**Std. Deviation**
Number of Pores	74	61	99	65	121	72	99	118	70	**87**	**23.0**
Minimum Pore Size(μm^2)	1.6	0.8	3.2	0.8	0.8	0.8	3.2	0.8	0.8	1.4	1.0
Maximum Pore Size(μm^2)	506.7	1153.7	97.5	425.0	230.0	144.3	181.6	1241.0	1864.2	649.3	623.0
Area of Pores (μm^2)	2090	2157	1224	1833	1148	1193	1516	3372	2866	1933	779.9
Area Pore Fraction	0.002224	0.002295	0.001303	0.001951	0.001222	0.001269	0.001613	0.003588	0.00305	0.00206	0.00083
% Porosity of Frame	0.22%	0.23%	0.13%	0.20%	0.12%	0.13%	0.16%	0.36%	0.30%	**0.21%**	**0.08%**
% Pores (0 - 10 μm^2)	52.70%	73.77%	64.65%	63.08%	84.30%	55.56%	72.73%	72.03%	77.14%	68.44%	10.27%
% Pores (10 - 20 μm^2)	25.70%	8.20%	12.12%	21.54%	7.44%	22.22%	15.28%	15.25%	15.71%	15.94%	6.26%
% Pores (20-30 μm^2)	8.11%	6.56%	7.07%	3.08%	3.31%	11.11%	13.89%	3.39%	0.00%	6.28%	4.36%
% Pores (30 - 100 μm^2)	8.11%	4.92%	10.10%	7.69%	4.13%	6.94%	2.78%	5.08%	2.86%	5.85%	2.51%
% Pores (> 100 μm^2)	5.41%	6.56%	0.00%	4.62%	0.83%	4.17%	5.56%	4.24%	4.29%	3.96%	2.17%
Average Pore Size(μm^2)	28.2	35.4	12.4	28.2	9.5	16.6	15.3	28.6	40.9	**23.9**	**10.9**

Table A.3.2: Sample B (HIP (2125F, 4 hours, 15ksi)) Porosity Reduction Study Results.

Frame	**1**	**2**	**3**	**4**	**5**	**6**	**7**	**8**	**9**	**Average**	**Std. Deviation**
Number of Pores	66	53	81	60	34	95	31	65	34	**57**	**22.0**
Minimum Pore Size(μm^2)	3.2	0.8	0.8	2.4	0.8	0.8	1.6	0.8	0.8	1.3	0.9
Maximum Pore Size(μm^2)	54.7	804.0	586.0	53.9	1460.6	65.8	332.2	369.5	114.2	426.8	468.3
Area of Pores (μm^2)	631	2163	1392	599	1821	726	827	905	338	1045	613.5
Area Pore Fraction	0.000672	0.002302	0.001482	0.000637	0.001937	0.000773	0.00088	0.000963	0.00036	0.00111	0.00065
% Porosity of Frame	0.07%	0.23%	0.15%	0.06%	0.19%	0.08%	0.09%	0.10%	0.04%	**0.11%**	**0.07%**
% Pores (0 - 10 μm^2)	74.24%	54.72%	71.60%	66.67%	55.88%	78.95%	48.39%	69.23%	82.35%	66.89%	11.61%
% Pores (10 - 20 μm^2)	15.15%	18.87%	18.52%	23.33%	29.41%	13.68%	32.26%	21.54%	8.82%	20.18%	7.45%
% Pores (20-30 μm^2)	6.06%	13.21%	4.94%	5.00%	2.94%	5.26%	9.68%	7.69%	5.88%	6.74%	3.07%
% Pores (30 - 100 μm^2)	4.55%	7.55%	2.47%	5.00%	8.82%	2.11%	3.23%	0.00%	0.00%	3.75%	3.06%
% Pores (> 100 μm^2)	0.00%	5.66%	2.47%	0.00%	2.94%	0.00%	6.45%	1.54%	2.94%	2.44%	2.39%
Average Pore Size(μm^2)	9.6	40.8	17.2	10.0	53.5	7.6	26.7	13.9	9.9	**21.5**	**16.7**

Table A.3.3: Sample C (Homogenize (2125F, 4 hours)) Porosity Reduction Study Results.

Frame	**1**	**2**	**3**	**4**	**5**	**6**	**7**	**8**	**9**	**Average**	**Std. Deviation**
Number of Pores	105	140	240	286	155	84	129	102	149	**154**	**66.8**
Minimum Pore Size(μm^2)	0.8	0.8	1.6	0.8	0.8	4.0	0.8	0.8	3.2	1.5	1.2
Maximum Pore Size(μm^2)	370.3	2739.6	256.1	502.7	173.7	885.7	81.7	545.5	146.7	633.6	828.3
Area of Pores (μm^2)	2187	4325	3928	5379	1252	2582	1196	1841	1894	2732	1472.2
Area Pore Fraction	0.002327	0.004602	0.00418	0.005723	0.001332	0.002747	0.001272	0.001959	0.002016	0.00291	0.00157
% Porosity of Frame	0.23%	0.46%	0.42%	0.57%	0.13%	0.27%	0.13%	0.20%	0.20%	**0.29%**	**0.16%**
% Pores (0 - 10 μm^2)	76.19%	71.43%	42.92%	47.20%	89.03%	77.38%	71.32%	75.49%	54.36%	67.26%	15.49%
% Pores (10 - 20 μm^2)	10.48%	17.86%	36.67%	30.07%	3.87%	11.90%	21.71%	10.78%	34.90%	19.80%	11.78%
% Pores (20-30 μm^2)	1.90%	5.00%	11.67%	11.89%	2.58%	0.00%	3.10%	3.92%	5.37%	5.05%	4.14%
% Pores (30 - 100 μm^2)	5.71%	4.29%	7.50%	8.74%	3.23%	4.76%	3.88%	7.84%	4.70%	5.63%	1.95%
% Pores (> 100 μm^2)	5.71%	1.43%	1.25%	2.10%	1.29%	5.95%	0.00%	1.96%	0.67%	2.26%	2.12%
Average Pore Size(μm^2)	20.8	30.9	16.4	18.8	8.1	30.7	9.3	18.1	12.7	**18.4**	**8.2**

Appendix A.4

Investment Cast ES-1 Study Results

Table A.4.1: Complete Tensile Results for Investment Cast ES-1 Study for heat #2.

Heat Treatment	Sample ID	Temp. °F	Energy (ft-lbs)
1	Heat1-HIP-40F-C1	-40	28
	Heat1-HIP-40F-C2	-40	26
	Heat1-HIP+72F-C1	74	31
	Heat1-HIP+72F-C2	74	30
2	Heat2-HIP-40F-C1	-40	26
	Heat2-HIP-40F-C2	-40	22
	Heat2-HIP+72F-C1	74	30
	Heat2-HIP+72F-C2	74	29
3	Heat3-NOHIP-40F-C1	-40	21
	Heat3-NOHIP-40F-C2	-40	22
	Heat3-NOHIP+72F-C1	74	20
	Heat3-NOHIP+72F-C2	74	23
4	Heat4-NOHIP-40F-C1	-40	20
	Heat4-NOHIP-40F-C2	-40	21
	Heat4-NOHIP+72F-C1	74	23
	Heat4-NOHIP+72F-C2	74	23
5	Heat5-NOHIP-40F-C1	-40	17
	Heat5-NOHIP-40F-C2	-40	19
	Heat5-NOHIP+72F-C1	74	21
	Heat5-NOHIP+72F-C2	74	22
6	Heat6-NOHIP-40F-C1	-40	15
	Heat6-NOHIP-40F-C2	-40	19
	Heat6-NOHIP+72F-C1	74	25
	Heat6-NOHIP+72F-C2	74	24

Table A.4.2: Complete Tensile Results for Investment Cast ES-1 Study for heat #2.

Heat Treatment	Sample ID	Temp.	UTS (ksi)	0.2% YS (ksi)	Elong %
1	HEAT1-HIP-T1	Room	234.8	180.6	13
	HEAT1-HIP-T2	Room	232.2	178.4	10
2	HEAT2-HIP-T1	Room	228.3	175.3	13
	HEAT2-HIP-T2	Room	231.9	175.8	14
3	HEAT3-NOHIP-T1	Room	237.5	181.0	5
	HEAT3-NOHIP-T2	Room	218.1	177.1	4
4	HEAT4-NOHIP-T1	Room	237.6	178.3	10
	HEAT4-NOHIP-T2	Room	215.1	177.9	3
5	HEAT5-NOHIP-T1	Room	230.9	176	10
	HEAT5-NOHIP-T2	Room	230.8	177.9	9
6	HEAT6-NOHIP-T1	Room	229.2	174.5	8
	HEAT6-NOHIP-T2	Room	225.8	172.6	6

Table A.4.3: Complete Tensile Results for Investment Cast ES-1 Study for heat #3.

Heat Treatment	Sample ID	Temp. ^{0}F	Energy (ft-lbs)
1	Heat1-HIP-40F-CH1	-40	26
	Heat1-HIP-40F-CH2	-40	26
	Heat1-HIP+72F-CH1	74	27
	Heat1-HIP+72F-CH2	74	32
2	Heat2-HIP-40F-CH1	-40	22
	Heat2-HIP-40F-CH2	-40	24
	Heat2-HIP+72F-CH1	74	27
	Heat2-HIP+72F-CH2	74	28
3	Heat3-NOHIP-40F-CH1	-40	22
	Heat3-NOHIP-40F-CH2	-40	20
	Heat3-NOHIP+72F-CH1	74	29
	Heat3-NOHIP+72F-CH2	74	24
4	Heat4-NOHIP-40F-CH1	-40	22
	Heat4-NOHIP-40F-CH2	-40	20
	Heat4-NOHIP+72F-CH1	74	26
	Heat4-NOHIP+72F-CH2	74	24

Table A.4.4: Complete Tensile Results for Investment Cast ES-1 Study for heat #3.

Heat Treatment	Sample ID	Temp.	UTS (ksi)	0.2% YS (ksi)	Elong %
1	HEAT1-HIP-TE1	Room	232.8	176.7	13
	HEAT1-HIP-TE2	Room	241.1	183.8	11
2	HEAT2-HIP-TE1	Room	233.6	177.4	13
	HEAT2-HIP-TE2	Room	233.9	177.9	10
3	HEAT3-NOHIP-TE1	Room	238.6	181.2	11
	HEAT3-NOHIP-TE2	Room	206.6	178.4	2
4	HEAT4-NOHIP-TE1	Room	235.4	179.6	12
	HEAT4-NOHIP-TE2	Room	235.4	178.9	8

Bibliography

[1] Malakondaiah, G.; Srinivas, M., and Rao, P., "Ultrahigh-Strength Low-Alloy Steels With Enhanced Fracture Toughness," *Progress in Materials Science*, Vol. 42, pp. 209-242, 1997.

[2] Totten, George E., "Steel Heat Treatment Metallurgy and Technologies: Steel Nomenclature," Taylor & Francis Group, Boca Raton, FL, 2007, pp.2-8.

[3] Steel Founders' Society of America, "Steel Castings Handbook: Structural Carbon and Low Alloy Steels," Edwards Brothers Inc., 1980, pp. 15-1 to 15-65.

[4] Abbaschian, Reza, "Physical Metallurgy Principles," PWS-Kent Publishing Group, Boston, MA, 3rd Ediction, 1992, pp. 644-651.

[5] Roberts, George; Krauss, George; Kennedy, Richard, "Shock-Resisting Tool Steels," *Tool Steels*, ASM International, Materials Park, OH 44073-0002, 1998, pp. 4, 165-179.

[6] Chatterjee-Fischer, R., "Internal Oxidation During Carburizing and Heat Treating," *Metallurgical Transcations A*, Vol. 9A, 1978, pp. 1553-1560.

[7] ASM International-Revised by Philip, ThoniV (TVP, Inc.); McCaffrey, Thomas J. (Carpenter Steel), "Ultra High Strength Steels," ASM International Handbook Online, accessed January 25, 2010 pp.1-22.

[8] Owen, W.S., "The Effect of Silicon on the Kinetics of Tempering," ASM Transactions, Vol. 46, 1954, pp. 812-829.

[9] Bhadeshia, H.K.D.H., "Bainite in Steels," *Institute of Materials*, London, 1992, p. 73.

[10] Bhadeshia, H.K.D.H.; Edmonds, D.V., "The Bainite Transformation in a Silicon Steel," Metallurgical Transactions A, Vol. 10A, 1979, pp. 895-907.

[11] Roberts, G.; Krauss, G., and Kennedy, R., "Principles of Tool Steel Heat Treatment," *Tool Steels*, ASM International, Materials Park, OH 44073-0002, 1998, pp. 67-107.

[12] ASM International, "High Strength Structural and High-Strength Low-Alloy Steels, Properties and Selection: Irons, Steels, and High Performance Alloys, *ASM Handbook*, Vol. 1, ASM International, 1990, pp. 389-423.

[13] Roberts, George; Krauss, George; Kennedy, Richard, "Tool Steels," ASM International, Materials Park, OH 44073-0002, 1998, pp.4, 102-104.

[14] Bain, E.C. and Pain, H.W., "Alloying Elements in Steel," 2nd Edition, *American Society for Metals*, 1962.

[15] American Society for Metals, "Metals Handbook: 1948 Edition," The American Society for Metals, Cleveland, Ohio, 1948 edition; pp. 453-488.

[16] Poole, S.W.; Franklin, J.W., "High-Strength Structural and High-Strength Low-Alloy Steels," ASM Handbook, Volume 1, pp. 403-420.

[17] Kroneis, M., "Tungsten in Steel," 1st International Tungsten Symposium, Printed in Mining Journals Books Ltd., London, 1979, pp. 96-107.

[18] Takemoto, S., Nitta, H., Iijimas, Y., and Yamazaki, Y., "Diffusion of Tungsten in α-iron," *Philosophical Mag.*, Volume 87, No. 11, April 11, 2007, pp. 1619-1629.

[19] Hong, S.G., Lee, W.B., and Park, C.G., "The Effects of Tungsten Addition on the Toughness of Modified 9Cr-Mo Steels," *Scripta Materialia*, Volume 43, Number 2, 2000, pp. 181-186.

[20] Bhadeshia, H.K., Honeycombe, R.W., "The Tempering of Martensite," *Steels: Microstructure and Properties,* Elseiver, Ltd., Oxford, UK, 3rd Edition, 2006, pp. 183-208.

[21] MMPDS Handbook (formerly MIL Handbook), Edition 03, October, 2006.

[22] MMPDS Handbook (formerly MIL Handbook), Edition 01, January, 2003.

[23] Philip, T.V. and McCaffrey, T.J., "Ultrahigh Strength Steels," ASM Handbook Online, Volume 1, 2002, pp. 424-433.

[24] ASM International, *Alloy Digest, ASM International*, 2002.

[25] ASM International, "Ultrahigh-Strength Steels," Heat Treater's Guide: Practices and Procedures for Iron and Steels, ASM International, Materials Park, OH 44073-0002, 2nd Edition, 1998, pp. 671-717.

[26] Krauss, G., "Heat Treated Martensitic Steels: Microstructural Systems for Advanced Manufacture," ISIJ International, Vol. 35 (1995), No. 4 pp. 349- 359.

[27] Wood, W., "Effect of Heat Treatment on the Fracture Toughness of Low Alloy Steels," *Engineering Fracture Mechanics*, Volume 1, 1975, pp. 219-234.

[28] Cox, T.B., Low, J.R., "An Investigation of the Plastic Fracture of AISI 4340 and 18 Nickel—200 Grade Maraging Steels," Metallurgical Transactions, Vol. 5, June 1974, pp. 1457 – 1470.

[29] Little, C.D., Machmeier, P.M., "High Strength Fracture Resistant High Strength Steels," United States Patent No. 4,076,525 B2, Feb 28, 1978. *Microstructure and Properties*, Elseiver, Ltd., Oxford, UK, 3rd Edition, 2006, pp. 183-208.

[30] Hemphill, R.; Wert D.E., "High strength, high fracture toughness structural alloy Eglin Steel-A Low Alloy High Strength Composition," United States Patent No. 5,087,415, February 6, 1990.

[31] Blair, Malcom, "Steel Castings: Classifications and Specifications," A*SM Handbooks Online*, Volume 1, 2002.

[32] Bhadeshia, H.K., Honeycombe, R.W., *Steels: Microstructure and Properties*, Elseiver, Ltd., Oxford, UK, 3rd Edition, 2006.

[33] Youngblood, J.L.; Raghavan, M., "Correlation of Microstructure with Mechanical Properties of 300M Steel," Metallurgical Transactions A, Volume 8A, Sept. 1977, pp. 1439-1447.

[34] Totten, G.E., *Steel Heat Treatment Handbook: Steel Heat Treatment: Metallurgy and Technologies*, New York, NY: Marcel Dekker, 1997.

[35] Ritchie, R.O., Cedeno, M., Zackay, V., and Parker, E., "Effects of silicon additions and retained austenite on stress corrosion cracking in ultrahigh strength steels," *Metallurgical and Materials Transactions A*, Volume 9, January 1978, pp. 35-40.

[36] Dilmore, M., Ruhlman, J.D., "Eglin Steel-A Low Alloy High Strength Composition," United States Patent No. 7,537,727 B2, May 26, 2009.

[37] Torres, K.L.; Clements, H.A., et al., "Dynamic Strength Estimates for a High-Strength Experimental Steel," Journal of Pressure Vessel Technology, Volume 131, April 2009, pp. 021414: 1-6.

[38] Lai, G.Y., Wood, R.A., Clark, V., Zackay, F., and Parker, E.R., "The Effect of Austenitizing Temperature on the Microstructure and Mechanical Properties of As-Quenched 4340 Steel," *Metallurgical Transactions*, Vol. 5, July 1974, pp. 1663-1670.

[39] Wegman, D.P., "An Introduction to Premium Melting," *Carpenter Technology Corporation White Papers*, June 2009, pp. 1-8.

[40] Schmidt, Norman B., "Selecting Optimal Stainless Steels for Bio-Pharmaceutical Service," *Carpenter Technologies Tech Center Publication*, Carpenter Technologies, Reading PA, December 1991.

[41] Parker, E.R., and Zackay, V.F., "Microstructural Features Affecting Fracture Toughness of High Strength Steels," *Engineering Fracture Mechanics*, vol. 7, 1975, pp. 371-375, Pergamon Press, Great Britain, 1975.

[42] Fredriksson, H. and Akerlind, U., "Microsegregation in Alloys – Peritectic Reactions and Transformations," *Materials Processing During Casting*, John Wiliey & Sons, Ltd., England, 2006, pp. 183-223.

[43] Gruzleski, J.E., *Microstructure Development During Metalcasting*, American Foundry Society, Des Plaines, IL, 2000.

[44] Totten, George E., "Fundamental Concepts in Steel Heat Treatment," *Steel Heat Treatment Metallurgy and Technologies*, Taylor & Francis Group, Boca Raton, FL, 2007, pp.121-164.

[45] Speich, G.R. and Leslie, W.C., "Tempering of Steel," *Metallurgical Transactions*, Volume 3, May 1972, pp. 1043-1054.

[46] Fredriksson, H. and Akerlind, U., "Heat Treatment and Plastic Forming," *Materials Processing During Casting*, John Wiliey & Sons, Ltd., England, 2006, pp. 227-251.

[47] Lebeau, C., "Production and Control of HSLA Steel Castings," *AFS Transactions*, Volume 92, Paper 84-47P, 1984, pp. 645-654.

[48] Leger, M.T., "Characterization of HSLA Cast Steel 12 MDV6-M Influence of Wall Thickness and Heat Treatment," *Proceedings of 1st International Steel Foundry Conference, sponsored by SFSA*, Chicago, IL, Nov. 11-13, 1985, pp. 145-162.

[49] Eddy, C.T. and Marcotte, R.J., "Determination of the Effect of Homogenization on the Hardenability and Impact Strength of Cast Steels," *Final Report on Research Project No. 11*, Steel Founders' Society of America, 1947.

[50] Floreen, S., "The Fracture Toughness of Cast High-Strength Steels," *Journal of Engineering Materials and Technology, Transactions of the ASME*, January 1977, pp. 70-75.

[51] Flemings, M. C., "Processing and Properties," *Solidification Processing*, McGraw-Hill Publishers, New York, NY, 1974, pp. 328-344.

[52] Askeland, D.R., The Science and Engineering of Materials, Brooks/Col Engineering Division, Monterey, CA: 1984.

[53] Krishtal, M.A., and Mokrova, A.M., "Mobility of Atoms of Alloyed Elements in Austenite", Translated from *Metallovedenie i Termicheskaya Obrabotka Metallov*, No. 5, May 1966, pp. 2-5.

[54] Nohara, K., and Hirano, K., *Journal of Japanese Industrial Metals*, Vol. 40, 1976, pg. 1053.

[55] Parke, H., *Trans. ASM*, Vol. 31 (4), 1943, pg. 877.

[56] Alberry, P.J., and Haworth, C.W. “Interdiffusion of Cr, Mo, and W in Iron”, *Journal of Metal Science*, Vol. 8, 1974, pp. 407-412.

[57] Růžičková, J., Million, B., Kučera, K., *Kovové Materials*, Vol. 19, 1981, pg.3.

[58] Gruzin, P.L., *In Coll: Problems of Metal Science and Physics of Metals* [In Russian], No. 4, 1955.

[59] Krishtal, M.A., Fiz. *Metal. I Metalloved.*, Vol. 14, No. 2, 1966.

[60] Umanskii, Y.A., Finkel’shtein, B.N., Blanter, M.E., *Physical Metal Science* [In Russian], Metallurgizdat, 1955.

[61] Kupalov, I., and Zemskii, S.V., “Diffusion of Tungsten in Austenite In High-Speed Steels”, Translated from *Metallovedenie I Termicheskaya Obrabotka Metalov*, No.2, Feb. 1968, pp. 10-12.

[62] Nohara, K., and Hirano, K., *Trans. Iron Steel Inst. Jpn.* (Suppl.), Vol. 11, 1971, pg. 1267.

[63] Hoshino, A., and Araki, T., *Trans. Nat. Res. Inst. Metals*, Vol. 13, 1971, pg. 99.

[64] Wells, C., and Mehl, R., *Metals Technology*, Jan. 1941.

[65] Bowen, A., and Leak, G., *Metall. Trans.*, Vol.1, 1970, pg. 1965.

[66] Grigorev, G., and Palinov, L. *Fiz. Met. Metalloved*, Vol. 25, 1968, pg. 377.

[67] Smith, A., “The Diffusion of Chromium in Type 316 Stainless Steel”, *Journal of Metal Science*, Vol. 9, 1975, pp. 375-378.

[68] MacEwan, J., and Yaffe, L. *Can. J. Chem.*, Vol. 37, 1959, pg. 1629.

[69] Adda and Ohiliber, J., *La Diffusion dans les Solides* Vol. 2, Presses Université de France, Paris, 1966, pg. 893.

[70] Badia, M., Vignes, A., *Acta Metall.*, Vol. 17, 1969, pg. 177.

[71] Hirano, K., Agarwala, R.P., Avaerbach, B.L., and Cohen, E., *J. Appl. Phys*., Vol. 33, 1962, pg. 3049.

[72] Wells, C., and Mehl, R. *Metals Technology*, Feb. 1941.

[73] Borg, R. J., and Lai, D., *Acta Met.*, Vol. 11, 1963, pg. 861.

[74] Totten, G. E., “Tool Steels,” *Steel Heat Treatment Metallurgy and Technologies*, Taylor & Francis Group, Boca Raton, FL, 2007, pp. 651-694.

[75] Totten, George E., "Effects of Alloying Elements on the Heat Treatment of Steel," *Steel Heat Treatment Metallurgy and Technologies*, Taylor & Francis Group, Boca Raton, FL, 2007, pp.165-211.

[76] Richards, V., Van Aiken, D., "High Performance Cast Steels," 2009 American Metalcasting Consortium (AMC) Technology Review Presentation, Chicago, IL, June 24-25, 2009, http://amc.ati.org/tech-review.html, accessed online 3 April, 2011.

[77] Ritchie, R.O., Francis, B., and Server, W., "Evaluation of Toughness in AISI 4340 Alloy Steel Austenitized at Low and High Temperatures," *Metallurgical Transactions A*, Volume 7A, June 1976, pp. 831-838.

[78] Shedunov, A.I., and Lat'eva, *Metallovedeni i Term. Obrat. Metallov.* 10, 63, 1966.

[79] Stratton, P., Surbery, C. H., "Retained Austenite Stabilization," *Heat Treating Progress*, March/ April, 2009, pp. 25-27.

[80] Totten, G.E.; Xie, L., and Funatani, K., Handbook of Mechanical Alloy Design, CRC Press, 2004, p. 236.

[81] Roberts, G.; Krauss, G., and Kennedy, R., "Tool Steel Alloy Design," *Tool Steels*, ASM International, Materials Park, OH 44073-0002, 1998, pp. 45-65.

[82] Sugimoto, K.I.; Usui, N., et al., " Effects of Volume Fraction and Stability of Retained Austenite on Ductility of TRIP-aided Dual-phase Steels," ISIJ International, Volume 32, No.12, September 1992, pp. 1311-1318.

[83] Matsumura, O.; Sakuma, Y., et al., " Effect of Retained Austenite on Formability of high Strength Sheet Steels," ISIJ International, Volume 32, No. 10, July 1992, pp. 1110-1116.

[84] Suimoto, K.I.; Nakano, K., et al., " Retained Austenite Characteristics and Stretch-flangeability of High-strength Low-alloy TRIP type Bainitic Sheet Steels," ISIJ International, Volume 42, No. 4, January 2002, pp. 450-455.

[85] Resiner, G.; Werner, E.A., et al., "The Modeling of Retained Austenite in Low-Alloyed TRIP Steels," Journal of Materials, September 1997, pp. 62-83.

[86] Parrish, J., "Retained Austenite: A New Look at an Old Debate," A*dvance Materials Processes*, Vol. 145, No.3, March 1994, pp. 25-28.

[87] Webster, Donald, "Development of a High Strength Stainless Steel with Improved Toughness and Ducility," *Metallurgical Transactions*, Volume 2, August 1971, pp. 2097-2104.

[88] Birat, J.P., Gerberich, W. W., "A Metastable Austenite with Plane Stress Fracture Toughness Near 500ksi.," *International Journal of Fracture Mechanics*, Vol. 7, 1971, pp. 108-110.

[89] Antolovich, S.D., Singh, B., "On the Toughness Increment Associated with the Austenite to Martensite Phase Transformation in TRIP Steels," *Metallurgical Transactions*, Vol. 2, August 1971, pp. 3135-2141.

[90] Rao, B.V., Thomas, G., "Structure-Property Relations and the Design of Fe-4Cr-C Base Structural Steels for High Strength and Toughness," *Metallurgical Transactions A*, Volume 11A, March 1980, pp. 441-457.

[91] Miihkinen, V.T.T., Edmonds, D.V., "Tensile Deformation of Two Experimental High-Strength Bainitic Low-Alloy Steels Containing Silicon," Materials Science and Technology, Volume 3, June 1987, pp. 432-440.

[92] Tomita, Y., "Mechanical Properties of Modified Heat Treated Silicon Modified 4330 Steel," Materials Science and Technology, Volume 11, Number 3, March 1995, pp. 259-263.

[93] Tomita, Y., Okawa T., "Effect of Modified Heat Treatment on Mechanical Properties of 300M Steel," Materials Science and Technology, Volume 11, Number 3, March 1995, pp. 245-251

[94] Tomita, Y., Okawa T., "Effects of Modified Austemper on Microstructure and Mechanical Properties of Silicon-Modified 4340 Steel," *J. Soc. Mater. Sci.*, Japan, Volume 44, Number 499, pp. 438-444, 1995.

[95] Totten, George E., "Classification and Mechanisms of Steel Transformation," *Steel Heat Treatment Metallurgy and Technologies*, Taylor & Francis Group, Boca Raton, FL, 2007, pp.91-120.

[96] Brooks, C. R., "Hardenability and Heat Treatments," *Heat Treatment of Ferrous Alloys*, Hemisphere Publishing Corporation, New York, NY, 1979, pp. 48-88.

[97] Krauss, G., "Tempering of Steel," *Steels: Heat Treatment and Processing Principles*, ASM International, Materials Park, OH, 1990 edition, 1997 Printing, pp. 205 – 261.

[98] Bhadeshia, H.K., Honeycombe, R.W., "The Embrttlement and Fracture of Steels," *Steels: Microstructure and Properties*, Elseiver, Ltd., Oxford, UK, 3rd Edition, 2006, pp. 235-258.

[99] Krauss, G., "Deformation and fracture in martensitic carbon steels tempered at low temperatures." *Metallurgical and Materials Transactions A*, vol. 32, 2001, pp. 867-877.

[100] Bhadeshia, H.K.D.H., "Bainite in Steels," *Institute of Materials*, London, 1992.

[101] Totten, George E., "Steel Heat Treatment," *Steel Heat Treatment Metallurgy and Technologies*, Taylor & Francis Group, Boca Raton, FL, 2007, pp. 277-414.

[102] Mirak, A.R.; Ahmadabadi, M.N., et al., "Effect of Modified Heat Treatments on the Microstructure and Mechanical Properties of a Low Alloy High Strength Steel," Materials Science and Technology, Volume 20, July 2004, pp. 897 – 902.

[103] Tartaglia, J.A.; Lazzari, K.A., et al., "A Comparison of Mechanical Properties and Hydrogen Embrittlement Resistance of Austempered vs Quenched and Tempered 4340 Steel," Metallurgical Transactions A, Volume 39A, March 2008, pp. 559-576.

[104] Li, Y. and Chen, X., "Microstructure and mechanical properties of austempered high silicon cast steel," *Materials Science and Engineering*, A 308, 2001, pp. 277-282.

[105] Li, Y. and Chen, X., "Effects of Ti, V, and Rare Earth on the Mechanical Properties of Austempered high Silicon Cast Steel," *Metallurgical and Materials Transactions A*, Volume 37A, November 2006, pp. 3215-3220.

[106] Putatunda, S.K., "Influence of austempering temperature on microstructure and fracture toughness of a high-carbon, high-silicon and high-manganese cast steel," *Materials and Design*, Volume 24, 2003, pp. 435-443.

[107] Atkinson, H.V.; Davies, S., "Fundamental Aspects of Hot Isostatic Pressing: An Overview," Metallurgical and Materials Transactions A, Volume 31A, Dec. 2000, pp. 2981-3000.

[108] Coble, R.L. and Flemings, M.C., "On the Removal of Pores from Castings by Sintering," *Metallurgical Transactions*, Volume 2, February 1971, pp. 409 – 415.

[109] King, S., Fletcher, A.J., Atkinson, H.V., Rickinson, B.A., "Removal of Voids in 70/30 Cupronickel Castings by Hot Isostatic Pressing," *Proceedings of the Internatoinal Conference on Hot Isostatic Pressing '93*, Anthwerp Belgium, April 21-23, 1993, 145-155.

[110] Novotny, P.M., and Maguire, M., "Navy Fighter Demands Evolve into Tough Castings," *Foundry Management & Technology*, December 1993, pp. 33-36.

[111] Bhadeshia, H.K., Honeycombe, R.W., "Formation of Martensite," *Steels: Microstructure and Properties*, Elseiver, Ltd., Oxford, UK, 3rd Edition, 2006, pp. 95-128.

[112] Bhadeshia, H.K., Honeycombe, R.W., "The Bainite Reaction," *Steels: Microstructure and Properties*, Elseiver, Ltd., Oxford, UK, 3rd Edition, 2006, pp. 129-154.

[113] Roskosz, S., Staszewski, M., and Cwajna, J., "A complex procedure for describing porosity in precision cast elements of aircraft engines made of MAR-M 247 and MAR-M 509 superalloys," *Materials Characterization*, vol. 56, 2006, pp. 405-413.

[114] American Society for Metals, "Metallograpy and Microstructures*," Metals Handbook: 9th Edition*, vol. 9, 1985, p. 170.

[115] Anton, D.L., Giamei, A.F., "Porosity Distribution and Growth During Homogenization in Single Crystals of a Nickel-base Superalloy," *Materials Science and Engineering*, vol. 76, 1985, pp. 173-180.

[116] H & M Analytical Services. "Retained Austenite Analysis", H&M Analytical Services, Inc., Allentown, NJ, 2003.

[117] Seagrave, S., and Canty, T., "Crystallography Tutorial: Diffusion," *University of Southamption Engineering Materials Website*, accesed 11/10/2010. http://www.soton.ac.uk/~engmats/xtal/diffusion/index.html.

[118] Campbell, J., *The New Metallurgy of Cast Metal Castings*, Butterworth-Heinemann, Jordan Hill, Oxford: Second Edition, 2003.

[119] Reill, W., Hoffman, H., Röll, K., "Interdiffusion in amorphous FeB multilayer thin films," *Journal of Materials Science Letters 4*, 1985, pp. 359-362.

[120] Röll, K., Reill, W., "A Study of Interdiffusion in Multilayer Cu/Ni Thin Films by Auger Electron Depth Profiling", *Thin Solid Films*, Vol 89, 1982, pp. 221-224.

[121] Lippard, H., *et al*, "Microsegregation Behavior during Solidification and Homogenization of AerMet100 Steel" *Metallurgical and Materials Transaction B*, Vol 29B, Feb. 1998 pp. 205-210.

[122] Sprinkle, J., Keverian, J., "Effect of High Temperature Homogenization and Other Factors on Mechanical Behavior of a Low Alloy Steel," *Modern Casting*, September 1966.

[123] Chandley, Dixon G., " Use of Vacuum for Countergravity Casting of Metals," *Materials Research Innovation*, vol. 3, pp. 14-23, 1999.

[124] Barre, Charles, "HIP Increasingly Used for Upgrading of Castings as Process Becomes More Economical," *International News Magazine of the Investment Casting Institute*, pp. 14-15, August 1998.

[125] Barre, Charles, "Hot isostatic pressing," *Advanced Materials & Processes*, March, 1999.

[126] Flemings, M.C., "*Behavior of Metal Alloys in the Semisolid State," Metallurgical Transactions A*, Volume 22A, May 1991, pp. 957-963.

[127] Carlson, M., Rao, N., Thomas G., "The effect of austenitizing temperature upon the microstructure and mechanical propertiesof experimental Fe/Cr/C steels," *Metallurgical and Materials Transaction A,* vol. 10, 1979, pp. 1273 – 1284.

[128] Haidemenopoulos, G.N., and Vasilakos, A.N., "On the thermodynamic stability of retained austenite in 4340 steel," *Journal of Alloys and Compounds*, vol. 247, Jan. 1997, pp. 128 – 133.

[129] Sastry, K., Khan, K., Wood, W., " Mechanical Stability of Retained Austenite in Quenched and Tempered AISI 4340 Steel," *Metallurgical and Materials Transactions A*, vol. 13, Apr. 1982, pp. 676-680.

[130] Zurecki, Z., "Cryogenic Quenching of Steel Revisited," *Heat Treating: Proceedings of the 23rd Heat Treating Society Conference*, September 25-28, 2005, David L. Lawrence Convention Center, Pittsburgh, PA, USA, 2006.

[131] Meng, F., "Role of eta-carbide precipitations in the wear resistance improvements of FE-12Cr-Mo-V-1.4C tool steel by cryogenic treatment," ISIJ *international*, vol. 34, 1994, p. 205.

[132] Xuan, F., Huang, X., and Tu, S., "Comparisons of 30Cr2Ni4MoV rotor steel with different treatments on corrosion resistance in high temperature water," *Materials & Design*, vol. 29, 2008, pp 1533-1539.

[133] Hebsur, M., "Recent attempts of improving the mechanical properties of AISI 4340 steel by control of microstructure – A brief review," Journal of Materials for Energy Systems, vol. 4, June 1982, pp. 28-37.

[134] Banerji, S., McMahon, C., and Feng, H., "Intergranular fracture in 4340-type steels: Effects of impurities and hydrogen," Metallurgical and Materials Transactions A, vol. 9, Feb. 1978, pp. 237-247.

[135] Tomita, Y., "Fracture toughness of calcium-modified ultrahigh-strength 4340 steel," *Metallurgical and Materials Transactions A*, vol. 21, Oct. 1990, p. 2739-2746.

[136] Paules, J.R., Dilmore, M.F., and Handerhan, K.J, "Development of Eglin Steel- A New, Ultrahigh Strength Steel for Armament and Aerospace Applications," *Materials Science & Technology 2005 Conference and Exhibition*, Sept. 2005, pp. 1416-1426.

[137] The London Metals Exchange, "Metal Prices & Price Tables," www.lme.com & www.metalprices.com, Accessed 22 March, 2011.

CURRICULUM VITAE

Paul C. Lynch

EDUCATION

PhD. **Industrial Engineering, Penn State University (May 2011)**
Dissertation title: "The Development of UltraHigh Strength Low Alloy Cast Steels with Increased Toughness"

M.S. **Industrial Engineering, Penn State University (2007)**
Thesis title: "The Effects of Non-Contact Acoustic Vibrations on the Solidification and Microstructure of Aluminum Casting Alloy A356"

B.S. **Industrial Engineering, Penn State University (2004)**
Minor in Business/Liberal Arts

PUBLICATIONS

1. Lynch, P.C., Abrahams, R.A., Paret, K.E., and Voigt, R.C. (2010). "Modeling of Segregation Reduction in Steel Castings During Hot Isostatic Processing (HIP) and Homogenization," *64th Steel founders Society of America Technical & Operating Conference*, December 9-11, 2010.
2. Abrahams, R.A., Lynch, P.C., Voigt, R.C. (2010). "Composition Development & Improved Processing of High Strength Low-Alloy IC Steels," *57th Annual Technical Conference and Expo*, October 10-13, 2010.
3. Lynch, P.C., Voigt, R.C., Furness, J.C., and Paulsen, P.D. (2010). "The Effects of Non-Contact Acoustic Vibrations on the Solidification and Microstructure of Aluminum Casting Alloy A356," *AFS Cast Expo '10*, March 20-23, 2010.
4. Abrahams, R.A., Lynch, P.C., Voigt, R.C. (2009). "Processing and Composition of High Strength Cast Steels," *63rd Steel Founders Society of America Technical & Operating Conference*, December 9-12, 2009.
5. Lynch, P.C., Voigt, R.C., Grenko, T.M. (2009). "Cast Iron Solidification with Non-Contact Acoustic Stimulation," *The Carl Loper Cast Iron Symposium*, May 27-29, 2009.
6. Lynch, P.C., Voigt, R.C., Grenko, T.M. (2009). "Cast Iron Solidification with Non-Contact Acoustic Stimulation," *International Journal of Metalcasting*, Vol. 3, Issue 4, Fall 2009.
7. Lynch, P.C., Voigt, R.C., Furness, J.C., and Paulsen, P.D. (2007). "Ultrasonic-Assisted Solidification and Feeding of Aluminum Alloy A356," *Aluminum Cast House Technology 10th Australasian Conference & Exhibition*, August 6-9, 2007.

PRESENTATIONS

1. Lynch, P.C., Abrahams, R.A., Paret, K.E., and Voigt, R.C. (2010). "Modeling of Segregation Reduction in Steel Castings During Hot Isostatic Processing (HIP) and Homogenization," *64th Steel founders Society of America Technical & Operating Conference*, Chicago, Illinois, December 11, 2010.
2. Lynch, P.C. (2010) "The Development of High Strength Cast Steels with Increased Low Temperature Toughness", 2010 Penn State Center for Innovative Sintered Products Industrial Members Meeting, Days Inn Penn State, April 13-14, 2010.
3. Lynch, P.C., Voigt, R.C., Furness, J.C., and Paulsen, P.D. (2010). "The Effects of Non-Contact Acoustic Vibrations on the Solidification and Microstructure of Aluminum Casting Alloy A356," *AFS Cast Expo '10*, Orlando, Florida, March 20-23, 2010.

TEACHING EXPERIENCE

Graduate Student Instructor, Penn State University, 2007-2010
Courses: IE 302: Engineering Economy, IE 311: Principles of Solidification Processing,
IE 312: Product Design & Manufacturing Processes, IE 322: Probabilistic Models in Industrial Engineering
Teaching Assistant, Penn State University, 2005-2006
Courses: IE 450/ IE 470: Manufacturing Systems Engineering
Teaching Intern, Penn State University, 2004
Course: IE 302, Engineering Economy

HONORS and AWARDS

1. 1st Place Overall Winner for Best Poster: 2010 AFS/FEF Student Technology Student Research Poster Contest, (2010)
2. Institute of Industrial Engineers – John L. Imhoff Award, (2010).
3. Alpha Pi Mu National Award for Excellence, (2008).
4. Penn State IE Department Outstanding TA of the Year, (2006).
5. Graduated with Highest Distinction Honors (B.S. IE), (2004).
6. Dean's List Every Semester at Penn State University, (2000-2004).
7. Penn State University Senior Evan Pugh Award, (2004).
8. Penn State IE Department Wilbur & Judy Meier Award, (2004).
9. Alpha Pi Mu National Award for Excellence, (2003).
10. Penn State IE Department Seville Outstanding Community Service Award, (2003).
11. Automobile Hall of Fame Awards, (2003 & 2004).
12. USAA All-American Scholar, (2003 & 2004).
13. USAA National Engineering Award, (2003).
14. Penn State Schuylkill Academic Honor in Mathematics, (2002).
15. Penn State Schuylkill Academic Honor in Engineering, (2002).
16. National Dean's List Publication, (2001).
17. Penn State President's Freshman Award, (2001).